Displacement-based verification of unreinforced masonry walls acting out-of-plane within a structural system

By

Renato Granata

In partial fulfilment of the requirements for the degree of

Master of science

in Structural Engineering

Delft University of Technology

Faculty of Civil Engineering and Geosciences

5th July 2017

Displacement-based verification of unreinforced masonry walls acting out-of-plane within a structural system

By

Renato Granata

Thesis Committee:	Ir. Mark Spanenburg	BAM A&E
	Prof. Dr. Ir. J.G. Rots	TU Delft
	Dr. Ir. Drs. C.R. Braam	TU Delft
	Dr. F. Messali	TU Delft

Delft University of Technology

Faculty of Civil Engineering and Geosciences

5th July 2017

Preface

This Master thesis research was written in partial fulfillment of the requirements for the degree of Master of Science in Structural Engineering at the Civil Engineering Department of Delft University of Technology. The work involves the numerical modelling of one-way vertically-spanning unreinforced-masonry walls subjected to the out-of-plane failure during the dynamic excitation.

The investigation was carried out under the guidance of Delft University of Technology and Bam A&E. Therefore, I would like to spend few words to thank all the members of my graduation committee for their support and for taking the time to meet me in the interim meetings throughout the academic year to check my progress. Also, I want to thank them for going to the effort of carefully reading and identifying the points of improvements in this document.

I am also grateful to all of my colleagues in Bam A&E, who were always available for listening to my doubts and helped me to stay motivated. Special thanks goes to Rick, for his valuable advice and consistent support and encouragement.

Finally, thanks to my friends Costantino, Giorgio and Daniele for making a difficult time much easier, and to my family for their unconditional love and support.

Renato Granata

Delft, University of Technology

July 5, 2017

Summary

This thesis research deals with the out-of-plane assessment of unreinforced masonry walls vertically spanning between the floors of a structural system. Their stability is analyzed in the context of the induced earthquakes that have been striking the area of Groningen in recent times as a result of gas extractions.

Present codes evaluate the structural capacity of a wall element either by comparing its physical strength to the applied load, following a so called force-based approach, or by making use of a combination of kinematic and limit analysis, generally referred as displacement-based methodologies. Displacement-based approaches such as the ones followed by the New Zealand standard (NZS) and the Italian code (NTC) seem to be more coherent with the out-of-plane failure mechanism considered as an instability problem. However, these codes are based on earthquakes whose nature is tectonic, and the used design spectra are not consistent with the induced nature of the Dutch events. Therefore, this thesis aims to verify whether the adoption of displacement-based methodologies from foreign countries is appropriate for the Groningen scenario and, in that case, if it is possible to derive more accurate results by making use of a numerical 2D modeling approach.

The methodology developed to answer the research questions consisted in mainly two parts. At first, attention was given to the modeling of a rocking wall only. Its inherent nonlinear behavior was analyzed by addressing its physical and geometrical properties and a variety of boundary conditions. Three alternative 2D wall models were developed and employed for carrying out several quasi-static and nonlinear transient analyses with the aim of choosing the most appropriate wall model for its implementation in an expanded building discretization. These models were validated against the results of experimental researches and analytical formulas found in relevant literature. Through a sensitivity analysis on material model parameters, it was found that a discretization of the rocking wall consisting of numerically integrated curved beam elements with 11 integration points over the thickness and nonlinear material model lumped in the areas where cracking is expected to occur is a valid finite elements representation for a rocking wall. In that case, a smeared approach with the Total Strain Fixed crack constitutive model was used to model conveniently the crack propagation in the cracked sections.

In the second stage of the research, the wall model was introduced inside a building system, which was represented by a frame model with linear elastic properties. In the model, only the nonlinearity of a single wall was considered at a time. This model was employed on different levels of the frame building and its resistance to the out-of-plane failure was investigated by exciting the primary structure with incremental base motions. The records used to perform these nonlinear analyses were derived in accordance to prescription of the NPR9998:2015, and the resulting output was elaborated to construct graphs showing the resistance of walls to the out-of-plane failure as a function of their location in the frame. The URM walls pertaining to top floors showed a tendency to tolerate smaller values of PGA than those on lower levels, even though this increase of vulnerability was not proportional to the solicitation, which seemed to raise linearly along the structure. In order to investigate this aspect, linear transient analyses were run on the frame model with the previous batch of records. The output of these analyses was processed with a Fast Fourier Transform procedure and the elastic response spectra at floor level were obtained.

By looking at the obtained response spectra it became clear that the interaction between the response of the primary and the secondary system determines the magnitude of the inertia forces acting on the walls. It was observed that the period of vibration of a rocking wall is a function of its deformation, and that the "period elongation" caused by its mid-height displacement may determine an abrupt reduction of the instabilizing forces acting on it, preventing it from failing.

Once the effects of height amplifications and systems-interaction on the URM walls within a building were unveiled, their resistance to out-of-plane excitations that resulted from numerical analyses was compared to the results extrapolated from the foreign normative. The comparison showed that for walls on lower floors the maximum PGA tolerable by the numerical model stands in between the values derived from the codes, whereas for wall on higher levels the maximum accelerations at the base of the buildings is similar for the numerical and the analytical models. Also, the maximum PGA's found in the New Zealand normative seem to be conservative, especially for lower-level walls. In conclusion, although the models developed do not allow to increase the accuracy of the analytical formulae found in international standards, they can be employed to verify the appropriateness of their use in the Groningen scenario.

Table of Contents

Part 3

Table of figures

Table of tables

1 Introduction

The ongoing gas exploitation pursued by the Dutch government in the region of Groningen has made necessary to investigate the seismic vulnerability of local buildings. If on the one hand all the structures today are erected according to recent prescriptions that enforce seismic design (Eurocode 6 and 8, National annexes, NPR 9998), on the other hand the largest part of the historical building stock in The Netherlands comprises structures where unreinforced masonry is part of the main load bearing structure.

Intuitively enough, plain masonry is not the best construction material to choose when it comes to the design of earthquake-resistant structures. Its composition and mechanical response lack important features that are crucial in the seismic situation such as tensile strength and ductility. For these reasons the mechanical behavior of unreinforced masonry better suits scenarios where a structure is subjected to static stresses rather than those of a dynamic nature.

In confirmation to this, in recent years the structural response to seismic events of the existing buildings in the area of Groningen appeared to be inadequate, and extended researches have been carried out with the aim of improving the assessment procedures with special regards to reliability and accurateness of the outcome. In order to do that, it is of fundamental importance to accurately identify the underlying characteristics of the Groningen scenario, such as the induced nature of its earthquakes and the rather slender wall systems with low lateral stiffness.

Figure 1 - A measure for collapse prevention in Loppersum.

Together with other consultancy engineering companies and Academic Institutions in the Netherlands, Bam A&E was commissioned by Nederlandse Aardolie Maatschappij (NAM) to assess the state of art of several existing structures in the area interested by the seismic phenomena, yet providing possible strengthening measures for their retrofitting. Although compelling, the current assessment procedures for masonry elements presented in foreign codes appear to be conservative and too specific for the characteristics of foreign situations. As a result, applying foreign normative on the Dutch buildings result in economically inconvenient solutions which can be realistically mitigated by carrying out further investigations on this matter.

1.1 Masonry as a construction material

Masonry is a composite material used to erect structures in every part of the world since very ancient times. To its simplest configuration, it consists of units that are brought together and bound with mortar. The systematic use of masonry and its corresponding developments coincide with the advent of the large urban civilizations and, in the period where mainly wood was adopted for construction purposes, marked the transition to an era of more durable and solid structures. The technology as we know it today is the outcome of the progresses made over thousands of years and to this day a large portion of the buildings in world cities are made from masonry.

Notable characteristics of masonry are the affordability and accessibility of its constitutive materials that together with its exceptional fire resistance make this construction material particularly attractive for residential use. Besides that, masonry is strong in compression but acts poorly in tension, showing brittle failure when subject to stretching or bending. Thus, construction of gravity structures (high compressive strength under vertical loads, high mass provided by the material itself) where arch action would be predominant is also popularly attained by means of unreinforced masonry. Although aspects such as the large variability in the mechanical characteristics of bricks and mortar may justify some of the

complications that are encountered when using masonry, authors agree that the major feature determining the general behavior of this material is the relation between its constituents. Their interaction in fact increases in complexity with increased deformation, making the overall material behavior highly nonlinear and difficult to model. Nowadays, the ongoing applications of masonry for the erection of slender structures particularly prone to instability phenomena and for the restoration of buildings of historical value require an even more in-depth knowledge on the way this material respond to a range of loading conditions.

1.2 Context of the present study, object of investigation and motivation

Given the limitations in structural performance of the masonry, one could wonder why in the Netherlands this material is generally found as the major building component even for structures located in a seismic region. The origin of this problem can be found in the loading typologies which were taken into consideration at the time of construction of the existing building stock around Groningen. Back in times the possible exposure of these buildings to seismic events was not accounted for as the area had hardly ever been subjected to this sort of phenomena. In fact, it is only in the late '50s of last century that the biggest natural gas field of Europe was found in the northern part of The Netherlands. Soon after that discovery, in 1963, activities related to the exploitation of the gas started. In 1991, seismic activity in the area of Groningen was observed for the very first time. Since then, several earthquakes have struck the area, suggesting some kind of correlation between the activity of gas extraction and the manifestation of seismic events. Nowadays, this phenomenon is known as *induced seismic activity* and it is studied as a specific branch of the earthquake engineering.

According to researchers who collected and analyzed the data in the last decades, the intensity and frequency of seismic events in the Groningen area have so far exhibited an increasing trend. Recent registrations showed that intensities of 3.6 on the Richter scale were already reached in 2013 (KNMI, 2013).

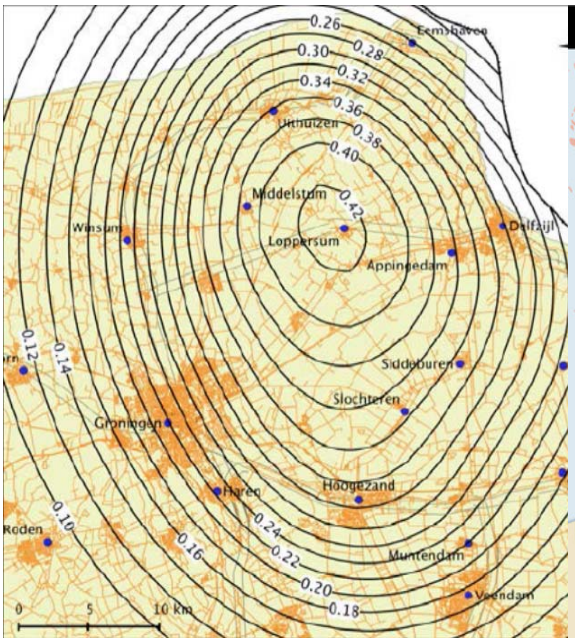

Figure 2 – Contour plot of reference PGA in g with a repeat period of 475 years (KNMI, 2016)

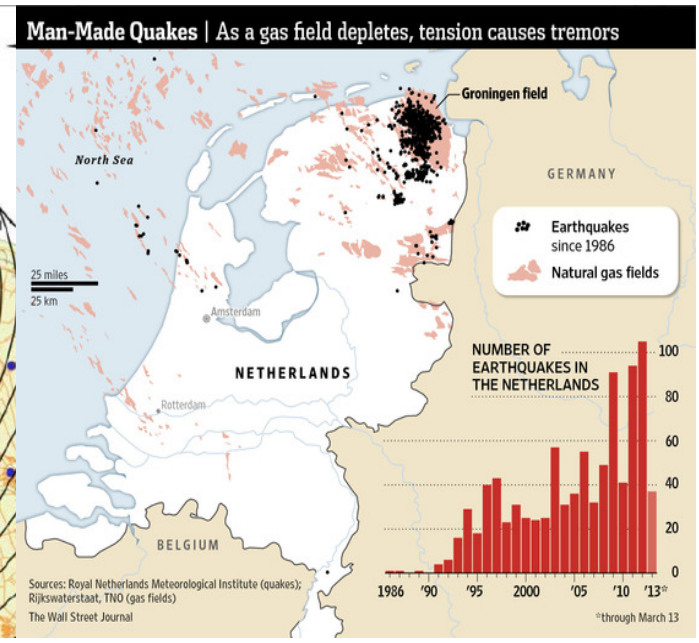

Figure 3 – Occurrence of earthquakes in the Netherlands in recent years (TNO, 2013).

Under this scenario it is of crucial importance to evaluate the capacity and stability of existing masonry structures in order to mitigate the detrimental effects caused by repetitive seismic actions on the buildings. These are not only related to the structural damages, but also to the diminishing sense of safety the inhabitants have shown in the region affected by these phenomena. In particular, the area of Groningen contains well over 150000 populated buildings of which about 90% of them consists to a great extent of unreinforced masonry. The goal set by the government is restoring trust and confidence for the people living in that area and, by consequence of that, improving their quality of life. Revealing

possible sources of conservativeness in current methodologies for the stability assessment of masonry elements, together with predicting their capacity before (and after) the strengthening measures adopted, may represent a key step for an effective action plan.

In general practice, the resistance of a masonry building to earthquakes is estimated by analyzing the seismic response of the structural elements which are assembled together to form the load-bearing system. Among all the others, walls represent a part of the structure which is particularly affected by inertia loads. The walls exhibit a behavior that may be conveniently analyzed by considering it in their in-plane and out-of-plane direction. For both circumstances specific failure mechanisms can be found, and thus the structural problem may be addressed by resorting to a number of different approaches. The scope of this master thesis research is trying to make a positive contribution to the ongoing researches being carried out to broaden the knowledge on and overcome the challenges related to the URM walls acting out-of-their-plane due to seismic loads. This topic in fact, seems to incorporate many of those aspects which make the assessment of the face-loaded walls rather over-conservative. This is particularly true in the case of walls located on higher levels of a building, for which the out-of-plane failure is more likely to occur due to the smaller load applied above them. The latter consideration stands as a starting point for this master thesis investigation, as discrepancies were found in the expected resistance of wall elements in Groningen. Indeed, question is whether it would be possible to capture some sources of conservatism when dealing with the out-of-plane action of walls in the current analytical methodologies and by making use of a numerical approach based on a 2D finite elements discretization. It should be noted that, since those methodologies can be found in the foreign normative, it might be that their application in the Dutch building typologies leads to inaccurate results due to factors or coefficients used which are sit-dependent to the foreign scenario. Thus, the main research question is:

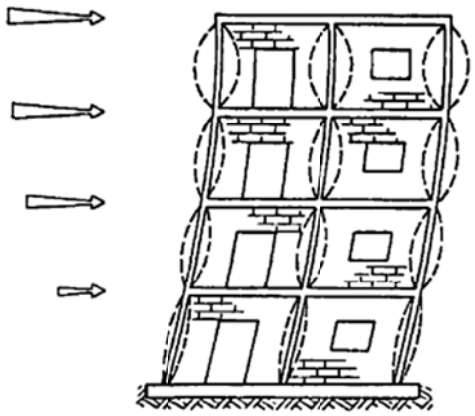

Figure 4 - Out of plane vibration of walls more pronounced for higher levels (Tomazevic, 1996).

"Is it possible to create an adaptation of foreign methodologies for the out-of-plane assessment of a URM wall to the Groningen scenario, by making use of a simple 2D frame model?"

Speaking of the out-of-plane behavior of walls, the assessment methods used nowadays try to integrate aspects which are based on both strength and stability considerations. Hence, it is convenient to have an understanding of both these contribution to correctly elaborate on the stability of URM walls. This can be accomplished through a more general literature study on the topic of URM walls in earthquake-prone environments, which will also reveal what is meant when those methods are labelled as "displacement-based". While doing so, additional (minor) research questions will progressively arise and be included in the investigation.

The choice of investing a relatively long period of time on the OOP of URM walls for the elaboration of a master thesis project is an appealing opportunity as it is a really stimulating topic and it enables to be actively involved in an extensive research plan conducted by hundreds of people sharing their knowledge on a regular basis.

1.3 Synopsis

This document is divided in three main parts. Part 1 includes the Introductory chapter, together with the Literature Review and the Action Plan for the development of the research in agreement to the time schedule. Next, Part 2 addresses the creation of the finite elements models generated in order to run a set of quasi-static and dynamic analyses and collect the associated data. This part is divided in two areas: the models pertaining to the local system (a URM wall rocking) and the those representing the entire global system (the building around it + the URM wall). Finally, Part 3 includes the chapters related to the numerical response of the models and the post-processing of results to draw the conclusions. These are presented in the last chapter of this master thesis, followed by some recommendations for future studies and investigations.

2 Literature review

This chapter presents a collection of the material consulted throughout the writing of this document. A number of topics are addressed in a rather concise way. For more extensive reading, the reader is referred to the bibliography at the end of this report.

2.1 Induced earthquakes

The event of ground shaking may be the manifestation of earthquakes at the earth's surface. If this is the case, this circumstance is called "seismic event" and the cause of it has to be found in the sudden release of stored energy in the earth's crust.

In the past, earthquakes were classified as natural events associated with the tectonic nature of the Earth: as the moving tectonic plates get stuck beneath the ground, an enormous quantity of energy would require to be released so as to allow straining, breaking and eventually sliding of these plates in the three spatial directions. Yet, it is clear today that the energy underneath the soil may also be artificially accumulated due to human activities. Confining this matter to national boarders, extraction of gas from the ground and its subsequent storage are both found to be sources of shallow quakes, which are thus classified as induced earthquakes (Ellsworth, 2013).

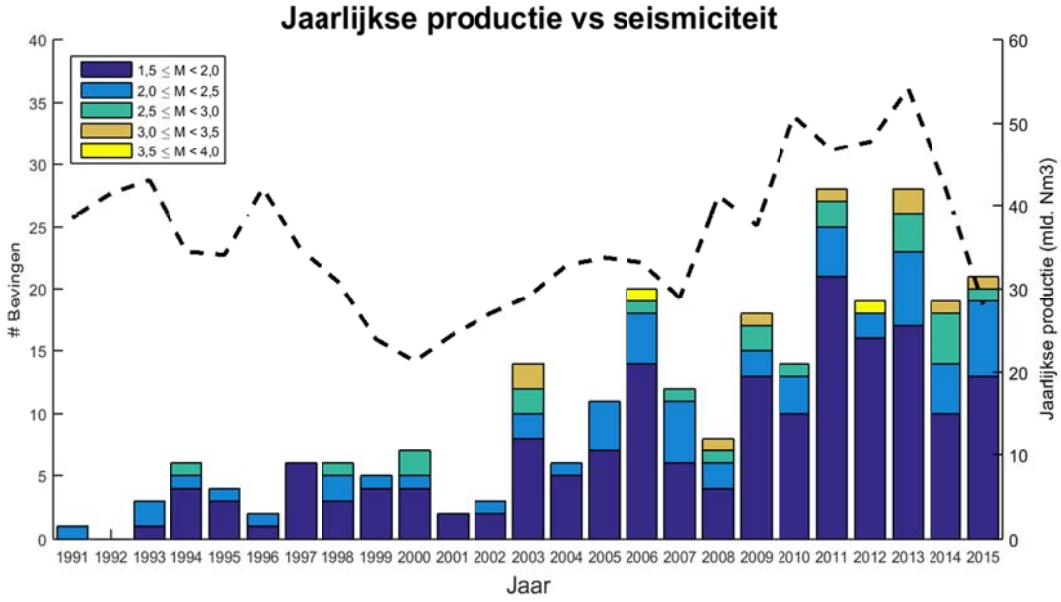

Figure 5 - Induced seismicity (>1.5) of the Groningen field in time sorted by magnitude vs. the annual production.

In the decades, seismic events of this typology in The Netherlands have increased in number and magnitude (Thienen-Visser & Breunese, 2015), becoming an important scientific and political topic. Unlike tectonic ones, the energy released by induced earthquakes is spread out over a narrow spectrum of high frequencies and the duration of this type of event is very short as in the case of pulse excitations.

2.2 Unreinforced Brick Masonry

The use of masonry in structures is well justified by the easy erection, the availability of its constituent materials and their costs. In masonry, bricks or stones usually act as single units that are placed on top of each other and bound together by means of bindings such as mortar. When assembling the units to shape walls, one can follow determined patterns which result in masonry structures with specific mechanical characteristics.

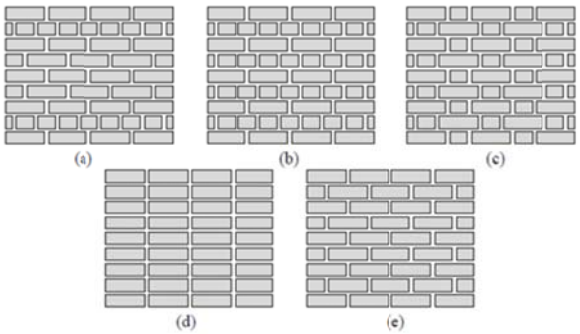

Figure 6 – Different arrangements for brick masonry: (a) common (b) cross (c) Flemish bond (d) stack bond (e) stretcher.

In general, however, the two most distinctive properties of masonry walls are their anisotropic nature enforced by the arrangement of the joints in vertical and horizontal direction, and the poor performance exhibited in tension.

These characteristics of the material led in the past to the misconception of masonry being not an adequate material for the use in seismic areas. Yet, several cases of masonry structures are found where the buildings proved to be able to withstand larger forces than those expected when confining the strength analysis to the physical resistance of the material only (Doherty, 2000 and Derakhshan et al, 2014). This suggests that for a correct seismic assessment of a masonry structure, attention should be given to the deformation capacity of its structural elements rather than focusing on the mechanical properties of the material only.

As the main goal of this thesis is to explore the out-of-plane behavior of masonry walls considered as continuum elements, detailed study on the mechanical and physical properties of its constitutive materials is not further addressed, unless clearly stated in dedicated sections. Masonry will thus be examined as a composite material.

2.2.1 Mechanical behavior of brick masonry

Despite the high variety of masonry, laboratory tests were undertaken in an attempt to generalize its mechanical behavior. Furthermore, masonry has intrinsic anisotropic properties due to its highly non-homogenous composition. However, given a wall configuration the behavior of masonry can be approximated as orthotropic and, sometimes, even isotropic. In general, its mechanical performance is characterized by strong nonlinear behavior, and should be assessed in the direction parallel and perpendicular to the bed joints of the wall.

Aiming at this, (Backes, 1985) tested the tensile resistance of masonry in the direction of the bed joints, and found that it is strictly related to the relative tensile strength between the mortar, the bricks and their interface. The latter usually exhibit a resistance which is ten times larger than the mortar, which justifies a step cracking pattern along the height of the wall. Compared to the case where mortar has a greater tensile strength than the bricks, the failure mechanism shows a more ductile behavior and thus dissipates a relatively large amount of energy before collapsing.

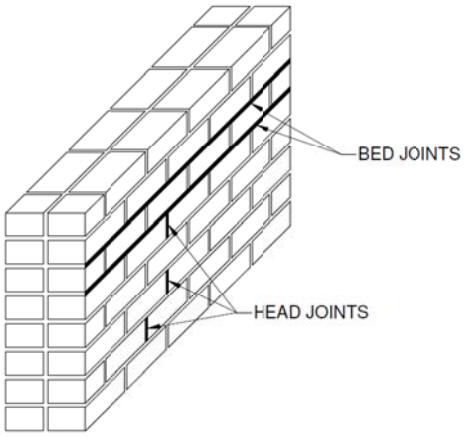

Figure 7 - Head and bed joints of a masonry wall.

Although no literature studies can be found on the tensile loading orthogonal to the bed joints, it may be reasonable to expect a softening behavior of the material, in a similar fashion to the softening of concrete.

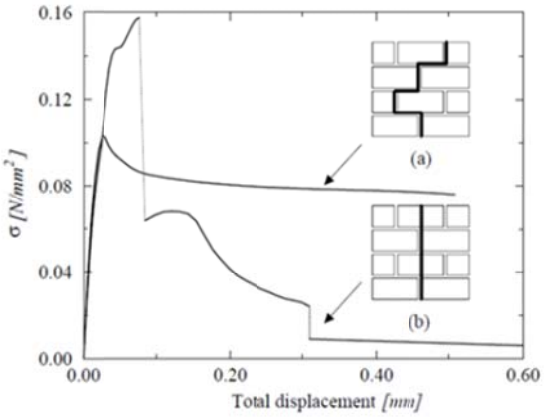

Figure 8 – Tensile resistance of masonry parallel to bed joints (Backes, 1985).

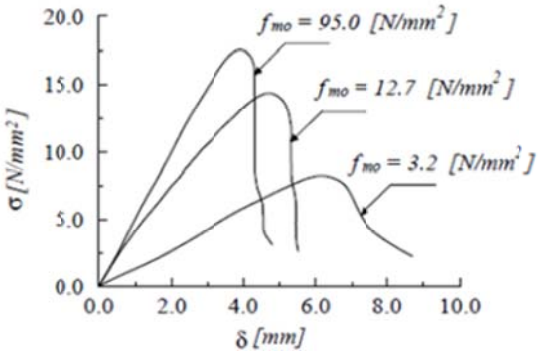

Figure 9 - Influence of the mortar strength on compressive resistance of masonry (Binda et al, 1988).

Similar tests were performed by (Binda et al, 1988), (McNary & Abrams , 1985) for static uniaxial compression loads on masonry prisms. It was found that the type of mortar used has a great influence on the way masonry fails in compression. The results illustrated on the graph indicate that compared to the bricks, for much larger compressive strength of the mortar, the masonry element experiences explosive failure. At the same time, the bricks compressive strength seems to have little influence on the nonlinearity of the stress/strain relationship of prisms, which depends mainly on the mortar properties beyond the linear range. Compared to static loading, cyclic compression resistance diminishes prism compressive strength by a factor 0.7 (Naraine & Sinha, 1989).

A series of experiments were also carried out to research the behavior of masonry subjected to biaxial loading. The work presented by Page (1981-1983) and Dhanasekar et al (1985), culminated in the formation of graphical results which are coherent with the typical behavior of brittle materials.

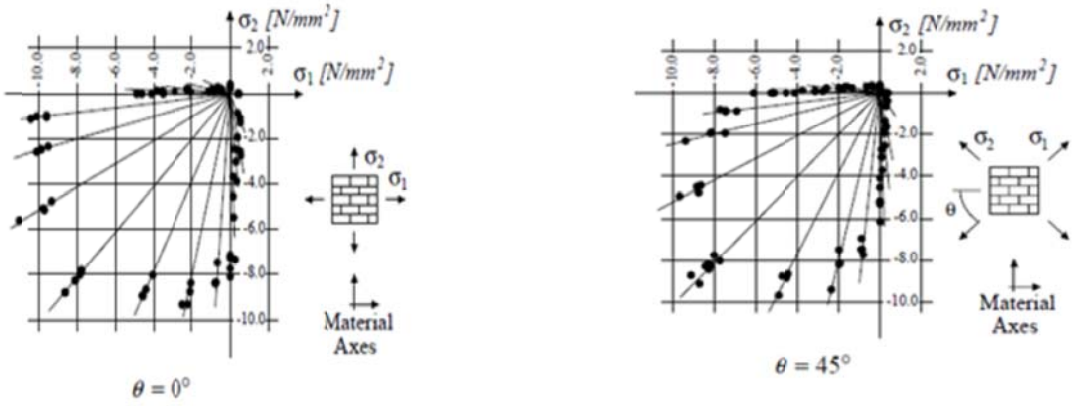

Figure 10 - Results found by Page, biaxial loading of masonry samples.

With respect to the stress-strain relations, the tests showed that nonlinear behavior of masonry was mainly determined by slippage of bricks and mortar at the interfaces, confirming the central role of the interface on the mechanical properties of masonry. Shear behavior of masonry is directly correlated to the properties of mortar and the roughness of the connection with the bricks. More in detail, the shear resistance of the masonry element is linearly proportional to the tensile resistance of the mortar parallel to the bed joints (Borri, -).

Shear behavior is also dependent on normal stress: if axial compression is applied, the shear strength of masonry increases. (Lourenco et al, 1995) found that a Mohr-Coulomb model is appropriate for modeling the shear behavior along the masonry joints.

In conclusion, from a material point of view, masonry behaves similarly to concrete both in compression and in tension. Compressive stresses follow a linear trend that shifts to a hardening behavior while crushing of the material occurs. When in tension, stresses increase until the formation of a crack, and at this point do not abruptly go to zero but undergo softening. In a modeling process of the material, these constitutive laws may be described by a number of pre-defined models that one can combine within the particular method of structural analysis used. In most cases, the interface between its constituents' materials is the weakest link of the system, resulting in assuming the tensile strength of masonry as negligible.

2.2.2 Degradation and dissipation for cyclic loading

The seismic capacity of URM walls is difficult to quantify not only due to the limited non-linear deformation capability of masonry and its highly variable mechanical properties. Being a degrading material, masonry is sensitive to inelastic deformations as they reduce its strength and stiffness in time. By consequence of that, masonry is a material particularly vulnerable to the incremental damage generated by earthquake action. Deterioration of the material is usually identified as cracks occurring between bricks and mortar. This interface area determines much of the masonry mechanical properties, and the complexity of the interaction between the materials increases with the plastic deformations.

The degrading behavior of masonry can be observed from the stress-strain relations or load –displacement curves of a masonry element subjected to cyclic loads. The dependency of the mechanical response to the loading history is called hysteresis. In the quasi-static cyclic tests performed by (Griffith et al, 2007), results diagrams show two typical aspects of the hysteresis on masonry: the reduced unloading stiffness and the partial regain of stiffness that follows the closing of cracks. The area enclosed by the hysteresis loops gives a graphic impression of the amount of energy dissipated by the system during a response cycle to an applied excitation.

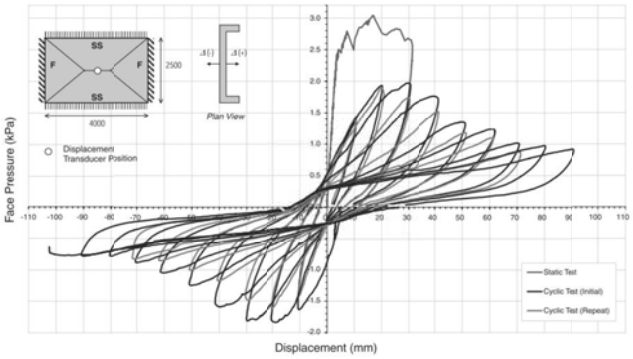

Figure 11 - Hysteresis loops obtained in experimental investigation (Griffith, 2006).

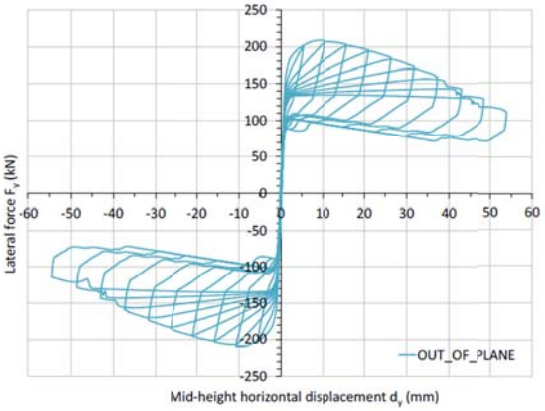

Figure 12 - Hysteretic behavior of a masonry wall acting out-of-plane. "Masonry wall under OOP cyclic loading", TNO DIANA Course Material, 2016.

2.3 URM walls

When the load definition on the masonry element is not limited to vertical and gravity components, undergoing flexural or stretching stresses may culminate in brittle failure and sudden collapse. In such cases, the use of reinforcement provides additional strength to the masonry that is consequently defined as "reinforced masonry". Walls may be thus erected with unreinforced (URM) or reinforced masonry. For the scope of this thesis the first typology only is of interest, so that the properties of reinforced masonry walls are here not regarded.

Within a complete building where the walls are part of the main bearing system, masonry walls are ideally expected to act as part of a rigid box and transmit the loads to the foundation by means of in-plane action. A wall engaged on its plane embodies the fundamental load path for the transmission of forces to the ground. Nevertheless, the connection between adjacent walls, the way they are constraint and the occurrence of dynamic forces cause the walls to act in flexure, or out-of-plane, as well (Priestley, 2007). The mechanisms that may lead to a failure of the wall in the direction perpendicular to its plane are called *first mode collapse mechanisms* and they must be prevented so as to allow the structure to activate the in-plane resistance of walls. This is usually much larger than their lateral strength, and it is pertinent to the so called second mode collapse mechanisms.

The out of plane mechanism of a wall under face load may be the cause of global collapse if the wall is supporting the floor beams or the roof of a building. How well a wall performs out of plane depends on the quality of its connections to the surrounding structural elements and on the type of diaphragm connected to it. In multi-stories URM buildings subjected to seismic action, the walls tend to be more exposed to flexural action at upper levels. It is interesting to see that out-of-plane demands appear to be more pronounced where the flexural capacity is lower due to a lack of vertical load on top (Tomazevic, 1996). Nevertheless, evidences show that in the past decades masonry walls acting out of plane during an earthquake outperformed in comparison to their expected seismic resistance (Priestley, 1985). This suggests that the problem of walls loaded by a dynamic excitation should not be limited to investigations on their material failure behavior. Rather than that, the out of plane action of a wall need to be addressed as a problem about stability, where large geometrical nonlinearities allow the wall to take advantage of its displacement reserve capacity.

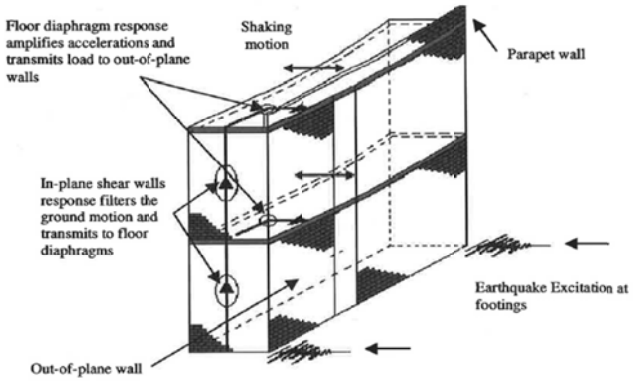

Figure 13 – Seismic Load Path for Unreinforced Masonry building (Extrapolated from Tomazevic, 1996)

These geometrical nonlinearities can be explained by the shifting of the workline of the forces acting on the wall as it deforms under the action of a lateral load. Basically, as long as this workline does not pass through the point of rotation of the mechanism, the reaction forces on the wall generate a stabilizing moment, and the wall is able to increase the rotation provided that the applied lateral force decreases accordingly. In his PhD project, Doherty, 2000 elaborated on the nature of this mechanism and provided a mechanical description of this phenomenon.

Among all the variables determining the lateral strength capacity of walls subjected to out-of-plane loading, the manner

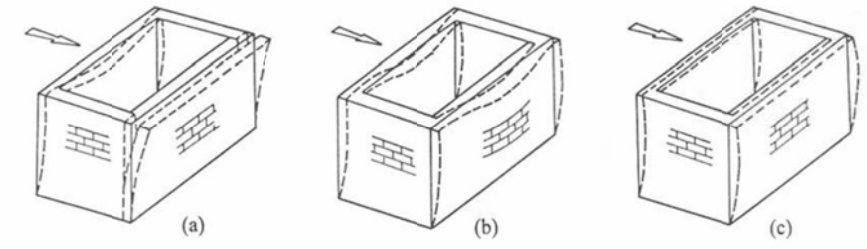

Figure 14 - Effect of types of diaphragm on face-loaded walls – a) inferior wall-to-wall connection and no diaphragm, b) good wall-to-wall connection and ring beam with flexible diaphragm, c) good wall-to-wall connection and rigid diaphragm (Picture from NZSEE, Corrigenda 4 April 2015).

of spanning between supports plays a big role. When the effect of return walls or stabilizing elements at the sides is negligible, the masonry wall may be treated as infinite long and assumed to be supported on bottom and top sides only. A lateral load applied on walls with such a configuration causes them to bend vertically, whereas the case of a wall supported also on sides makes they experience horizontal bending as well. As the two-way flexure involves the activation

of more resistant mechanisms, the lateral resistance of two-way bending walls is larger than that of one-way spanning walls of the same size. It is here underlined that this thesis focuses on one-way spanning walls only.

A vertical load applied on top of a wall, commonly referred as "overburden", may have a significant impact on its lateral stability. According to (Lourenco, 2000), the effect of a force acting along the vertical axis of a masonry wall is comparable to pre-compression. In short, the wall benefits from the presence of a top load as it increases in magnitude, provided it remains smaller than the value at which crushing of masonry occurs. Giving the due weight to the role of applied top forces, in his research, Doherty (2000) made a clear distinction between masonry walls with high and low overburden, identifying different behaviors and their failure modes.

The point of application of the vertical top loads determines the initial stress of the wall. Large eccentricities are usually found in the so called *endwalls* and result in the presence of bending moments at the edges. On the other hand, *partition walls* are assumed to be loaded symmetrically on their sides and the normal force acting on top has no initial eccentricity.

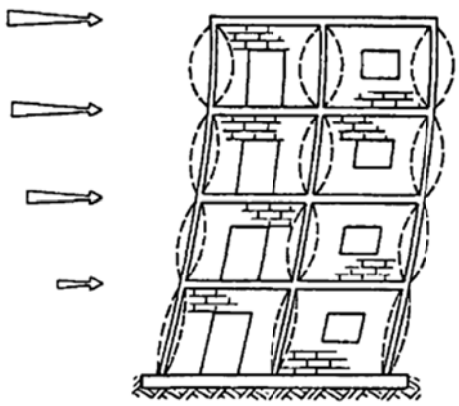

Figure 15 - Out of plane vibration of walls more pronounced for higher levels (Tomazevic, 1996)

2.3.1 Principal failure mechanisms

In general, failures of URM buildings may be classified as local or global. One may talk about global failure when the stability of the entire structural system is endangered, whereas local stability pertains to the verification of parts of the structure only. If it is true that local failures result in a smaller life hazard than global mechanisms, it should be noted that usually they are the main cause of damage suffered by masonry structures during an earthquake. The topping of parapet elements as well as collapse of walls not carrying joists fall into this category. Within the context of earthquake engineering, masonry buildings are particularly sensitive to peak ground accelerations in view of their quasi brittle behavior.

The most common failure modes of URM structures are related to the system loss of integrity:

- Lack of anchorages;
- Connections poorly designed;
- In plane failures;
- Out of plane failures;
- Combination of in and out of plane effects;
- Diaphragm-related failures.

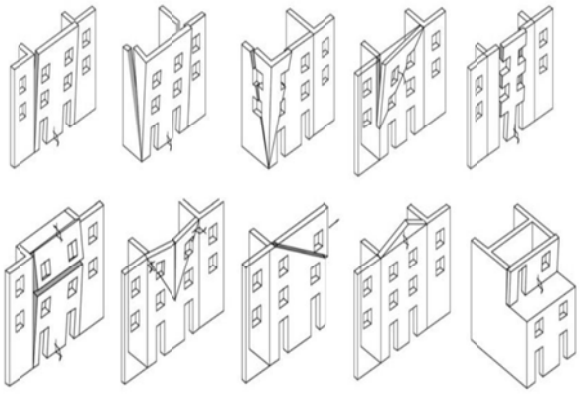

Figure 16 - Kinematic out of plane failure mechanisms of URM buildings by D'Ayala and Speranza (2002).

The in-plane failures recognized by codes are the rocking of wall elements, bed joint sliding, toe crushing and diagonal tension and they are categorized as mode II collapse mechanisms. On the other hand, the out-of-plane failures, or mode I mechanisms, may be classified as one-way bending, two-way bending and corner mechanisms, and their occurrence depends not only on the way the load is applied on the wall but also on the constraints configuration along its edges. An important difference between in-plane and out-of-plane mechanisms lies in the amount of energy dissipated during the

inelastic deformations. Although in-plane rocking cannot be defined as a dissipative mechanism tout-court, they are much more resistant than the out-of-plane. The latter release much less energy and, therefore, manifest through brittle behavior. In many codes the out-of-plane failure is presented as a local mechanism. However, in historical structures not intended for seismic areas, as it is the case in Groningen, the possibility that a partition or endwall is load-bearing makes this categorization rather far-fetched for this case, as the total stability of the structure may be endangered.

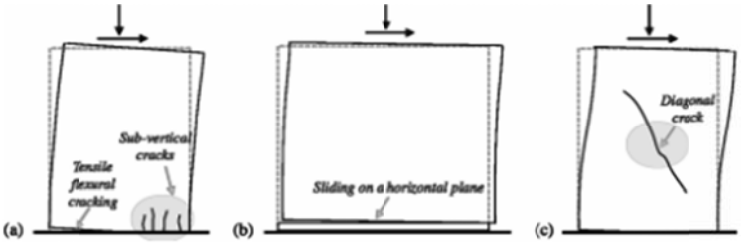

Figure 17 - Typical failure modes of masonry piers due to horizontal loads: (a) rocking; (b) sliding shear; (c) diagonal cracking. (Calderini, 2009)

2.4 Calculation philosophies in structural engineering

One of the primary objectives of an erected structure is to be able to achieve specific levels of performance when subjected to the design loads. When assessing the seismic response of an existing structure it is thus crucial to follow procedures which are capable of controlling its structural performance by referring to reliable parameters.

Traditionally, the design as well as the assessment of structures is based on the comparison between the resulting design forces acting on structural elements and their resistance: Rd ≥ Ed. This approach consists in estimating the structural stiffness of the elements considering their initial geometric properties, making use of this value to compute the strength of the structural members and eventually check that the resulting design forces are smaller than this value. Hence, the stiffness, considered as the main parameter for calculations, is not a function of the members' strength which, in turn, is the end product of the calculations. This is what it is called a *force-based approach*. In seismic design, force-based approaches imply the application of force-reduction factors in order to account for the ductility of the systems that manifests with a decrease of the structural stiffness proportionally to the increase of deformations.

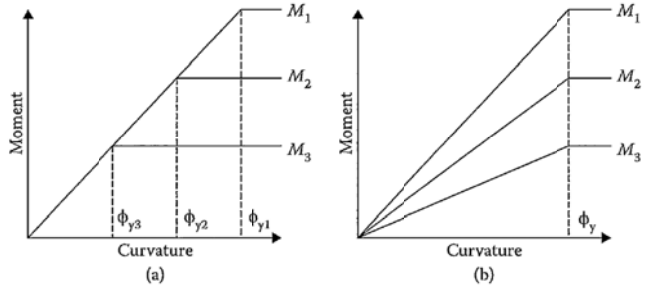

Figure 18 - Influence of strength on moment-curvature relationship. (a) Force-based: constant stiffness (b) Displacement-based: constant yield curvature (Priestley, 2007).

Through the reduction-factors it is possible to reduce the elastic response force of the systems according to the expected or target ductility (see section 2.5.2). In recent years, it was established that this way of making up for an initially assumed constant stiffness may be inappropriate, as the underlying assumption behind these types of approach is that the inelastic response of a system subjected to seismic loading is equal to the elastic response of the same system under the influence of reduced forces. This is especially wrong in case of dissipative systems such as masonry walls.

A viable alternative to the force-based methodologies is found in addressing structural problems by referring to deformation quantities (Priestley, 2007). In fact, parameters such as the curvatures, the displacements and the ductility allow to follow the evolution of damage in a building from a quantitative perspective and to account for its inelastic behavior more accurately. This approach is known as direct *displacement-based* and it is based on the concept that the stiffness is directly related to the deformation and thus it changes with the development of the structural response. The concept was first introduced in New Zealand two decades ago and since then it has allowed to assess the inelastic response of structures to earthquakes in a more reliable way. Among all the benefits arising from such an innovative approach, considering the stiffness as a deformation-related quantity brought huge advantages in structural engineering as this parameter is directly related to the structural vibration period of members and the way external forces are

distributed in the structure. In short, the displacement-based philosophy in seismic engineering considers the maximum accepted displacement as the main objective of the investigation and by consequence of that as the starting point of the assessment procedure rather than a parameter to be checked in a second moment as it happens with forced-based approaches.

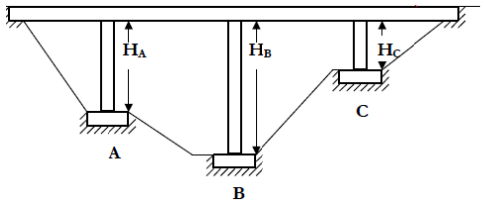

Approach	Force-based	Displacement-based
Stiffness	Proportional to $1/H^3$	Proportional to $1/H$
Shear	Proportional to $1/H^3$	Proportional to $1/H$
Moment	Proportional to $1/H^2$	Equal
Reinforcement	Proportional to $1/H^2$	Equal
Ductility	Equal	Proportional to $1/H^2$

Figure 19 - Implications of using different approaches. Example extracted from the work of Lourenco P.

The confrontation between displacement capacity and displacement seismic demand is the core of the *displacement-based assessment (DBA)*. Doherty et al (2002) have studied the OOP bending response of parapet and simply supported masonry walls and concluded that a displacement-based approach is particularly adapt for analyzing the dynamic stability of rocking masonry elements.

2.5 Structural idealization

This section briefly presents some of the aspects that are pertinent to the conceptual representation of structural systems subjected to seismic motion. Since it may not be intuitive to grasp the underlying concepts of this branch of engineering, a number of tools for approaching this topic are presented.

2.5.1 System representation

In engineering practice a continuum, structural system needs to be simplified in order to be analyzed. The methods developed in the field of structural analysis require the idealization of objects in assemblages of discretized elements, whose structural behavior better approaches reality as the modeling complexity increases (Ghali et al, 2009). The use of dedicated software such as DIANA FEA for numerical resolution of structural problems is made possible thanks to this concept.

When dynamic problems are addressed analytically, the resolution of equations governing the mechanical behavior of structures is usually limited to specific locations of simplified models where the structural properties are homogenized. A model commonly applied in seismic engineering is the *lumped-mass model*. In order to idealize a building in such a way the mass is concentrated at the nodes of the discretized structure. Each structural element is then replaced by points masses at its two edge nodes based on static analysis of those elements under their own weight. Eventually it is possible to sum up all the mass contributions of the structural elements at each node. It is a common practice in seismic engineering to model multi-story buildings as tower lumped mass systems.

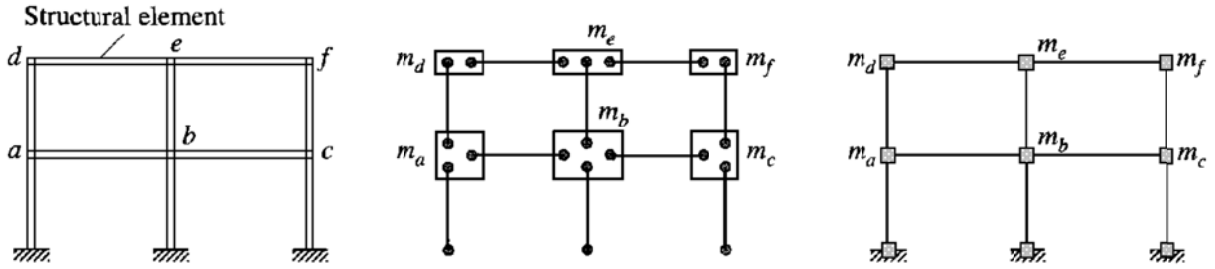

Figure 20 - Idealization of a building as an equivalent lumped mass system. Chopra (2012).

Together with the previous simplification, the *static condensation method* also permits to decrease the complexity of a structural problem enabling to elaborate on the behavior of a structural system in an approximate way.

In short, this method excludes the degrees of freedom not directly affected by the structural analysis, either because restrained or not associated to a mass in a dynamic analysis, and simplifies the system of equations defining the problem.

The modeling procedures mentioned above have the goal of decreasing the number of degrees of freedom characterizing the behavior of a structure. Consequently, similar methodologies turn out to be particularly efficient especially in dynamic problems where a large number of parameters are taken into account. Besides, in the assessment of seismic actions on a structure, great attention is given to the maximum response (in the form of displacement demands or induced acceleration) of the system as a function of the exciting frequency. This and more structural aspects can be easily analyzed by making use of *equivalent single degree of freedom approximations* as an ultimate representation of an entire building.

For instance, the pushover analysis used for assessing the global lateral resistance of a building compares the deformation capacity of a multi degree of freedom system with its displacement demand by means of a transformation to an equivalent single degree of freedom system with ideal elasto-plastic behavior.

Specific mechanisms can be described by equivalent single degree of freedom systems as well. Shibata & Sozen (1976) and later Doherty et al (2002), developed a model based on a substitute single degree of freedom structure with elastic behavior for investigating the out of plane rocking mechanism of unreinforced masonry walls subjected to seismic motion. The characterization of a representative stiffness for the rocking mechanism is the main feature of this idealization.

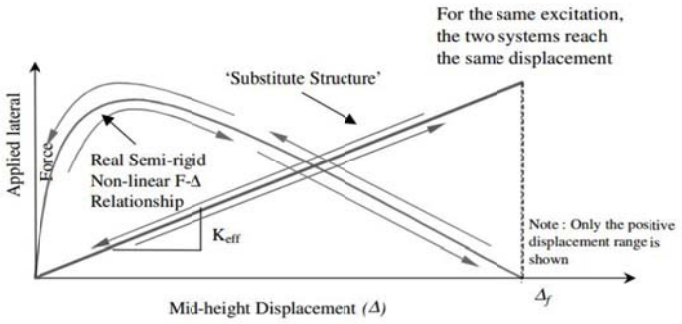

Figure 21 - Equivalent linear SDOF system describing the rocking mechanism of the wall out-of-plane (Doherty, 2000).

2.5.2 Ductility

The ductility of a structure is of fundamental importance for its stability assessment under earthquake loads. By definition, the ductility corresponds to the ability of the structure to undergo large deformations beyond the elastic field without experiencing strength and stiffness reduction until failure.

For an inelastic system, the *ductility* is defined as the ratio between the ultimate deformation and the value of the elastic deformation at which yielding occurs.

$$\mu = \frac{\delta_{max}}{\delta_y} = \frac{\theta_{max}}{\theta_y}$$

Even though it is not possible to define a unique ductility factor for unreinforced masonry buildings, as it is a structure-dependent parameter, a value between 1.25 and 2.5 is generally found in most design codes (Allen & Masia, 2013).

Ductility of a structural system is usually addressed in design codes through the *reduction (or behavior) factor*. By making use of it, nonlinear response of a structure can be accounted for also in linear analysis. The reduction factor decreases the seismic design forces below those corresponding to the elastic response requiring the system to accommodate much larger deformations.

Estimating the ductility of a structural system is crucial when approximating it with an equivalent SDOF elastic system. Considered as an oscillator, the seismic response of a ductile structure may not be the same as the corresponding elastic

system. Depending on the structural period of the system analyzed, either the *equal displacement* or the *equal energy principle* applies (Priestley, 2007).

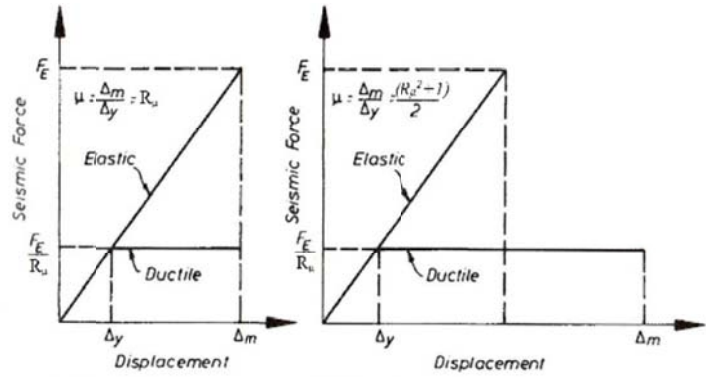

Figure 22 - Equal displacement and equal energy principles (Priestley, 2007).

Equal energy	Equal displacement
$q = \mu$	$q = \sqrt{2\mu - 1}$

$$q = \frac{F_E}{F_R}$$

Table 1 - Definition of reduction factor q.

In the latter case, the maximum displacement response of the building is larger than in the ideal indefinitely elastic system. Masonry structures are dissipative systems and as such, they follow this rule. The reduction factor q can be expressed as a function of the ductility factor by making use of the equations shown in Table 1.

2.5.3 Numerical representation

Numerical simulations of masonry behavior are essential for supporting the derivation of design and assessment rules. Since there is no established modeling strategy for this material, a number of different alternatives was developed over the last years. They are based on robust and accurate constitutive models, and they comply with the advanced solutions procedures of the system of equations that results from the discretization of the structural system of interest.

The representation of masonry can be pursued through three different levels of complexity. These are distinguished by their accuracy in describing the mechanical behavior of the material.

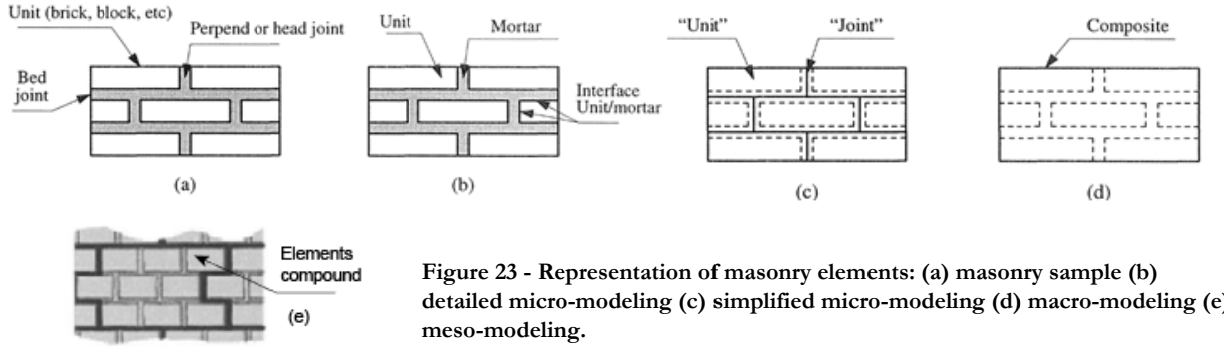

Figure 23 - Representation of masonry elements: (a) masonry sample (b) detailed micro-modeling (c) simplified micro-modeling (d) macro-modeling (e) meso-modeling.

In the *micro-modelling approach*, the masonry behavior is described by the constitutive models of all its components. While the units and the mortar are implemented as continuum elements, the interfaces between these two materials are modeled by means of discontinuum elements. Sometimes the mortar is given a zero thickness and its highly nonlinear properties are assembled to the interface ones. When the mortar and interface elements are lumped into a unique discontinuum element representing the joints, the approach being used is called *simplified micro-modeling*. The micro modeling approaches enable to capture strong heterogeneous states of stress and strain of the material and thus they are suitable for analyzing the local behavior of small structural elements. The failure characterization of masonry within this modeling strategy is illustrated by the *composite interface model* (Lourenco & Rots, 1997).

Alternatively, the main feature of the *macro-modelling approach* is neglecting the distinction between units and mortar. In other words, the mechanical properties of these two components are smeared out in a homogeneous continuum. In this way, the masonry material is regarded as anisotropic or, to the full macro-modelling potential, as orthotropic. The concept behind this approach is relating the average stresses of masonry to its average strains. Using average parameters is justified by the periodic arrangement of the units and mortar that allows a partial homogenization of this composite material. The macro-model approach is reflected by the *anisotropic continuum model* (Lorenco & et al, 1998).

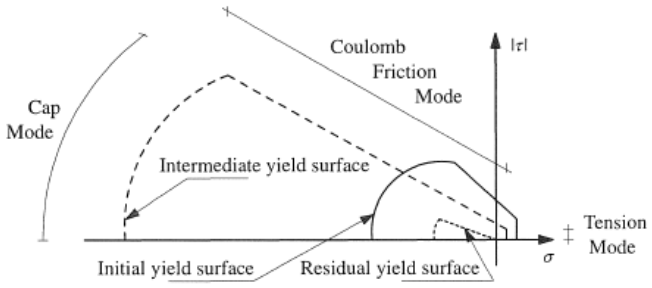

Figure 24 - The composite interface model for micro-modeling (Lourenco & Rots, 1997).

When addressing the functionality and applicability of models, the *meso-modelling approach* also deserve to be mentioned. Meso-modelling constitutes an intermediate between the previous two approaches. In fact, it considers a compound of a set of bricks and mortar joints as a base element for the modeling. These elements are connected between them by planes of cracking. Such modeling strategy is used in the "rigid elements method" (Casolo, 2000) and "equivalent frame method", where the latter is the basis of the 3Muri software.

In his studies, (Lorenco, 2008) proposed a methodology for linking micro and macro modelling by means of *homogenization techniques*. Comparable studies in numerical representation of masonry (Gambarotta & Lagomarsino, 1997) led to additional micro and macro models particularly suitable for seismic analysis. These are the basis of the 3Muri software.

To conclude, the differences between these modelling strategies mainly lie on their field of applicability. The micro modelling approach is able to describe in detail the material behavior. Although all different failure mechanisms of masonry can be considered, the computational weight and the related storage requirements limit its applicability for practical use. On the contrary, the macro modelling approach is much more practice-oriented and can be applied on large structural systems for more global structural analyses. The meso-modeling is particularly adapt for implementing masonry behavior in software for structural analysis.

2.6 Implementation of seismic assessment

An earthquake event produces seismic waves that generate stresses at the foundation of structures. These waves may be seen as a signal of varying amplitude and frequency which may be recorded by a seismograph. It is possible to apply the recorded signal on a structural mathematical model in order to assess what is the effect that the earthquake has on similar buildings.

In engineering applications, however, real records specific for a location of interest may not be available or appear to be of impractical use in the context of an approximated calculation. Therefore, a number of different approaches are available so as to simulate the action of quakes on a building and assess their stability. The main distinctions lie on the method used to account for the structure (single degree of freedom system, detailed three-dimensional model...) and the way to specify the seismic hazard. The way the seismic load is applied also defines the structural analyses that can be run on the model, the degree of complexity being dependent on the structural aspects taken into account in the modeling phase of the structure. A variety of the solution strategies that are currently adopted can be found in (Pantazopoulou, 2013).

With regards to masonry structures, their seismic performance may be evaluated through different analysis techniques. These may be categorizes as Quasi-static analysis methods and Dynamic analysis methods. Both typologies are used for local and global seismic assessment of masonry constructions. However, the (NPR9998) clearly states (section 4.3.3.2.1) that methods based on the application of a lateral load may be used for those buildings whose response is not significantly affected by vibration modes other than the fundamental one.

2.6.1 Quasi-static analysis methods

In quasi-static analysis methods, the dynamic effects are entirely neglected. Since the inertia forces are not taken into account, calculations are simpler and results are easy to interpret. For this reason, they are primary tools in engineering practice. They are divided in strength and equilibrium methods.

In the *non-linear static* analysis, also called pushover, the seismic action is simplified as an increasing distributed acceleration over the height of the building. The effect on the structure is evaluated in its displaced configurations. It is a very popular analysis because it gives insight into the lateral resistance of the entire structural system. The outcome of this analysis is a graph showing the relation between the force acting on the structure, the base shear, and the displacement of a particular point, called target point. The structure is verified when the displacement capacity of the structure represented by this graph is larger than the displacement demand given by the seismic excitation. When calculating the capacity curve, the input force distribution along the height of the building may be uniform or varying along the height by following defined shapes. Even though different configurations of the lateral load lead to different results, with a pushover analysis it is not always possible to obtain the amplification effects of the response that would be disclosed by a dynamic analysis. In their studies, (Lourenco e. a., 2011) also noticed that adaptive pushover techniques do not provide improvements in terms of load displacement diagrams or identification of failure mechanisms.

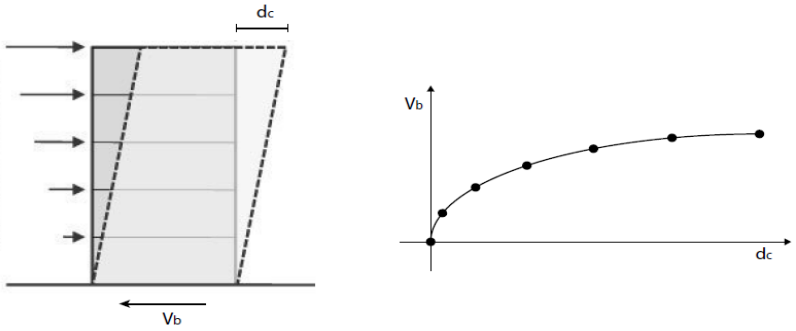

Figure 25 - Pushover analysis representation and resulting base shear force development as a function of the target point displacement.

Equilibrium methods consist in verifying the balance of the forces acting on the structure and therefore they are also called stability methods. In this way the static analysis of the masonry structure is reduced to a stability problem only. The seismic action, represented by a horizontal constant force, may be described by a design spectrum. The global seismic assessment is carried out through a *linear kinematic* approach with the use of the principle of virtual work, and appears to be an efficient tool. With this type of analysis it is crucial to select the meaningful collapse mechanisms in order to obtain reliable results.

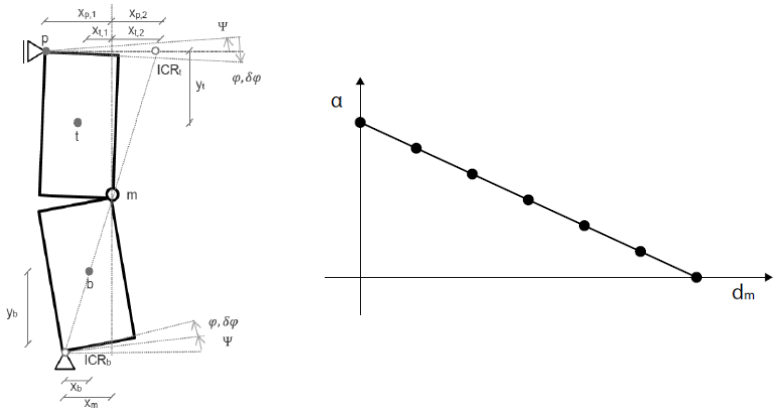

Figure 26 – Representation of a nonlinear kinematic analysis (NLKA) of a rocking mechanism through the use of virtual work principle. On the right, the decreasing of the horizontal force multiplier as the mechanism develops.

When the right collapse mechanisms are difficult to select due to the structure's complexity or inability to take a detailed inspection of the building, more sophisticated methods becomes necessary. (Vinci, 2016) identifies the dissipative nature of buildings made of masonry and discourages the use of linear analysis methods as they underestimate the deformation

capacity of the structure. Moreover, equilibrium methods usually require the specific assumption to be adopted such as no tensile strength of material and infinite compressive strength. For such a reason, (DeJong, 2009) stresses that the application of quasi-static equilibrium methods should be limited to pure compression structures only.

With regards to local mechanisms such as the out-of-plane failure, and in analogy to the pushover analysis for global verification of the structure, the *nonlinear kinematic analysis* is a valid tool for assessing the lateral stability of walls. This analysis allows to determine the horizontal forces that the wall is able to withstand as the failure mechanism develops. Eventually, the verification of the wall at matter can be reduced to the comparison between displacement capacity and displacement demand.

In conclusion, while the strength methods are particularly suitable for predicting or assessing when the damage at material level occurs, stability methods are more suitable for predicting the collapse of the entire or part of a structure.

2.6.2. Dynamic analysis methods

Approaching the seismic assessment of masonry structures by means of dynamic methods allows to investigate the stability of a structural system in more detail. The nature of the seismic action is addressed where instability phenomena such as resonance effects may arise. Dynamics approach can be analytical or numerical.

In analytical approaches, the dynamic response of masonry structures is derived through the formulation of one or more equations of motion. Usually the equations that can be found on literature represent the dynamics of simple rocking bodies such as parapets or walls represented by two rigid bodies. (Derakhshan et al, 2014) derived the equation of an equivalent single degree of freedom system representing the nonlinear out-of-plane behavior of a masonry wall, and proposed a method to transform the nonlinear problem to a corresponding linear equivalent.

The dynamics of multi-degree of freedom systems or in the continuum can be better addressed with numerical methodologies.

A *(modal) response spectrum analysis* is a linear-dynamic method which indicate the likely maximum response of a structural system to an excitation by making use of the superposition principle. The contribution of each of the natural mode of vibration is taken into consideration, but the nonlinear behavior of the system is neglected. Modal analysis, being a procedure assuming elastic behavior, uses the elastic spectrum. Therefore, the results should be scaled by the ductility factor to accord with the inelastic spectral acceleration.

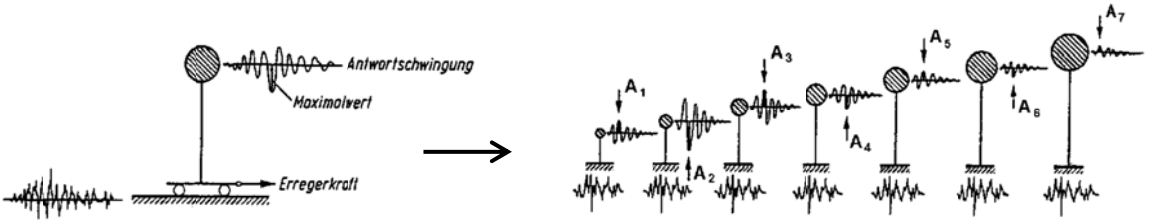

Figure 27 – A modal analysis accounts for those modes of the system associated to a relevant range of natural frequencies.

Performing *non-linear dynamic* analyses on numerical models requires more elaborated input. The external excitation at the base of the structure produces horizontal instabilizing forces over the height of the building which together with inertia forces determine the stability of the system at matter. The horizontal forces can be related to the self-weight of the structure and gives an impression on how its stiffness re-distributes in time, showing amplifications of the response for higher levels. This type of analysis accounts for both physical and geometrical nonlinearities of the system and it is usually carried out in the form of a *nonlinear time history analysis*.

Occasionally dynamic analysis may be performed by scaling an artificial signal which is then used to excite the system. In such a case the procedure is called *incremental dynamic analysis* (IDA) and it may be interpreted as the dynamic equivalent of the pushover analysis. The reference value chosen for each scaling procedure is the PGA of the signal.

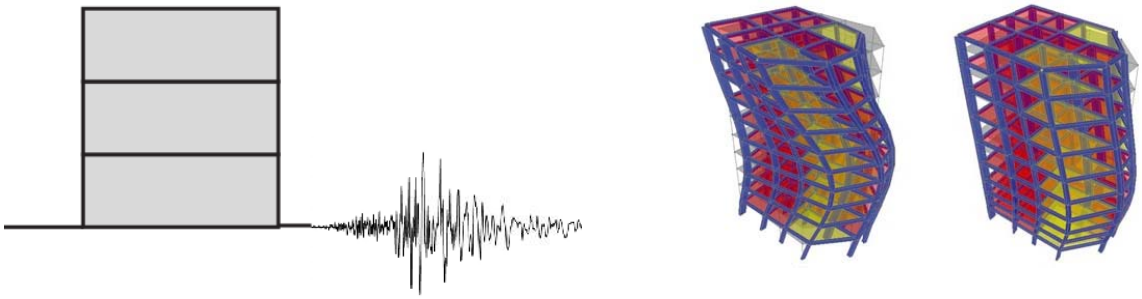

Figure 28 – Dynamic analysis of a frame structure: a base acceleration simulates the action of the earthquake.

To conclude, although all the presented methodologies are useful tools in the assessment of the seismic behavior of unreinforced masonry structures, experimental results show that those approaches based on nonlinear analyses are more appropriate as they are able to account for the high inelastic deformation capacity of walls.

2.7 Out-of-plane behavior in flexural walls

As mentioned before (section 2.3), a masonry building is expected to respond to lateral loads by means of in-plane action of its walls, provided that connections between structural elements are properly designed. If this is not the case, the out-of-plane behavior of walls may arise and the nature of this mechanism should be analyzed through dynamic analyses (Lourenco e. a., 2011).

Traditional approaches based on elastic stress calculations for the assessment of the out of plane seismic performance of existing walls proved to be too conservative. Previous sections hinted that methods of assessment based on stability and energy considerations are more suitable for addressing the inelastic deformation capacity of unreinforced masonry walls. From an financial point of view, accounting for this aspect makes a significant difference in deciding whether or not strengthening measures are necessary.

It is thus crucial to address the out-of-plane vulnerability of URM walls by taking into account their "reserve displacement capacity". Following the work done by (Doherty, 2000), the behavior of URM walls loaded perpendicularly to their plane is briefly introduced by characterizing their force-displacement relationship in the pre and post-crack phase. The procedure adopted is the *non-linear kinematic approach*, so called because it considers the equilibrium of forces in consecutive displaced configurations of the system characterized by the occurrence of geometric nonlinear phenomena.

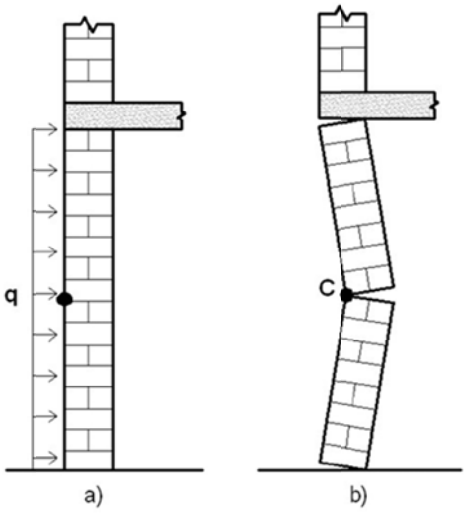

Figure 29 - Endwall acting out-of-plane under the action of a distributed lateral load

2.7.1 Pre-crack behavior

Prior to cracking, the wall acts elastically and there is no impact on the distribution of the inertia forces. The lateral resistance of the wall, which is essentially governed by the tensile strength of the masonry in flexure, increases linearly with the displacements. If the peak lateral resistance of the wall in the cracked configuration is smaller than its elastic capacity, no reserve lateral capacity of the wall can be found and the stability of the wall is reliant on the applied forced being reduced to the cracked lateral capacity of the wall. This case is typical of non-bearing walls, in which the occurrence of the rocking mechanism is less likely than for the walls with high overburden applied.

On the other hand, when the applied overburden is large, the beneficial effect of the generated stabilizing moment outweighs the tensile resistance of the masonry. The lateral force inducing cracking of the wall is not sufficiently large to bring it to collapse. The dynamic problem shifts from strength to stability considerations.

2.7.2 Post crack behavior

When the applied accelerations exceed the elastic capacity of the wall cracks form at locations of maximum bending moments. These are usually the top and bottom support levels and in a second moment an area which is typically assumed to be at mid-height. These three cracks act as joints and therefore the wall is split in two bodies that are able to rock around their points of rotation. The bodies may be assumed to be rigid, which means that they have infinite compressive strength.

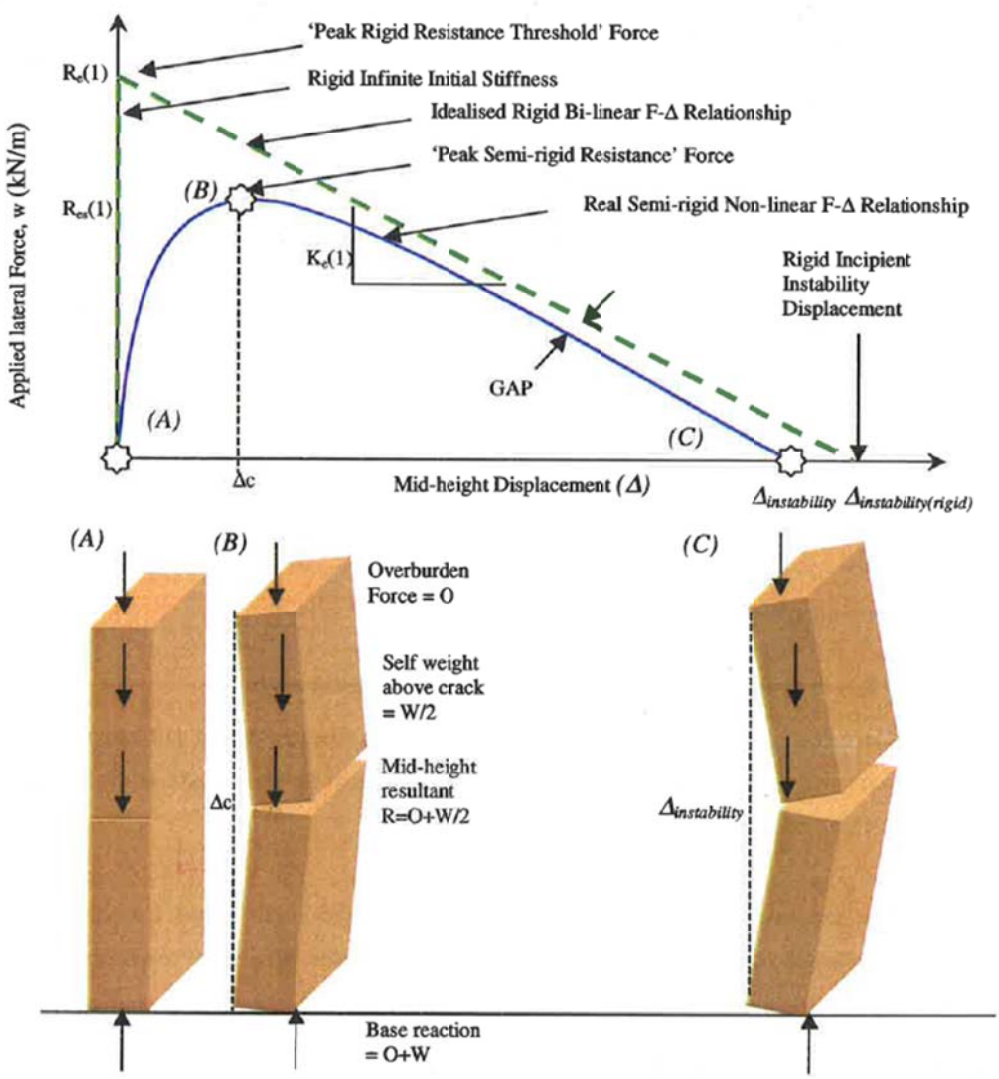

Figure 30 - Rocking mechanism of a wall acting out-of-plane under the rigid bodies assumption. Illustrations extracted from Doherty (2000).

The balance of forces follows the interaction between gravity restoring moments, shifting of vertical reactions with the mid-height displacements and the P-delta effects of the top load. The wall peak resistance is displayed on the graph as the point on the vertical axis. When the lateral force is larger than this value, the wall starts to display and the stability of the mechanism is governed by the balance of restoring and overturning moments. Restoring moments decrease as the

mechanisms develops, which corresponds in the force-displacement relationship to a trend characterized by a negative stiffness. The ultimate displacement at which there is no reserve resistance to overturning is called "rigid instability displacement".

During rocking configurations, the wall is said to be in unstable equilibrium, and its stability depends on the removal or reduction of the applied lateral force. The distribution of accelerations along the height of the wall is not uniform anymore since relative accelerations act on the wall as well. From a practical point of view, the fact that the lateral stiffness of the rocking wall is a function of the displacement suggests that a natural frequency for this mechanism cannot be computed. This evidence is coherent with the inherent nonlinear behavior of the wall acting out of plane. However, as Doherty suggests, it is possible to derive an effective resonant frequency of excitation for which the response of the wall is amplified the most. This frequency is associated to the average incremental secant stiffness of the mechanism. In analytical and numerical calculations, the force displacement relation illustrated above is usually approximated by bi-linear and tri-linear models.

2.7.3 Filtering effect

The earthquake action is directly applied at the foundation level of a building. In masonry structures the signal reaching the upper levels is modified by the in-action of the walls and the dynamic characteristics of the diaphragms. Therefore, the input excitation for walls at higher levels should be corrected accordingly and may lead to different demands that may greatly affect their out of plane performance. This "filtering effect" is also related to the modes of vibration of the entire structure and is thoroughly addressed in the scientific investigations about the stability of rocking walls. (Tomazevic, 1996) found that the out of plane demands on walls are much larger on higher floors. (Lourenco e. a., 2011) and earlier (Priestley, 1985) account for the filtering effect by amplifying the deformation demands of walls through correcting coefficients also called "seismic coefficients". Finally, codes like the Eurocode 8 (EN1998-1 2004) and NZSEE guidelines embraced these findings and assimilated them in their prescriptions.

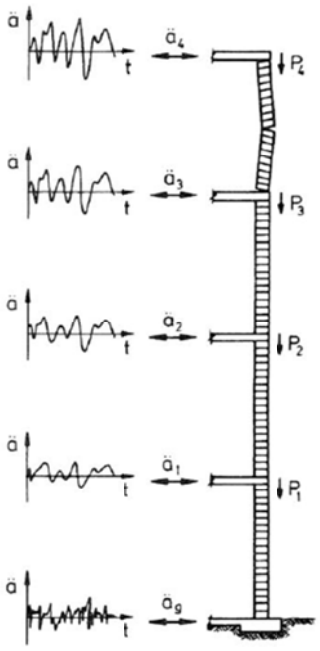

Figure 31 - Resulting accelerations on floors: filtering effect.

2.8 Analytical verifications for walls

The adequacy of a masonry structure to seismic loads can be evaluated in many ways of which the pushover analysis is the most popular one. However, the pushover is a global verification, where all the structural elements of the building at matter contribute to its lateral resistance and the parameter used to verify the stability is unique for the whole structure. In the context of a local mechanism as the one captured by the out of plane behavior of the wall, the supporting conditions of each wall may differ within the structural system and thus a verification specific for each wall element becomes necessary.

In this section the methodology adopted by three codes (Italian NTC, New Zealander NZSE and Dutch NPR) is presented for masonry walls spanning vertically between supports, also known as "one way bending" walls. One way bending failure of URM walls (ULS) is determined by three main phenomena: tension cracking of masonry, compression crushing of masonry and ultimate instability of the wall. Unless the walls have a very high compressive axial loading, crushing and shearing of elements do not play a big role and can be therefore neglected as a simplification. As such, although the procedures illustrated in the three codes may differ in the way they approach the problem, authors like (Lagomarsino, 2014), (Doherty, 2000) and (Giuffre' & Carocci, 1993) agree that the most appropriate way to address the assessment of the seismic lateral resistance of slender masonry structures subjected to out-of-plane actions is by making use of a combination of kinematic limit analyses and spectral analyses.

2.8.1 NZSEE approach

A step by step methodology is presented in the NZ code. First, the wall panel is assumed to form hinge lines at the position of the horizontal supports and at mid-height. The center of compression of this lines forms a pivot point around which rotation occurs. The wall is thus divided in two parts which are assumed to be rigid. Then, the most unfavorable set of eccentricities for the acting forces is calculated.

By making use of the virtual work principle, the instability mid-height deflection of the wall is calculated. With the application of safety factors, 60% of this displacement is eventually taken as the maximum usable deflection of the wall, in other words, its deformation capacity.

$$\Delta_{max} = 0.6 \times \Delta_{ins}$$

For the calculation of the displacement demand, the vibration period of the wall is derived in an approximated way. Taking into account that the wall subjected to a rocking mechanism has no specific natural period, the secant stiffness of the wall system corresponding to a mid-height displacement equal to 60% of the deformation capacity of the mechanism is chosen, thus accounting for the 36% of the (real) instability displacement.

$$\Delta_t = 0.6 \times \Delta_{max} = 0.36 \times \Delta_{ins}$$

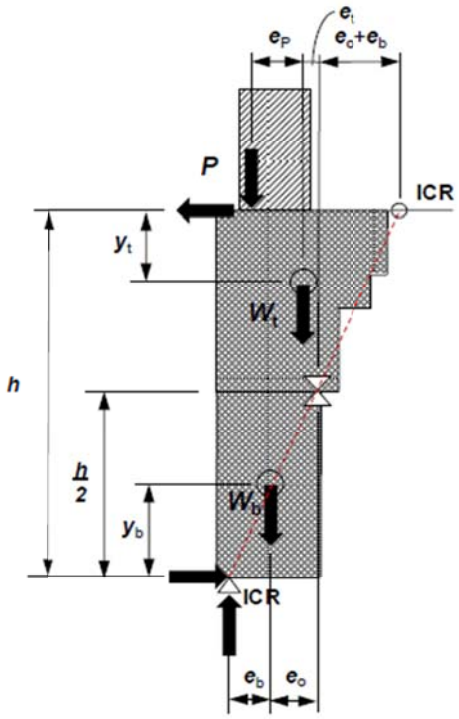

Figure 32 - Configuration of the wall at incipient rocking (Picture extrapolated from NZSEE Guidelines)

The displacement demand is then calculated by assembling correction coefficients which are used to scale the output obtained by an applicable displacement spectrum. These coefficients account for the dependency of the wall response on that of the entire building (part coefficient), for the correlation between actual response of the rocking system and that approximated by an equivalent elastic SDOF oscillator (participation factor), and for the type of analysis performed – ULS or SLS - together with the importance of the element (wall) analyzed in the general context of the entire structure stability (part risk factor).

$$D_{ph} = \gamma (T_P/2\pi)^2 C_P(T_P) R_P g$$

The part coefficient relates to the interaction between local (rocking wall) and global (whole building) modes and the height effects. Hence, it embodies the filtering effects already addressed beforehand (section 2.7.3). One of the coefficients present in its definition, namely $C_i(T_P)$, the *parts coefficient*, was revised and capped to a smaller maximum value as explained by (Shelton, 2004). According to this document, the period of the earthquake is too short for affecting the parts of the structure.

The last step of this method consists of comparing the displacement demands with the capacity and later to estimating the adequacy of the analyzed wall to the New Zealand standard as a percentage:

$$\%NBS = 100 \times \Delta_m / D_{ph}$$

The NZSEE code deems that a masonry wall has sufficient out of plane capacity and does not need strengthening as long as the %NBS achieved is higher than 33%.

Charts are provided for estimating the %NBS of regular vertical spanning walls knowing their boundary conditions, load configurations and geometric properties. Also, values of the maximum acceleration a wall is able to withstand and its

instability displacement are tabulated for a set of different boundary conditions. For cantilever walls, such as parapets, the same procedure applies with the difference of multiplying the instability displacement by a factor 0.3 instead of 0.6.

Boundary Condition Number	0	1	2	3
	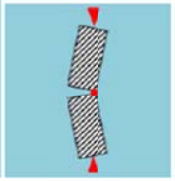	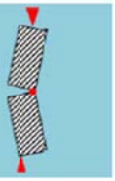	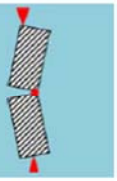	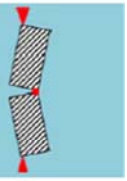
e_p	0	0	$t/2$	$t/2$
e_b	0	$t/2$	0	$t/2$
b	$(W/2+P)t$	$(W+3P/2)t$	$(W/2+3P/2)t$	$(W+2P)t$
a	$(W/2+P)h$	$(W/2+P)h$	$(W/2+P)h$	$(W/2+P)h$
$\Delta_i = bh/(2a)$	$t/2$	$\frac{(2W+3P)t}{(2W+4P)}$	$\frac{(W+3P)t}{(2W+4P)}$	t
J	$\{(W/12)[h^2+7t^2]+Pt^2\}/g$	$\{(W/12)[h^2+16t^2]+9Pt^2/4\}/g$	$\{(W/12)[h^2+7t^2]+9Pt^2/4\}/g$	$\{(W/12)[h^2+16t^2]+4Pt^2\}/g$
C_m	$(2+4P/W)t/h$	$(4+6P/W)t/h$	$(2+6P/W)t/h$	$4(1+2P/W)t/h$

Table 2 - Maximum multiplier of horizontal forces (Cm) and instability displacement (Δi) of a wall for different configurations of boundary conditions. New Zealander approach (Picture taken from NSEE Guidelines).

2.8.2 NTC approach

The approach followed by the Italian code is essentially analogue to the New Zealand one, with minor differences that will be highlighted later. In short, the kinematic approach used permits to determine the trend of the horizontal action that the wall system is able to withstand as it displays laterally. The latter is expressed through the amplification parameter α (expressing the ratio between applied horizontal forces and the corresponding weights of the masses of the system) as a function of the displacement of a target point (usually at mid-height). The curve obtained is transformed to the capacity curve of an equivalent SDOF system where it is possible to define the ultimate displacement capacity of the mechanism which has to be compared to its seismic displacement demand.

Hence, the wall is again modelled as a kinematic chain composed of two rigid bodies with infinite compressive strength. Then, by making use of the virtual work principle, the parameter α is derived and its values computed in the displaced configurations of the system. The curve is adapted to the equivalent SDOF system expressing the accelerations and displacements by their spectral value. All of this is accomplished through a detailed procedure. The vulnerability of the wall and its compliance to the normative are estimated on the spectral capacity curve by accounting for an average secant stiffness for calculating the vibration period of the wall. The stiffness value should be taken as the smaller between those representing:

- 40% of the instability displacement (α=0);
- The displacements corresponding to local system configurations which are not acceptable.

It should be noted that the 0.4 safety factor is directly related to the "salvaguardia della vita (SLV)" limit state, which in the Eurocode corresponds to a "significant damage (SD)" limit state.

FEMA 356	OP	Operational Performance
	IO	Immediate Occupancy
	LS	Life Safety
	CP	Collapse Prevention
EC8	DL	Damage Limitation
	SD	Significant Damage
	NC	Near Collapse
NTC 2008	SLO	Stato Limite di Operatività
	SLD	Stato Limite di Danno
	SLV	Stato Limite di Salvaguardia della Vita
	SLC	Stato Limite di Collasso

Comparison		
FEMA 356	EC8	NTC 2008
OP	DL	SLO
IO		SLD
LS	SD	SLV
CP	NC	SLC

Table 3 - Correspondence between limit states of different normatives. (Brebbia C.A, Maugeri M., 2011)

As a last step of the procedure, the ultimate deformation capacity of the walls is compared to the displacement demands that are computed with formulas accounting for the filtering effects:

$$d_u^* \geq S_{De}(T_1) \cdot \Psi(Z) \cdot \gamma \cdot \frac{\left(\frac{T_s}{T_1}\right)^2}{\sqrt{\left(1-\frac{T_s}{T_1}\right)^2 + 0.02\frac{T_s}{T_1}}}$$

Where $S_{De}(T_1)$ is the elastic spectral displacement response of the building in its first vibration mode, T_s the vibration period of the wall as derived above, and γ and Ψ are modal correcting factors that are function of the wall position in height. The vibration period of a masonry building lower than 40 meters is derived in the italian normative by an approximated equation in which $C_1 = 0.05$:

$$T_1 = C_1 \cdot H^{3/4}$$

2.8.3 NPR (v.2015) approach

This approach is really straight-forward as it consists in consulting the table 9.2 of section 9.5 of (NPR9998). The masonry wall is first categorized as endwall, partition wall or cavity wall depending on its boundary conditions. Successively, the maximum value of the peak ground acceleration that the wall is able to resist for lateral actions is found by selecting the right wall geometrical properties on the table and the magnitude of the compressive action on top of it.

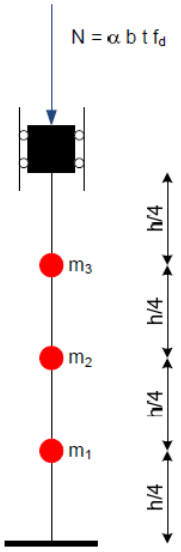

Wandtype	Wanddikte *t* [mm]	Benuttings-graad α [a]	*T* [s]	*q* [-]	S_{Rd} [*g*]	$a_{g;R;norm}$ [*g*]
Tussenwanden [c]	100	0,02	0,080	5.39	0,196	0,28
		0,03	0,074	4.69	0,295	0,48
		0,04	0,068	4.35	0,393	[b]
	120	0,01	0,081	6,46	0,165	0,24
		0,02	0,066	5,53	0,295	0,50
		0,05	0,055	4,10	0,595	[b]
	150	0,02	0,053	5,47	0,491	[b]

Table 4 - Maximum acceleration values resisted by unreinforced masonry walls according to NPR – Partition walls.

Figure 33 - Idealization of the wall as a lumped mass system in NPR9998.

For different values than those present in the table, interpolation is necessary. It is possible to see the underlying procedure through which this table is derived in the document *Dossier 8550 – Metselwerkwanden belast uit het vlak* (2015). From it, it becomes clear that the NPR approach has an "hybrid" nature, as it is essentially based on strength checks that are only partly supported by displacement capacity considerations.

In short, the masonry wall is discretized as a lumped mass model and thus divided in four deformable sections. A moment-curvature relation is derived from the cross sectional properties and as a function of the normal force expressed through the utilization factor. After this two pushover analyses are analytically carried out for both an even and a modal distribution of the point loads applied on the lumped masses. It is noted here that geometric nonlinearities are not accounted for in this step. Then, the force-displacement diagrams are transformed into those of an equivalent SDOF mass-spring system with bilinear behavior. By making use of the procedure described in another section of the NPR, the

vibration period T and the behavior factor q can be computed and it appears that there is no significant distinction between the results of the modal and even distribution of nodal forces.

At this point a modified design spectrum for ductile systems is applied to calculate the dynamic amplification factor of the wall. The latter is used for deriving the equivalent static forces acting on the wall as a function of the peak ground acceleration and proportionally to the displacement configuration of the lumped masses for a representative load.

Finally, the lateral strength of the masonry wall is verified according to EN 1996-1-1. The second order effects as well as the initial eccentricities should be accurately taken into account in this final check.

In the document explaining the procedure it is suggested that only one of the three wall typologies may be verified directly with displacement based approaches: the load bearing partition walls. These walls in fact seem to have good lateral capacity when it comes to force-based calculations. On the other hand, for the other two typologies of walls, strength capacity checks are as important as the displacement verifications when assessing their ultimate seismic performance for lateral loads (out-of-plane behavior).

2.8.4 Remarks on the above methods

In the previous paragraph three methodologies currently used in design codes were described. Their analogies and differences are briefly presented here.

Clearly, the main difference lies between the NPR approach and the other two, as it is essentially based on strength considerations and neglects to address the stability of the rocking walls. In fact, only the pushover analyses are displacement-based calculations. Since the development of the out of plane mechanism is not analyzed, the ability of the wall to accommodate large inelastic displacements is not accounted for. Consequently, the displacement reserve capacity characterizing the spanning wall between supports cannot be captured by the NPR method, and may result in rather conservative estimations when assessing seismic performance of a masonry wall. Moreover:

- The masonry wall is not considered as a kinematic chain of rigid bodies and the compressive strength of masonry is an input of the procedure;
- The wall is discretized as a stick-lumped mass model;
- The second order effects on the wall subjected to both compression and flexure are considered;
- Initial drift of the wall cannot be taken into account;
- The filtering effect is not accounted for.

The New Zealand and Italian procedures are entirely built upon the idea that it is not the physical strength of the wall to govern its seismic performance. On the contrary, the capacity of the wall to act out of plane can be conveniently seen as a stability problem and thus addressed through limit analyses applied on kinematic models. The analogies between the two methods are many, and the underlying hypothesis and set of assumptions are the same:

- The wall is assumed to form three hinges and thus split in two rigid bodies;
- The strategy adopted relies on assessing a SDOF substitute-structure showing equivalent displacements;
- Filtering effects are clearly accounted for by means of correcting coefficients and factors;
- The verification of the wall consists in comparing the displacement capacity with the displacement demand of the wall.

Nonetheless, between these two foreign codes there are differences as well:

- The safety factors applied are different, as the Italian code performs checks for the "significant damage" limit state, whereas the New Zealander checks use "near collapse" limit state. This has an impact on the factors used

to compute the secant stiffness and the ultimate displacement permitted in the two codes (40% vs 60%). Refer to section 2.8.2.

- Obviously, the two codes use elastic response spectra relevant to their country;
- When calculating the average stiffness of the rocking walls system, NTC also accounts for unacceptable wall configurations with regards to the global stability of the structure;
- The NTC code to accurately perform the transition from MDOF to the equivalent SDOF by calculating the participating mass and carrying out all the analytical steps provided. In the code from New Zealand these detailed steps may be disregarded in favor of consulting more (approximated) practical formulas and charts.

3 Action plan

The literature study raised awareness on the complexity of the out-of-plane behavior of masonry walls due to the inherent nonlinearity of both the material involved as well as the rocking mechanism itself. Also, it stressed the extension of this issue, a problem being perceived in every part of the world with special attention on those countries struck by the occurrence of seismic phenomena. Hence, examples were shown of foreign normative where the seismic demands assessment for masonry walls was addressed by making use of displacement considerations and culminated in the derivation of practical formulas specific for those countries.

The advantages delivered by these methodologies are clearly related to their ease of applicability and the efficient use in engineering practice, which make their utilization rather compelling for a diverse range of circumstances. Nonetheless, it was also noted that the procedures at matter are strictly related to site-specific conditions and their inappropriate use may result in large inconsistencies with regards to the structural behavior of the masonry walls. Since an inaccurate solution to a structural problem leads to potential safety issues or financial disadvantages, the possibility of adapting those methodologies to the Groningen situation is a query worth investigating.

In this chapter the research questions brought up after having familiarized with the topic are presented. Then, the strategy which will be adopted in the development of the project is illustrated.

3.1 Research questions

The scope of this thesis is to optimize the assessment procedure for the out-of-plane seismic demand of unreinforced masonry walls through the adaptation and possibly the extension of existing methods to the specific case of Groningen. This intent will be pursued by answering the following sub-questions:

- How can the out-of-plane rocking mechanism of a one-way bending wall be conveniently described through a 1D/2D finite elements model?
  That is: what could be a simple FE idealization of a wall able to capture the nonlinear nature of the rocking mechanism, where the stability is mainly governed by displacement considerations?

- What are the structural material aspects that should be included in the model and how to implement them numerically?
  That is: how to extend the FE model of the rocking wall to account also for the features defining the highly physical nonlinear behavior of masonry? What impact do these have on the overall seismic resistance of the wall?

- Can the additional lateral resistance given by the in-plane action of returning walls or external steel frames (strengthening measure) be effectively modelled in the 2D discretization for the out-of-plane behavior study?

- How to capture the interaction between the wall and the surrounding structural system in a 2D fashion?
  That is: how can the role played by the wall location in height be addressed in an efficient way? Is there an interaction between local vibration period and global modes of the structure? Is it possible to describe the way the energy is dissipated in the building subjected to an earthquake with that model ?

- Is it possible to reproduce the results presented in foreign displacement-based methodologies through the numerical FE approach applied on simple 1D/2D models?
  That is: Codes such as NTC assess the compliance of existing masonry wall to safety requirements by making use of formulas which are derived through a combination of NLKA and limit analyses. Correcting coefficients are applied to account for the amplification effects. By reproducing relevant site-specific conditions, it is crucial to check whether and to what extent the models developed can give results which are comparable to those methodologies.

- Is it possible to adapt the foreign approaches to the scenario of Groningen and to derive a set of coefficients to be used as correcting factors in analytical formulas for the out-of-plane assessment of masonry walls?
  That latter questions can also be recognized as the main one for this research. In other words:
  "Is it possible to create an adaptation of foreign methodologies for the out-of-plane assessment of a URM wall to the Groningen scenario, by making use of a simple 2D frame model?"

- Will the accuracy of the out-of-plane seismic assessment for existing masonry walls be increased after this research?

3.2 Strategy

The methodology to be adopted in the development of this master thesis can be idealized as an initiation-conclusion process with recursive characters composing the main part. This is evidenced in the flowchart provided below.

As a starting point, the literature study provides the essential knowledge for the topic at matter. This is necessary to targeting those aspects which deserve more investigations and evidences the difficulties related to the out-of-plane behavior of masonry wall in general. Now that the research questions are defined and sufficient information is collected, the first phase terminates with a reflection on what approach to follow. It is thus decided to tackle the out-of-plane behavior of masonry walls as a 2D problem, neglecting the direct role of the in-plane action and related failure modes.

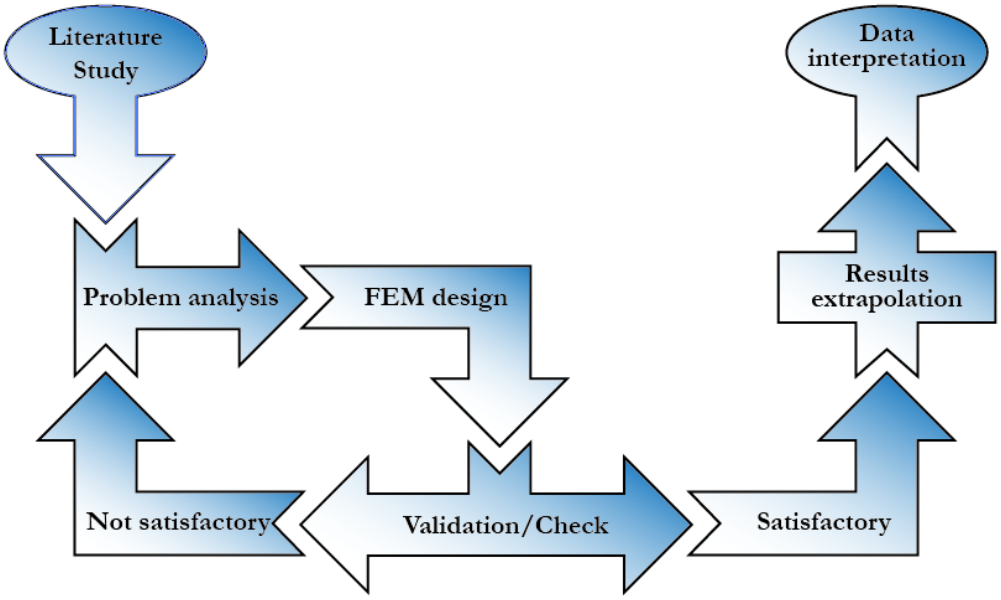

Figure 34 - Flowchart of the project development

The analysis phase will thus be followed by an iterative procedure, core of the research. This will consist of developing the right tools to answer the project questions in a structured way, by first reproducing results of proven validity and then shifting to structural aspects where interpretation of results played a major role. Two macro-areas of modeling will be delineated, the first one addressing the idealization of the rocking mechanism of a single unreinforced masonry wall only, and the second one consisting in extending the model by implementing the wall in a surrounding structural system with multi-floors. In both phases some features of the objects, the single wall or the frame structure, will be included stepwise to improve control on modeling. Hence, the models will be "upgraded" or abandoned when necessary and after each validation attempt until that point in which a 2D model able to effectively describe the structural behavior of the rocking masonry walls is obtained. The modeling goal is set as to generate a model able to reproduce the seismic performance of unreinforced masonry walls in a structural system with regards to their out-of-plane behavior independently of their site-specific conditions.

Once that goal is achieved, the features specific of the seismicity in Groningen can be implemented in the models and may allow to verify whether correcting coefficients for the displacement demands of the walls are derivable and if they are related to those of the foreign normative.

Since an attempt is made to reproduce a particular scenario with regards to the nature of the excitation as well as the structural response of an element in a building, it is important to make a remark. It should be stressed in fact that the modeling approach used for both the structural system and the unreinforced masonry wall is strongly simplified as it only takes into account 1D or 2D beam elements. In a similar fashion, also the external excitation during transient analyses will be modeled as single-component only horizontal motion. Consequently, the intention of "reproducing" a specific structural behavior taking into account all these assumptions is quite far-fetched, as it will mainly be limited to the following aspects:

- Investigating the URM wall response assuming the surrounding system to act in two extreme ways (fig.38):
  A) As a shear wall, with flexure behavior and a concave profile of deflections over the height of the building;
  B) As a moment resisting frame, with a shear behavior and a convex profile of deflection;

  Where it can be stated that a realistic response of a masonry structure to lateral loads is usually somewhat in between these two circumstances, which are closely correlated to the stiffness of the inter-story diaphragms.

- Dimensioning the unreinforced masonry walls over their thickness with the geometrical proportions commonly adopted in the building stock of Groningen;

- Resorting to an artificial signal for the base motion of the frame models that is agreement with the NPR9998 prescriptions and thus compatible from an energy point of view with the induced seismicity in Groningen.

The over-mentioned 1D/2D approximations are made intentionally due to time constraints. Certainly, they result in research constraints that will be addressed in more detail in the conclusive part of this report.

Speaking of how to derive of the amplification coefficients for the rocking motion of unreinforced masonry walls within a frame model, the methodology that will be adopted to carry out this investigation is now briefly presented. First, the lateral capacity of a wall within a single story building and for a set of boundary conditions will be assessed by scaling the peak ground acceleration (PGA) of a given artificial signal resembling the induced seismicity in Groningen. This will be addressed as the "reference case". Then, the same wall will be introduced in a variety of frame models where the following parameters are adjusted each time:

- For a frame that acts according to A) or B) as explained above, the number of floors is ranged between 1 and 7;

- Within these groups of buildings, the rocking wall model (nonlinear system) is located each time on different floors;

- Keeping the wall position fixed, the magnitude of load on top of it (overburden) is changed;

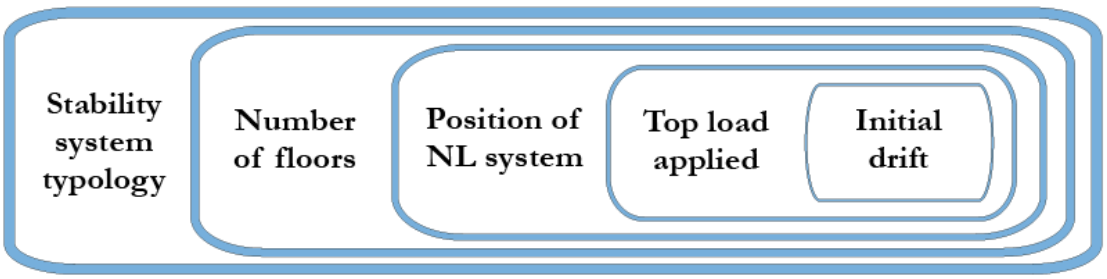

Figure 35 - Variations on model configuration and structural parameters.

For each case, an incremental dynamic analysis (IDA) will be run on the model until the failure of the URM wall caused by the achievement of its instable configuration is reached. Considering the large number of comparative analyses that will be involved in this investigation, attempts will be undertaken to compile a script for multiple-analyses.

For every condition the PGA of the (incrementing) signal for which the transient analysis diverges is compared to the reference case. The ratio of these two values represents what will be called "failure scaling ratio". That is:

$$FSR_{(n\_storey\,;\,i\_level)} = \frac{PGA_{MAX}(n\_storey; i\_level)}{PGA_{MAX}(1\_storey)}$$

The equation calculates the ratio between the PGA of a signal increasingly scaled until the out-of-plane failure of the wall system takes place, that is PGA_{max}, and that one corresponding to the same circumstance occurring in the case of a single-storey frame building. Collecting the amplification values for all the circumstances mentioned above will allow to construct the failure profiles of the wall systems as a function of their position in the structural system and other parameters. The pictures below show the example of a 3-story frame subjected to an IDA in which different positions of the nonlinear system representing the rocking wall are addressed. For each system a maximum PGA is derived and related to a reference value identifying a point in an failure scaling ratio(FSR)-height diagram.

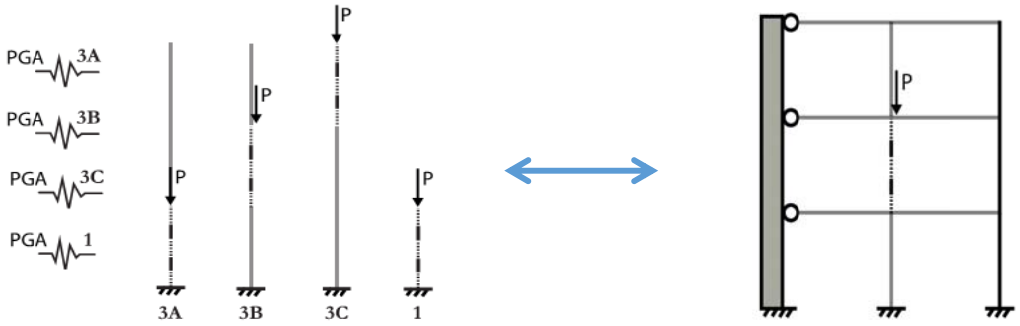

Figure 36 - Representation of an incremental dynamic analysis on a 3-story frame model. On the right: case 3B.

The obtained output will give insight on the occurrence of out-of-plane failure of walls as a function of their location, by taking into account both the "height effects" as well as "interaction effects" between the frame structural system and the nonlinear wall one. In order to investigate these two aspects in a separate way and evaluate their impact on the wall, a set of linear transient analyses can be run on the frame models in order to deduce how accelerations demands are amplified over the height and how the period of the rocking wall system determines the forces acting on it. In this way it should be possible to make considerations on the impact of the interaction between the URM wall and its surrounding structural system on its out-of-plane dynamic behavior.

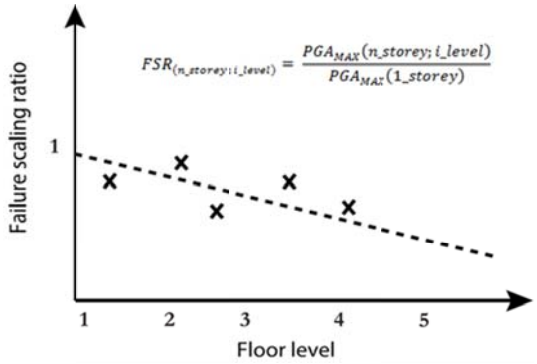

Figure 37 - Expected output of the research: amplification profiles of the structural systems.

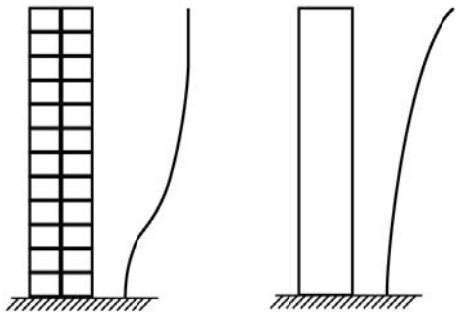

Figure 38 - Lateral deflection profiles of structures acting as moment resisting frames (left) and shear walls (right).

3.2.1 Validation of wall model

Before expanding the single wall model and analyze the dynamic behavior of this unreinforced masonry element inside a frame structure it is essential to prove its validity with regards to the geometrical as well as physical nonlinear properties. To this purpose the model is subjected to a pushover analysis in order to check its theoretical displacement capacity during rocking. Also, by making use of the same analysis it will also be possible to address the nonlinear nature of the masonry material and to elaborate on the cyclic nature of the damage undergone by the wall when such circumstances repeats in time. The experimental results derived by Doherty (2000) will at this first stage of the research be adopted as a benchmark to compare the reliability of the FE model. This will imply developing the model with similar boundary conditions and dimensions found in the reference research at least for the first wall models. At the same, time tables and analytical methods extrapolated from national and foreign codes will be employed for the same scope.

Although at the beginning Doherty is cited again, when dealing with transient analyses a validation methodology based mainly upon interpretation of numerical results will be chosen. For the rocking masonry wall in dynamic analyses the balance of vertical and horizontal forces acting on the model will be monitored. Then, for the input of material parameters a sensitivity study will be performed and thus the general framework of the models creation and development can be summarized as a trial and error approach. This is especially true for the modeling phase of the structural system surrounding the wall element due to the fact that there will be no specific case study to be used as a reference. How the masses involved in the extended model affect the wall response will also be investigated.

In particular, attention will be given to two aspects which are typical for the rocking mechanisms of walls constraint on the bottom and the top edge:

- The position of the points of rotation of the wall members and the correlated shifting of bounding vertical forces along the thickness of its cross sections during transient analyses;
- The progression of the bending moment curve over the height of a rocking wall, from the hinges creation at the level of the cracks to the achievement of instability displacement.

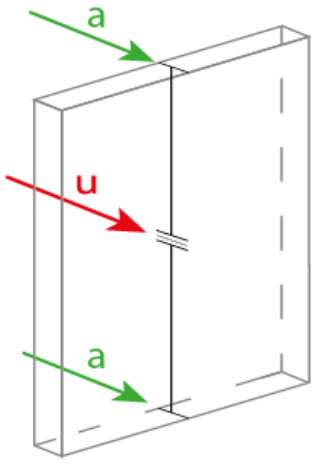

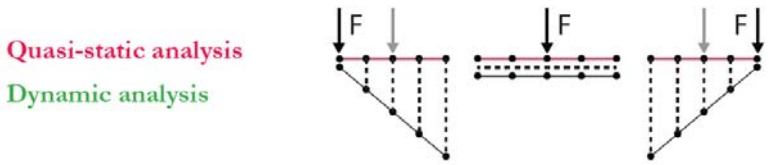

Figures 39 – On the left: overview of the loading scheme for the unreinforced masonry wall: pushover (red) and transient (green) analyses. On the right: shifting of the point of rotation for the wall top section.

4 Generation the FE models

Over the last decades, the seismic performance of unreinforced masonry walls has been evaluated with finite elements software which allowed to accurately predict their structural behavior and explore in detail specific dynamic phenomena. Theoretically, the idea behind finite elements methods is stimulating the trend from reactive and predictive problem-solving approaches to a preventive way of confronting with structural problems, especially in the design phase. With regards to the seismic activity in the province of Groningen, the magnitude of the seismic events is expected to increase in the next few years. Therefore, numerical approaches can help predicting the behavior of already damaged buildings and to effectively cope with the large amount of those that will be soon exposed to this kind of events.

The starting point of a good structural assessment is *idealizing* a building as a set of structural elements for which some simplifying assumptions are made. Subsequently, the structural elements are *discretized* as an assembly of connected nodes with assigned materials and geometrical properties. The *load idealization* and the *calculation* phase finalize the assessment procedure. This chapter present the models developed for estimating the out-of-plane demand of unreinforced masonry walls subjected to transient loading. For each model a description of the geometries, material properties, and finite elements used is provided. The software adopted is DIANA FEA version 10.1, which is considered appropriate for investigating the out-of-plane action of walls as it accounts for both the physical and the geometrical nonlinear nature of the rocking phenomenon.

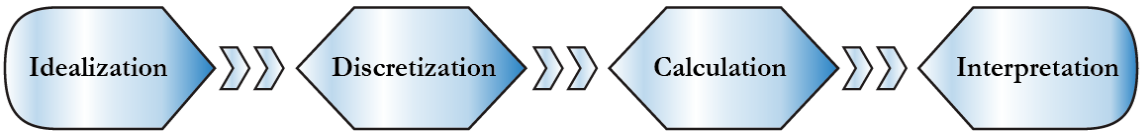

Figure 40 - Steps to be taken in the assessment of structural elements.

The goal of the modeling phase is to come up with a model able to describe the mechanism of a rocking wall with focus on its post-peak behavior and thus addressing its displacement reserve capacity up to instability achievement and failure. A wall can be discretized using finite elements of different kind, depending on the degree of approximation used and the level of detail chosen. For all of the models developed in this master thesis research, macro-modeling approach is followed. Also, it is assumed that the walls experience one-way bending only, and that it is thus possible to model them as thin strips. Since the behavior of the walls in their in-plane direction is not directly modelled, a full 2D description in the xy plane is deemed appropriate for the investigation at matter. The elements used are then all introduced in a xy plane and their cross section dimension are specified as a geometrical property.

The models in this chapter can be broadly divided in three groups:

1) The rocking-wall model based on a rigid-bodies definition, for which the physical resistance of the masonry material is only partly considered;

2) The alternative rocking-wall models, where the material models adopted are more realistic because it is taken into consideration the cracking and crushing behavior of the masonry material;

3) The frame models where the rocking mechanism of the walls is analyzed within a structural system.

In all cases the local zones close to where the cracking is expected to occur are made inhomogeneous, meaning that the nonlinear nature of the masonry material is all lumped or distributed in those confined areas. The models built for the research are depicted in the next page. Results interpretation, remarks and comments on the consequences of dealing with these models are presented in a separate chapter. The units adopted are those of the International System of Units (SI).

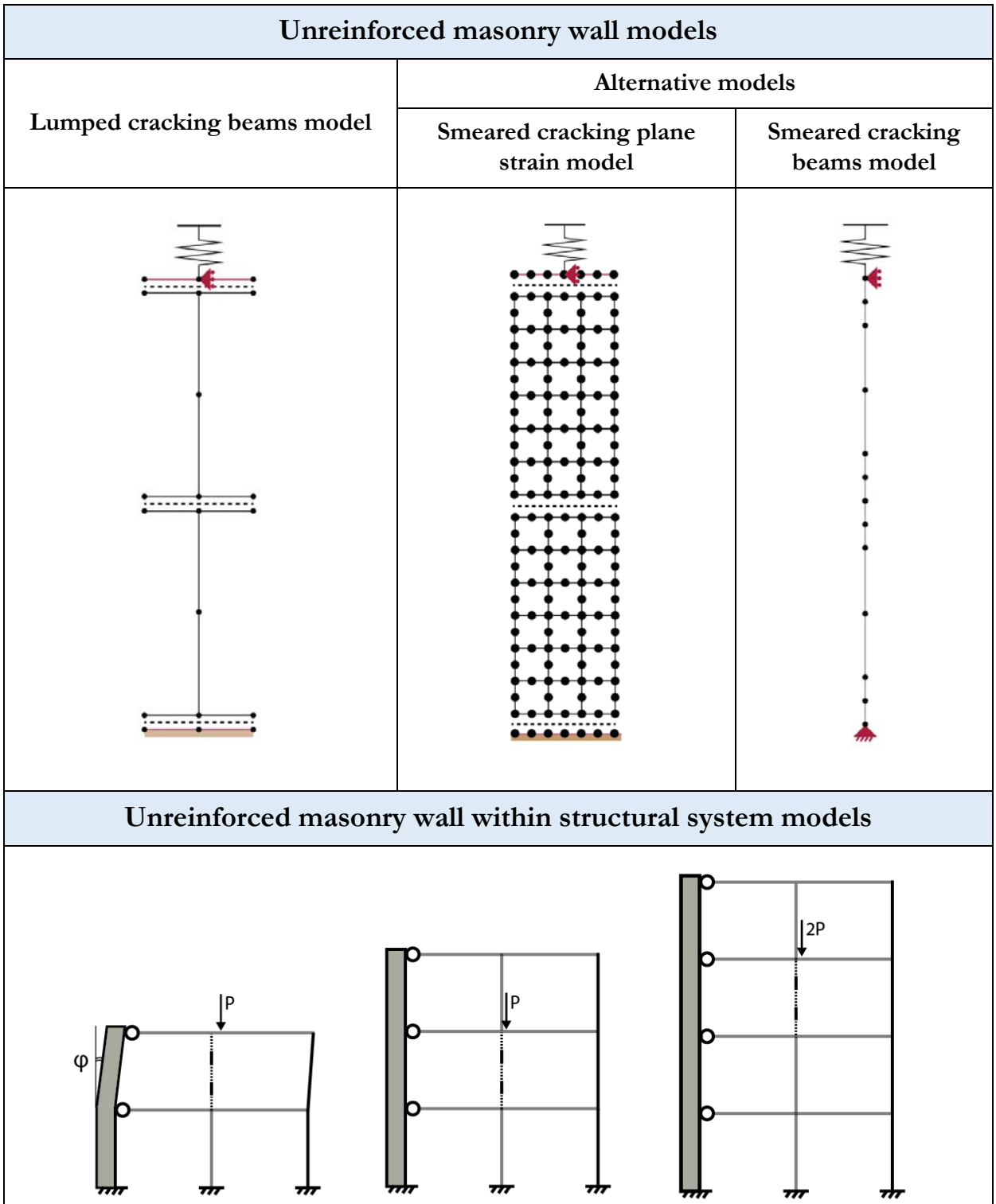

Figure 41 – Representation of the models developed and analyzed in the present research. With regards to the frame models, reference is made to the parameters that will be addressed as part of the sensitivity. Starting from the left: initial drift of the floor on top of the wall acting out-of-plane; variation of the number of floors; different values of overburden.

4.1 Lumped cracking beams model

The modeling phase is initialized by creating a simple structural system capable of capturing the displacement reserve capacity of a rocking wall. In practice, the goal is to reproduce the behavior explained in section 2.7 and 2.8 of this master thesis, and to gain knowledge on the factors governing the out of plane response of unreinforced masonry walls. At this stage a comparative analysis of the numerical behavior of the model against experimental findings is crucial for determining its reliability. In particular, the work of Doherty will often be called as the benchmark for the validation of this first model which, indeed, is shaped to mimic the experimental setup of his experiments. For more details, reference is made to the already cited document "An investigation of the weak links in the seismic load path of unreinforced masonry buildings", Doherty (2000). The model is greatly affected by the simplifying assumptions of the wall elements acting as rigid bodies and experiencing discrete cracking phenomena that are all lumped in a limited number of cross sections. In the chapter dedicated to the response of the models it will be shown that although it is not the case in quasi-static analyses, these assumptions are not appropriate for studying the dynamic out-of-plane behavior of unreinforced masonry walls.

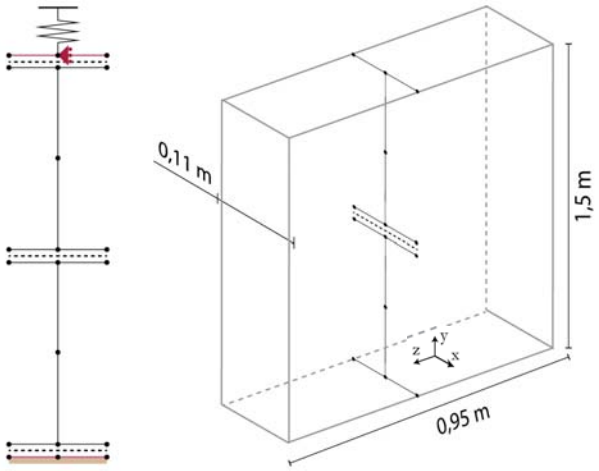

Figure 42 - FE representation of the lumped cracking beams model.

4.1.1 Geometry and FE types

The rocking mechanism of the wall involves the formation of cracks acting as hinges and around which the wall elements rotate. Since it can be demonstrated that these cracks will form at the top, bottom and mid-height of the wall, it is decided to make use of class III vertical beam elements to represent each of the two rocking portions. Then, additional beam elements of the same length as the wall thickness are added in the horizontal direction in correspondence of the expected hinge formations to simulate the rigid cross sections of the wall. The three variables representing the beams nodal degrees of freedom are all expressed through quadratic polynomials, and the integration scheme along the beams centerline is left to the default 2-point Gauss. On top of the wall model, a discrete vertical spring element is applied to control the compression force acting on the wall during rocking.

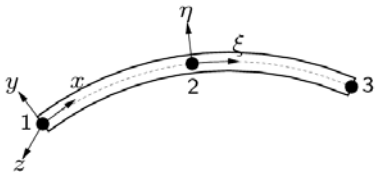

Figure 43 - CL9BE, 2D element, 3 nodes. Diana Manual 10.1, Element library.

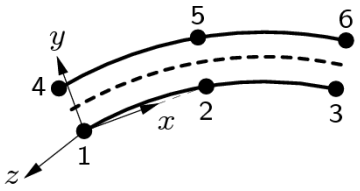

Figure 44 - CL12I, 2D element, 3+3 nodes. Diana Manual 10.1, Element library.

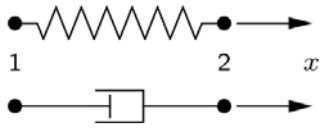

Figure 45 - SP2TR, 1D translation element, 2 nodes. Diana Manual 10.1, Element library.

To account for the cracks, a discrete cracking modeling approach is adopted with no-tension line interface elements placed in between the rigid cross sections. The three interface elements are based on quadratic interpolation and their integration scheme is left to the default 3-points Newton-Cotes. A disadvantage of this modeling procedure is that the horizontal elements introduced so far cannot be visualized in Diana when the model is in the undisturbed configuration due to overlapping. For this reason, the implementation of these elements together with the interface has to be carried out in the .dat file, connecting manually the nodes. The upper-side nodes of the top line interface are tied together in the

horizontal direction to simulate a rigid steel plate around which half of the wall can rotate. The following table shows the geometrical properties of the finite elements introduced for the URM wall modeling.

	CL9BE		CL12I	SP2TR
Width [m]	Vertical elements	Horizontal elements	[-]	[-]
	0.11	0.001		
Thickness [m]	0.95	0.95	0.95	[-]
Length [m]	0.75	0.11	0.11	0.10

Table 5 - Geometry specifications for the lumped cracking beams model.

The model is meshed so that there is one beam element for each of the vertical and horizontal members. This is the minimum number of elements required for carrying out the analyses. However, it can be demonstrated that for the rigid horizontal cross sections increasing the number of elements does not affect the model behavior.

4.1.2 Material properties

For this model five material definitions are required. The elements pertaining to the wall are all supplied with linear elastic material, where the one which is assigned to the rigid cross sections is given an elastic modulus that is three orders of magnitude larger than in the case of the vertical wall elements. For the translational spring a material presenting the stiffness in one direction only should be specified. Then, two material models are implemented for describing the wall behavior at the level of the cracks: no-tension and tension-resistant interfaces. The physical interpretation that justifies the use of two different crack materials is related to the possibility of analyzing the wall behavior in initial configurations ranging from a fully pre-cracked stage to a un-cracked stage. In the latter case the wall generally presents more lateral capacity as the hinges around which the wall members will rotate should first be formed and thus require some amount of energy cracks to develop.

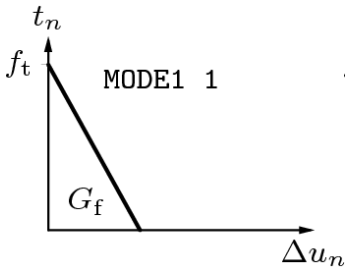

Figure 46 - Linear tension softening model. Diana 10.1 Manual, Material library

All elements are assumed to have fully elastic behavior in compression. No crushing of masonry material is accounted for. For the tension-resistant interface, a linear tension softening model is selected together with secant unloading/reloading model and a zero shear traction criterion. In a similar way, the shear stiffness in the case of the no-tension interface reduces to zero as soon as the crack opens. The table hereunder presents the material models specifications.

	Mass [kg/m^3]	E [N/m^2]	Poisson [-]	f_t [N/mm^2]	G_f [N/m]	K_n [N/m^3]	Ks [N/m^3]
Rigid CS	1800	$1.16 \cdot 10^{13}$	0.1	-	-	-	-
Linear masonry	1800	$1.16 \cdot 10^{10}$	0.1	-	-	-	-
No-tension int.	-	-	-	-	-	10^{10}	10^{12}
Tensile resist. int.	-	-	-	0.45	35	10^{10}	10^{12}
Spring	-	-	-	-	-	$9.60 \cdot 10^5 \cdot m^2$	-

Table 6 - Material specifications for smeared cracking beams model.

The intention is to use this model for quasi-static analyses as well as transient analyses. To do that, Rayleigh damping coefficients need to be derived through an eigenvalue analysis and applied to the material models. Two modes are usually selected to numerically compute these coefficients: the first shape of vibration of the system and that for which 90% of the mass of the system is activated in the direction of interest. By including the Rayleigh coefficients the energy

that would be accumulated by the system due to spurious modes is damped down, a practice that corresponds to applying an external fictitious damping to the system. However, it should be underlined that the eigenvalue analysis is a linear procedure. Consequently, the Rayleigh coefficients calculated in this way for the system do not account for nonlinear phenomena such as cracks opening and, therefore, may lead to inaccurate results. For the case of highly nonlinear problem the damping should better be assessed through experimental researches. In line with instructions found in literature (Doherty, 2000), a damping ratio of 2% is applied for computing the Rayleigh damping coefficients for this model. The coefficients are presented below.

Rayleigh coefficients for a damping ratio of 2%	
$a = 8.8804\ 1/s$	$b = 0.82124 \cdot 10^{-5}\ s$

Table 7 - Rayleigh damping coefficients for the lumped cracking beams model.

4.1.3 Boundary condition, tyings and loads

The wall strip is constrained horizontally and vertically at the bottom side, whereas the top end is kept free to displace in the vertical direction. Free vertical motion is ensured by providing the upper-side nodes of the top line interface, which are tied in the vertical direction and simulate a rigid steel plate on top of the wall, with a mid-horizontal-support. At the bottom, the lower nodes of the interface element are those to which the supports are assigned. At the same time, the wall rocking members need to be able to rotate around the edges of the rigid cross sections while keeping their shape straight. In order to that rotational tying are applied to the nodes of each horizontal beam. The top spring is connected to the steel plate and fixed on the other extremity. An additional horizontal support is introduced at the mid-wall level so as to apply the prescribed displacements for the displacement control analysis.

	u_x	u_y	φ_z
Lower nodes bott. int.	✓	✓	-
Central node steel plate	✓	×	✓
Node at wall mid-height	✓	×	×
Spring on top	✓	✓	×

Table 8 - Constraints configuration for the lumped cracking beams model.

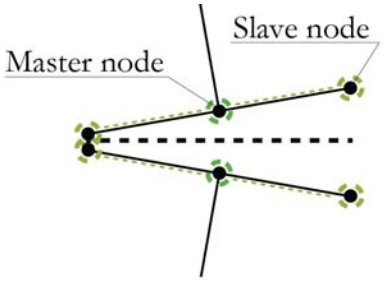

Figure 47 - Rotational tying in rigid cross sections.

A pushover analysis will be run on the model with a displacement control procedure. This is the only possible way to capture the decrease of the wall lateral resistance as the instability displacement is achieved. A set of load-cases is required to perform the analysis. First, the self-weight is applied followed by the application of the force on the wall resulting from the compression of the top spring. The initial compression load deriving from the spring action is taken equal to the one used in Doherty experimental research. At this point the prescribed displacement at mid-height can be introduced in steps. For comparative analysis, also the load-case of a constant vertical top force applied on the middle node of the steel plate is implemented in the model. Details of the model loadings for the quasi-static analysis are provided below.

	Point of application	Magnitude	Direction	Frequency
Self-weight	-	-	-	-
Prescribed displacement	Wall mid-height	0.11 m	x	-
Prescribed displacement	Spring top	0.017 m	-y	-
Concentrated force	Wall top	1-17 kN	-y	-
Base acceleration	Horizontal supports	Increasing harmonic	x	0.5 – 2.5 – 15 Hz
Base acceleration	Horizontal supports	Accelerometer	x	Variable

Table 9 – Definition of the loads applied on the lumped cracking beams model.

Apart from the quasi-static ones, a variety of transient analyses with different input excitations is used to investigate the dynamic behavior of the model and its response to inertial loading. A base excitation is applied to all nodes horizontally supported. Two typologies of signals are used. A set of increasing harmonic accelerations with three forcing frequencies is used to excite the system. Each of the three frequencies corresponds to a different branch of the design spectra that are commonly used for the seismicity in the area of Groningen, thus giving an general idea of the role played by the exciting frequency in this nonlinear problem. Then, an accelerometer corresponding to the Nahanni earthquake so as to compare the outcome with the Doherty experimental results. The input signals used are presented in the graphs hereunder. The vertical axis represents the multiplication factor of the acceleration of gravity.

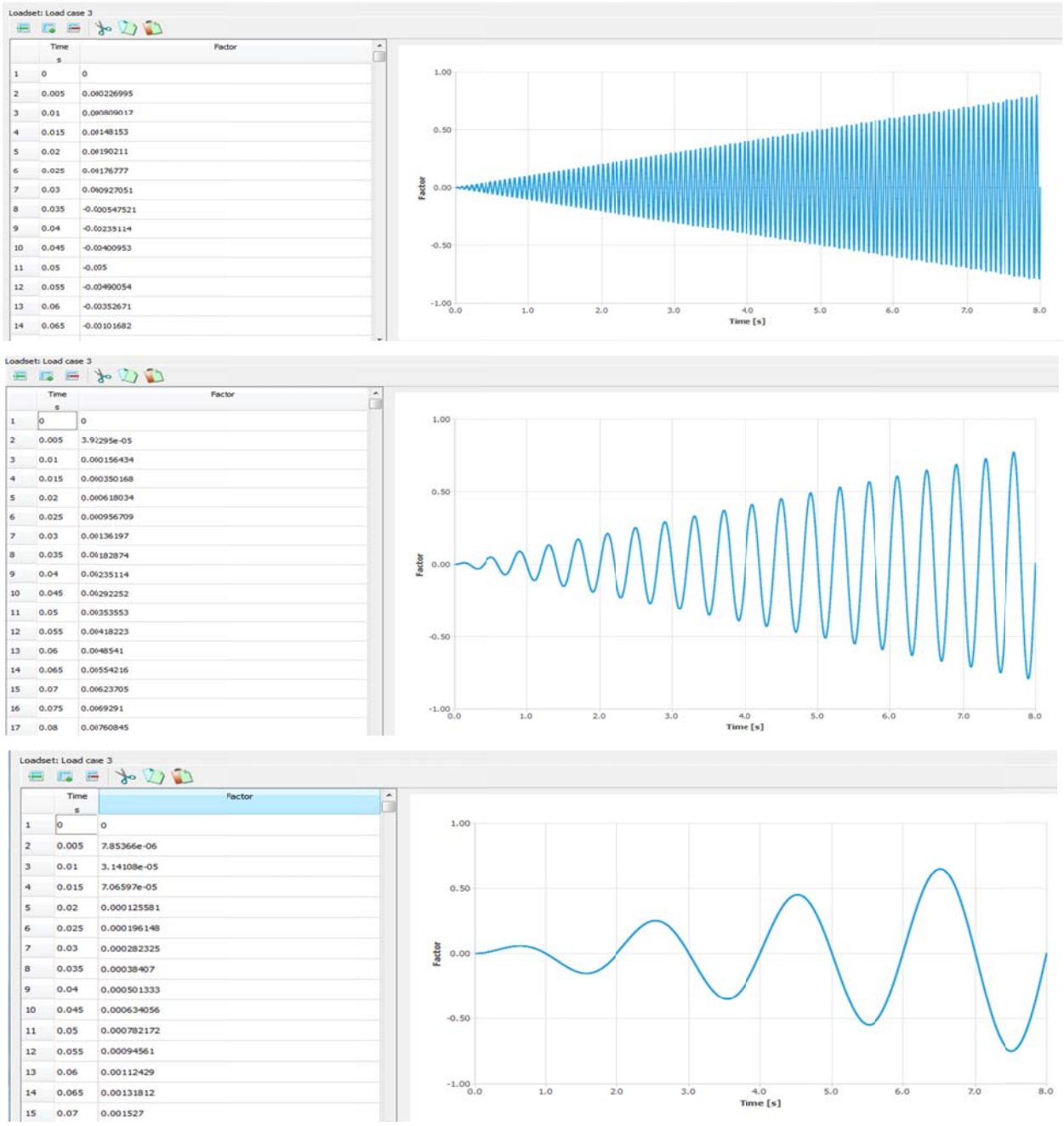

Figure 48 – Increasing harmonic signals used for the lumped cracking beams model: 15 Hz (top); 2,5 Hz (mid); 15 Hz (bottom).

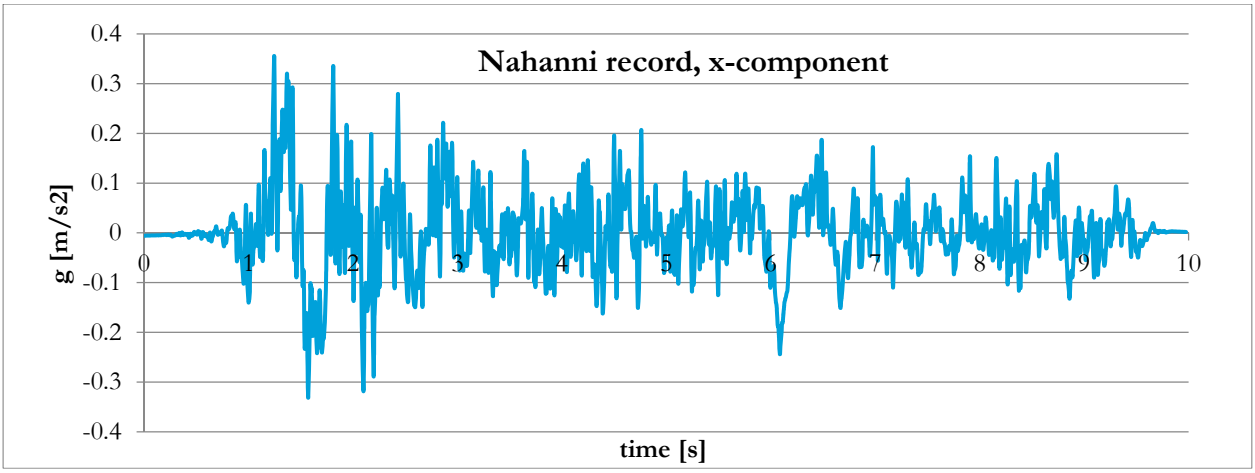

Figure 49 - Signals used for the lumped cracking beams model: Nahanni earthquake record.

4.1.4 Analysis control

The pushover analysis is carried out by controlling the prescribed displacement at the mid-height cross section of the unreinforced masonry wall. The geometrical nonlinear effects should be activated to account for the large deformations experienced by the system while it rocks. In the table provided below it is shown the step-size to be used as well as the convergence norm to be adopted for this type of analysis. Depending on the way the top load is applied, the overburden on the wall may be constant or induced by the spring (see two possible cases 2A and 2B in the table).

Application order	Loadcase	Load/Time steps	Iterative method	Convergence norm	Tolerance
Quasi-static analysis – Displacement control					
1	Self-weight	1	Newton-Raphson	Pre-defined	-
2A	Spring compr.	1	Newton-Raphson	Pre-defined	-
2B	Top force	1	Newton-Raphson	Pre-defined	-
3	Prescribed displ.	1.00000e-05(95) 1.00000e-06(100) 1.000000e-5(1000) 1.000000e-3(99)	Newton-Raphson	Force, Displacement	0.001
Transient analysis – Base acceleration					
1	Self-weight	1	Newton-Raphson	Pre-defined	-
2	Spring compr.	1	Newton-Raphson	Pre-defined	-
3	Base motion	0.00200000(4000)	Newton-Raphson	Energy	0.0001

Table 10 - Loads application procedure and settings for the numerical analysis of the lumped cracking beams model.

The arrangements for the transient analyses are left to the default settings apart from the time integration scheme which is set to the Euler Backward methodology. This integration method guarantees more stable solutions compared to the Newmark procedure even if the beta factor is set to 0.25 and the gamma factor to 0.5, values for which the method is implicit and unconditionally stable.

Alternative models

Dealing with the numerical models shows how limiting are those based on the rigid beams definition. Although the latter give good results with respect to quasi-static analyses for a variety of boundary conditions, it is not possible to achieve similar accuracy for dynamic analyses. Occurrence of numerical instability makes the investigation of the wall behavior difficult to control and hinders further development of the model. The difficulties encountered seem to be caused by the detrimental presence of concurrent features in the models definition rather than a single one. Among the others, the alleged incompatibility between the finite elements of the mesh and the modeling of the wall through its thickness by means of infinitely rigid beam elements may well be the main causes of its unreliability. A more detailed description of all the problems encountered with lumped cracking beams model is provided in the relevant section.

At this point, having gained sufficient insight on the out-of-plane action of the wall element and on the pre-requisites of its numerical representation, a new set of models can be developed. In this section not only an attempt to create a more stable model from a numerical point of view is made, but also to implement the masonry material behavior, for instance by taking into account its compressive strength and crushing energy to model the material damage in time. More than in the lumped cracking beams model, extra attention is given to the single wall modeling with respect to its final utilization, which is its implementation in a frame structure for transient analyses. Consequently, the overall modeling procedure adopted for this model is essentially purpose–driven.

Two approaches are presented in the following sections: modeling the masonry wall by means of plane strain elements along its vertical cross section from the side of the thickness, and again by making use of curved beams elements but this time only along the vertical axis of symmetry of the wall. The main advantages of both procedures is allowing for a more homogenous utilization of the elements type used and avoiding resorting to infinitely rigid elements to simulate the wall cross sections at cracks level. Nonetheless, the smeared cracking beams model almost immediately proved to be capable of a better performance compared to the smeared cracking plane strain model. Consequently, although these wall models were developed in parallel, the implementation in the frame structure only took place for the most efficient one, namely the smeared cracking beams model.

4.2 Smeared cracking plane strain model

Due to the fact that the wall length in the spanning direction is ten times as large as its thickness, it is possible to assume that the strains field has a zero component in the z direction. The choice of using plain strain elements allows to analyze with increased level of detail the nonlinear phenomena which take place during crack formation, and to overcome the alleged incompatibility between the default membrane configuration of the line interfaces and the beam elements adopted in the "lumped cracking beams model". In particular, the degradation of the material may now be accounted for. The same size as the previous model is used to schematized the wall.

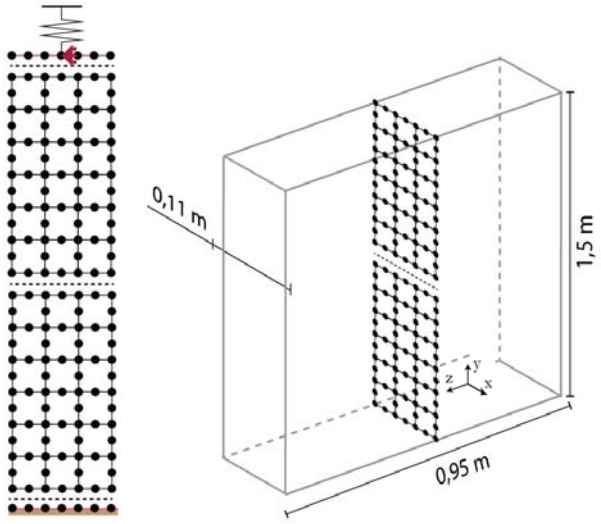

Figure 50 - FE representation of the smeared cracking plane strain model.

The "smeared cracking plane strain model" is developed in parallel to the "smeared cracking beams" one: its main function is to assess the minimum number of integration points required along the thickness of the wall and to implement as number of layers for the next model. This is done by comparing the behavior of this model during quasi-static loading with the results obtained with the lumped cracking beam one. Once this aspect is determined, the smeared cracking plane strain model is left apart to give space to the smeared cracking model which employs a smaller number of nodes, resulting in less computing time, and which also guarantees easier connecting solutions for its implementation into a frame system. Thus, as this wall

discretization is used a mean to make modeling choices in another model, and given the fact that the settings of the pushover analysis are the same as in the lumped cracking beams model, the following sections will only briefly present the modeling procedure to be adopted and highlight the its main features.

4.2.1 Geometry FE types

This model consists of a set of plain strain elements of a quadrilateral shape along the entire thickness as well as the height of the wall. The initial number of elements used in the thickness direction is assumed and later modified to increase the accurateness of the results. The line interfaces are constituted of the same elements that were introduced in the lumped cracking beams model. The same also holds for the spring element. The CQ16E plain strain element has an isoparametric definition and it is based on quadratic interpolation. The eight nodes belonging to this element have no rotational degree of freedom. If rotation results are desired, the bending moments can be calculated via composed line elements embedded throughout the height of the wall. By default Diana applies a 2-point Gauss integration scheme to this element. Table 11 shows the geometrical properties of the finite elements introduced for the URM wall modeling.

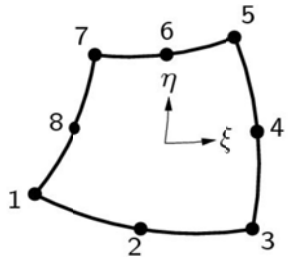

Figure 51 - CL9BE, 2D element, 3 nodes. Diana Manual 10.1, Element library

	CQ16E	CL12I	SP2TR
Width [m]	0.037	0.037	[-]
Thickness [m]	0.95	0.95	[-]
Length [m]	0.125	[-]	0.10

Table 11 – Overview on the size of the finite elements used in the wall smeared cracking plane strain model.

The mesh applied at the beginning is rather coarse. Sensitivity studies will be carried out to determine the most convenient number of plain strain elements required in the thickness direction of the wall. As the cross sections at the level of cracks are not rigid anymore, the accurateness of their nonlinear deformation is a function of the number of integration points adopted.

4.2.2 Material properties

For this model smeared cracking approach is used. To make the rocking possible, a no-tension line interface element is applied on top and bottom sides of the wall while the masonry material at mid-height level is modeled with nonlinear properties in order to accommodate the smeared cracking. Indeed, the plain strain elements all act in a linear way, apart from those adjacent to the mid-height crack. For the latter, the material model provided accounts for cracking and crushing of the masonry: the stress-strain relation in compression has a parabolic shape, and a linear tensile softening curve is enforced for its tensile resistance. Details are given in the table provided hereunder.

	Mass [kg/m³]	E [N/m²]	ν [-]	f_t [N/mm²]	G_f [N/m]	fc [N/mm²]	Gc [N/m]	K_n [N/m³]	Ks [N/m³]
L masonry	1800	$5 \cdot 10^9$	0.1	-	-	-	-	-	-
NL masonry	1800	$5 \cdot 10^9$	0.1	0.45	35	4.50	5000	-	-
No-tens. int.	-	-	-	-	-	-	-	10^{10}	10^{12}
Spring	-	-	-	-	-	-	-	$9.6 \cdot 10^5 \cdot m^2$	-

Table 12 - Material specifications for smeared cracking plane strain model.

The next two captions show the material models of Diana applied for the tensile softening behavior of the mid-height interface element and the nonlinear compressive behavior of the plain strain elements adjacent to the mid-height crack.

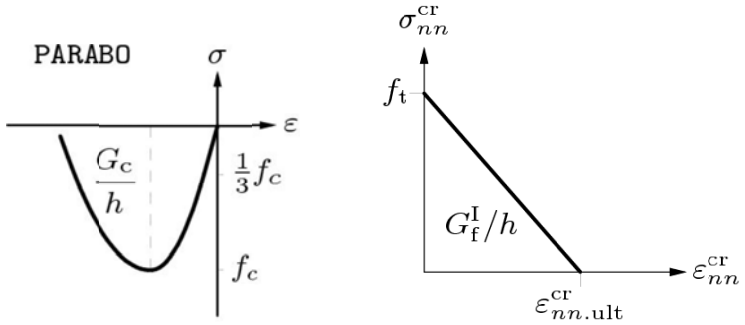

Figure 52 – Stress-strain relations in compression and in tension for the unreinforced masonry material and the discrete crack at mid-height.

4.2.3 Boundary conditions, loading and analysis control

The boundary conditions for this structural schematization are the same as those of the lumped cracking beams model. The spring on top has one edge supported in the x and y direction and the other end connected to the upper nodes of the top no-tension interface element which also act as a rigid member free to move in the vertical direction. To accomplish that these nodes are tied together in the x direction to the master middle node. The latter is supported in the horizontal direction with a roller. Again, one node in the middle section of the wall is supported by a "fictitious" horizontal support which is required for applying the prescribed displacement during a pushover analysis. Finally, the bottom nodes of the lower no-tension interface which are not directly connected to the plain strain elements are constraint in both the x and w directions.

As already mentioned in the beginning of this section 4.2, only pushover analyses will be run on this model to assess the minimum number of integration points required along the thickness of the wall to reach accurate results. This will be done by applying the top load both by means of the spring and with a constant vertical top force. The methodology used is the equal to the one described for the "lumped cracking beams model". Same control procedure is followed. Details are presented below.

	Point of application	Magnitude	Direction
Self-weight	-	-	-
Prescribed displacement	Wall mid-height	0.11 m	x
Prescribed displacement	Spring top	0.017 m	-y

Table 13 – Definition of the loads applied on the smeared cracking plane strain model.

	u_x	u_y	φ_z
Bottom int. nodes	✓	✓	-
Central node top int.	✓	×	×
Node mid-height	✓	×	×
Spring top	✓	✓	×

Table 14 – Constraints configuration of the smeared cracking plane strain model.

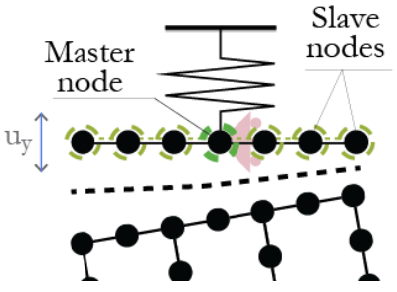

Figure 53 – On the right: horizontal tying of the upper-side nodes belonging to the top no-tension interface of the wall.

4.3 Smeared cracking beams model

As in the case of the plane strain one, the smeared cracking beams model accounts for the material behavior of the wall and thus for its physical nonlinearity besides the geometrical one. Nevertheless, using beams elements has immediate beneficial effects on the computational costs of numerical analyses since the number of nodes and integration points is drastically smaller than in the plane strain elements model meshed in a similar way. Moreover, using specific beam elements such as class III beams permit to increase the number of integration points in the direction of interest and decrease their number in others if necessary.

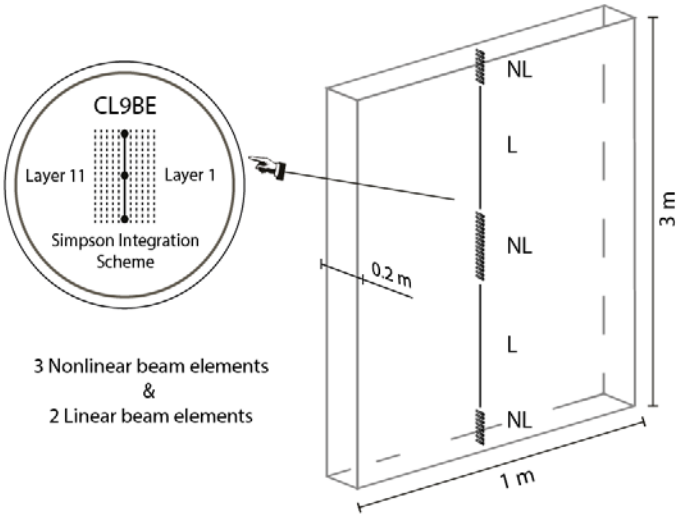

Figure 54 - FE representation of the smeared cracking plane strain model.

The model developed consists of beam elements with different material models applied depending on their position along the wall. Those areas of the wall where out-of-plane action is expected to originate cracks are modeled by assigning non-linear properties to the beams, whereas the remaining parts are approximated to deform linearly-elastic. Thus, during the development of the crack patterns as well as the occurring of the rocking mechanism the focus is given to larger areas compared to the lumped cracking beams model because the increase of curvature is smeared out along the height of the wall and the stress is distributed more effectively. Last but not least, this model is the easiest to implement in the frame building.

4.3.1 Geometry and FE types

The wall is discretized using two dimensional beams only, representing its vertical axis of symmetry. These elements have a rectangular cross section shape. The spatial dimensions of the wall are assigned to the beam elements as a property together with the material definition, the element typology and the data for additional input. Since no reference is made to any specific wall, dimensions that are commonly found in practice are chosen for the current model. For a partition wall, this may correspond to a wall height of 3 meters and a thickness of 20 centimeters. Another model with similar dimension to the previous ones is also developed for the sake of comparison and validation of results. Refer to the given table for the geometry of the beam elements employed.

Element / Size	CL9BE	CL9BE	SP2TR
Width [m]	Partition wall	Similar previous models	[-]
	0.20	0.11	
Thickness [m]	1	0.95	[-]
Length [m]	Nonlinear element	Linear element	[-]
	0.0375	0.375	0.10

Table 15 - Geometry specifications for the smeared cracking beams models.

For this model it is decided to use class III beam elements as they allow for second order interpolation polynomials for two translational degrees of freedom and a rotational one. Also, it is possible to adjust the preferred integration scheme over their cross-section and along their axis, which is a convenient feature when addressing physical nonlinearities such as crushing and cracking of a material. These elements are based on Mindlin-Reissner theory and thus they take into account shear deformations. They can be curved thanks to the presence of three nodes along the beam axis, and they act in a 2D environment.

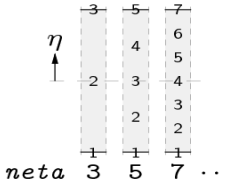

Figure 55 - Simpson integration scheme along wall thickness. DIANA 10.1 - User's manual

Integration scheme and number of integration points arranged in the model		
Along the beam axis ξ	Gauss	2
Along the beam cross section η	Simpson	11

Table 16 - Integration schemes for the beam elements

The elements are integrated with the default 2-point Gauss scheme along the beam axis, whereas a 11-point Simpson scheme is used for integration along their cross section. The latter is able to account for the shifting of the point of rotation of the wall to the extreme fiber in compression when the rocking mechanism occurs. This is set through a DATA input. The wall is split in areas with and without linear behavior. This is accomplished by referring to how concentrated loads spread within a structural element. For the case at matter this happens when the rocking wall is pushed close to its instability displacement and there is a compressive force applied to the extreme fiber of its cross sections acting as point of rotations. Thus, the wall can be conveniently given nonlinear features in those areas where the stress flaw presents high nonlinearities and the influence of the concentrated load is larger. In EC6-1-1 it is stated that for unreinforced masonry brickwork a dispersion angle of 60 can be adopted. Given a thickness of 12 cm, it is then reasonable to assign nonlinear properties to the wall up to a distance of around 20 cm from the (main) cracks. Same reasoning will be adopted also for the coming models. Illustrations are provided for the sake of clarity.

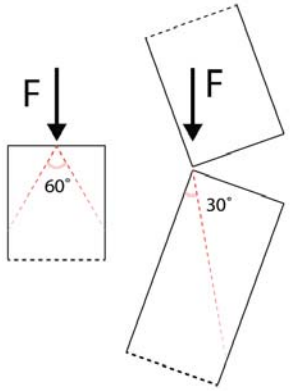

Figure 56 – Load dispersion in URM according to EC6-1-1.

A spring is applied on top of the model to simulate the action of the overburden on top of the wall during the quasi-static analysis. This is performed in a similar fashion to the previous models (Section 4.1.3 and 4.1.4). Characteristics and element type of the spring are presented above.

4.3.2 Material properties

There are three material models applied to the wall. The masonry is treated as a linear elastic material in areas of the wall that are not considered to experience large nonlinear behavior. On the other hand, nonlinear masonry is assigned to relevant sections in order to investigate cracks propagation and material degradation as the out-of-plane action develops. To this purpose, a total strain based crack model with fixed cracking propagation and Rots bandwidth is used. With regards to the behavior in tension and in compression, the constitutive models described by a linear tension softening curve and a parabolic compression curve are chosen. For the compression law, no reduction due to lateral loading nor stress confinement are accounted. The parameters input are specified in the table provided below.

	Mass [kg/m³]	Young's modulus [N/m²]	Stiffness [N/m]	Poisson [-]	f_t [N/mm²]	G_f [N/m]	fc [N/mm²]	Gc [N/m]
Nonlinear masonry	1800	$5 \cdot 10^9$	-	0.1	0.45	35	4.41	5000
Linear masonry	1800	$5 \cdot 10^9$	-	0.1	-	-	-	-
Spring	-	-	$9.60 \cdot 10^5$	-	-	-	-	-
Rayleigh coefficients for a damping ratio of 2%								
$a = 8.8804\ 1/s$				$b = 0.82124 \cdot 10^{-5}\ s$				

Table 17 - Material specifications for smeared cracking beams model.

With regards to the utilization of the model in a transient analysis, fictitious damping is applied again through Rayleigh damping coefficients derived through an eigenvalue analysis.

4.3.3 Boundary conditions and loads

The wall is clamped at both ends, with the top margin of the wall left free to move in the vertical direction. The resisting bending capacity of the cross section will be exceeded in those areas where cracking is expected to occur. When the cracks are sufficiently developed those areas will provide rotational capacity and thus act as hinges in the overall rocking mechanism. Again, a mid-height horizontal support is added to the wall so as to perform a displacement control analysis for the pushover calculation.

2D configuration	u_x	u_y	φ_z
Wall bottom edge	✓	✓	✓
Wall top edge	✓	×	✓
Wall mid-height	✓	×	×
Spring top	✓	✓	×

Table 18 - Constraints configuration for the smeared cracking beams model.

Similarly to the previous models for the rocking wall, different loadcases are defined for the investigation of the out-of-plane behavior of the unreinforced masonry wall subjected to quasi-static and transient excitations. The prescribed displacement at mid-height of the wall varies with the dimensions of the wall analyzed, as it calibrated in order to capture the achievement of the instability displacement for which the destabilizing forces threaten the stability of the system. As it was already discussed (see Table 2), the instability displacement also depends on the constraints configuration of the wall. The compression force given by the overburden is implemented by means of a spring forced to compression or by a static point load. Remarks to all these aspects will be provided when necessary.

	Point of application	Magnitude	Direction
Self-weight	-	-	-
Prescribed displacement	Wall mid-height	0.11 – 0.20 m	x
Prescribed displacement	Spring top	0.017 m	-y
Concentrated force	Wall top	1 – 5 kN	-y

Table 19 – Definition of the loads applied on the wall model.

4.3.4 Analysis control

The performance of the wall is evaluated by means of a quasi-static analysis on Diana. To this purpose, the application of the loads on the model takes place in steps that are refined, when necessary, to provide numerical stability of the system. As it can be seen from the table hereunder, first the self-weight of the wall is applied, followed by the overburden force and the prescribed displacement at mid-height.

Application order	Loadcase	Load steps	Iterative method	Convergence norm	Tolerance
1	Self-weight	1	Newton-Raphson	Pre-defined	-
2	Overburden	1	Newton-Raphson	Pre-defined	-
3	Prescrb. Displ.	1.00000e-05(95) 1.00000e-06(100) 0.000100000(1000)	Newton-Raphson	Displacement	0.01
				Force	0.01

Table 20 - Loads application procedure and settings of the numerical analysis on the smeared cracking beams model.

The methodology used to solve the system of equations describing the wall is again the Parallel Direct-Sparse with a tolerance of 10.e-08. The iterative procedure is left to the pre-defined settings with maximum 10 iterations for each load increment. The convergence criteria specified are also reported in the table above; however, the calculation is aborted by

Diana only when the solution diverges. As it was also the case in the lumped cracking beams model, the occurring and further development of the crack patterns may sometimes lead to sudden loss of convergence which is, however, recovered within few steps of the analysis. Hence, Diana is instructed to continue the analysis even if convergence is not reached provided that the latter is reached again in a following stage. It is underlined that the settings for the analyses here presented were chosen after comparison with other procedures as well. Details are presented in the section dedicated to the response of the models.

4.4 Frame building models

This research aims to evaluate in a quantitative way the out-of-plane performance of unreinforced masonry walls within a structural system and possibly to derive correcting coefficients for their use in analytical and practical approaches. Aiming at this, it is definitely necessary to develop a 2D model of a building in order to investigate a variety of realistic boundary conditions with respect to overburden of its walls and their degrees of constraint. Furthermore, the frame modeling is crucial for simulating the interaction between the local behavior of the walls and that one describing the building as a whole, with special attention to their dynamic response. The frame models should then be considered as a tool for this type of research.

The starting point of the modeling procedure for the structural system coincided with choosing, among those previously developed, the most appropriate wall model for its implementation in the building discretization. The role played by the following aspects was considered:

- Inherent numerical stability;
- Accurateness in describing the rocking behavior of the wall out-of-plane mechanism;
- Number of DOFs introduced in the model and related analyses computational cost;
- Ease of implementation in the frame model.

These requirements are all to be found in the "smeared cracking beams" model, which is thus introduced in a set of structural elements required for describing the building.

In parallel, several models were developed to account for single and multi-floor buildings. The lateral stability of the models is provided by systems that are modeled as either shear walls or moment resisting frames, being the real behavior of a residential building usually in between these two idealizations. The physical interpretation of the stability systems may be the representation of the elements acting in-plane in the structural system. The features of these models are briefly presented in paragraph 4.3.2.

4.4.1 Step-by-step development of an adequate model

Before explaining the modeling procedure adopted for the frame models this section wants to highlight the crucial steps that were undertaken in the development of the 2D model itself. In short, running transient analyses on it made it possible to understand several inconsistencies with regards to the structural behavior and to modifying the model accordingly.

First, a "basic frame model" was created, consisting of floors and walls elements only with the nonlinear URM wall systems on each floor. The lack of lateral rigidity determines drift values that are too large even for small accelerations. Thus, new models were elaborated with the introduction of stability elements to provide adequate inter-story drift limits and, also, realistic values of vibration period for the structural frames. The physical interpretation of the stability system may be addressed as the rigid in-plane action of the URM walls that are orthogonal to the 2D plane shown. Again, the nonlinear wall systems were included on each of the frame floors.

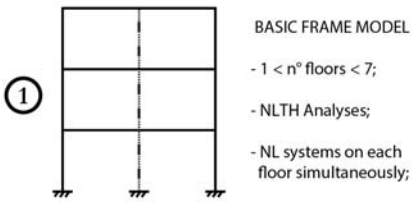

Figure 57 - First frame model.

Due to the rise of large normal forces on the walls, induced by the structural system defined as an assemblage of beams and column continuously connected (also known as "frame effects"), hinge elements were implemented in the model.

More specifically, hinges were applied at the connection between floors and stability systems. The floors were defined as continuous elements spanning over the nonlinear URM walls. This corresponds to model 3 depicted in the figure below.

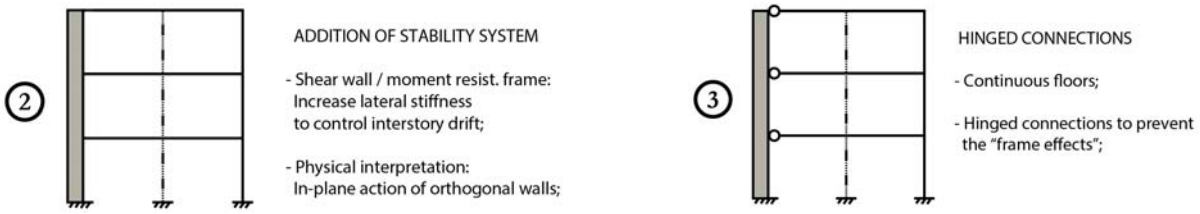

Figure 58 - Second and third models.

However, it was realized that in order to have all the walls analyzed comparable it was necessary to have the same boundary conditions (constraints, loads) for all of them. Since a ground-floor wall has always to withstand larger top loads compared to one on an upper level, different kind of "stair frame" models were developed, also taking into account the amount of DOFS involved to decrease the time of computations.

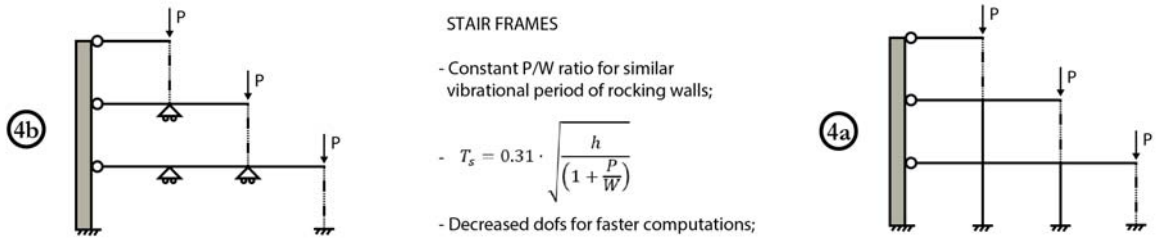

Figure 59 - Stair frame models.

Eventually, it became clear that as soon as one of the URM walls achieved its instable configuration due to the external excitation, the whole analysis would diverge and thus stop completely preventing the assessment of the behavior of the other elements in a later moment. A frame model made of dummy floor elements with no mass was finally chosen to meet this necessity. This model will be employed to verify the performance of one nonlinear system at a time on each floor. The major part of the mass pertaining to the frame structure will be thus lumped in the stability system and applied above the walls as a concentrated load.

Depending on the type of analysis that one wants to run, it will be possible to vary the magnitude of the force on top of the wall, the initial drift of the floor above it, the ground motion intensity at the base and the location of the system representing the URM rocking wall within the structural frame.

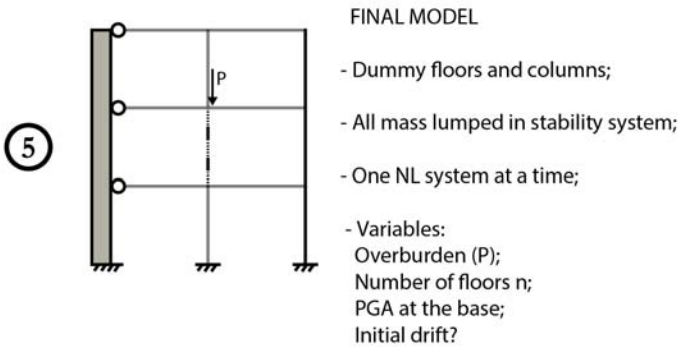

Figure 60 - Final model with dummy floor elements.

4.4.2 Geometry and FE types

Given the wall numerical definition as described in Section 4.2, additional beam elements of the same typology are adopted for discretizing the building system as a frame. Geometrical properties are assigned to these objects to reproduce the size of the structural elements which represent the floors and the stability system. Besides their dimensions, the way these elements are connected to each other may also be attributed at geometry level. Finite elements software offer a variety of possible ways for defining hinged connections. In the model at matter, hinges are implemented in the model by introducing extra elements, namely 2D point interfaces between the end of the masonry walls and the floors, or by keeping the same number of elements and characterizing the ends of relevant objects as hinged. Both the methodologies were used in the current research, and their pros and cons are presented in this section as the differences mainly deal with their definition procedure rather than the impact they have in the structural response.

Each floor of the frame measures 3 meters in height and the columns span for 4 meters. In the following tables the properties of the additional elements composing the frame model is presented. With regards to the characteristics of the masonry walls, reference is made to the "smeared cracking beam" model.

Object	Floor	Hinged-floor edge	Shear wall	Wall-floor connection
FE element	CL9BE	CL9BE	CL9BE	N4IF
Width [m]	0.15	0.15	2.00	[-]
Thickness [m]	1.00	1.00	0.25	[-]
Length [m]	2.00	2.00	Same as wall elem.	0.00
Surface [m^2]	[-]	[-]	[-]	0.20
Hinge	[-]	PHIZ1	[-]	[-]

Table 21 - Geometry specifications for the frame models.

As it can be observed from the table above, the hinged connections between the stability system and the beams representing the floor slabs are defined without the input of extra finite elements. In fact in Diana it is possible to give the beam elements not only their cross sectional dimension but also to activate hinges at their ends. However, the limit of defining hinges in this way is that the properties of the connection are given not to the whole geometrical shape but to all the beam elements composing its mesh. This being said, it is necessary to split up the floor in two parts when using this type of hinge definition, one part meshed with a single beam element and hinged to the stability system, and the other part with user-defined mesh refinement and continuous beam elements. The alternative way of defining hinges is by introducing nodal interface elements. In this way the model allows for more freedom in meshing the floor objects but at the expense of additional degrees of freedom and input needed such as interface material properties and geometrical characterization.

N4IF, 2D element, 1+1 nodes.
Diana Manual 10.1, Element library.

Since the focus of the research is on the highly nonlinear rocking mechanisms of the masonry walls, the extra elements included in this model should be intentionally given a coarse mesh. For the same reason the integration schemes adopted for this elements are left to their predefined schemes.

4.4.3 Material properties

The material definition for the unreinforced masonry wall elements is already addressed in the relevant section of the smeared cracking beams model (see 4.2.2.2). The final material parameters chosen for the frame model follow a sensitivity analysis performed in section 5.3 of this document. Also, the Young Modulus is now set to 5 GPa (values adopted for the lumped cracking beams model were taken from experimental settings of Doherty). For defining the frame model additional material models need to be introduced. The floors are assumed to be made of concrete, with an elastic modulus that is six times larger than the unreinforced masonry one and with a massless density. When the hinged stability system-to-floor connections are applied through nodal interface elements, the values of their normal and shear stiffness are required.

The Rayleigh damping coefficients for the models at matter depends on their structural configuration (number of floors) and structural performance (such as structural ductility, not addressed in this research) and are calculated through an eigenvalue analysis. As an example, the Rayleigh damping coefficients for a six-story building with shear walls as a stability system are presented in the table below.

	Mass [kg/m^3]	Young's modulus [N/m^2]	Normal stiffness [N/m^3]	Shear stiffness [N/m^3]	Poisson [-]
Floors	2200	$3.00 \cdot 10^{10}$	[-]	[-]	0.1
Point interface	[-]	[-]	$1.00 \cdot 10^{13}$	$1.00 \cdot 10^{13}$	
Rayleigh coefficients for a frame model and a damping ratio of 4%					
$a = 0.87835\ 1/s$			$b = 0.24634 \cdot 10^{-3}\ s$		

Table 22 - Material specifications for the frame model.

A remark is necessary on the cracking model applied to the masonry elements of the frame. Analyses of results on the smeared cracking beams model in the sensitivity analysis demonstrated that a fixed cracking approach better estimates the amount of energy involved in the rocking mechanism of a wall acting out-of-plane. Therefore, the fixed cracking model is chosen in place of the rotating one. For details on this aspect, reference is made to the next chapter of this master thesis.

4.4.4 Boundary conditions and loads

The frame is clamped to the ground. The walls within the structural system are, as it was mentioned before (section 4.3.1), continuously connected to the floors unless stated differently.

2D configuration	u_x	u_y	φ_z
Shear wall	✓	✓	✓
Ground-floor walls	✓	✓	✓

Table 23 - Constraints configuration for the smeared cracking beams model.

Hinges may be applied to the wall-floor connections either for forcing the cracks to occur at the wall mid-height or to prevent the structural system from experiencing frame effects. The first instance may be used to mimic the case of a building system in which the walls are already pre-cracked at the ends, a circumstance that may be present in existing buildings due to settlements or already partially damaged. The frame effects mentioned deal with the occurring of tension and compression forces through the frame system which provide the balance of forces but also prevents the rocking mechanism of the masonry walls to be captured in the right way during the analysis. As a final choice for the analyses made on the frame model, the hinges will be only applied to the floors-stability system connections.

With regards to the loads applied, again increasing harmonic base accelerations were used to test the model overall and local behavior as well as to calibrate the lateral stiffness of the stability system adopted. The increasing harmonic motions used were similar to those used for previous models. Note that this (intermediate) investigation is not reported in this document. Once it was demonstrated that the frame model is able to capture the out-of-plane action of masonry walls in dynamic analyses, a series of realistic signals compatible to those pertinent to Groningen are implemented. The procedure followed to derive these signals is briefly described hereafter.

	Point of application	Type of motion	Direction
Self-weight	-	-	-
Base acceleration	Horizontal supports	(Increasing) Harmonic	x
Base acceleration	Horizontal supports	Accelerometer	x

Table 24 - Definition of the loads applied on the frame models.

First, seven spectrally matched NPR bedrock time history records were taken, which were then scaled to two design spectra obtained as described in NPR9998 (2015) clause 3.2.2.2.1 and Annex F. These two design spectra, based on a reference ground acceleration of 0.2g and 0.3g respectively, were constructed by making use of other relevant factors which are provided in the following table. These records were passed through a specific software which determined the new batch of records at ground level taking into account the soil profile derived from three CPT tests carried out in the Loppersum area. For each record the components in either x and y direction were base corrected and then taken for the 2D frame model. The peak ground acceleration at ground level for these records ranges from 0.15g to 0.20g. The next two captions show the elastic design spectra of the scaled signals.

$a_{g,ref}$	k_{ag}(CC2)	γ_M	factor(n° records)	PGA(bedrock)
0.2/0.3	1.5	1.5	1.4 (7 records)	0.42/0.63

Table 25 - Factors used to derive the ground motions for the frame model.

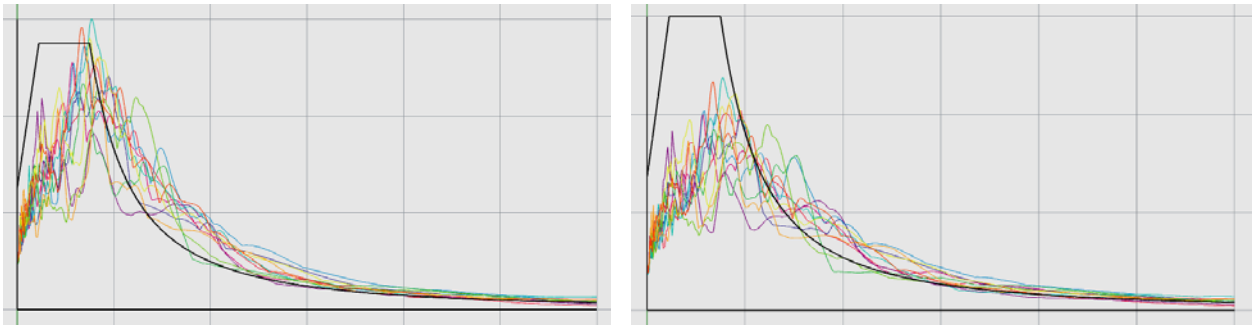

Figure 61 – Spectra of the signals adopted for the Non Linear Time History Analysis of the frame model. x-direction components. a_{gref} = 0.2 (on the left) and 0.3 (on the right).

These signals will allow to study the structural response of the elements for a range of exciting frequencies and are representative from an energy point of view of the ground motions acting in the area of Loppersum (reference acceleration 0.3g) and Groningen (0.2g).

4.4.5 Analysis control

The frame model undergoes non-linear dynamic analyses which are performed by applying the self-weight of the structure first and then imposing accelerations to its supports. The time step adopted for these analyses is presented in the following table.

Application order	Loadcase	Load/Time steps	Iterative method	Convergence norm	Tolerance
1	Self-weight	1	Newton-Raphson	Displacement, Force	-
2	Base motion	0.001 (8000)	Newton-Raphson	Energy	0.0001

Table 26 - Loads application procedure and settings of the numerical analysis on the frame models.

The numerical methodology used to solve the system of equations for the dynamic problem at matter is left to the default Diana settings. The time integration scheme used is the Euler Backward. Energy convergence criteria with a maximum of 20 iterations is employed. When the analysis does not converge, two aspects are examined. First, one should make sure that convergence of the result is recovered in few time steps. Secondly, lack of convergence in the analysis results are acceptable only if these are reasonably limited (<<1). If both these requirements are met, the solver is allowed to proceed with the analysis.

In order to efficiently process the analyses results and given the high number of time steps, Diana is instructed to logging results every 5 steps. Moreover, user-defined output is specified to obtain curvatures, crack pattern development and crack widths along the beam elements composing the walls.

5 Structural response of the Models

5.1 Lumped cracking beams model

The first part of the modeling phase was entirely dedicated to reproducing the structural behavior of a rocking wall in quasi-static conditions. Here, the numerical definition of the element does not account for the masonry material properties yet as it is solely intended to check the capabilities of Diana to capture the geometrical nonlinear nature of the out-of-plane mechanism. The wall, modeled by means of rigid beam elements, reacts to the horizontal imposed deformation by exhibiting a lateral resistance which is a function of the displacement at mid-height. Depending on the tensile resisting properties of the wall and the nature of the overburden on top of it, the trend of the resisting lateral load with the displacement is different. The following diagrams illustrate these circumstances and reflect the analytical and experimental findings addressed in the literature study and in Doherty experiments. Details on the loading conditions of the model and other relevant aspects are to be found in Chapter 4 if not specified explicitly in this section.

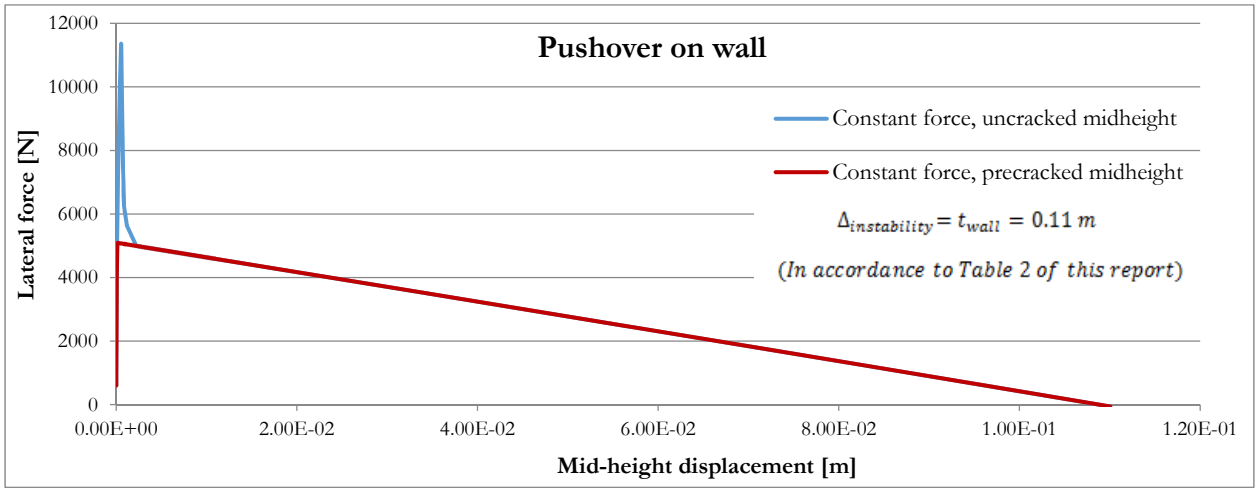

Figure 62 – Pushover analysis on the lumped cracking beams model: tensile resisting and no tension crack elements. No spring.

A number of pushover analyses output are presented. If the interface used to describe the cracks are defined as tensile resisting elements, the graph shows an initial peak which is due to the initial elastic strength of the wall. The area identified by the descending branch accounts for the crack energy being dissipated during cracks opening. After this stage, the horizontal force that the wall is able to withstand drops abruptly and the stability of the system is ensured only by the balance of the forces acting on it. This is depicted in the figure above. The next captions present the result of the same analysis performed on a wall upon which the overburden is applied by means of a spring element. Clearly, the curve depicts a negative stiffness of the system which is no longer represented by a straight line. Again, this is in agreement to the theory. Also, the model was employed to make a rough verification on the impact of the crack energy in the material model. Although this aspect will be addressed later on in more detail, in the section concerning sensitivity analyses on the material parameters, a zoomed-in caption on the first pushover steps is illustrated on the right. The numerical representation of the wall behaves as expected: the more tensile resistance is supplied to the system, the more energy is required to make it start rocking.

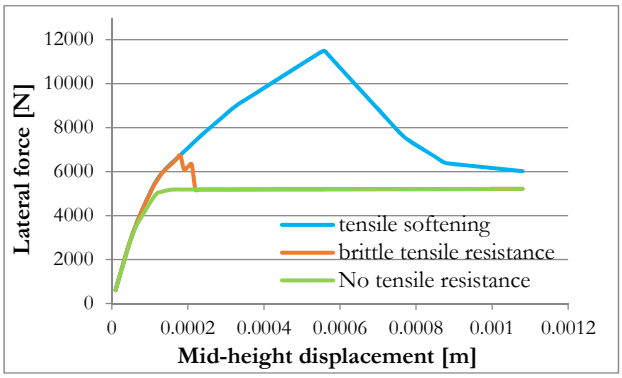

Figure 63 - Zoom-in on the first analysis steps: effect of tensile resistance of cracks. Spring element on top.

It is possible to compare the outcome of the pushover analysis depicted in Figure 64 with the experimental results of Doherty for a similar wall sample with a spring on top of it. Reference is made to Appendix A of this report.

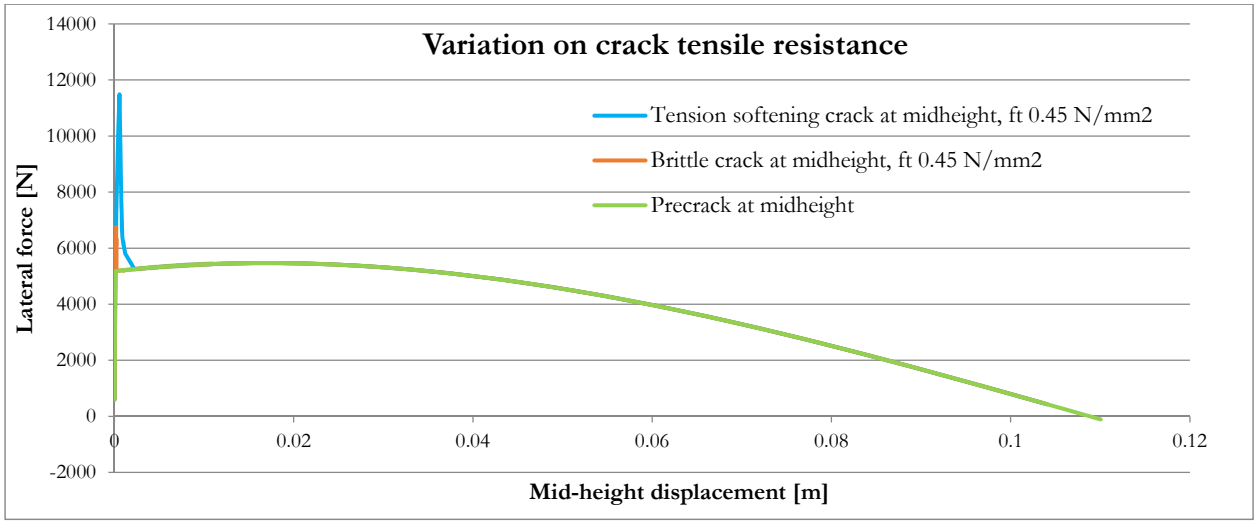

Figure 64 - Pushover analysis on the lumped cracking beams model: different types of tensile resisting crack elements. Spring on top.

The lumped cracking beams model is also used to assess how the magnitude of the overburden, its point of application and the wall constraints affect the system stability or, in other words, its displacement capacity. The caption below demonstrates that a large load acting on top of the wall has a beneficial effect and increases its lateral resistance. It should be stressed, however, that the material model being used in this numerical representation of the wall is not able to account for the compression strength of the masonry. Hence, it can be stated that the larger the top load the more the wall is stable provided that the masonry compression strength is not exceed. If that happened, masonry would experience crushing. This phenomenon will be investigated later on by means of a more detailed wall model.

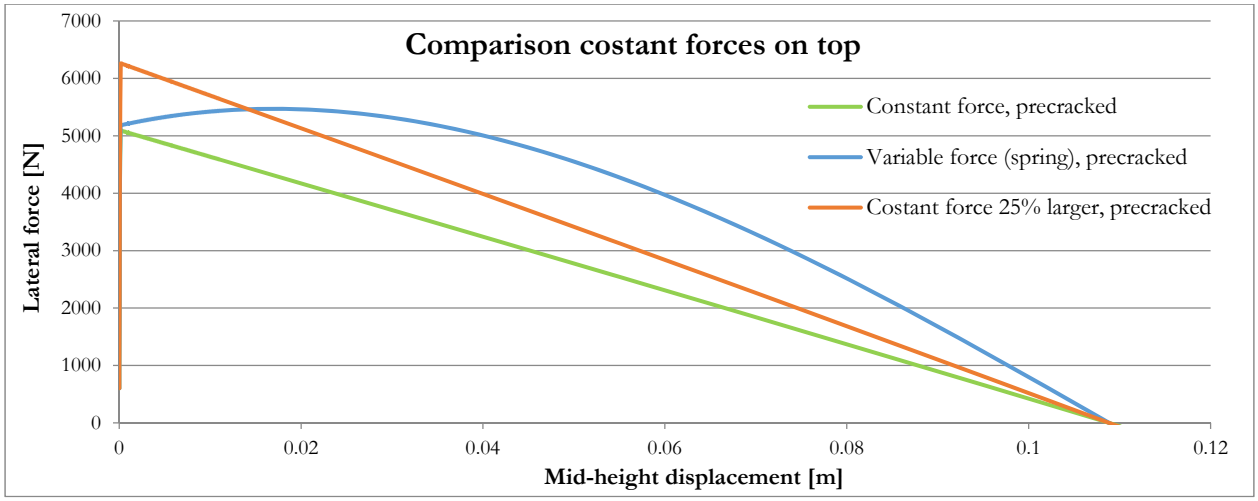

Figure 65 – Pushover analysis on the lumped cracking beams model: different top loads.

Although it is evident that increasing the overburden on a wall makes it more resistant to lateral deformation, another important aspect of it, namely its displacement capacity, remains unchanged. In fact, codes suggest that it is the way the wall ends are constraint to really play a role on this matter. A number of different constraint configurations was obtained by varying the position of the supports on the top and bottom rigid cross sections of the wall. The resulting pushover curves show that not only the displacement capacity of the walls varies, but the initial lateral resistance does too. The

increase of both these quantities is proportional to what in the New Zealand Code is called "seismic coefficient", the maximum horizontal multiplier (acceleration) for which the wall stability is guaranteed. The results obtained with the numerical lumped cracking beams model very well match the analytical formulas from Table 2 (See also Appendix B).

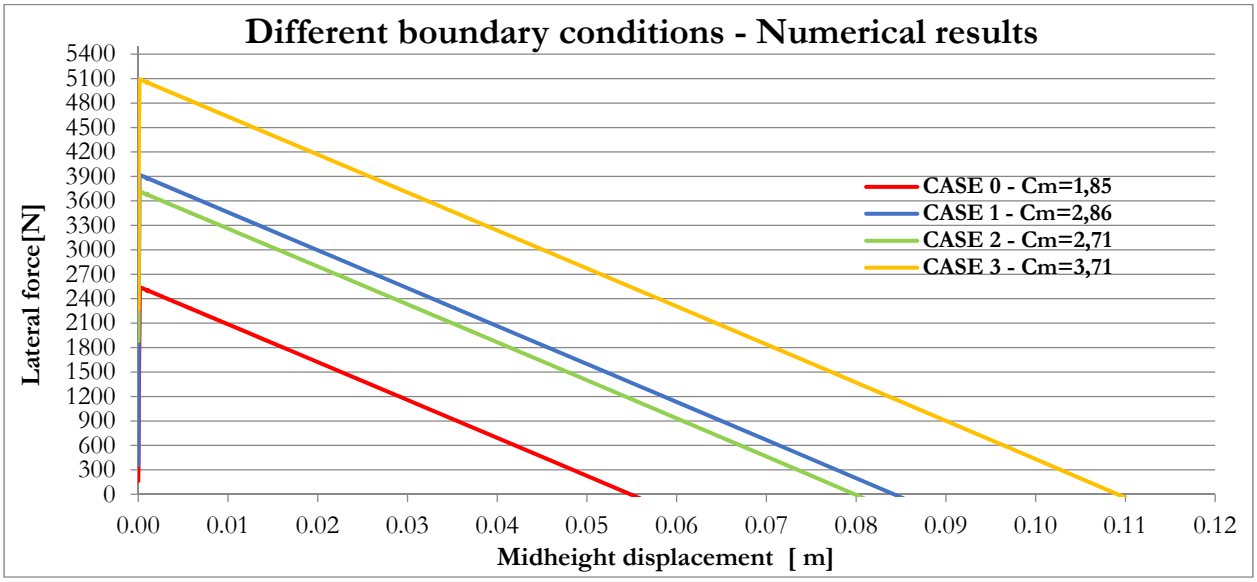

Figure 66 – Results of analytical formulas and numerical calculations on lumped cracking beams model, 17 kN overburden. Cm is the so called "seismic coefficient", which is reported on the legend of the figure.

The results describing the quasi-static behavior of the rocking wall system confirm that its inherent nonlinear nature may be explained in a great measure through stability considerations. Before resorting to an additional source of nonlinearity such as the physical resistance of the materials involved, the lumped cracking beams model is employed in some transient excitations. As explained in the modeling chapter, the energy consumption of the system will be entirely relegated to a fictitious damping defined at materials level.

First, an attempt is made to reproduce the experimental findings of Doherty on a real record, the Nahanni earthquake. The response of the numerical model to this excitation is found to be similar to the Doherty results (see Appendix A). Despite the differences in the number of peaks, the amplitude of the rocking oscillations is of the same order of magnitude and they do also occur at the same range of exciting frequencies. This is particularly true for the case where the wall is already pre-cracked at the mid-height cross section.

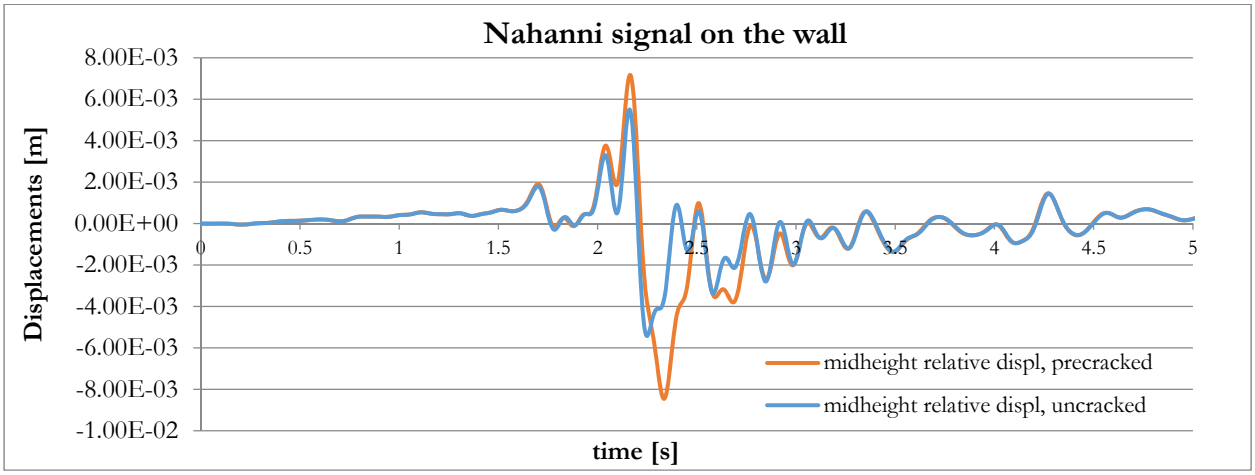

Figure 67 – Mid-height wall displacement resulting from the rocking motion caused by a Nahanni record base excitation.

Now a set of increasing harmonic base motions is applied on the supports of the wall system to analyze the rocking mechanism activation in relation to the magnitude of the top load and the forcing frequency. The signals adopted have three different forcing frequency: 15 Hz, 2.5 Hz and 0.5 Hz. For all walls, the pre-cracked situation is investigated. The case of zero force acting on top of a pre-cracked wall is shown below.

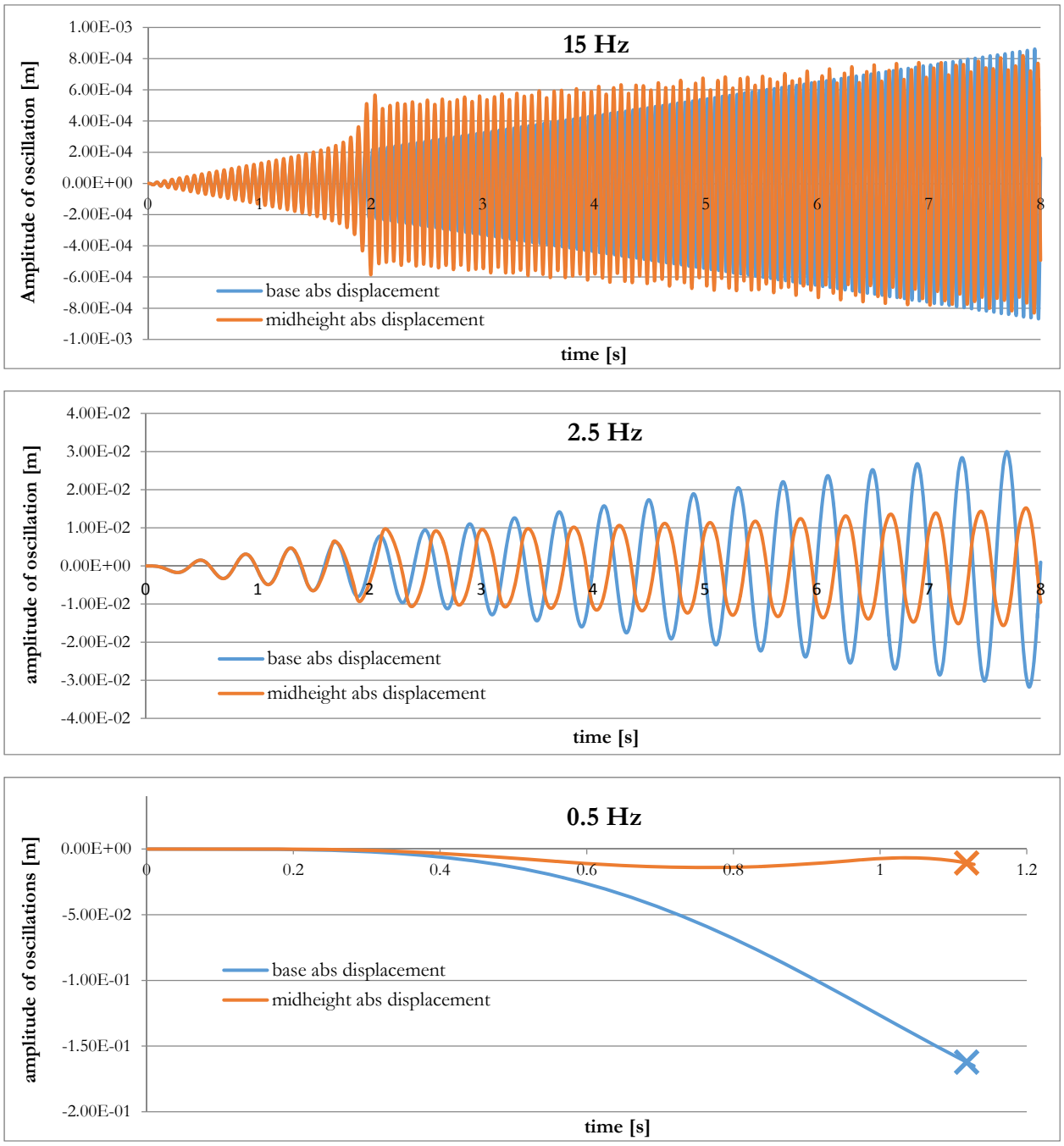

Figure 68 - Increasing harmonic excitations on the lumped cracking beams model. Absolute displacements at the base and mid-height.

The captions show the absolute displacements computed at the level of the base and the mid-height of the masonry wall. In order to elaborate on them the mid-height deformation of the wall relative to its supports is computed and

represented in the next pictures. It is possible to see that the signals with high frequency do not affect the stability of the wall for the whole duration of the excitation, which was set to 8 seconds. On the other hand, the opposite happens for the signal with a frequency of 0.5 Hz, for which the output curve stops much earlier than in the other examples. Indeed, soon after one second the wall loses its stability configuration due to the action of inertia forces. However, it is remarkable that the numerical solution diverges not when the theoretical instability displacement is reached at mid-height level, but in a later stage. Hence, Diana appears to be able to find a convergent solution even though the wall is failing. The lack of warning from the software on this matter will also be of concern for the upcoming analyses.

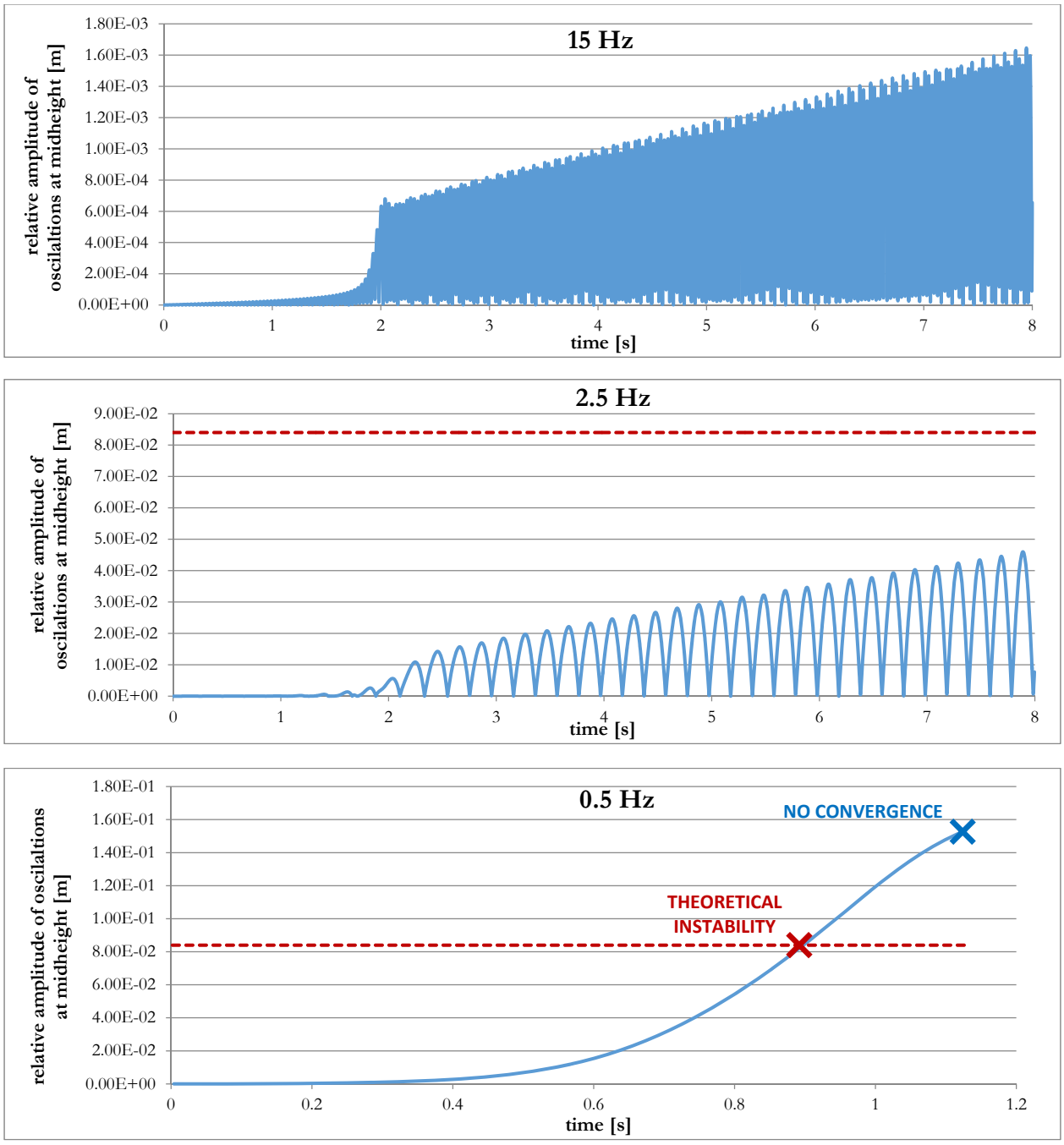

Figure 69 – Absolute mid-height relative displacement of the wall subjected to increasing harmonic excitations. The instability displacement is 0.084 m, which is less than the wall thickness due to the particular boundary conditions used.

The investigation on the effect of the top load continues by applying relatively small loads on the wall, namely 1 kN, 2 kN and 4 kN. Some representative results are plotted in the following captions representing the oscillations at mid-height of the wall relative to the base support. More results for different boundary conditions can be found in Appendix C of this report. Only the signals with forcing frequencies of 2.5 and 0.5 Hz are studied. Intuitively enough, the occurrence of rocking motion is delayed as the overburden load increases. As noted in section 2.3, the top load acts as a pre-compression force on the wall which prevents it from cracking.

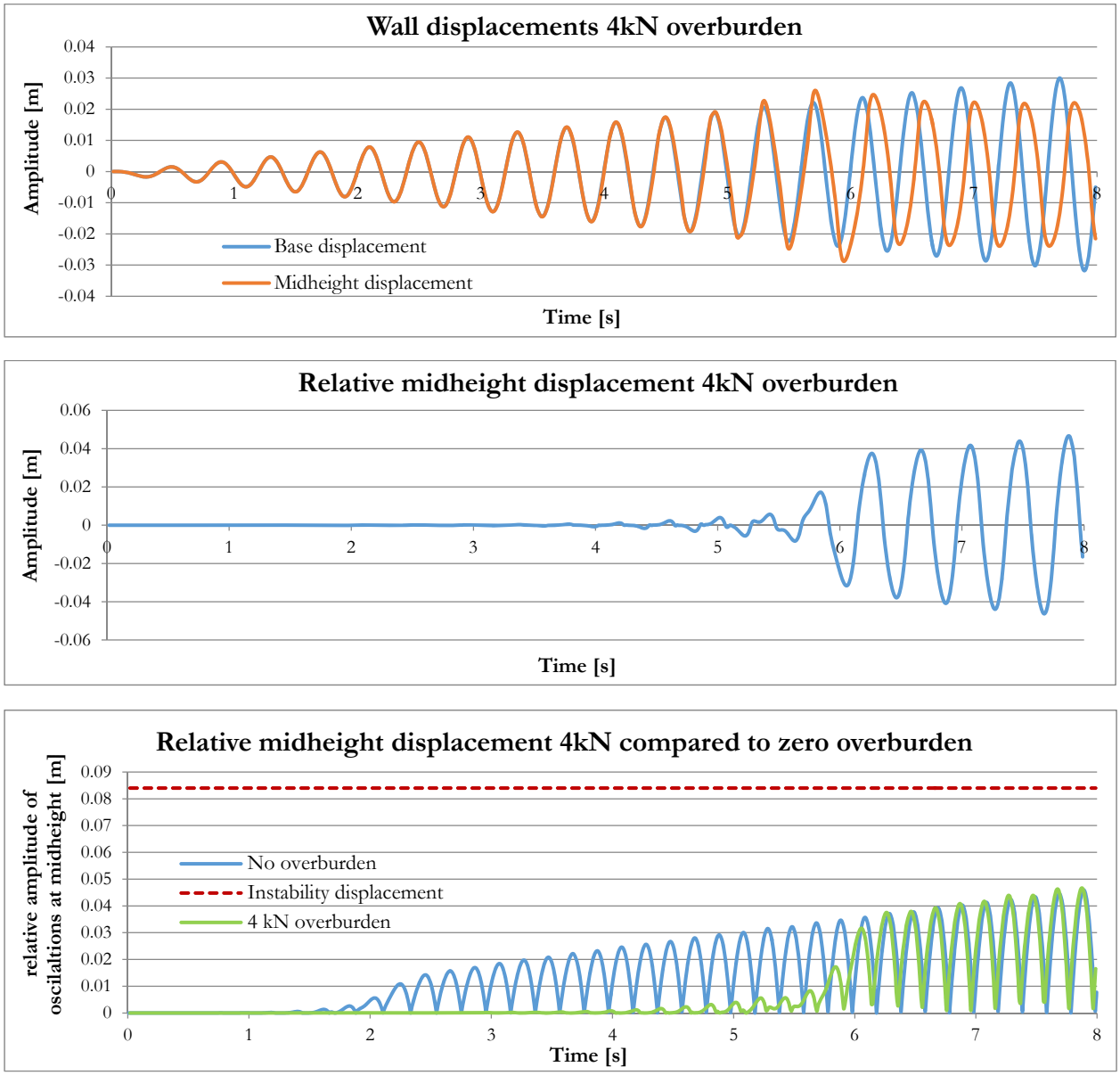

Figures 70 - Increasing harmonic excitation on 1,5 m tall wall. Overburden 4 kN, forcing frequency 2.5 Hertz.

The delayed occurrence of rocking compared to the case with no top load applied is visible in the last graph of the figures above. For a forcing frequency of 2.5 Hz the inertia force acting on the wall is far from affecting the stability of the wall even for accelerations in the order of 0.7g. On the contrary, a much smaller acceleration of around 0.25g is sufficient to cause instability of the system when the forcing frequency is 0.5 Hz, as presented in the following captions. An important remark should be made here. Earlier in this section it was noted that Diana is not able to warn the user when an instable configuration of the system is reached, and a numerical solution of the dynamic problem might be

found for several steps before the actual divergence occurs. This aspect may be seen as a real limitation to the study of the OOP behavior of walls since a transient analysis would potentially continue for an undetermined number of steps regardless of the wall integrity.

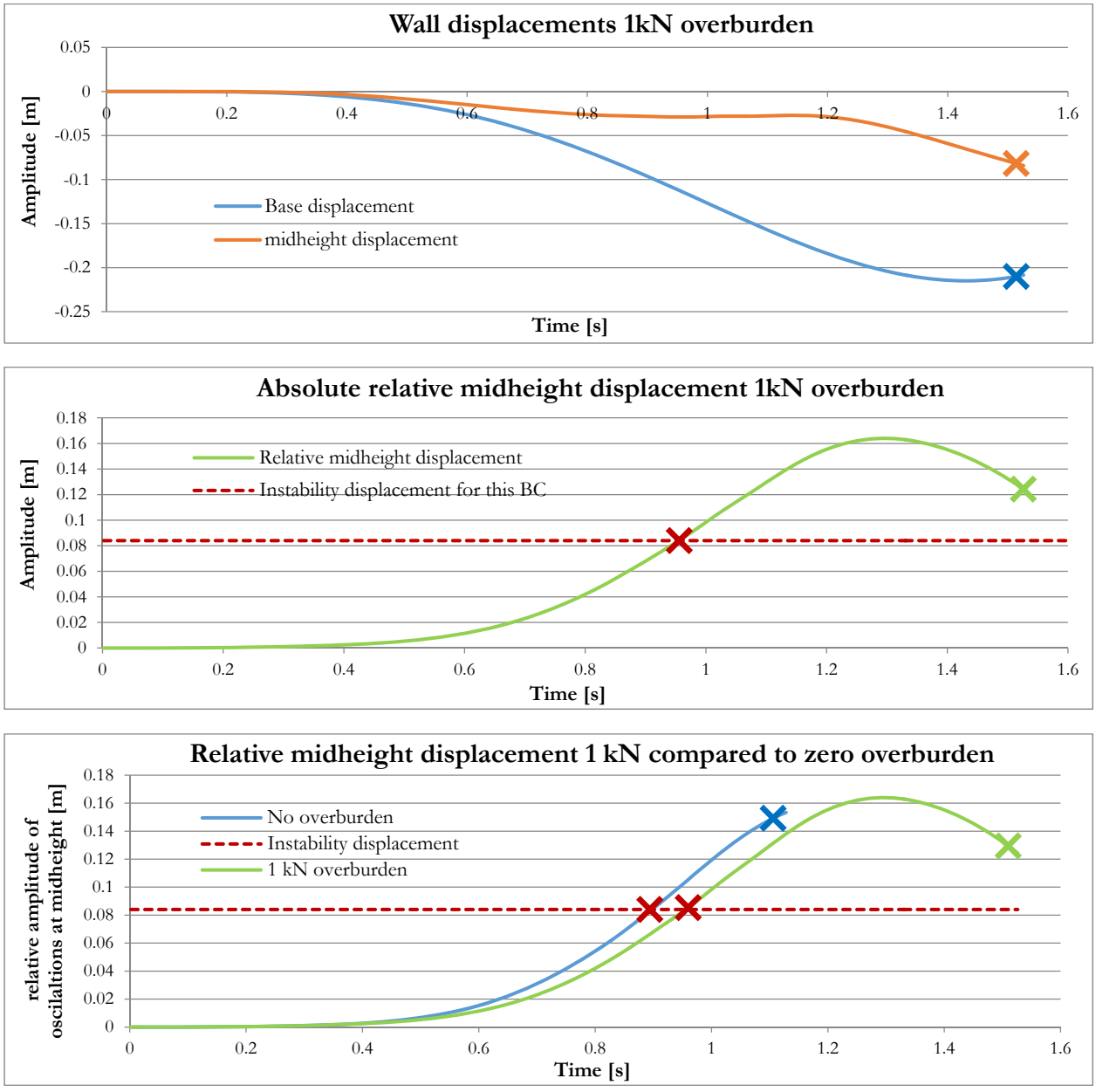

Figure 71 – Increasing harmonic excitation on 1,5 m tall wall. Overburden 1 kN, forcing frequency 0.5 Hertz.

As a consequence of that, the role played by the post-processing of the analyses results is of a crucial importance. If from one side it is true that convergence of results may be found for instable configurations of the wall, the development of total horizontal and vertical reaction forces at the supports may be of help to spot sudden variations of forces which occur at the moment the wall loses its stability. In the case at matter this is particularly true for the variation of the horizontal reaction forces. In the graphs illustrated so far the X marks in red represent the theoretical static instability displacement of the wall for the given boundary conditions whereas those with a different color identify the actual numerical divergence of the analysis performed through Diana.

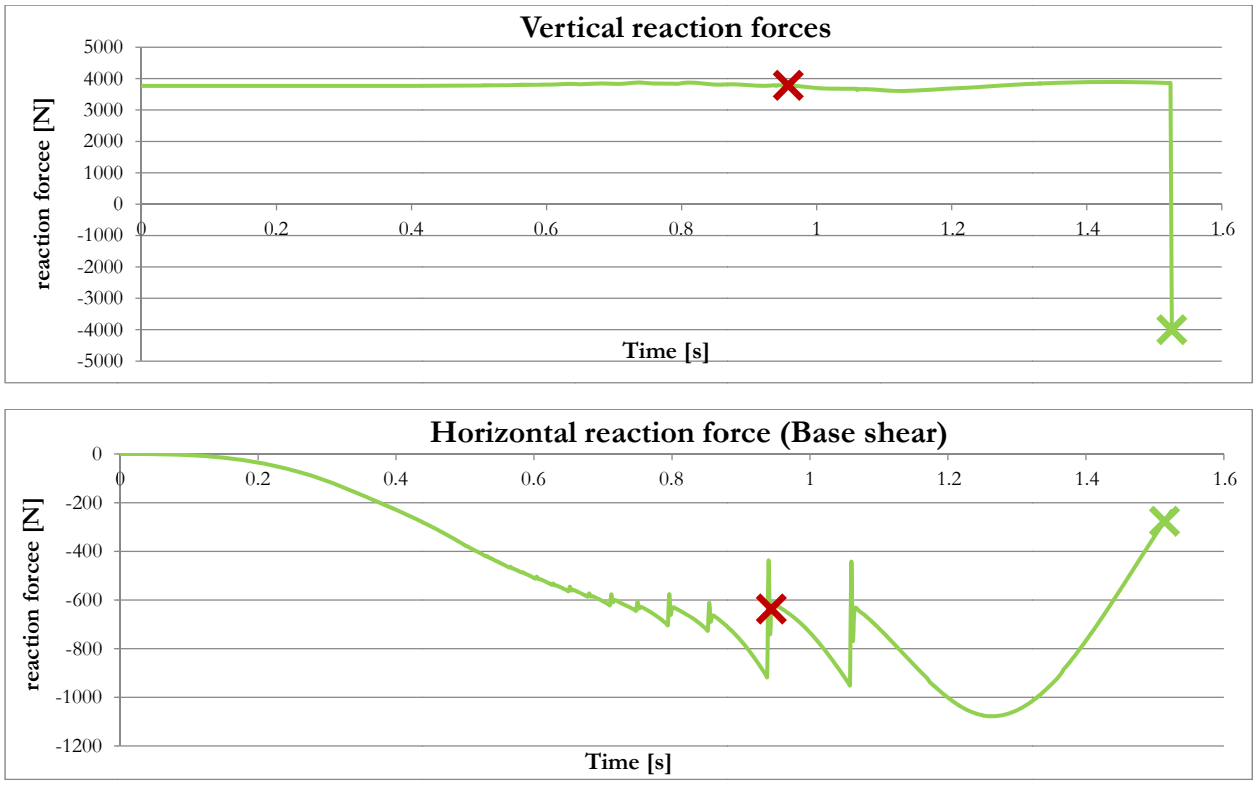

Figures 72 – Development of the horizontal and vertical reaction forces for the case of 1 kN overburden and 0.5 Hz.

In general, the control of the convergence criteria seems to be problematic when running transient analyses on this model. In fact, in addition to the limitations mentioned above, the model tends to be subjected to random divergence even for signals of a very small amplitude. After having performed several analyses, it was concluded that the difficulty to control the transient solution is mainly caused by two factors: the intrinsic numerical instability of the model and the lack of stiffness-related damping associated with the no-tension interfaces used at the bottom, mid-height and top of it.

The first aspect is related to the fact that this model tries to emulate the simplifications of analytical approaches used to assess the wall stability. These are, above all, the infinitely rigid cross sections and the cracking elements with zero tensile resistance. Assembling elements with opposite extreme properties as such may well lead to a finite elements model prone to numerical instability phenomena. Secondly, it was also noted that the system tends to accumulate energy in the vertical direction as the rocking cycles follow one another. The rigid cross section hit each other at the end of the their length and this dynamic and repetitive impact makes the rigid bodies to lose contact and start "bouncing". A caption representing this issue can be seen in the picture provided. This accident may be related to the fact that the interface no-tension elements adopted for this model do not give a contribution to the numerical damping of the model in the vertical direction, being their stiffness zero. Hence, the system accumulates energy in that direction and the wall parts start floating in Diana until the software is no longer able to find a convergent solution. For this reason it was decided to perform dynamic analyses for the most part in frame models where the wall system is encased in a structural cage that restrain its parts in the vertical direction.

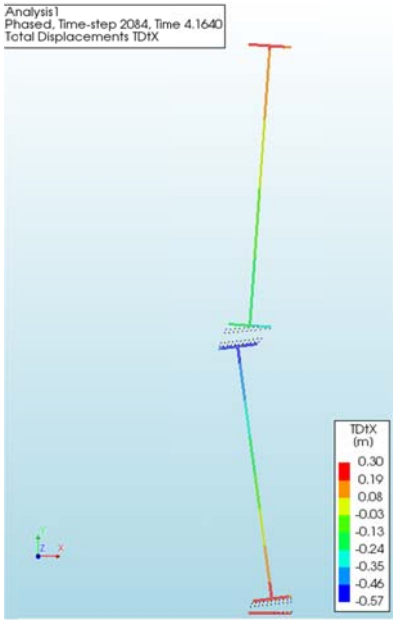

Figure 73 – Energy accumulated in vertical direction: loss of contact of elements.

5.2 Smeared cracking plane strain model

The numerical definition of the masonry wall by means of plain strain elements was undergone in parallel to the generation of the smeared cracking beams model. Thanks to the ease of implementation in the future frame model the smeared cracking beams wall was made object of several sensitivity investigations while the application of the model at matter was limited to finding the appropriate amount of integration points necessary along the thickness of the wall. The figure below shows a quasi-static analysis performed on the smeared cracking plane strain model with a variable number of integration points ranging from 3 and 11 corresponding to the minimum and maximum amount which is possible to use for a single CL9BE finite element. There are two areas that requires attention: the initial resistance of the wall to the lateral load applied and the maximum mid-height displacement that can be achieved by the wall. It appears from the diagram that for a number of three integration points only the lateral resistance of the wall is considerably overestimated (around 30% more) and, therefore, this amount of points should not be used. When the integration points entered in the model are increased to five or seven, the resistance to lateral loads goes back to acceptable values but the maximum mid-height displacement exceeds the theoretical stability configuration. As a matter of fact, a wall displacing more than its thickness (0.11 meters for the case analyzed) is not realistic. Hence, using nine or eleven integration points seem to be the only two options available. Although they do slightly differ with regards to their impact on the displacement capacity, both solutions are possible. However, sources in relevant literature recommend the use of eleven integration points as a minimum number along the thickness of a wall for which the rocking motion is investigated. For this reason, the maximum amount of integration points will be applied to the CL9BE elements for the next models of this research.

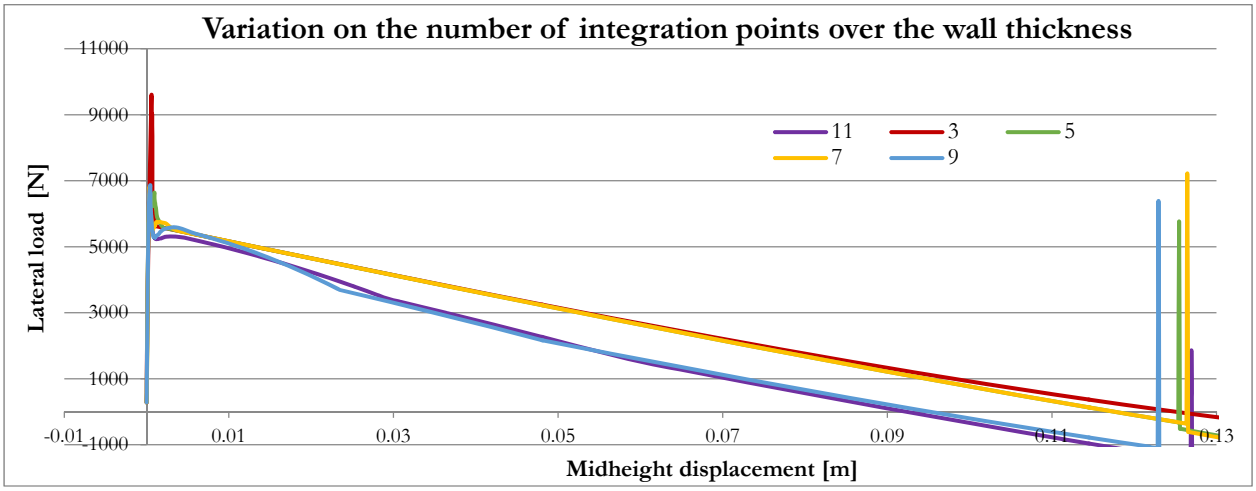

Figure 74 –Variation on the number of integration points used along the thickness of the wall.

It is noted that only the results obtained for a constant load on top are illustrated, the case of a top load applied through a spring leading to the same conclusion. Also, the parameters related to the tensile resistance of the masonry are related to considerations addressed in section 5.3.2. More in detail, in that section it will be justified the decision to assign a tensile resistance of 0,15 MPa and a cracking energy of 7 Nm to the unreinforced masonry material.

5.3 Smeared cracking beams model

This section may be considered as an introduction to the last wall model developed. Before the modification in size, the model of 1,5 meters in height was used to estimate the impact given by hinged connections at the wall ends, the mesh objectivity and an the tension softening model adopted for the cracks development. Moreover, it was verified whether the application of a spring on top of the wall for applying the overburden would act as expected.

Impact of the spring element on top

Given the one-dimensionality of the model, it was questioned whether the possibility of applying a spring on top of the wall would lead to tension forces in its displayed configurations. In order to check that, the vertical displacement of the node at the top of the wall was tracked as the rocking mechanism developed. At some point of the deformation the top

node indeed starts lowering. However, much before the point the spring would undergo tension stresses the wall fails out of its plane due to instability. Thus, overburden applied through the application of a spring are not of concern.

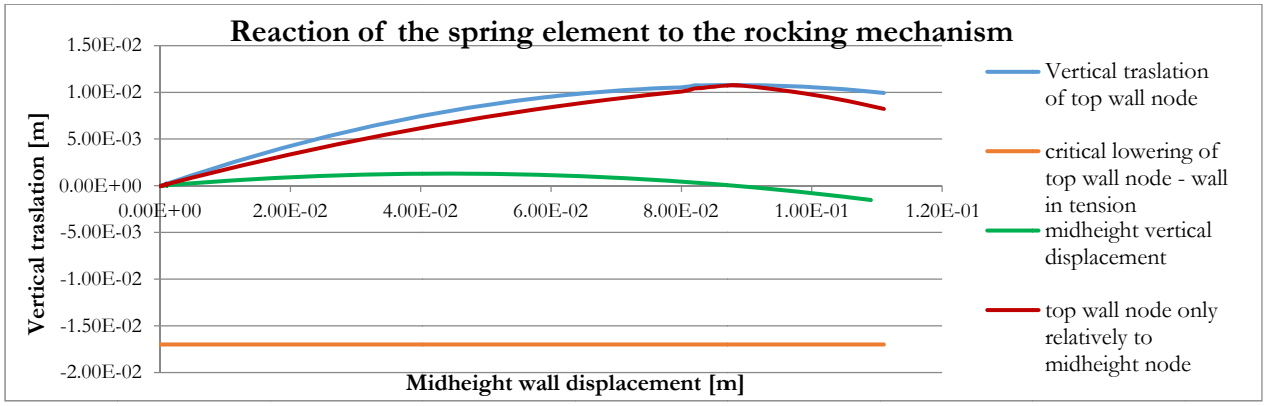

Figure 75 – Reaction of the spring element to the rocking mechanism for the smeared cracking beams model.

Hinged ends

The application of hinges at the wall ends implies that the boundary conditions of the structural problem change and the wall parts are only able to rotate around their mid-thickness. This case corresponds to that depicted in the table of the New Zealand Code labelled as Table 2 in this report. As suggested by analytical approaches, the instability displacement of the masonry wall simplified with the rigid bodies theory should correspond to roughly half the wall thickness, which is this case is 0.11 m. This circumstance is very well matched by the output depicted in the following graph. If hinges are used, the maximum lateral load the wall is able to withstand is much lower than in the clamped-clamped case and the instable configuration is reached for displacements equivalent to half the wall thickness. The graph also presents the effect of the crushing phenomenon occurring at the level of the wall mid-height: the wall section deteriorates and the lever arm of the forces for the equilibrium of moments decreases. As a result, the instable configuration is reached even earlier. More details on crushing will be given later.

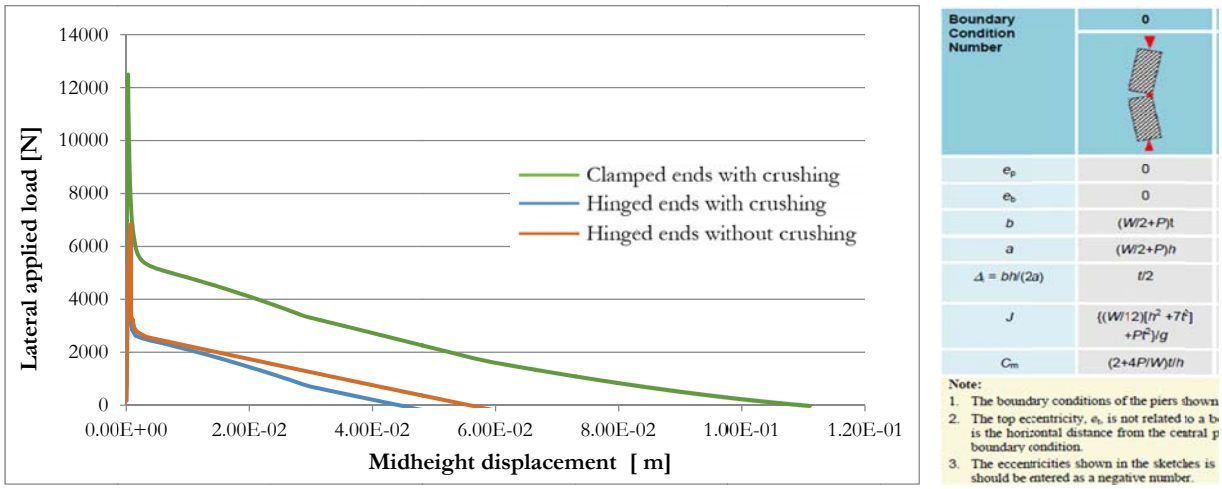

Figure 76 - Effect of hinged ends on the wall and crushing: smeared cracking beams model 1.5 m, 17 kN overburden.

Mesh objectivity

The appropriate mesh refinement along the beams composing the wall representation is addressed in this paragraph. Again, the wall cross sections experiencing nonlinear phenomenon to a greater extent are those around which the wall parts rotate. While the mesh refinement investigation is reserved for the beam elements in those areas, the wall parts acting essentially in a linear way are kept constant to 1 finite element only. So, if the nonlinear wall parts are divided in 5

parts each, there would be 5 x 4 + 2 = 22 elements in total. After the wall peak lateral resistance is overcome, its capacity to withstand horizontal loads lightly increases for the coarse meshed wall, showing a small bulge before decreasing to zero with the same trend as in more refined cases. Also, the wall elastic resistance to lateral deformation is a bit underestimated. Using more refined mesh leads to more accurate results. Thus, it is chosen to make use of 22 elements.

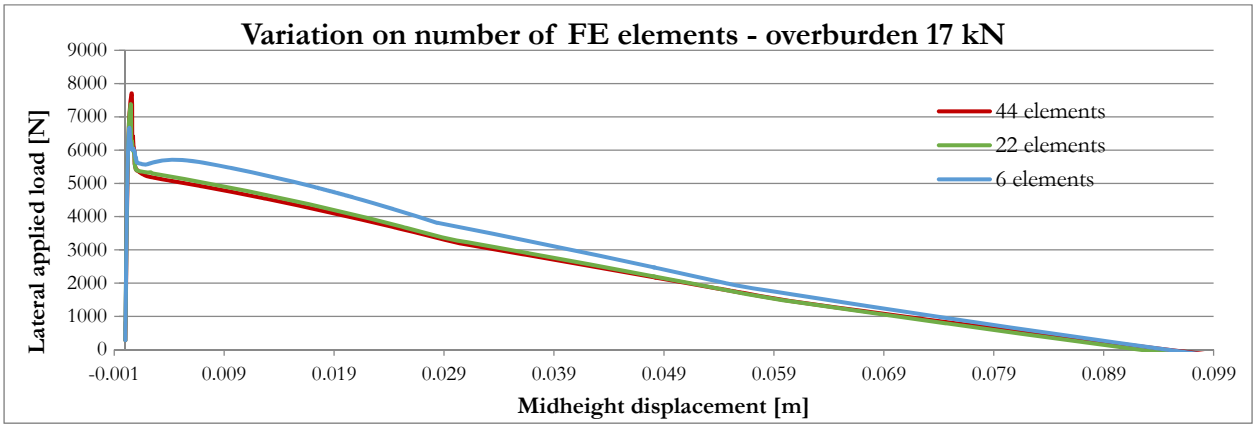

Figure 77 – Variation on the number of finite elements used: mesh objectivity on the smeared cracking beams model. Note that for this analysis a tensile strength of 0.15 MPa and a crack energy of 7 Nm was used. Their use is justified later on.

Tension softening/brittle behavior

Diana offers various tension softening models for the tensile resistance of the materials. Three alternatives were analyzed for the smeared cracking beams model: linear and Hordijk curves and brittle behavior. Comparison was also made to the output obtained in case of rigid bodies approximation. Reasonably enough, the initial elastic resistance to lateral deformation of the wall presents a peak if a tension softening model is supplied to the model. Resorting to a Hordijk softening type seems to have a beneficial effect on the maximum mid-height displacement that the wall is able to reach in spite of a small decrease in the initial peak resistance of the system, which is believed to be underestimated. Decision is made to apply from now on the linear tension softening model to the material as the results are similar to the other cases. In terms of computational costs and numerical stability however, the latter model guarantees a better performance for the future transient analyses.

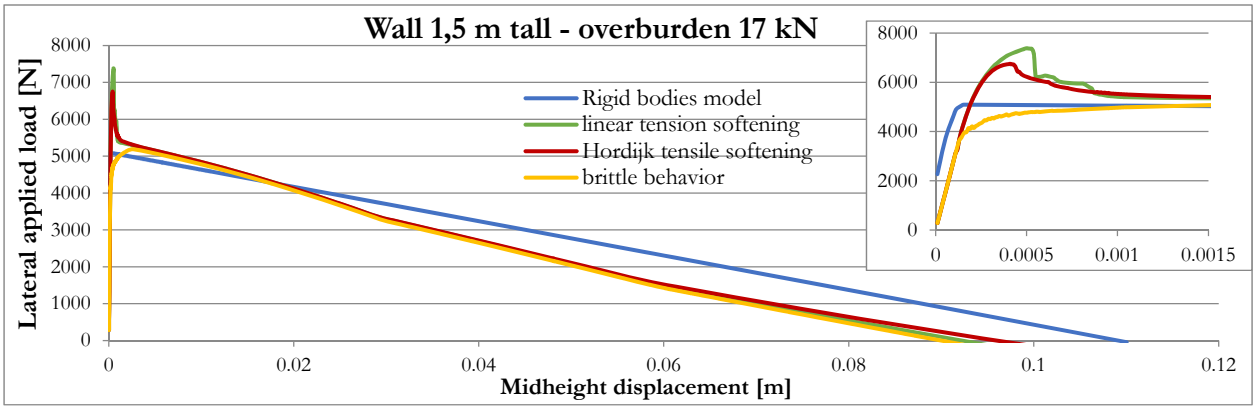

Figure 78 - Different tensile resisting models for crack development, 1.5 m wall, 17 kN.

Hysteresis

An attempt is made to capture the hysteretic behavior for the finite elements representation of the unreinforced masonry wall developed in this section. This means that the system response to the lateral horizontal action should be affected by the level of material damage in cyclic analyses. Thus, this section deals with an increasing pushover analysis on both sides

where the masonry is expected to degrade due to crushing of its extreme fibers. As a result, the thickness of the wall at mid-height decreases and this phenomenon should be visible in the F-Δ curve. The analysis output is plotted hereunder.

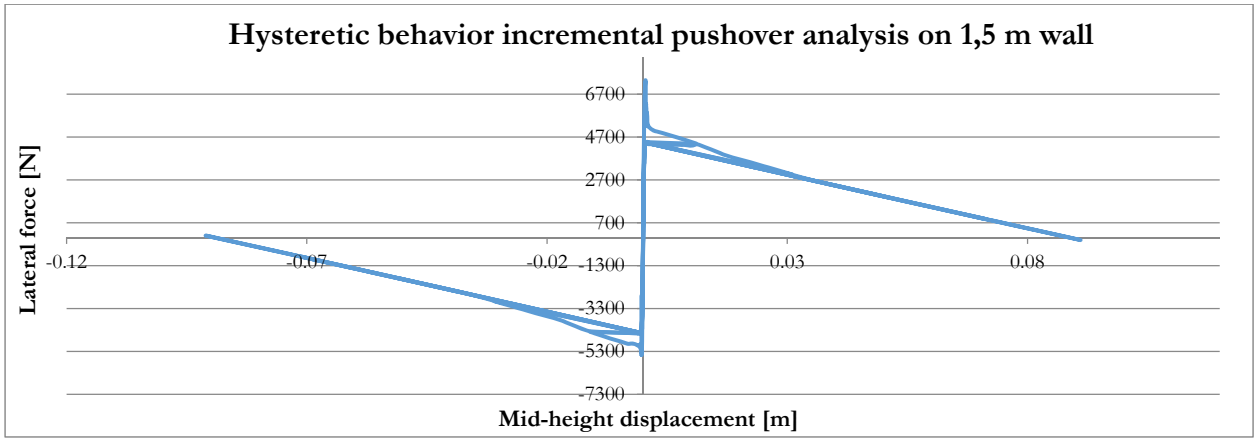

Figure 79 - Hysteretic behavior of the unreinforced masonry material on the wall subjected to the Nahanni excitation.

The force displacement curve obtained is derived mainly through considerations on the equilibrium of forces characterizing a stability problem. This explains why the graph obtained presents a behavior that can be generally classified as *nonlinear elastic*, meaning that the curve shape remains always the same. However, the hysteretic behavior for the OOP behavior is reflected, for the case at matter, by the slight translation in the bottom-left direction of the curve after every cycle. Note that only the first cycle on both sides present a peak due to the initial cracking tensile resistance of the masonry. A caption representing the initial pushover steps of one cycle is available in Appendix D.

5.3.1 Sensitivity study on material parameters

This section presents the results of all the analyses performed on the latest unreinforced masonry wall model, 3 meters tall. These will serve as a mean for validating the model as well as for justifying its later use in the expanded frame schematization. Several material parameters were investigated to study their impact in the nonlinear behavior of the wall. This sensitivity study will lead to the choice for the most appropriate set of parameters to discretize the structural system with respect to its numerical efficiency and accurateness.

It is decided to use the smeared cracking beams model for the NLTH analysis of the frame structure. For this reason the wall model needs to be scaled to a realistic size since the previous dimensions were adopted to reproduce the experimental settings of the Doherty research for comparative reasons. Scaling the model to 3 meters high and 200 millimeters thickness wall evidenced an unexpected behavior of the model.

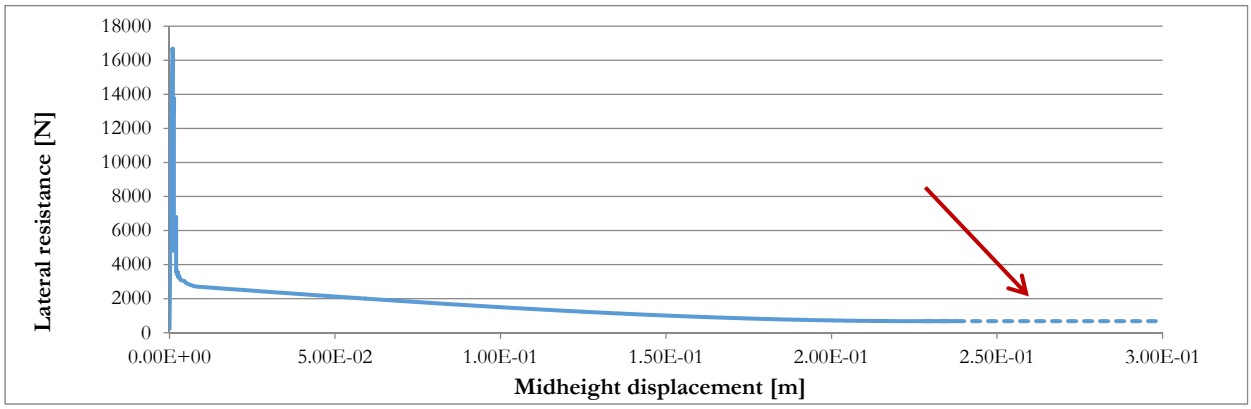

Figure 80 - Force-Displacement diagram for the 3m high URM wall. Smeared cracking beams model. 5 kN overburden.

It can be noted in fact that even though all material properties and boundary conditions are kept constant with respect to the 1,5 m tall wall, the model scaled to a height of 3 meters presented much larger deformation capacity when subjected to a pushover analysis. While rocking, the stability of the wall system is ensured by the equilibrium of forces and corresponding moments: as the mechanisms develops towards the instability displacement, the lateral capacity is expected to decrease to zero. Initially, this was not the case for the scaled smeared cracking beams model, as it can be seen from the graph above. It can be stated that this behavior may not be a problem in view of a dynamic analysis due to the fact that the remaining lateral capacity of the wall at the theoretical point of instability is around 15% of the initial one. The inertia forces acting on the wall at such level of deformation would likely cause it to fail anyway. However, an attempt is done to correct this aspect and improve the model reliability. Hence, a number of quasi-static analyses was carried out to identify the parameters responsible for this particular behavior. It is underlined here that the theoretical instability displacement, for the given boundary conditions of this model (clamped ends) is equal to the thickness of the wall itself.

Variation of the shear retention factor

At first, there are suspects of a shear locking phenomenon occurring in the model. It appeared that the shear retention factor in the definition of the nonlinear masonry material, which was up to now considered with its default value on Diana, has indeed quite a significant impact on this matter. By increasing its value from 0.01 to 0.1 the trend of the lateral resistance is even more inconsistent to the real behavior as not only it does not reach zero, but it increases as it get closer to the instability displacement. On the other hand, decreasing the shear retention factor by a factor 10^{-2} results in a lower resistance curve which still does not goes to zero. The same behavior is observed also for much smaller values of the shear retention factor. Using a damaged-based model to describe this factor also proved not to be of any help.

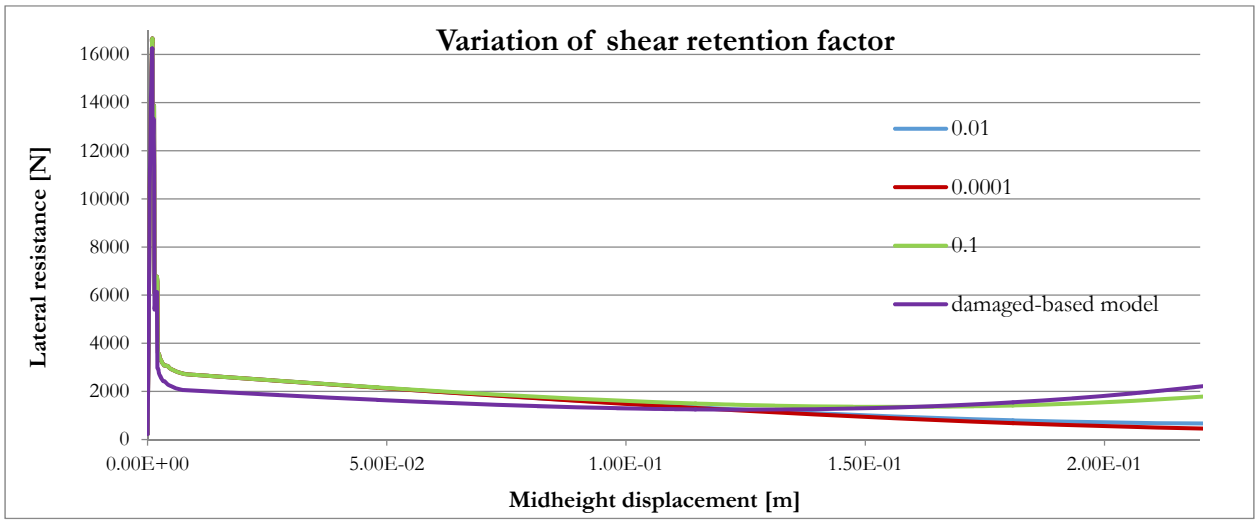

Figure 81 - Variation of the shear retention factor for the smeared cracking beams model. 5 kN overburden.

It is noted that the red, green and blue curves follow the same trend until around 0.06 m so that the graphs are essentially overlap until then. It may be concluded that, although the shear retention factor has a relevant impact in the final part of the force-displacement curve, it is not able to fully correct the infinite stability of the system which manifests for very small lateral forces applied on the wall.

Applied overburden

Varying the applied vertical force on top of the wall showed that this problem may be related to the energy required by the crack to develops in the masonry. In other words, for a larger magnitude of applied overburden the masonry experiences crushing and the hinges generated at the level of the cracks shift towards the inner side of the cross section. The damaged cross section has a smaller thickness compared to the undamaged one, and the instability displacement is reached earlier. Indeed, for large top loads, the wall system succeeds in achieving the instable configuration. This is illustrated in the figure below.

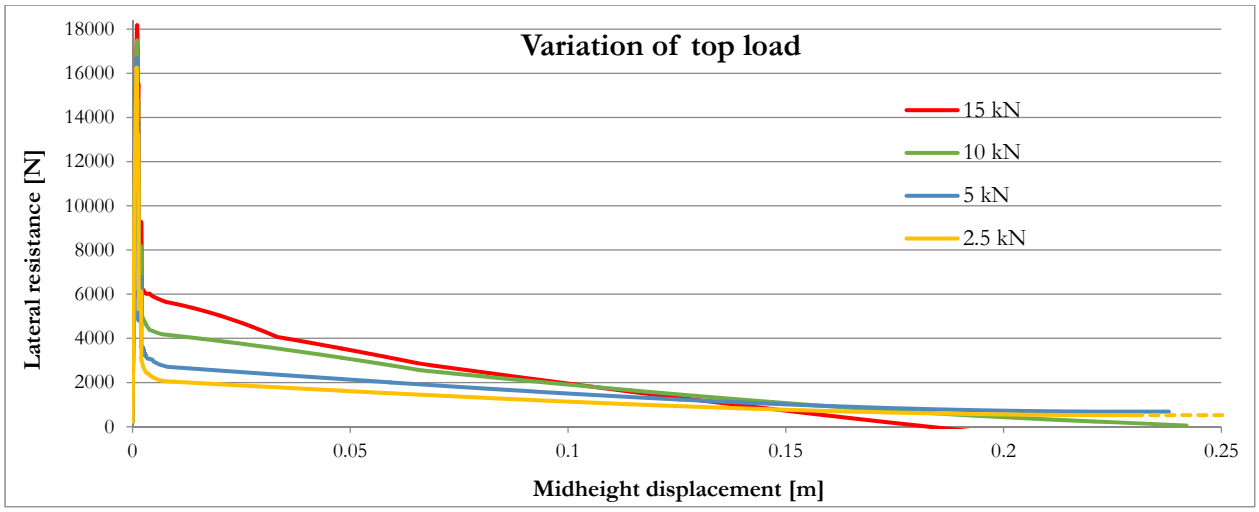

Figure 82 - Response of the smeared cracking beams model for different magnitude of top loads. 3m wall.

The system which experience less "pre-compression" on top requires more energy from the lateral load to enable the rocking mechanism of the wall members. The trend described by the tail of the diagram still is unrealistic. Further investigations are necessary to correct the model parameters and reach the zero lateral resistance of the wall system. Still, it is noted that the model acts as expected with regards to the total energy required to display the system horizontally: the larger the top load (which originates a stabilizing moment at first), the larger the energy needed. This is represented by the larger area beneath the curves.

Cracks orientation

An additional step made for this investigation was related to how the cracking model adopted influences the behavior of the wall system. There are three options available on Diana for the total strain cracking model. Their difference lies in the orientation of the developing crack, which could be fixed, rotating or a combination of the two. It is interesting to plot the behavior of the wall system for the two extreme cases for deformations beyond the theoretical instability of the wall. This may help to have a broader understanding of the impact of parameters variations in the model.

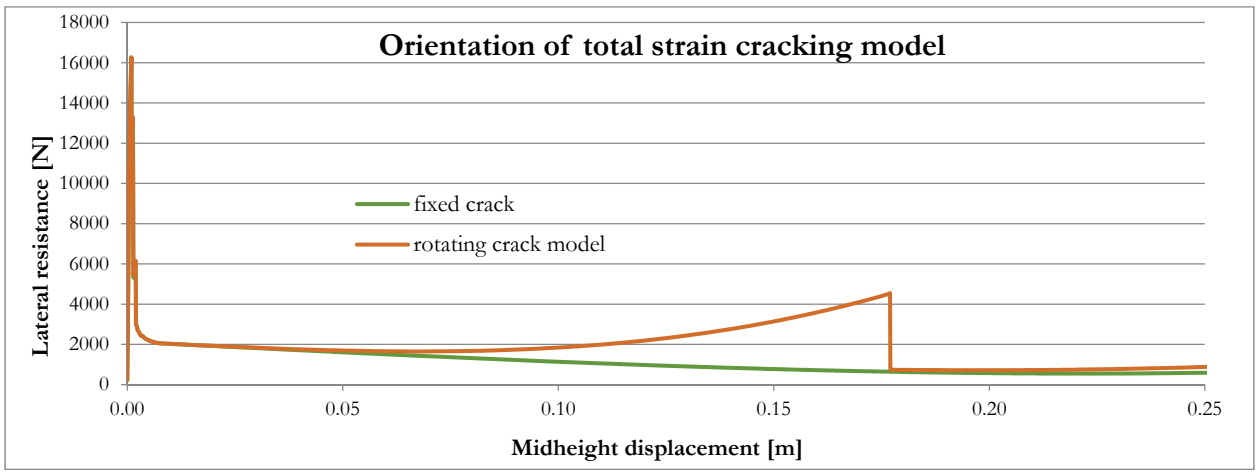

Figure 83 - Different models for the total strain cracking approach, 3m tall wall, 5 kN overburden. Note: the peaks overlap.

When the lateral resistance of the system reaches zero, the wall should be considered to have failed due to its instable configuration. From the illustration above, it is clear that the wall still presents a much larger deformative capacity than 0.2 meters for both approaches. However, it is evident that the latter case requires a large amount of additional energy to alter the orientation of the cracks, while the fixed cracking presents a more regular trend until the point it necessitates a

rather large quantity of energy to overcome what appears to be an obstacle to the cracks widening. It may be assumed that the cracks developing at the bottom, top and mid-height of the wall propagates along a single plane only and, as a consequence, that they have fixed orientation. Alternatively, it is also possible that this unexpected behavior is caused by numerical problems in Diana. This justifies the choice of relying on this cracking model, but leaves unsolved the problem of the wall displacement capacity. The positive impact of the fixed crack orientation in the model is also confirmed by the results obtained for the 1.5 m tall wall model.

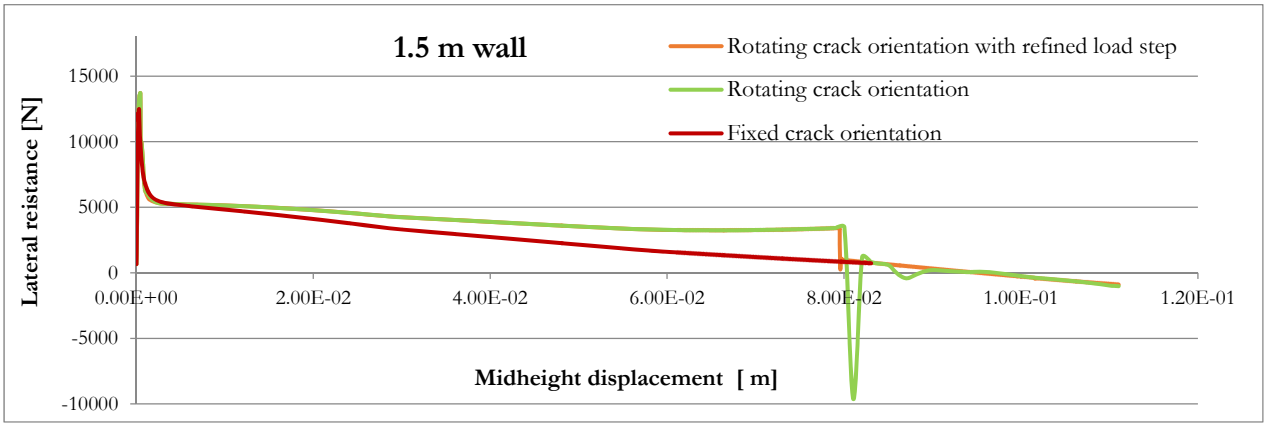

Figure 84 – Effect of rotating crack model on the 1.5 m tall wall, 17 kN overburden. Note: green and orange peaks overlap.

Crushing and cracking of masonry

In this section the impact on the FE model for the crack and crushing parameters of the nonlinear masonry material is evaluated. The reference values used are presented in the table hereunder together with the range of parameters adopted. This means that while a parameter is being varied, all the rest are assigned to the value given in the table unless otherwise stated. Due to the fact that the following document has a speculative background and as it is not accompanied by experimental findings, many of the model parameters related to the strength of the masonry were deducted by literature.

E [N/m²]	Compression curve [-]	Tensile curve [-]	ν [-]	f_t [N/mm²]	G_f [N/m]	fc [N/mm²]	Gc [N/m]	Shear retention [-]	Crack model [N/m]
$5.00 \cdot 10^9$	Parabolic	Linear	0.2	2.50	35	4.50	5000	Constant, 0.001	Fixed, Rots
Range f_t		Range G_f			Range fc			Range Gc	
0.15 Mpa – 0.45 Mpa		25 N/m – 40 N/m			2.50 Mpa – 8.50 Mpa			2000 N/m – 10000 N/m	

Table 27 - Sensitivity study on strength parameters. Reference values and range of investigation.

The variation of the material parameters is mainly based on the studies of Lourenco as reported in his PhD thesis (Lourenco, 1996), but also on those commonly used in the research programs conducted by EUCENTRE and TU Delft (2015) in the last few years which are also focused on the masonry type distinctive of Groningen (URM walls made of calcium silicate bricks). Unless specified differently, a top load of 5kN is applied in the next analyses. The table above also reports the range of investigation used for the sensitivity analysis concerning the compression and tension strength of masonry, two aspects that will be dealt with in the following paragraph.

The energy released during the formation of a crack may be quantitatively identified as the area delimited by the tension softening curve adopted to describe the nonlinear response of the masonry in tension. Since the rocking mechanism of the wall implies the creation and widening of cracks through the whole thickness of the wall section, it is interesting to check to what extent the cracking energy chosen for this model determines its resistance. Although in previous sections it was chosen to make use of the fixed orientation cracking, the influence of the cracking energy is evaluated on the rotating model as well.

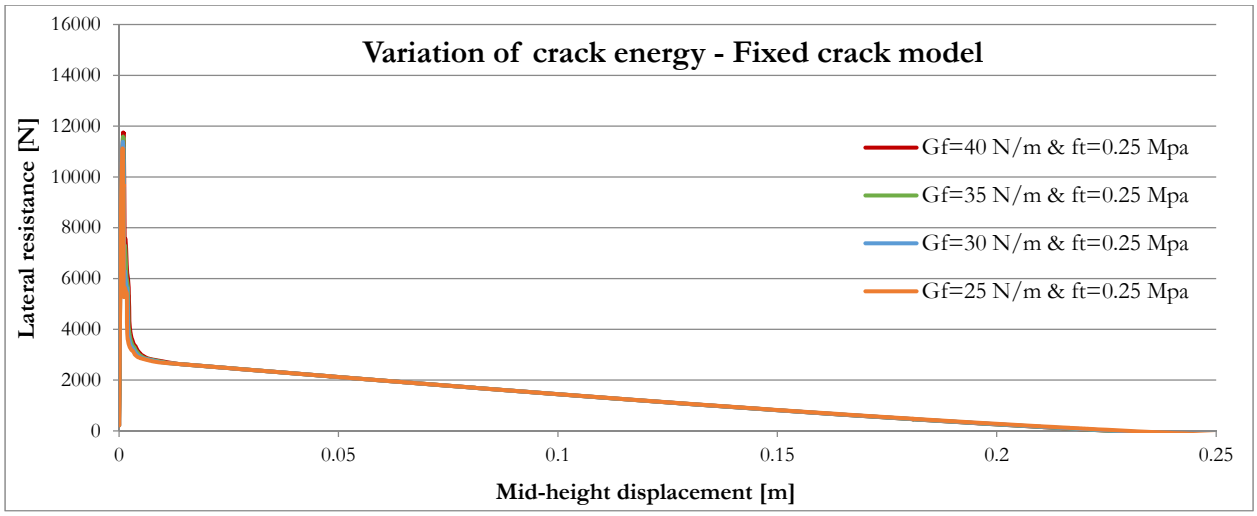

Figure 85 - Sensitivity study: variation of cracking energy on the model of 3 meters – fixed crack model.

Figures 85 and 86 show the lateral horizontal force that the wall is able to withstand as a function of its displacement at mid-height. The variation of the cracking energy parameter has an impact in the first and last part of the diagram. However, only the portion related to a positive value of the lateral force is meaningful for the pushover analysis. Zooming in to the initial steps, it is clear that modifying the cracking energy has a relatively small impact on the peak lateral capacity of the URM wall, whereas it does not affect at all its behavior around the instability displacement.

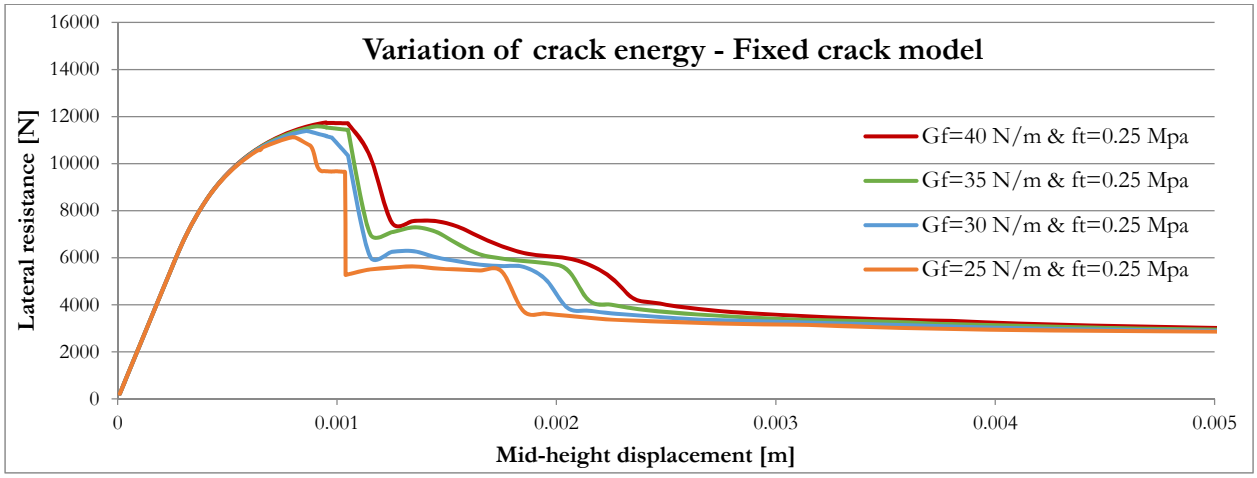

Figure 86 - Sensitivity study: variation of cracking energy on the model of 3 meters – zoom-in of figure 82.

In a similar way the rotating crack model does not lead to much different results. Zooming in on the first portion of the diagram, which correspond to the formation of the hinges on top and bottom of the wall, produces the same graph of figure 86. However, in a later stage, the higher cracking energy corresponds to a slightly larger lateral capacity. This is visible in the second caption of figures 88. As expected, also in this last case the parameter at matter did not greatly affected the behavior of the curve in its descending branch.

Next page also presents the resulting trends of the force-displacement diagrams in case of crushing energy variation. It is clear that for the given top load the wall behavior is not affected at all by the variation of this parameter in the range 2000 N/m to 10000 N/m. The latter stands also for the stage of cracks formation, in the beginning of the rocking mechanism. However, it might be the case that the overburden acting on top of the wall is not sufficiently large to cause enough crushing of the material and to capture the impact of a larger crushing energy. Figure 90 shows the same study using a larger top load of 15 kN. The larger overburden induces crushing over the thickness of the wall, thus slightly

decreasing its displacement capacity from around 220 mm to 190 mm. This findings are in accordance with the results represented in figure 85. With regards to the crushing energy, applying a larger top load points out the role played by this parameter: the curve in the force-displacement diagram exhibits a little more lateral capacity for a higher value of Gc.

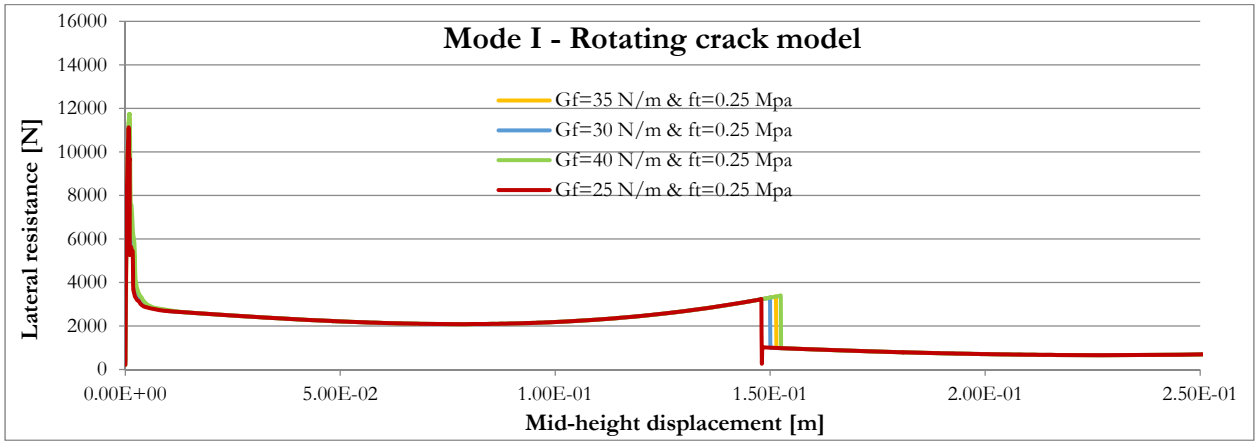

Figures 87 - Sensitivity study: variation of cracking energy on the model of 3 meters – rotating crack model.

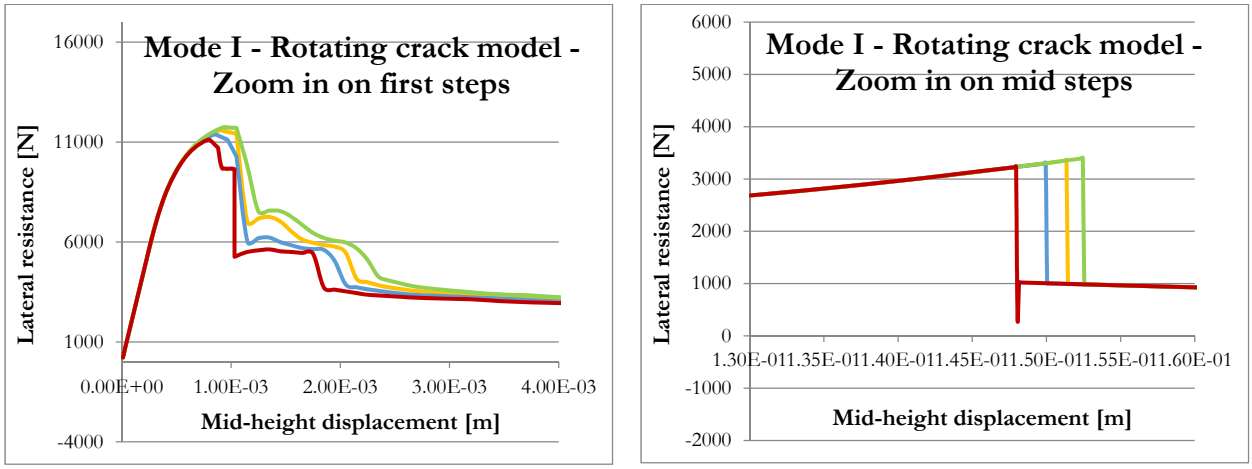

Figures 88 - Sensitivity study: variation of cracking energy on the model of 3 meters – zoom-in of figure 84.

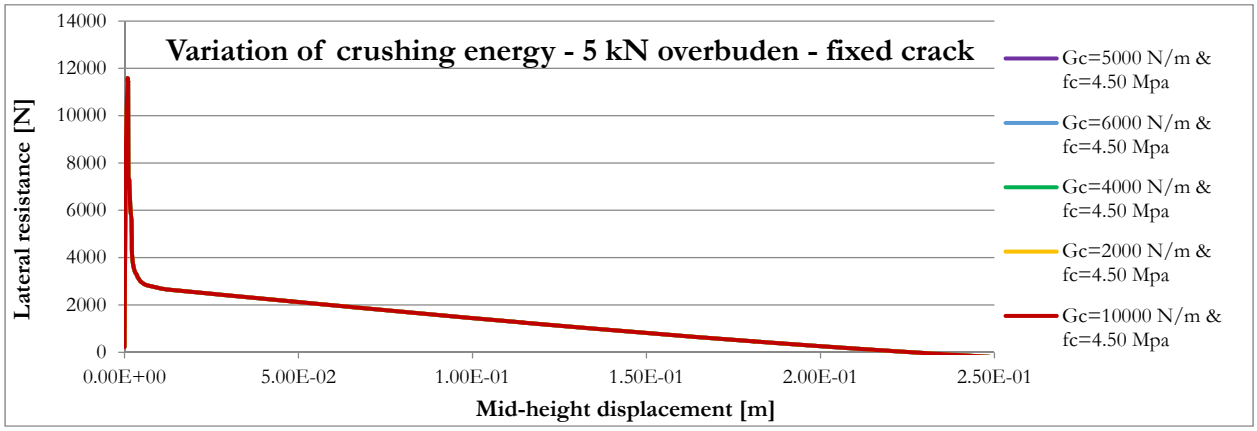

Figure 89 – Modification of the energy related to crushing of masonry material has no effect on the 3 meters tall model. Note that all the curves overlap.

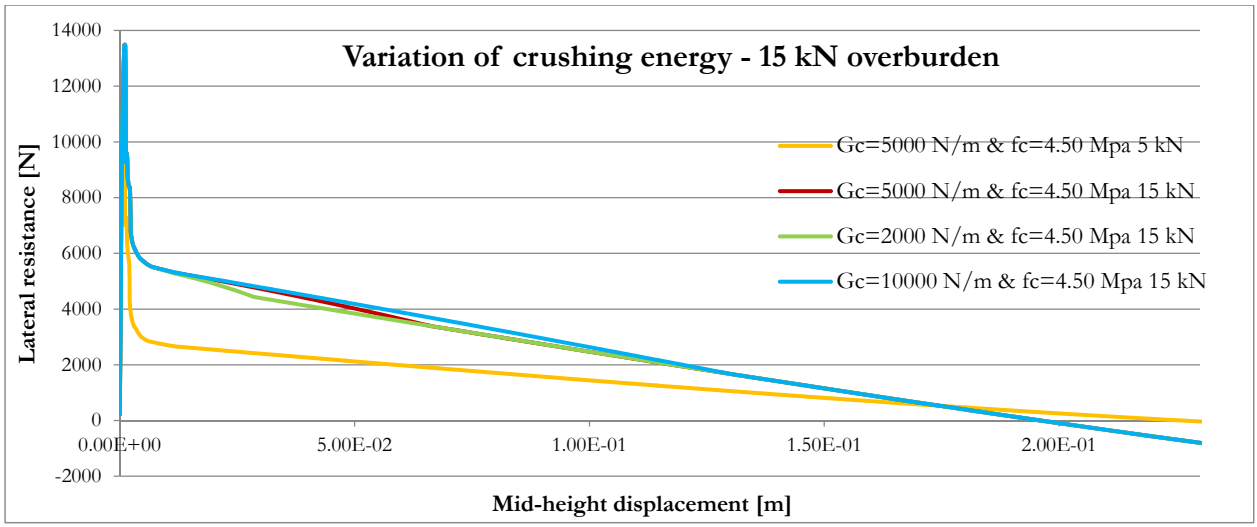

Figure 90 – Modification of the energy related to crushing of masonry material on the 3 meters tall model, 15 kN. The peak value of light-blue, red and green curves is the equivalent.

It is concluded that the rocking mechanism is mainly governed by cracking phenomena rather than the occurring of crushing. In the last investigations the strength parameters of the masonry were set as fixed parameters. Next sections justifies their values.

Variation in tensile and compressive strength of masonry

In the beginning of this section, which is entirely dedicated to the sensitivity studies on the wall model, it was noted that the URM wall may presents a much larger displacement capacity than expected when re-sized to 3 meters. Although relying on different boundary conditions such as larger top loads to allow crushing may mitigate this situation, it is important to identify the parameters responsible of this behavior. Here it is demonstrated that adjusting the strength parameters of the masonry, namely the compression and tensile strength, has a strong impact on the way the force-displacement curve develops.

The next two captions present the lateral resistance of the unreinforced masonry wall for a range of compression strengths assigned to the material and for two possible overburdens: 5 and 15 kilonewtons.

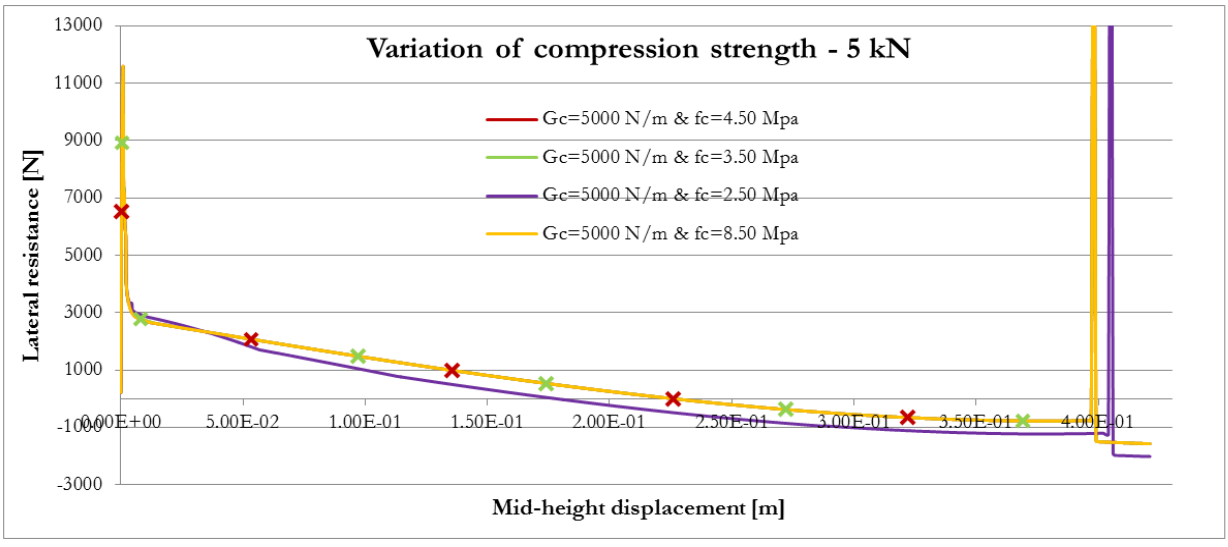

Figure 91 - Sensitivity study: variation of compression strength of masonry material, 3 meters tall model, 5 kN.

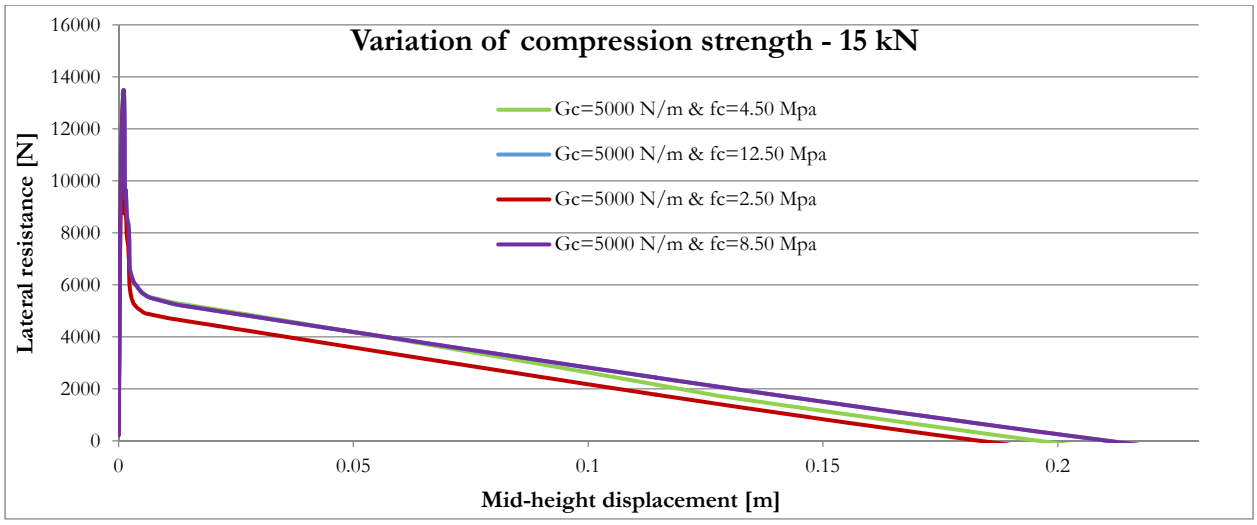

Figure 92 - Sensitivity study: variation of compression strength of masonry material, 3 meters tall model, 15 kN.

Again, it appears that varying the compression resistance of the material properties does not lead to significant changes in the model response unless the top load is incremented as well. In the case of 5 kN overburden, there seems to be a threshold value for the compression strength beyond which this parameter does not affect at all the response of the model. Indeed, in Figure 91 the curves related to a compressive resistance of 3.50, 4.50 and 8,50 MPa correspond, while for 2.5 MPa only the lateral resistance of the wall experiences a steeper decrease and, probably, more crushing. As it was done for the crushing energy analyses, the top load is increased. For a 15 kN top load and varying compression strength the curves exhibits slightly different trends compared to the 5 kN case. Note that the case of 12.5 MPa and 8.50 MPa coincide. With regards to lateral resistance, the wall with 15 kN overburden shows only 2 kN larger initial peak to form the hinges on the wall compared to the other case, while the overall energy required for a complete rocking cycle is of course much bigger. A much bigger influence on the peak resistance of the wall is displayed by the tensile strength of masonry: the top load acts as a pre-compression force that prevents the material from cracking. See graph below.

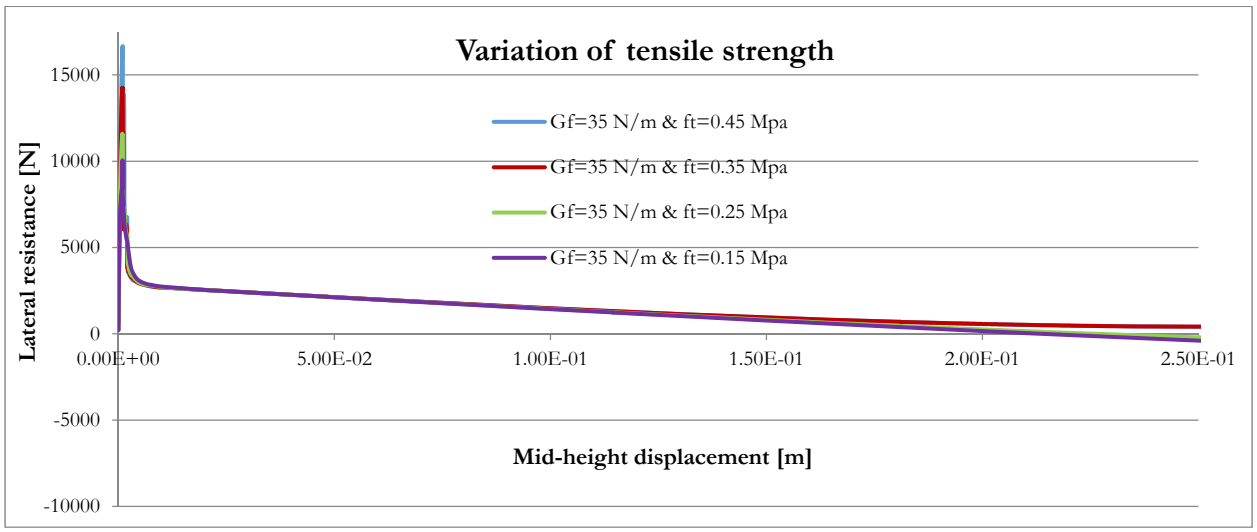

Figure 93 - Sensitivity study: variation of tensile strength on the smeared cracking beams model of 3 meters.

For a given cracking energy, modifying the tensile resistance of the wall generates not only different initial peaks but also distinct tails of the curve. Hence, with reference to the issue evidenced beforehand regarding the infinite displacement capacity of the wall of 3 meters (beginning of section 5.3.1), adjusting the tensile resistance of the wall seems to be the suitable solution.

It may be concluded that when dealing with the strength in compression of the masonry wall and for evaluating the effect given by varying either the crushing energy or the compression resistance of the material itself, it is recommendable to apply a larger top load on the wall. However, it is the tensile strength of the masonry to have the biggest influence on the model resistance to horizontal loads. Also, the slope of the curve around the instability displacement of the wall model is greatly influenced by the value of the tensile strength of the unreinforced masonry.

5.3.2 Extras and conclusions

Before moving to the dynamic response of the frame model, additional results of some investigations made on the smeared cracking beams model of the wall are presented here. These analyses were conceived during the development of the single wall models as well as in the process of implementing it in a structural frame system. They highlight the importance of using an appropriate load step size when dealing with highly nonlinear phenomena such as cracking and geometrical nonlinear effects, the reasons behind the decision of modeling the vertical top load on the wall by means of a translational spring (reference is made to the experiments carried out by Doherty) and they also verify whether the finite elements adopted in the modeling procedure are capable of capturing the shifting of the position of the hinges along the thickness of the wall while it rocks.

Load steps size

In numerical analyses the occurrence of cracking may easily lead to unstable solutions that are reflected by sudden divergence of the procedure or unreliable results. The following illustration shows that at the stage of incipient cracking of the masonry wall, the vertical reaction force located at the bottom end of it experiences some fluctuations. For this specific size of the wall the self-weight produces a vertical reaction force equal to 10.6 kN, to which an additional 5 kN should be added as a result of the applied vertical load. Regardless of how the cracks pattern develops, the total vertical reaction force is expected to stay constant as the wall displays. The diagrams provided below demonstrates that in numerical analyses this is not the case since there are usually small variations in calculating the forces due to the numerical approach. However, for the sake of the accurateness it is important that such fluctuations are limited. Therefore it is of crucial importance to choose an appropriate step size when applying the external load. The case represented below refer to a pushover analysis carried out with a displacement control procedure.

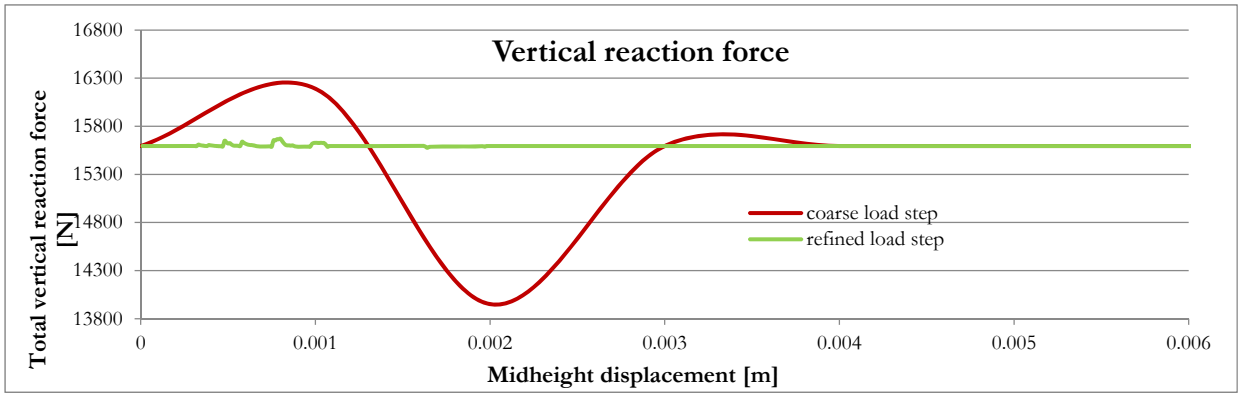

Figure 94 - Check on the impact of load step size in development of vertical reaction forces. 3 m tall wall model.

In a similar fashion and for the same reasons explained above, in transient analyses the time step is chosen in such a way that divergence of the solution is avoided and that the inertial forces are accounted for by relying on small time intervals (unless stated differently, 0.002 seconds).

Increase of the wall overburden

While developing the frame model a number of unexpected problems related to the assumptions made for the wall arose. Also, some aspects of the system required adjustments as the response of the model showed occurrence of unrealistically large dynamic forces in the vertical direction during transient analyses. In order to make the results of the analyses suitable for processing, it became essential to understand how and why these vertical forces developed. For this

reason a very simple T model was constructed representing a rocking wall beneath an horizontal beam simulating the action of a supported concrete floor on top of it. The floor spans 4 m on both sides and has a thickness of 0.15 mm. The mass density of the concrete is 2200 kg/m^3. This model is subjected to both quasi-static and transient analyses. By looking at the vertical reaction forces that originates at the supports and to the normal forces and moments that occur at specific nodes, it is possible to make some verifications. A schematization of the T model in its static and deformed configurations is presented hereunder.

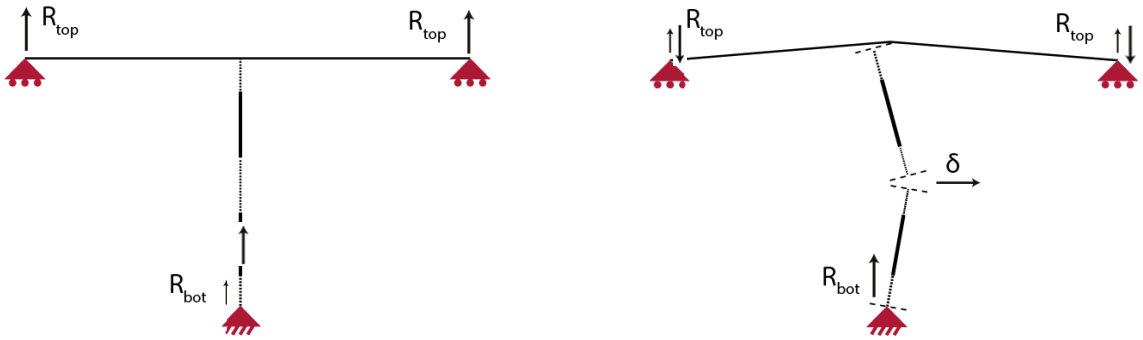

Figure 95 - Representation of the T model used to check behavior of rocking wall implemented in the structural system.

The connection between the wall and the floor is continuous. Due to the prescribed horizontal displacement applied to the wall mid-height (pushover analysis) or to the inertia load activated by the base motion (dynamic analysis) the wall cracks. In order to make it possible for the wall to rock around the hinges developing at the level of the cracks, the concrete floor above needs to move vertically to accommodate this motion. The side supports prevent the floor from deforming and try to push it back down. It is stressed that the masonry wall has a certain thickness even though it is modeled by making use of one dimensional elements. The stresses and strains along the cross sectional direction are computed through the addiction of integration points to which the Simpson integration scheme is applied. The beam element describing the wall may thus be considered as a set if sheets or "layers", each one referring to an integration point. Reference on this matter is made to the chapter dedicated to the modeling procedure. In the next illustrations the trend of the vertical reaction force is represented as a function of the mid-height displacement, in case of the quasi-static analysis, and of the time in case of a transient analysis.

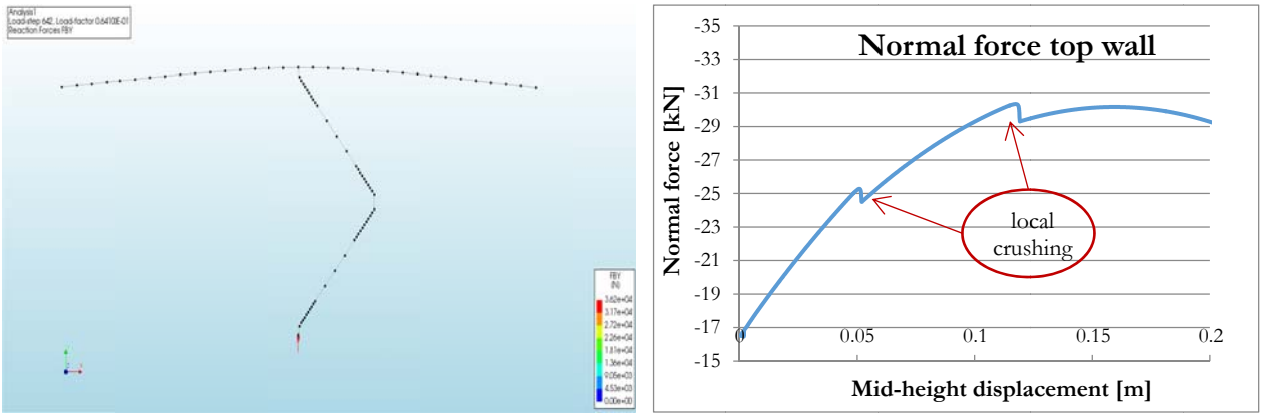

Figure 96 – Pushover analysis on the T model: increase of top load due to floor constraints.

What stands out from the quasi-static analysis is that due to the rocking of the wall the top load on it increases if the floor is schematized as a vertically supported element for which reaction forces in the downward direction originate, see figure 95. Although the experimental settings of Doherty research are supported by practical arguments, the behavior of the wall evidenced here shows that in a construction applications the top load sustained by the wall may indeed increase if the floors are not free to display vertically. This configuration reflects the modeling arrangements made for the frame

schematization, where the floors are continuously connected to the whole system. Applying a constant vertical force on top of the wall in the following investigations is a choice dictated by the necessity to simplify the structural problem: if the floor beam on top of the wall is given a mass, the vertical motion induced on the floor by the rocking mechanism beneath it accelerates the floor and increases its impact on the wall. If not controlled in numerical analyses, this situation may become rather unrealistic, with the wall failing due to achievement of its physical resistance instead of its unstable configuration.

Although it is possible to introduce some damping in the model to counteract the effect of the vertical impact of the floor on the wall, it is decided to make use of dummy floor elements for the structural frame model. In this way the inertia load given by the mass of the floors is not taken into consideration and the equivalent floor weight is applied on top of the wall as a vertical point load of constant magnitude throughout the whole analysis. This would allow to carry out, if necessary, a sensitivity analyses based on different magnitudes of the top load, without the need to monitor its oscillations in magnitude. As an example, the figure below shows the amplification of the top force acting on a wall within a frame model due to the impact of the floor above it if the latter is given a mass. The wall is located higher than the ground floor and the case refers to an harmonic base excitation where the vertical motion of the floor is undamped. The peaks in the variation of the top load identifies the moments in which the top floor impacts on the wall. The values of the force are so high that they do not have a physical meaning anymore.

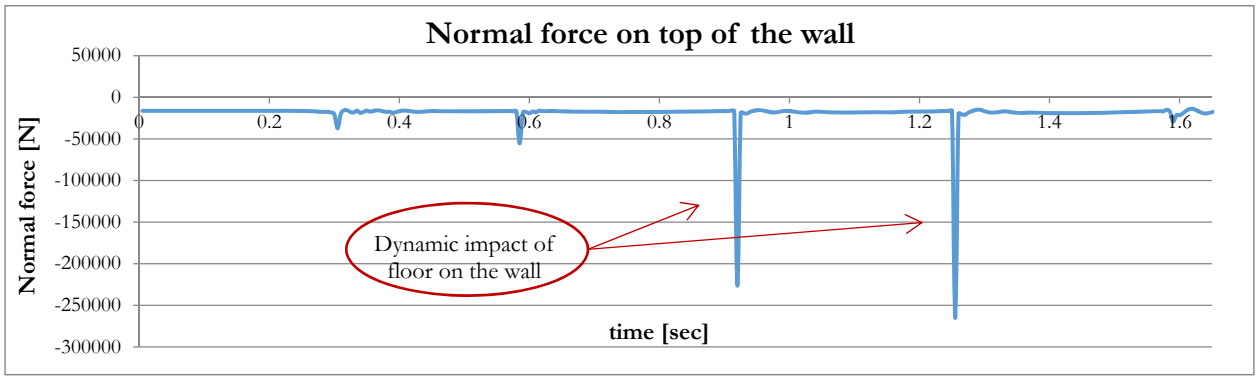

Figure 97 – Top normal force on a URM wall in a frame model: transient analysis on harmonic excitation.

Shifting of the top load above the wall: eccentricity check

When rocking occurs the upper point of rotation of the wall is located at the connection with the floor. There, following the direction the system displays, a hinge is formed and shifts along the cross section of the wall as the mechanism develops. At incipient failure, the top load is applied on the extreme fiber of the cross section and the eccentricity is maximum. The T model was used to check whether the one-dimensional definition of the nonlinear system is able to capture this behavior in both quasi-static and transient analyses. According to the wall size, the maximum eccentricity possible should correspond to half of the wall thickness, which is 100 mm. The investigation conducted by means of pushover numerical analyses and displacement control procedure is shown below. There are two points drawing attention. First, it appears that the eccentricity is larger than half the cross sectional dimension for very small values of displacement. Secondly, that there is a sudden drop of eccentricity around 120 mm of wall deformation.

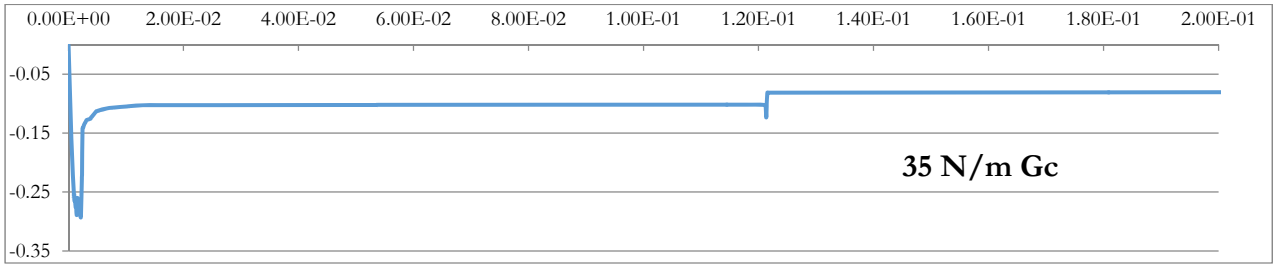

Figure 98 - Eccentricity of top vertical force applied on top of the URM wall during a pushover analysis: Gf = 35 N/m.

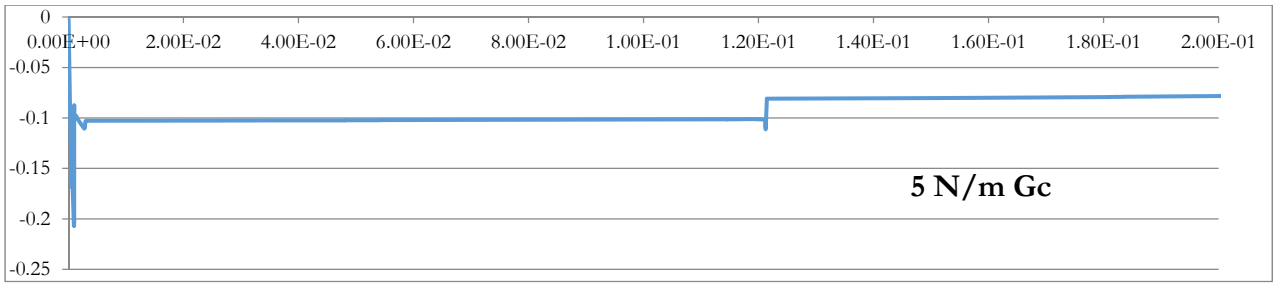

Figure 99 - Eccentricity of top vertical force applied on top of the URM wall during a pushover analysis: Gf = 5 N/m.

The first situation can be explained by the nonlinear behavior of the masonry material. In the chapter dedicated to the modeling procedures it is shown that the material has a stress-strain relationship with a parabolic shape in compression and a linear tension softening based on crack energy. While cracking, the hinge shifts to the extreme fiber until, theoretically, only compression stresses are concentrated in one point. The value of the moment divided by the resulting point force gives its eccentricity respect to the center of the cross section. However, due to the tensile strength assigned to the material, an additional moment is originated which makes the eccentricity larger than expected. Until the tensile strain resistance of the all the extreme fibers is reached, resulting in a consumption of crack energy by the application of the external force, this phenomenon occurs. A representation of this circumstance is provided in the picture hereunder.

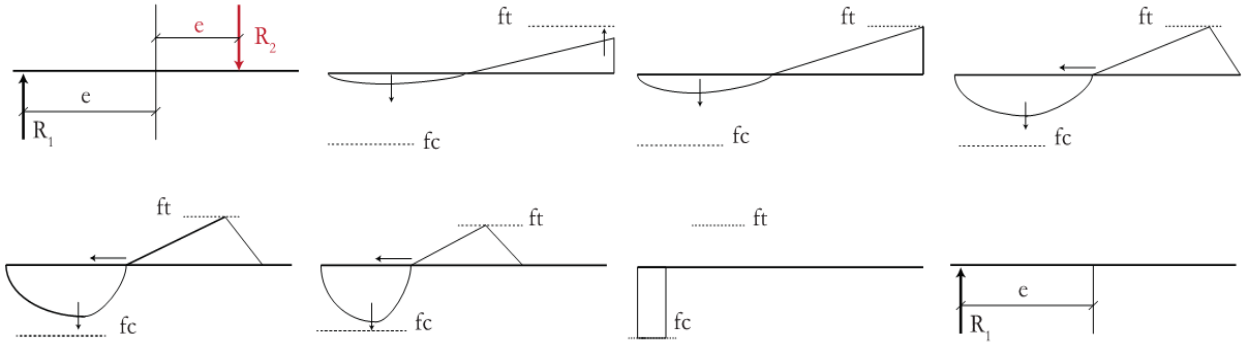

Figure 100 - Additional moment component acting on the cross section due to tensile strength of the material.

As this behavior is caused by the way the material definition, it is reasonable to check what is the effect of modifying the material parameters related to the tensile strength. The next illustrations represent the eccentricity values that were found for different values of cracking energy Gf and tensile strength ft. Only the first stage of deformation is represented. The case with zero crack energy and 0.25 MPa corresponds to the eventuality of brittle cracking.

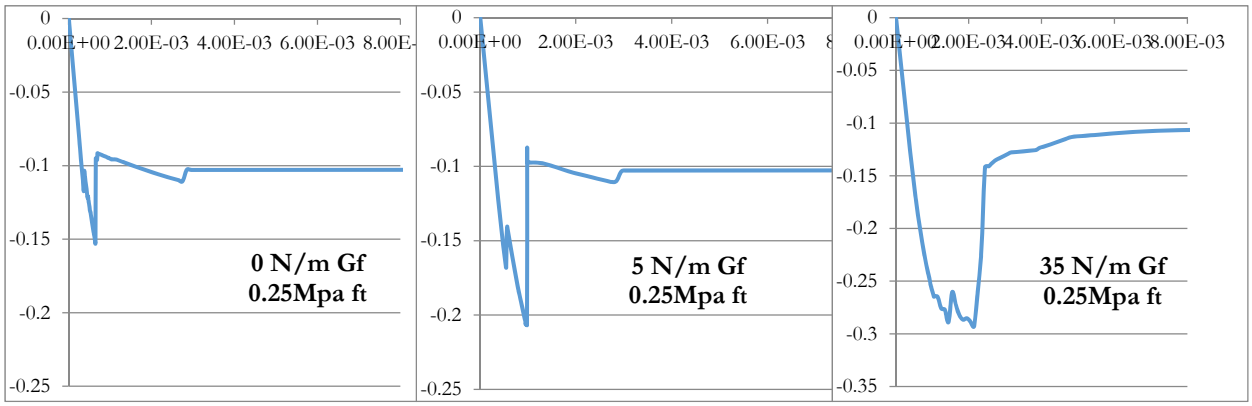

Figure 101 - Eccentricity of top load on the URM wall. Variation of cracking energy Gf with tensile strength of 0.25 MPa.

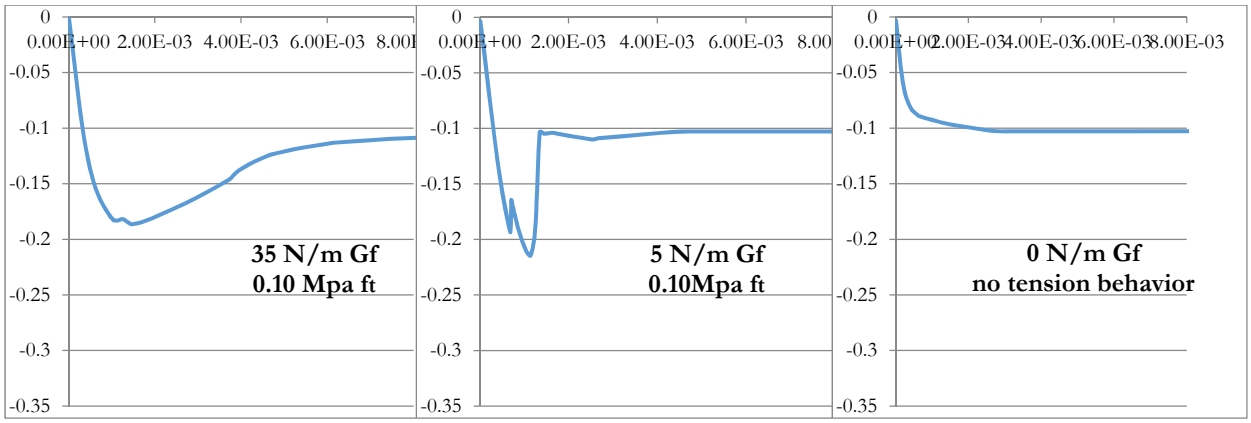

Figure 102 - Eccentricity of top load on the URM wall. Variation of cracking energy Gf and tensile strength of masonry.

The figures above show that when the nonlinear material is given a tensile resistance there is always an additional component of the moment which resists cracking. The more energy is required to reach the ultimate strain in tension of the masonry, the more developed is the curve describing the eccentricity as a function of the mid-height displacement of the rocking wall. The bottom-right caption shows the limit case of the no-tension material. As expected, the resulting graph presents a smooth trend towards the value of 100 mm.

When running transient analyses a similar behavior should be obtained. Indeed, the results obtained for an URM wall within a frame structure subjected to an harmonic base excitation is represented in the next picture. The masonry is modeled with a 0.45 MPa tensile resistance and 35 N/m cracking energy (linear tension softening). The initial eccentricity is due to the different end constraints of the upper floor that is supported by the wall (hinged-clamped). Before the actual rocking motion of the wall starts, the system requires a certain amount of energy to overcome the tensile resistance of the masonry and fully open the cracks where the hinges form. Also when the rotation point on top of the wall shifts to the opposite edge there is still some cracking energy left. Then, when the material is no longer able to respond in tension, the eccentricity is finally bounded between the values ±100 mm.

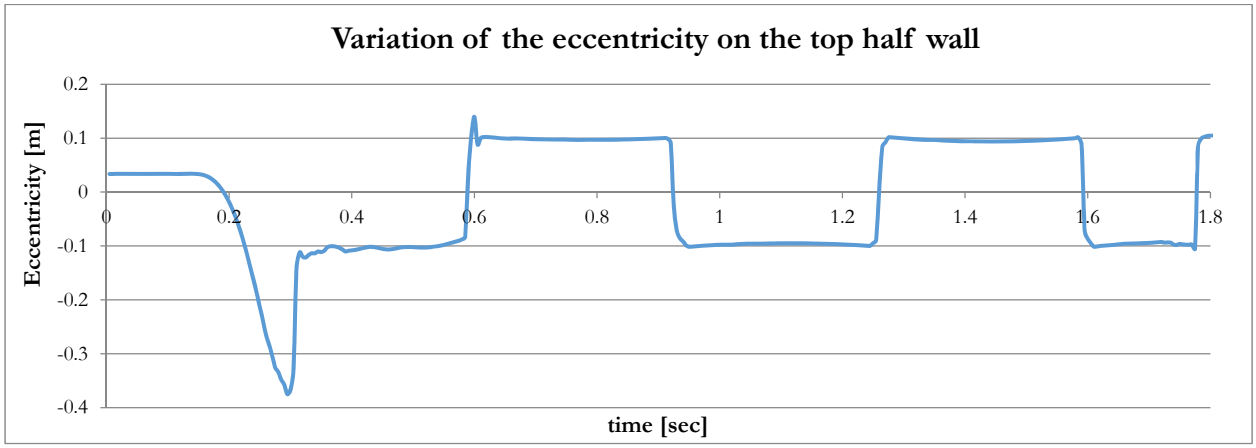

Figure 103 – Eccentricity of the top load acting on a wall during a transient analysis which induces the rocking motion.

Going back to the representation of figures 98 and 99, the sudden kink around a mid-height displacement of 120 mm may be caused by the crushing of the masonry which decreases the wall thickness and, therefore, the maximum moment acting on top of the wall.

Hence, it is concluded that the model developed for the present research is able to capture distinctive aspects of the rocking mechanisms and that it is thus possible to make use of it for describing an URM wall inside a frame structure.

5.4 Frame model results

The considerations made throughout the sensitivity analyses of the previous sections led to development of a set of frame models. These were used for carrying out some investigations in accordance to the research plan as illustrated in Chapter 3. However, the intended research plan would consist in performing a large number of incremental nonlinear dynamic analyses on the frame models and for a variety of boundary conditions. Due to time constraints the variations on the model itself and on the range of loading excitations were adjusted. First, it was decided to keep the overburden on walls with a constant value of 15 kN and to apply no initial drift to the walls. Also, the frames used in the transient analyses were limited to a maximum of 5 floors. With regards to the adoption of an alternative stability system present in the structure, it became necessary to only examine one representative case for each of these circumstances. Finally, it was decided to make use of 4 signals (2 in the x direction and 2 in the y direction) for the base motion excitation out of a total number of 44 artificially-derived available records. Recurring to such small number of records can be justified by taking into account that this project is not associated to a structural design process which needs to comply with the normative guidelines.

It was found that a crucial aspect of the frame models is the necessity to employ two sets of damping coefficients in their definition. In fact, although the model seems to be rather simple, it consists of two structural series systems each of them characterized by their own damping properties. The Rayleigh coefficients applied to the frame structure, which acts linearly elastic, depends on its height, whereas the damping properties of the rocking mechanism are constant for every wall experiencing the OOP deformation. The table depicted below presents the vibrational period and the damping coefficients computed for the frame models through an eigenvalue analysis. It is noted that due to the assumption made of a stability system with constant structural properties over the height, the short frame structures appears to be rather stiff. However, the building period of the five-storey frame reported is acceptable. On the next page another table is presented with the vibration period of the clamped-clamped elastic beam and the rocking mechanism as reported by foreign codes.

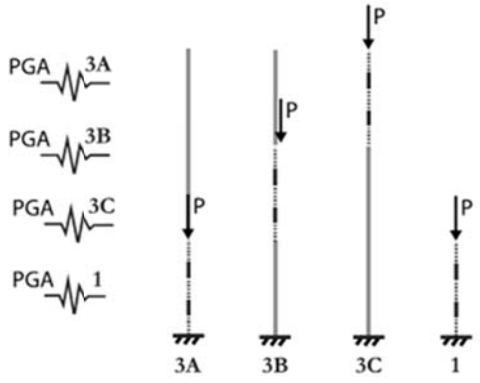

Figure 104 – Incremental dynamic analysis on frame models equipped with rocking walls: schematization.

Rayleigh damping parameters - 4% damping Stability: shear wall system.			
N° floors	Period	Mass coeff.	Stiffness coeff.
[-]	[s]	[1/s]	[s]
1	0.0391	12.078	0.29784 · 10E-4
2	0.07178	6.4226	0.7576 · 10E-4
3	0.1475	3.194	0.11727 · 10E-3
4	0.2544	1.8785	0.15953 · 10E-3
5	0.3958	1.12385	0.19586 · 10E-3
Assumption: structural properties of the stability system in the frame model are constant over the height!			

Table 28 - Vibration periods and damping coefficients for the frame systems. 4% damping assumed.

The figure on the left above is a schematic representation of the analyses performed on the frame models. The location of the rocking mechanism was varied along the height of a frame structure with a fixed number of floors. For each of the given records, the base excitation was scaled until the rocking wall system within the frame reached its instability displacement due to rocking. The maximum scaling factor was recorded and it was then compared to the reference case of a URM wall at ground level. By making the ratio of these two values it was possible to derive the "Failure Scaling Ratio" as a function of the wall location for each of the given signal and frame models. By post-processing the data obtained in these analyses, the maximum PGA that the wall on each floor is able to resist OOP were outlined for all the frame models. More details on the definition of the Failure Scaling Ratio (FSR) will be given in section 5.4.1.

Successively, the set of records was again employed to run some linear transient analyses on the models. The acceleration outputs of the rocking wall at mid-height were numerically elaborated to derive elastic acceleration response spectra at floor levels. Those graphs served as a backbone for the estimation of the *parts correcting coefficients* in the assessment of the

seismic response of wall elements within a building system. In a similar fashion, the outcome of the linear transient analyses was post-processed to construct the trends of the amplification in acceleration demands as a function of the height, which is related to the derivation of the *height-effects coefficients*. The two contributions of parts and height-effects are related to the so called *filtering effect* of the building on the ground motion (See section 2.7.3).

Rayleigh damping parameters of clamped-clamped elastic beam - 2% damping – 3 meters wall.			
Height [m]	Vibration period [s]	Mass coefficient [1/s]	Stiffness coefficient [s]
3	0.027	8.8804	0.82124·10E-4
Vibration period of rocking mechanism according to NZSEE and NTC2008 – 3 meters wall			
NTC2008	NZSEE	Mass coefficient [1/s]	Stiffness coefficient [s]
0.274 sec	0.540 sec	8.8804 (approx.: l.e. beam)	0.82124·10E-4 (approx.: l.e. beam)

Table 29 – Damping coefficients for the clamped-clamped elastic beam in the horizontal direction assuming 2% damping.

The computations to derive the vibration periods of Table 29 are available for consultation in the Appendix F. The next sections present the results obtained in this investigation. The records used are labelled as A, B, C and D and they were all derived from a reference acceleration at bedrock level of 0.63g. The full step-by-step procedure is illustrated for the signal A, whereas the results obtained with other signals are accounted for by referring to their post-processed output.

5.4.1 Max values of PGA and FSR profiles

The strategy followed to derive the set of FRS profiles for the frame models was addressed in the previous section. The step-by-step procedure is now shown for one of the signals, while for all the others the outcome is summarized in tables and graphs in order not to interrupt the flow of the text. The reader can refer to the Appendix G the results of the IDA analysis on Record D. It is noted that the output is presented up to 9 seconds even though the excitation lasts for 10 seconds. This has nothing to do with the response of the model and it is only related to the designing of the pages layout. No significant deformation of the walls was recorded in that time window in the present investigation.

Record A

The caption below illustrates the signal labelled as A. It corresponds to the base excitation adopted for all the frame models and it has a peak acceleration of 0.176 m/s2. Starting from the reference case of a wall at the ground-floor level, the output of the incremental dynamic analysis is shown next.

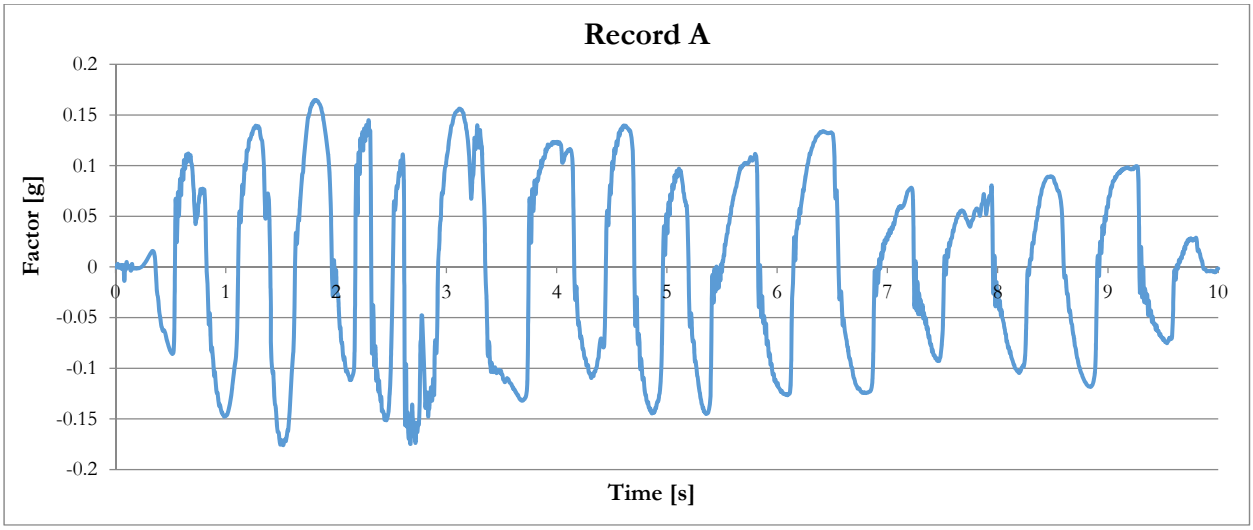

Figure 105 - Representation of the signal A used as an acceleration base motion excitation for the frame models.

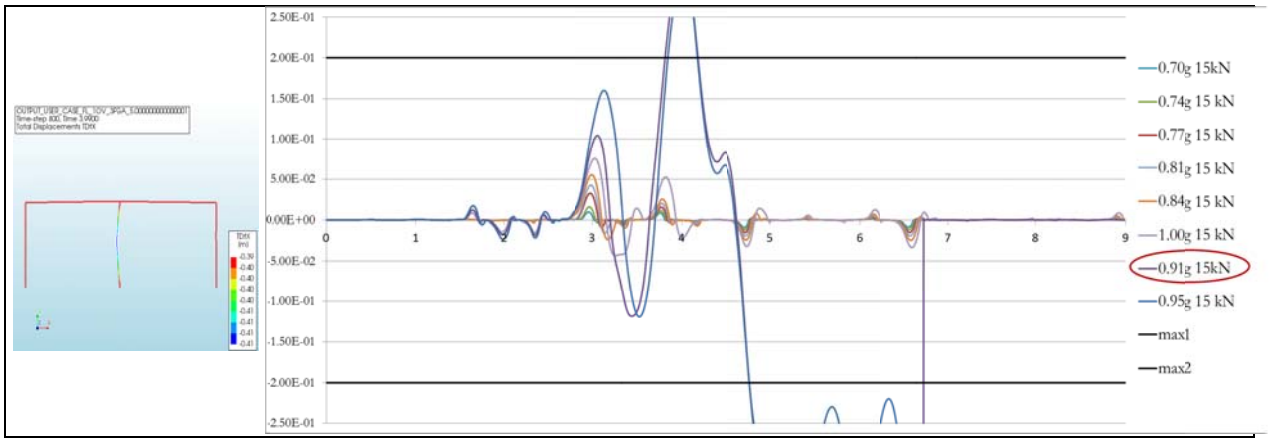

Figure 106 - IDA on frame model with one floor and rocking system at ground floor. Record A.

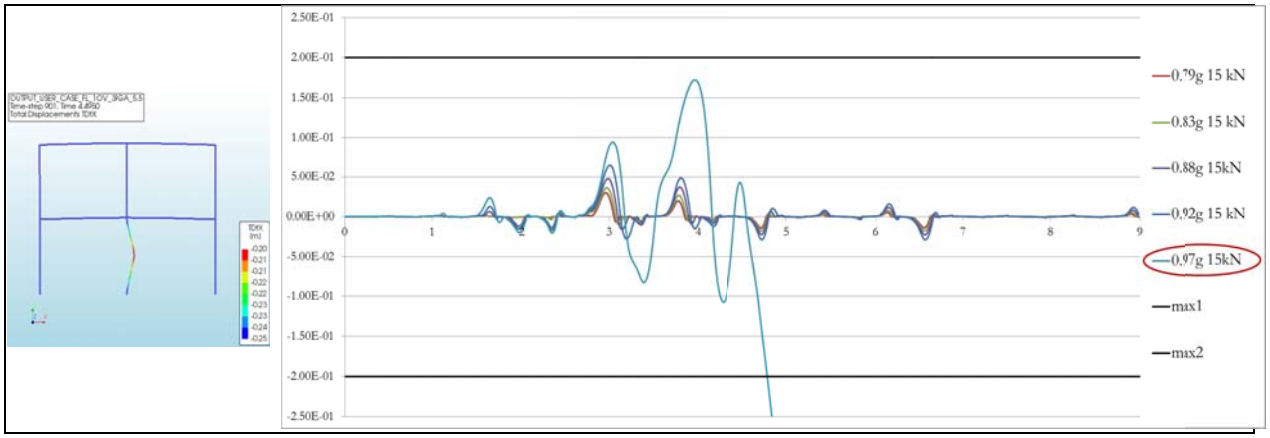

Figure 107 - IDA on frame model with two floors and rocking system at ground floor. Record A.

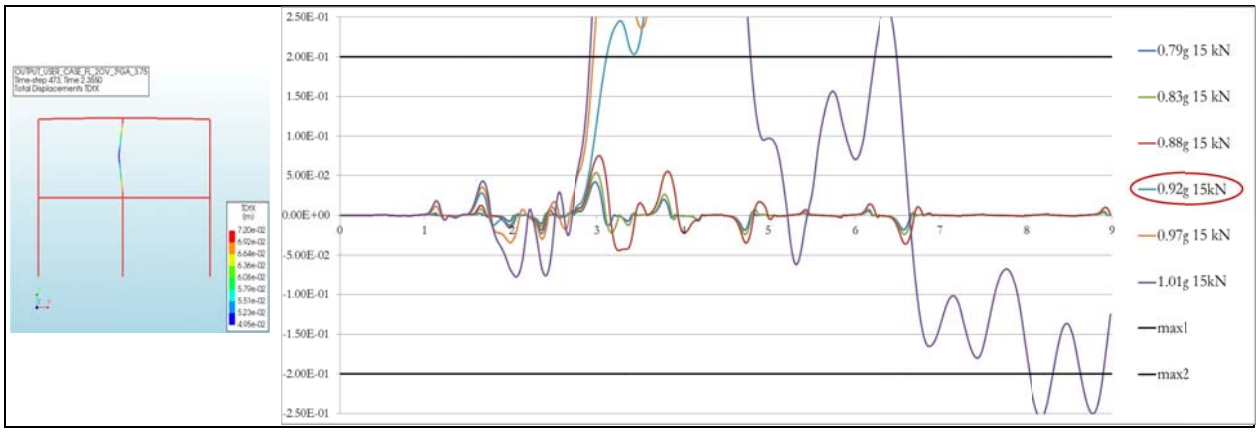

Figure 108 - IDA on frame model with two floors and rocking system at second floor. Record A.

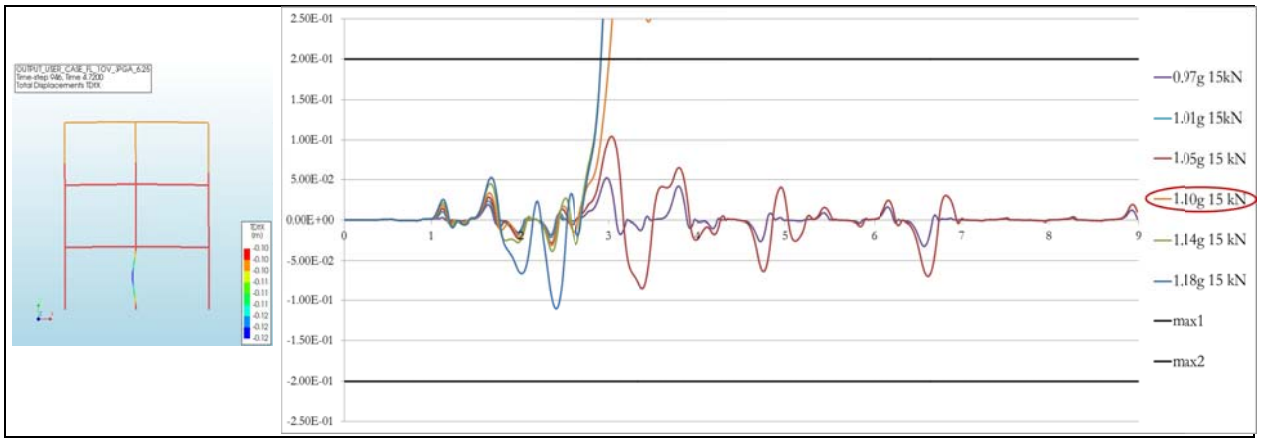

Figure 109 - IDA on frame model with three floors and rocking system at groundfloor floor. Record A.

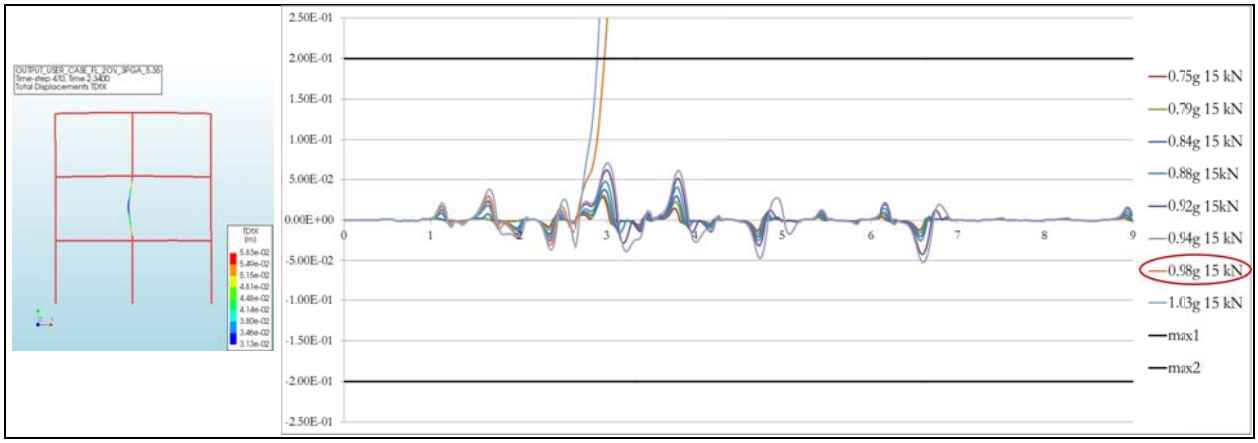

Figure 110 - IDA on frame model with three floors and rocking system at second floor. Record A.

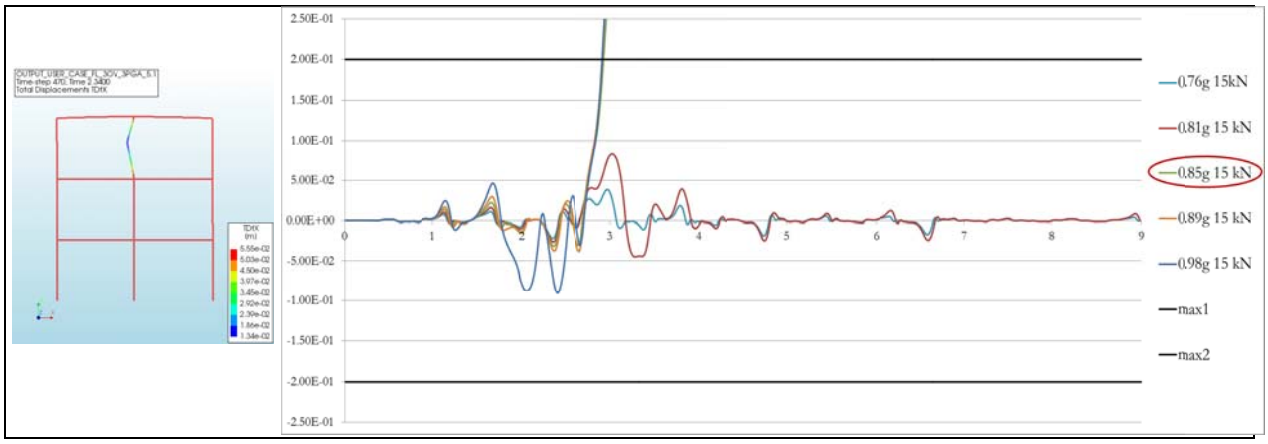

Figure 111 - IDA on frame model with three floors and rocking system at third floor. Record A.

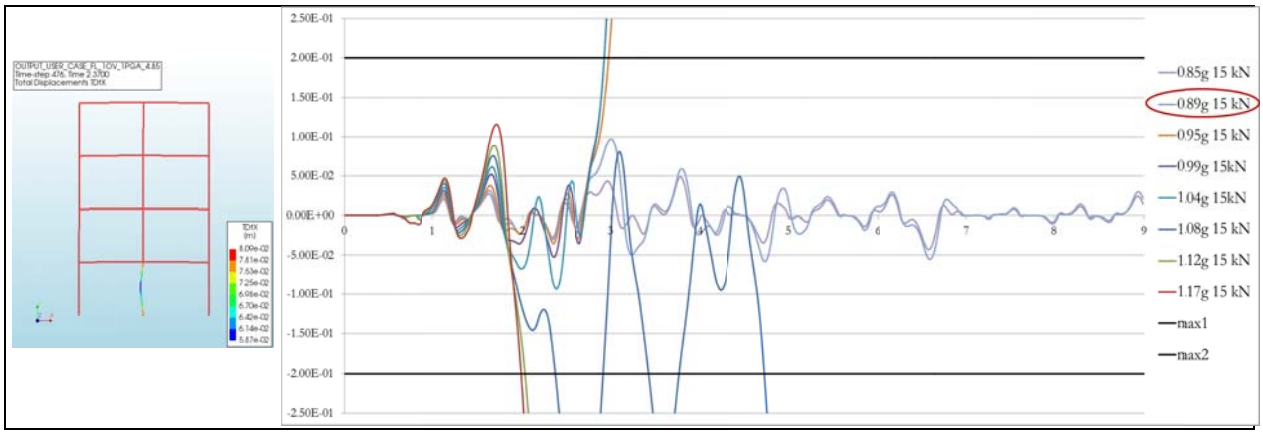

Figure 112 - IDA on frame model with four floors and rocking system at groundfloor floor. Record A.

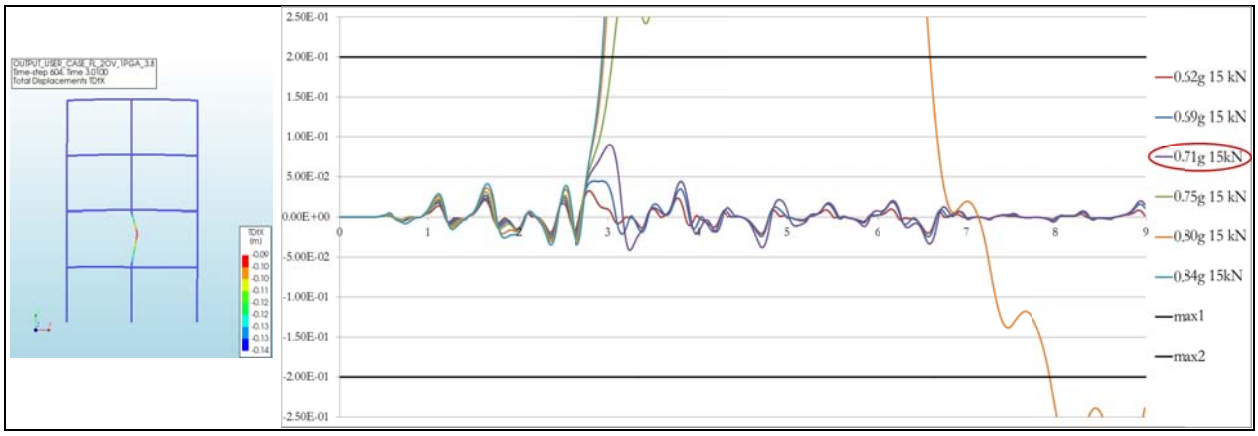

Figure 113 - IDA on frame model with four floors and rocking system at second floor. Record A.

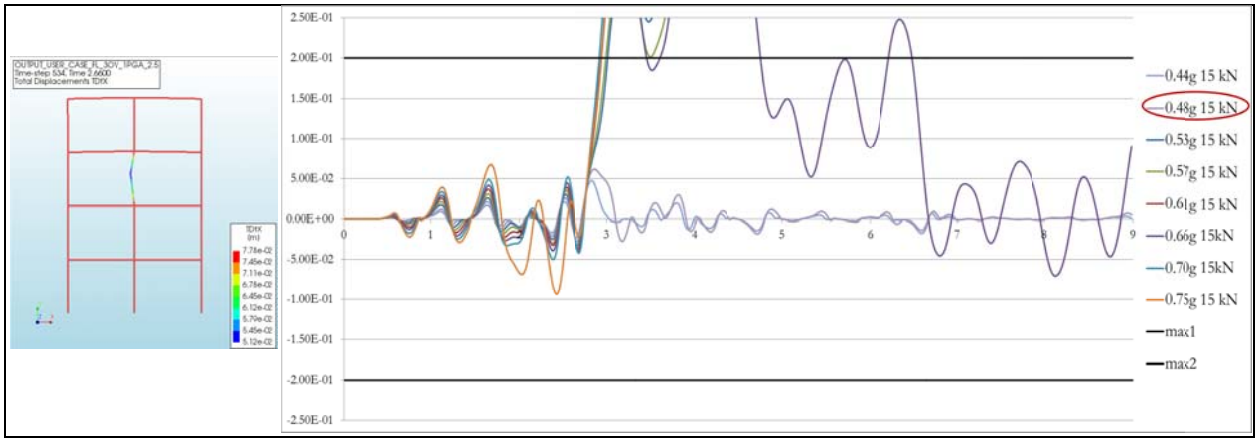

Figure 114 - IDA on frame model with four floors and rocking system at third floor. Record A.

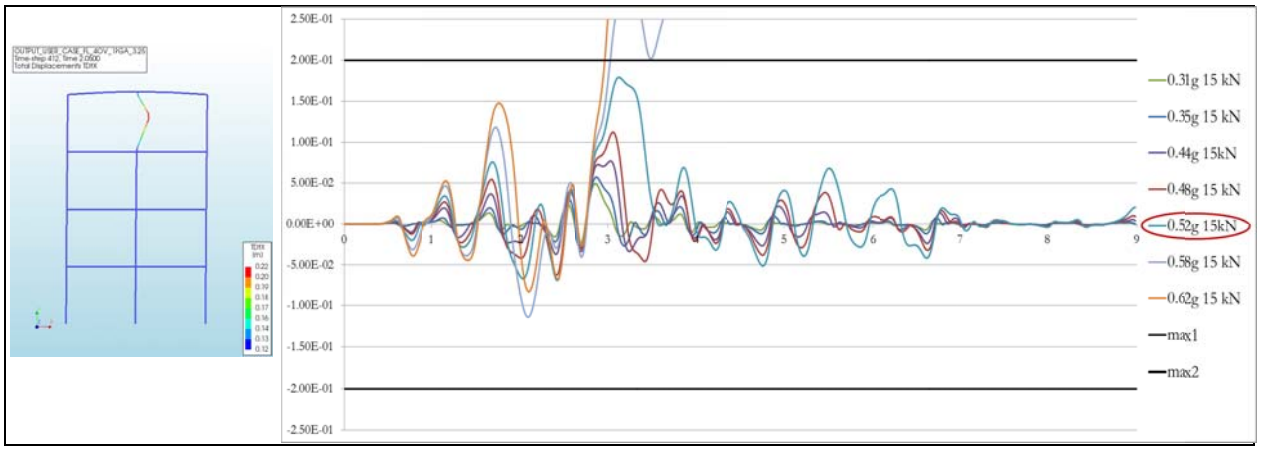

Figure 115 - IDA on frame model with four floors and rocking system at fourth floor. Record A.

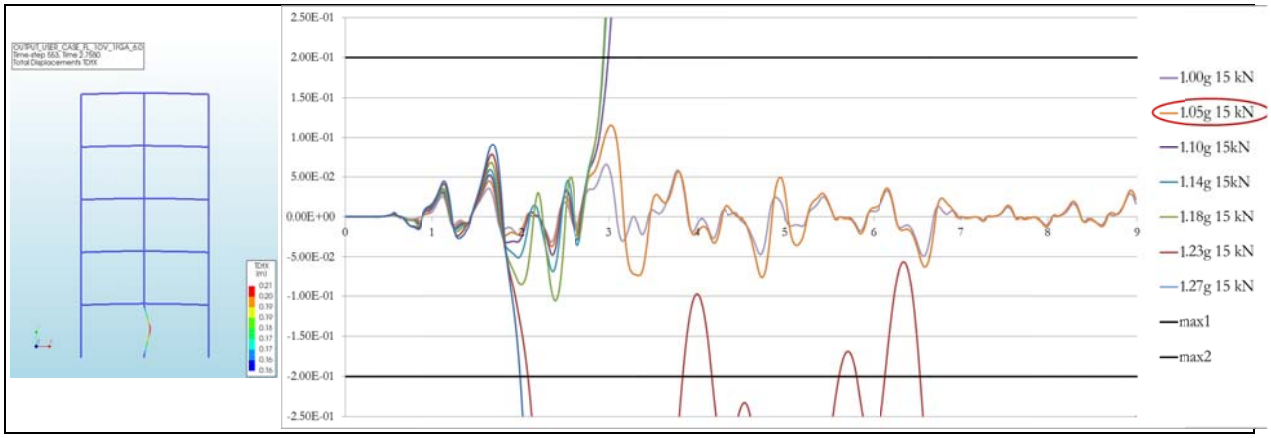

Figure 116 - IDA on frame model with five floors and rocking system at ground floor. Record A.

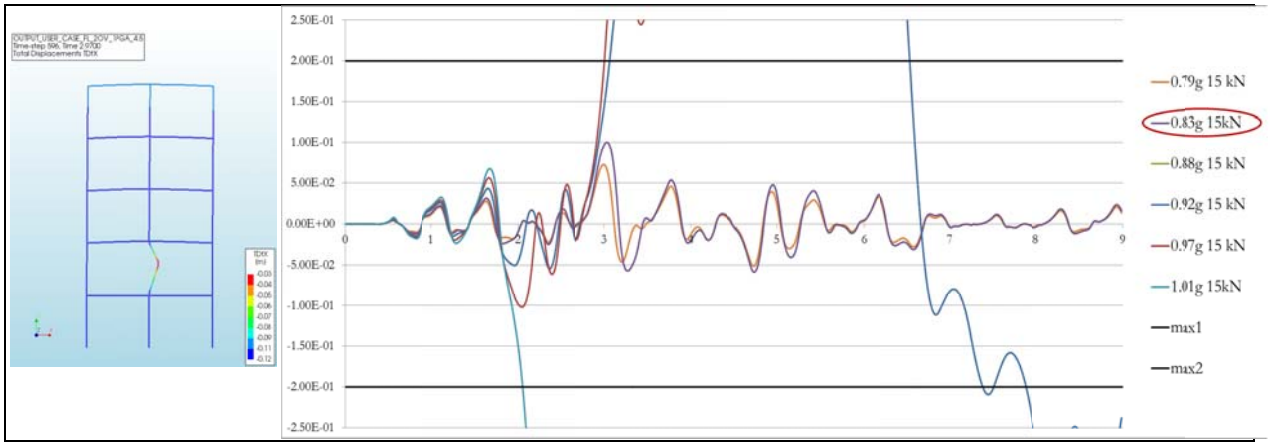

Figure 117 - IDA on frame model with five floors and rocking system at second floor. Record A.

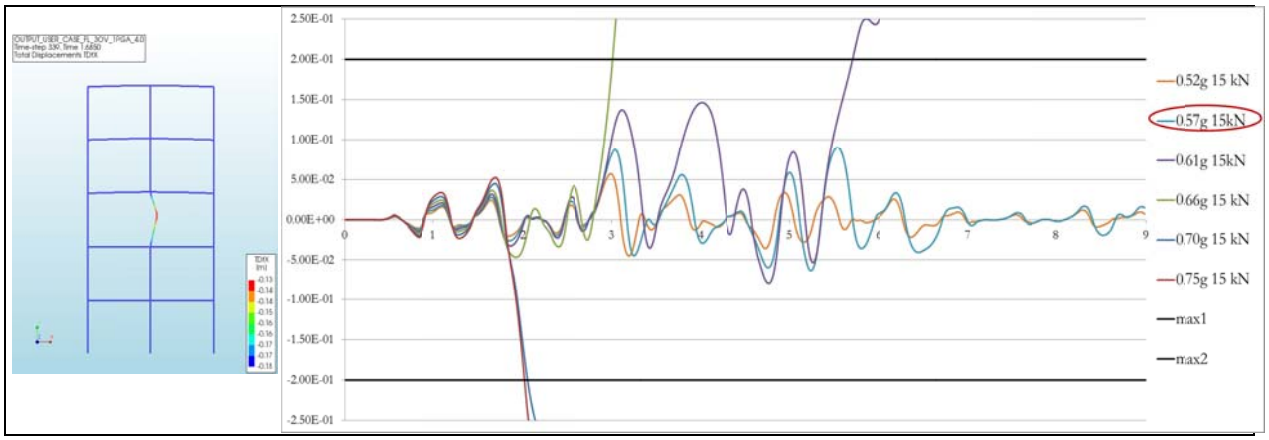

Figure 118 - IDA on frame model with five floors and rocking system at third floor. Record A.

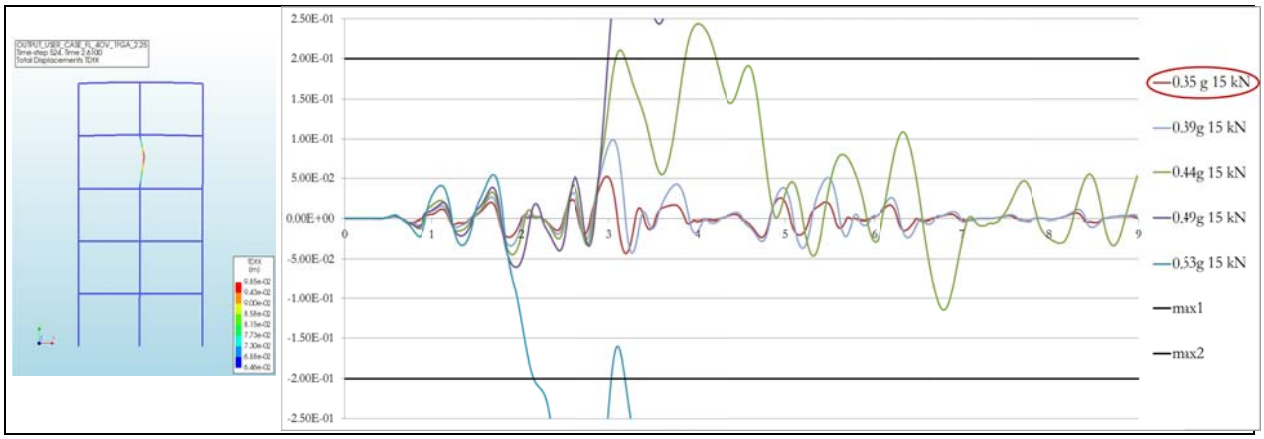

Figure 119 - IDA on frame model with five floors and rocking system at fourth floor. Record A.

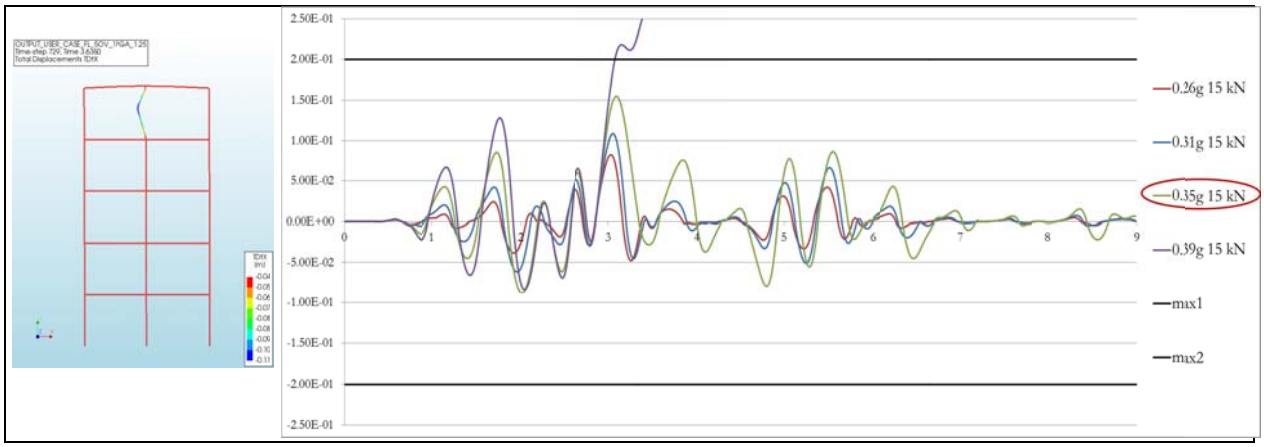

Figure 120 - IDA on frame model with five floors and rocking system at fifth floor. Record A.

Each scaled signal corresponds to a maximum ground acceleration. The increments used in the IDA are visible on the right of each graph, and the value rounded in red represent the peak ground acceleration of the scaled record A for which the wall at a specific location loses its stability due to the out-of-plane deformation. A remark is here necessary. In the section dealing with the response of the smeared cracking beams model it was underlined that DIANA appears not always to be able to warn the user when the unstable configuration of the rocking walls is reached (Section 5.1). For this reason the graphs plotted above present two thick lines which represent the theoretical deformation limits for the wall system, and the OOP failure of walls is considered to be achieved whenever the mid-height displacement of walls touches those lines or numerical divergence occurs. Therefore, post-processing the analyses output graphically is a crucial aspect in the assessment procedure for the OOP resistance of walls for the numerical models, especially when no numerical divergence takes place. With respect to the failure of walls, two important aspects are neglected:

1) It is assumed that the instability displacement at mid-height is the one corresponding to the undamaged masonry cross section. However, it was seen before that the instability displacement is a function of the material deterioration (for instance due to crushing. See section 5.3, "hinged ends" and section 5.3.1, "crushing and cracking of masonry" and "applied overburden"). Therefore, the approach used may be considered un-conservative to this respect.
2) The sudden change in direction of the inertial forces due to the base motion may be able to push back the wall to a stable configuration even if it has already displayed beyond its instability displacement. In the illustrations shown above the occurrence of such a circumstance is detected few times. This behavior is of course possible in reality but, given the strong approximations made throughout the development of the model, it was decided to consider the wall as collapsed as long as the mid-height displacement curves touched the thick bounding lines.

Also, given the level of approximation adopted so far for the development of the numerical model of the wall and frame systems, it is deemed reasonable to use increments of the signals in the order of not less than 0.25 times the original record.

The pictures on the next pages present tables with an overview of maximum scaling factors and the resulting "Failure scaling ratio (FSR)" profiles associated to the rocking mechanism for all the walls analyzed and collected from the graphical elaboration of the output in previous pages. The quantity "Failure Scaling Ratio" is expressed by the following formula, as anticipated in Chapter 3:

$$FSR_{(n\_storey\,;\,i\_level)} = \frac{PGA_{MAX}(n\_storey; i\_level)}{PGA_{MAX}(1\_storey)}$$

The equation calculates the ratio between the PGA of a signal increasingly scaled until the out-of-plane failure of the wall system takes place, that is PGA_{max}, and that one corresponding to the same circumstance occurring in the case of a single-storey frame building (that is the reference case commonly considered in the international standards). The evolution of the value of the FSR parameter is shown in the following figures. For each of the signals the scaling procedure up to the OOP failure of walls is applied to frame models ranging from one to five storeys. As an example, the results represented in Table 31 are considered. If the global (primary) system is a 4-storey frame, the following applies:

- The external excitation (in this case record B, PGA = 0.1799 m/s2) needs to be 1.41 times larger than in the case of a single storey-frame building to cause the OOP failure of the wall system at ground-floor level. However, the wall system in a single-storey frame model fails OOP and under the given signal only if the latter is scaled at least 3 times larger than the original one (see Table 31). Therefore, the original record B needs to be amplified 1.41 x 3 = 4.22 times in order to determine OOP failure of the (secondary) wall system at ground level.

It is clear that the higher the wall location, the smaller is the maximum PGA they can withstand before failing out-of-their-plane. Although this conclusion matches the findings of several researches of the theory, it is noted that the

overburden on top of the wall is kept constant regardless of the wall location within the building in the IDA. Hence, this behavior cannot be explained by the smaller top load acting on higher walls and must be related to the amplification of acceleration demands on higher floors due to filtering effects. The filtering effects are associated to the interaction of vibration modes of the structural systems involved (primary – the frame building – and secondary – the wall with nonlinear material properties) and to the amplifications caused by height effects. Focus on these two aspects will be given in the upcoming sections. The presentation of the FSR profiles is followed by a comparative study where the results on the tables are plotted, overlapped and examined in order to better elaborate on them and draw conclusions.

Record A

Record A - PGA: 0.175984 m/s2 - Duration: 10 sec		
N° floors	Max scaling up to failure	Failure scaling ratio
1	5.97	1.15
2	4.72	0.91
3	3.24	0.63
4	1.99	0.38
5	1.99	0.38

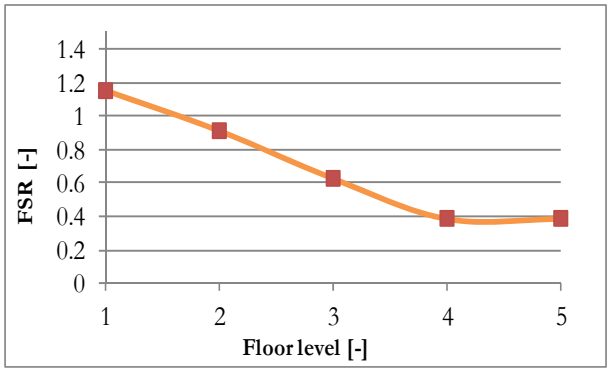

N° floors	Max scaling up to failure	Failure scaling ratio
1	5.06	0.98
2	4.03	0.78
3	2.73	0.53
4	2.95	0.57

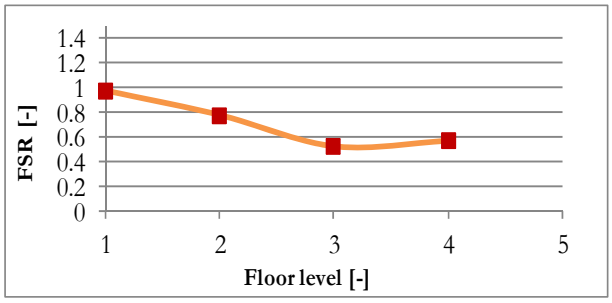

N° floors	Max scaling up to failure	Failure scaling ratio
1	6.25	1.21
2	5.57	1.08
3	4.83	0.93

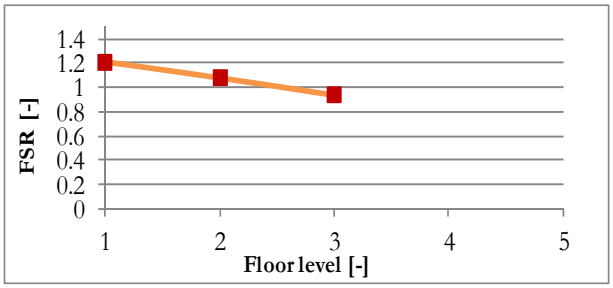

N° floors	Max scaling up to failure	Failure scaling ratio
1	5.51	1.07
2	5.23	1.01

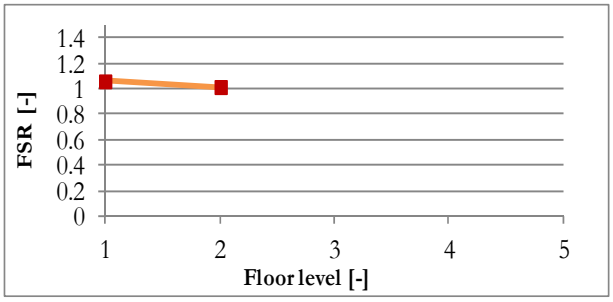

N° floors	Max scaling up to failure	Failure scaling ratio
1	5.17	1.00

Table 30 – Failure scaling ratio for the frame models. Record A.

Record B

Record B - PGA: 0.179895 m/s2 - Duration: 10 sec		
N° floors	Max scaling up to failure	Failure scaling ratio
1	5.00	1.67
2	3.50	1.17
3	2.50	0.83
4	1.72	0.57
5	1.72	0.57

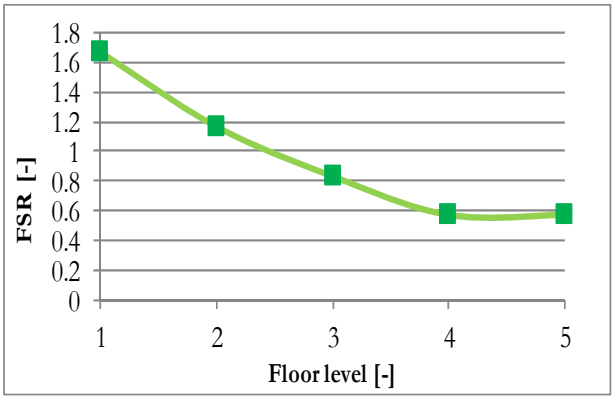

N° floors	Max scaling up to failure	Failure scaling ratio
1	4.22	1.41
2	3.50	1.17
3	2.72	0.91
4	2.72	0.91

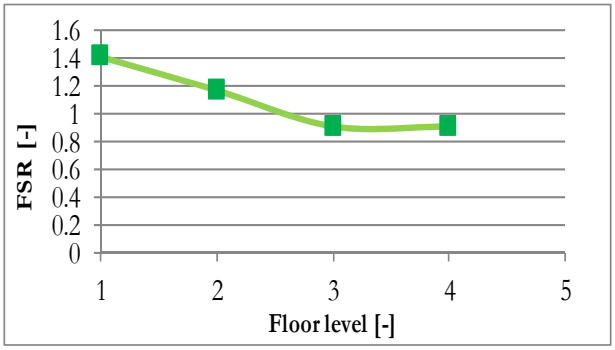

N° floors	Max scaling up to failure	Failure scaling ratio
1	3.72	1.24
2	3.22	1.07
3	2.72	0.91

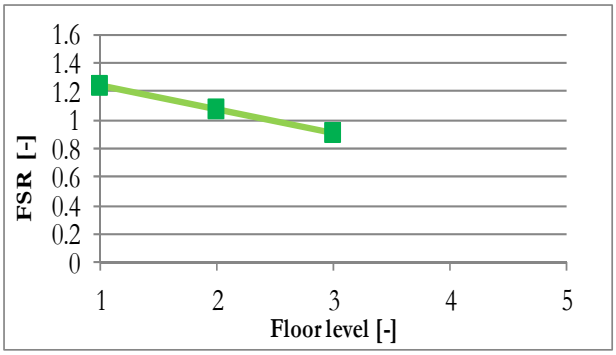

N° floors	Max scaling up to failure	Failure scaling ratio
1	3.50	1.17
2	2.78	0.93

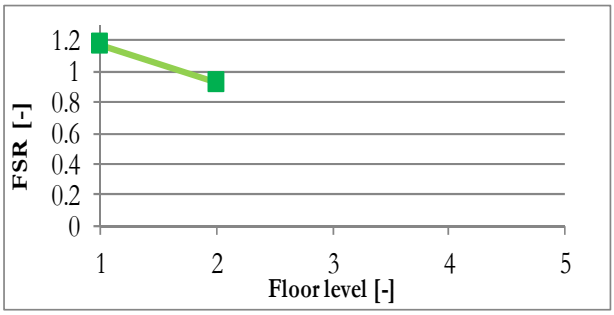

N° floors	Max scaling up to failure	Failure scaling ratio
1	3.00	1.00

Table 31 – Failure scaling ratio for the frame models. Record B.

Record C

Record C - PGA: 0.19553 m/s2 - Duration: 10 sec		
N° floors	Max scaling up to failure	Failure scaling ratio
1	6.75	1.40
2	5.22	1.09
3	3.17	0.66
4	2.15	0.45
5	1.64	0.34

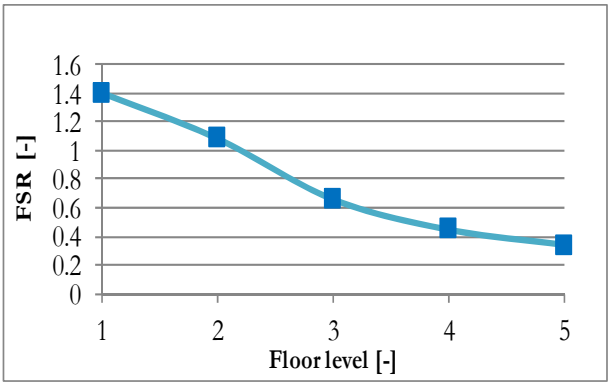

N° floors	Max scaling up to failure	Failure scaling ratio
1	6.14	1.28
2	5.32	1.11
3	4.09	0.85
4	2.97	0.62

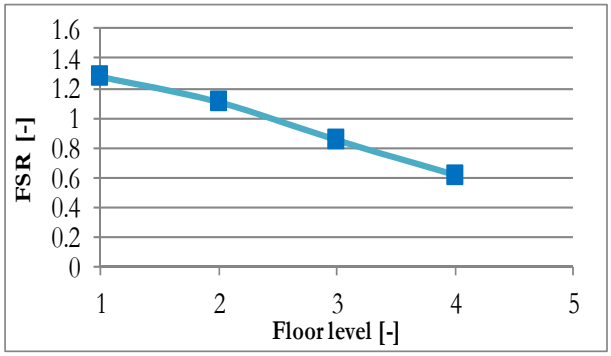

N° floors	Max scaling up to failure	Failure scaling ratio
1	5.73	1.19
2	5.11	1.06
3	4.40	0.91

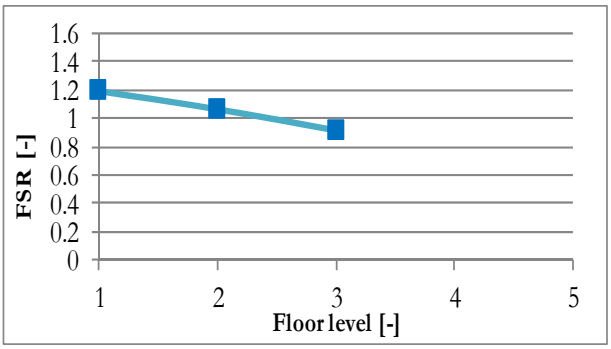

N° floors	Max scaling up to failure	Failure scaling ratio
1	5.32	1.11
2	4.91	1.02

N° floors	Max scaling up to failure	Failure scaling ratio
1	4.81	1.00

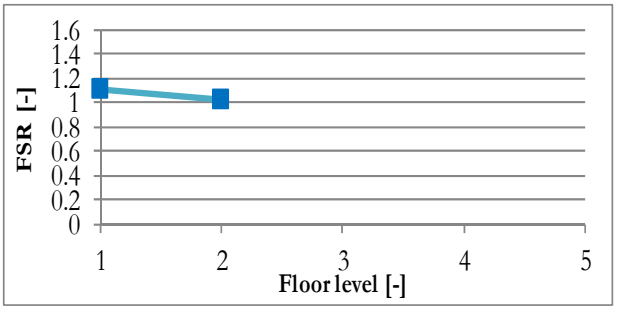

Table 32 – Failure scaling ratio for the frame models. Record C.

Record D

Record D - PGA: 0.188608 m/s2 - Duration: 10 sec		
N° floors	Max scaling up to failure	Failure scaling ratio
1	5.25	1.62
2	3.71	1.15
3	2.49	0.77
4	2.01	0.62
5	2.01	0.62

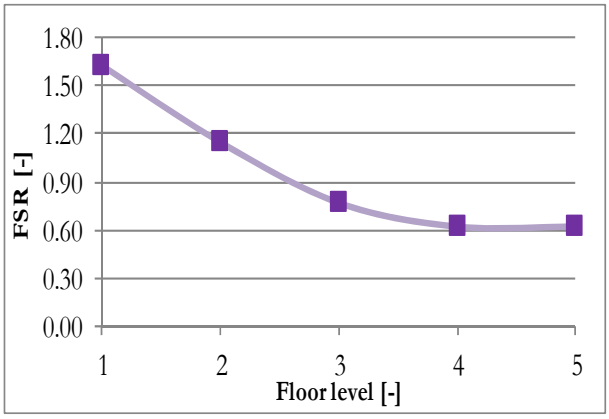

N° floors	Max scaling	Failure scaling ratio
1	4.51	1.39
2	3.50	1.08
3	2.70	0.84
4	2.70	0.84

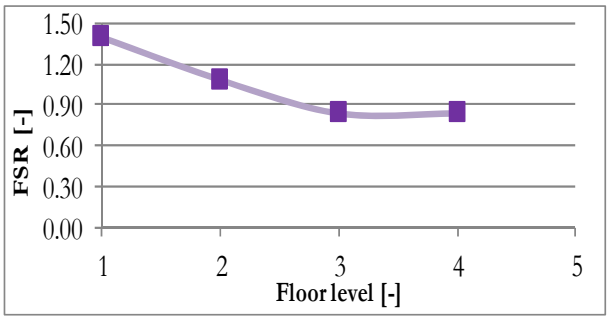

N° floors	Max scaling up to failure	Failure scaling ratio
1	4.51	1.39
2	3.50	1.08
3	2.97	0.92

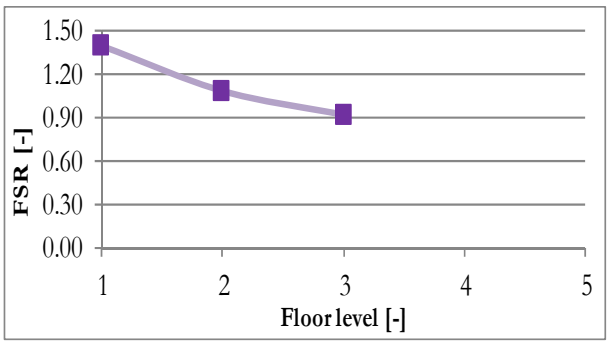

N° floors	Max scaling up to failure	Failure scaling ratio
1	3.71	1.15
2	3.23	1.00

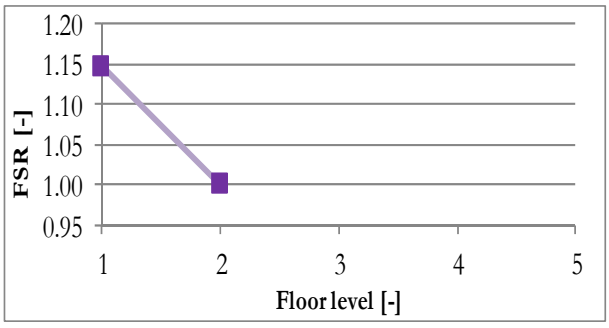

N° floors	Max scaling up to failure	Failure scaling ratio
1	3.23	1.00

Table 33 – Failure scaling ratio for the frame models. Record D.

The Figures 121-122-123-124 present a graphical representation of Tables 30-31-32-33. The vertical axes in the graphs identify the "failure scaling ratio" (FSR) for a wall located on the i-floor of a n-storey frame building subjected to a base motion representing the records A, B, C and D. The horizontal axis is the floor level taken into consideration.

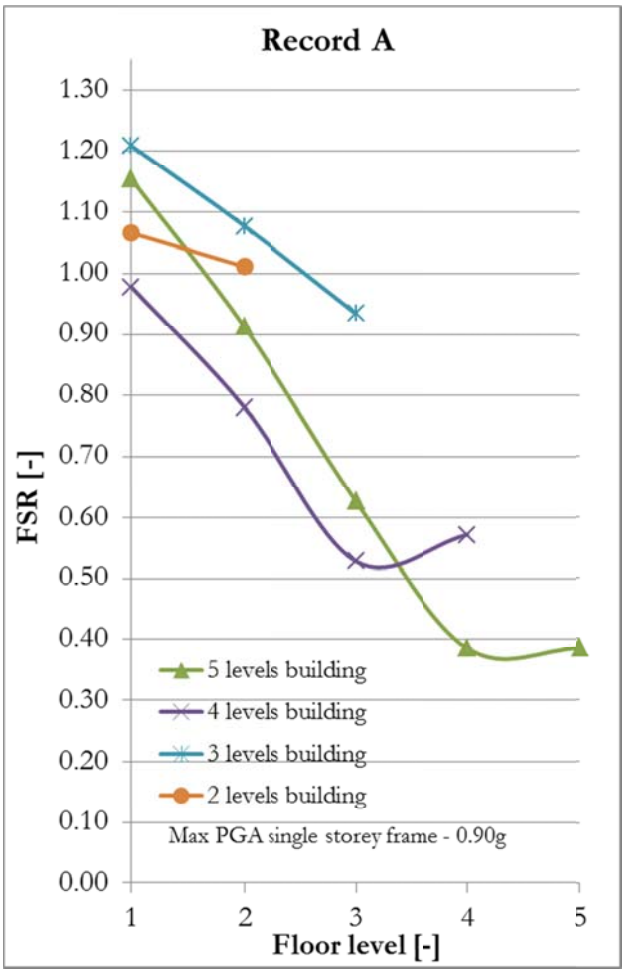

Figure 121 – Signal A, graphical output.

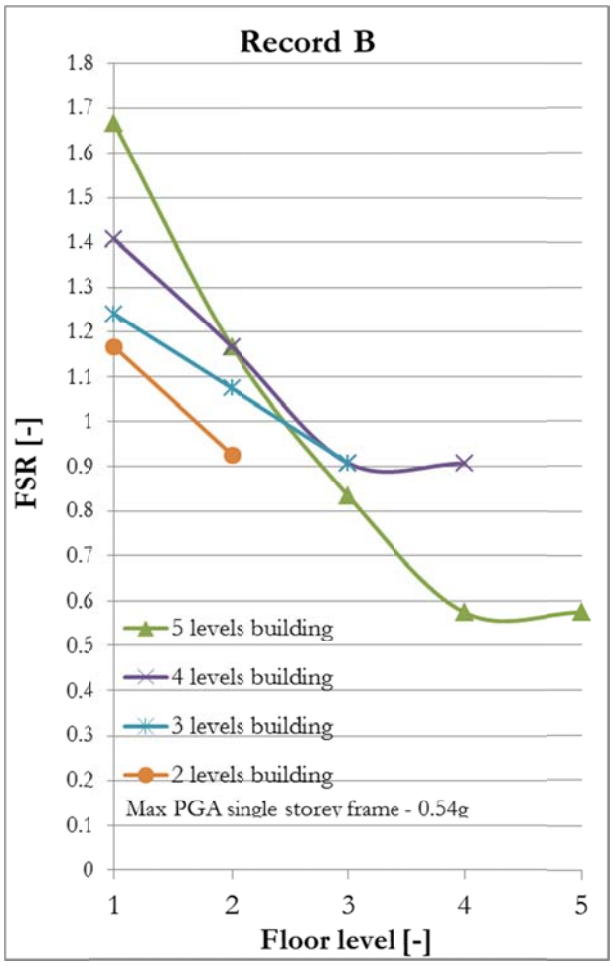

Figure 122 – Signal B, graphical output.

The limited number of records used and the level of simplification adopted in the models do not allow to draw practical conclusions from these graphs. However, some interesting observations can be made:

- First of all, it should be noted that according to the numerical results, none of the records adopted in the analyses is able to cause the out-of-plane failure of the walls in any of the configurations analyzed (size of the building up to five floors, location of the wall system inside it..) unless scaled appropriately. This finding might be easier to observe in Tables 30-31-32-33-34: the values under the column "maximum scaling factor up to failure" are never smaller than the unity for all locations of the wall system. The out-of-plane failure seems not to be of any concern for the URM walls in the frame models. This may indeed be confirmed by the results of hand calculations performed in accordance to NZSEE prescriptions. See Appendix E.

- As the total number of floors of the frame models increases, a larger scaling factor is required to make the wall system at ground-floor level fail for each of the given signals. This is due to the rigidity of floors above the wall system that exhibit a resistance to bending deformation and prevent the wall from rocking.

- The general trend of the curves shows that for systems located at higher floors the scaling factor required to reach the wall OOP failure decreases (see Figure 13 where all the records are applied on a 5-storey frame model). However, in Figure 121-122-123 and 124 this trend is not confirmed, being the walls on higher floors capable of resisting similar or even higher base accelerations than those below them, as one can see from their FSR. This is a clear evidence of the nonlinear nature of the problem, and it suggests that the response of the rocking walls on the different floors (or the secondary systems) is influenced by that of the frame structure (or primary system) which filters out the forces acting on them.

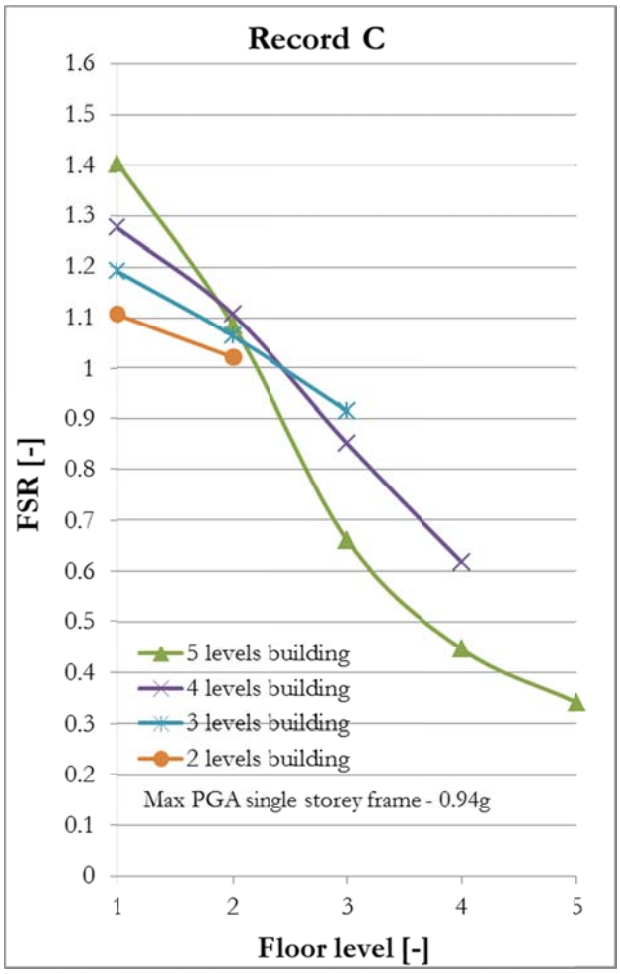

Figure 123 – Signal C, graphical output.

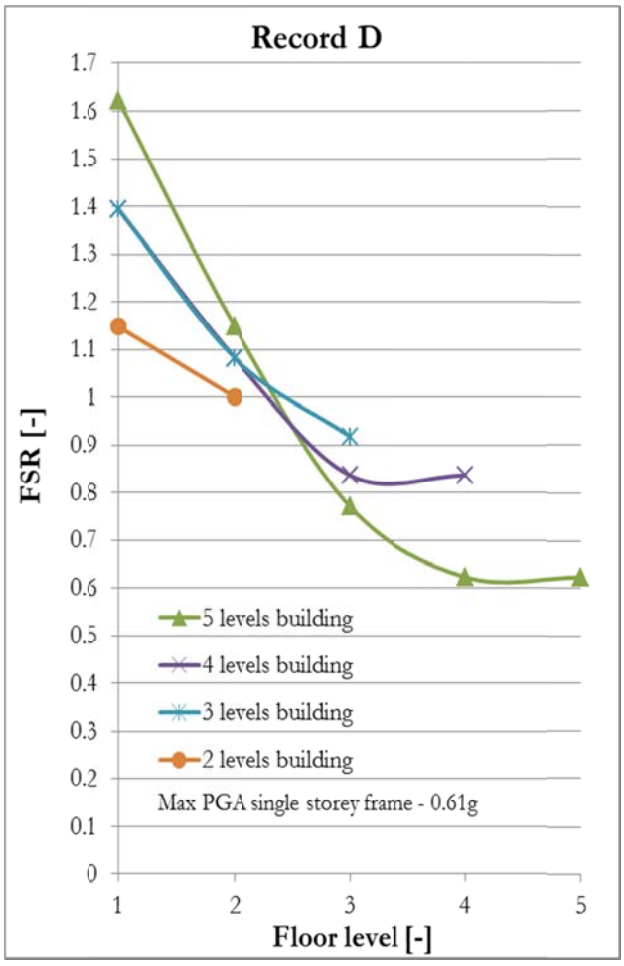

Figure 124 – Signal D, graphical output.

In the next page the curves are arranged in a different way and the trend of the FSR is presented in such a way that it is possible to compare it by varying the record applied at the base of frame models of the same size, see Figure 125. In general, the shape of the curves is similar for all the signals adopted.

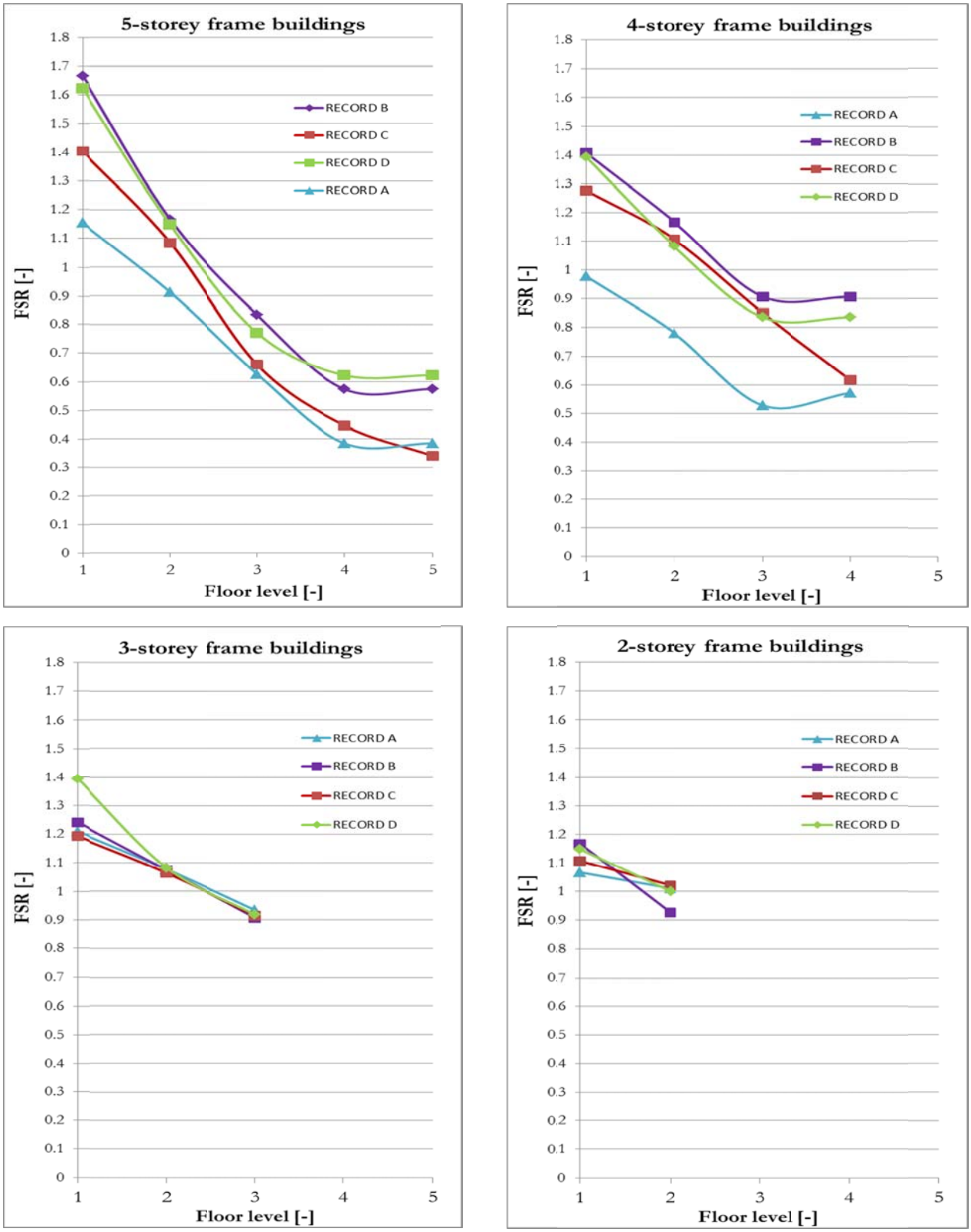

Figure 125 – Comparative analysis on Failure Scaling Ratio of the systems as a function of the building height.

5.4.2 Variation on stability system adopted

The response of the structural system is influenced by the stability system chosen for the frame buildings. This determines how the base excitation is filtered through the building and the way the energy is dissipated throughout the structure in a dynamic context. An example of a comparative analysis is addressed in this section. The set of frame models is supported in the horizontal direction by means of a shear wall system in one case and by a moment resisting frame system in the other.

Before exciting the systems with one of the records adopted in section 5.4.1, a check on the static response of the numerical models is made. A uniform distributed load of 5000 N is applied on the five-storey frames with shear wall system and moment resisting frame. As expected, the structure stabilized by the moment resisting frame presents a large inter-storey drift for the lower floors which decreases with the height. On the contrary, the application of a shear wall as a lateral resisting system results in inter-storey drifts which increase to a great extent for upper levels. Thus the models act as expected and can be used in the dynamic analyses of this research. This check is represented in Figure 126.

The case of the primary system with a moment resisting frame used to resist the lateral loading in opposition to the shear wall adopted in all the previous frame models is addressed now. Similarly to the previous cases, the output is presented in Table 34 and graphically in Figure 128. The use of such an alternative stabilizing system seems to have a beneficial effect on the out-of-plane resistance of the walls located on the last floors of the 4 and 5-storey frame models. If one compares the curves of Figure 127 and 128, which are both associated to record D, the different trend of the FSR for the top floors is evident. This might be an indication of higher modes affecting more the response of the primary structure when a moment resisting frame is used. Having said that, the lack of data to support this argument (only record D was employed in the analyses) does not allow to further speculate about it. The aim of this supplementary analysis is demonstrating how the choice of a different stabilizing system has an impact on the response of the primary and, by consequence of that, the secondary system.

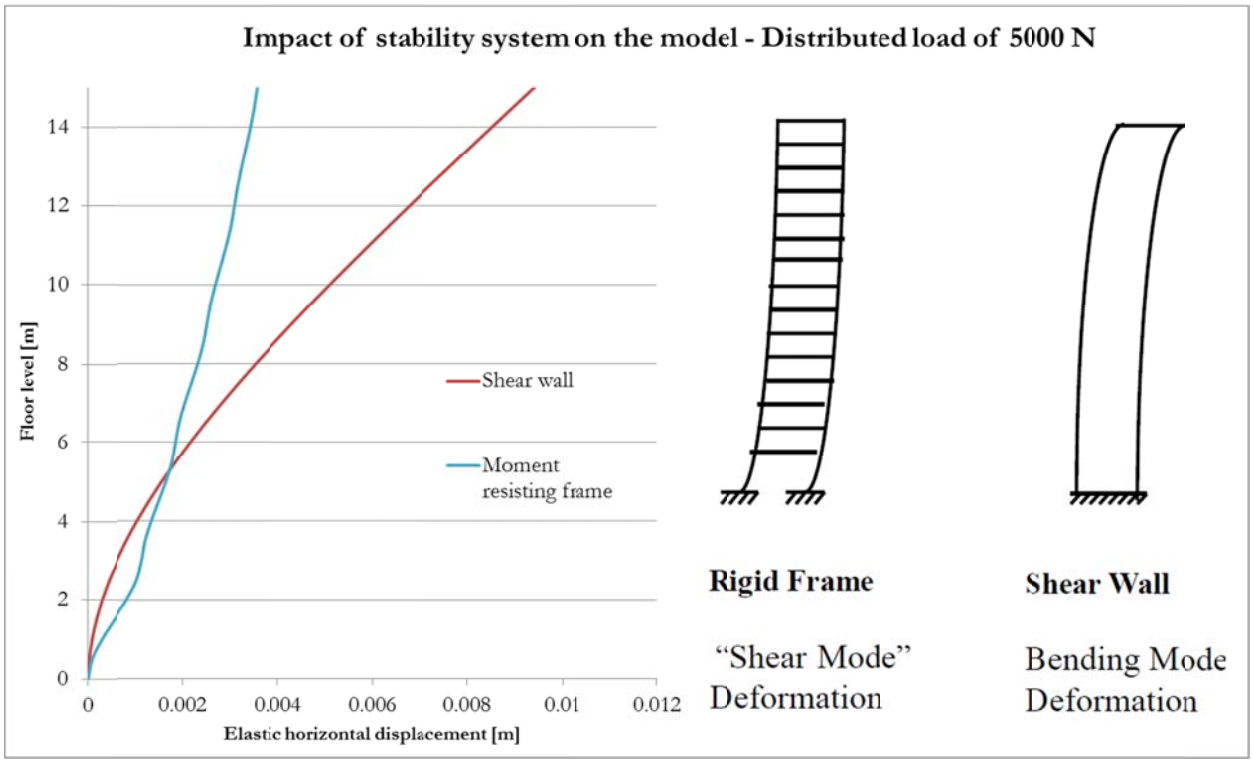

Figure 126 – Impact of the stability system adopted for the frame model on the displacement demands over the height. Note: the number of floors for the pictures on the right is note representative of the models developed.

Record D

Record D - PGA: 0.188608 m/s2 - Duration: 10 sec		
N° floors	Max scaling up to failure	Failure scaling ratio
1	4.72	1.46
2	3.50	1.08
3	2.23	0.69
4	1.48	0.46
5	2.23	0.69

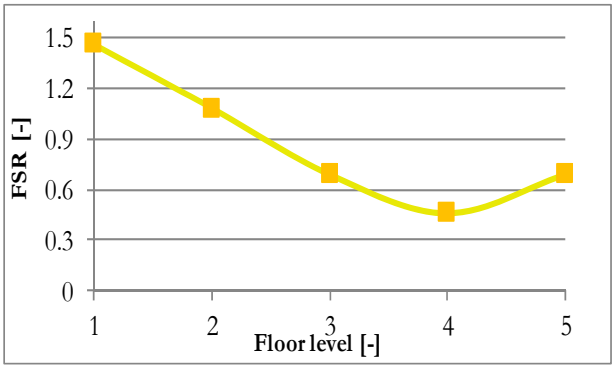

N° floors	Max scaling up to failure	Failure scaling ratio
1	4.51	1.39
2	3.02	0.93
3	2.23	0.69
4	2.76	0.85

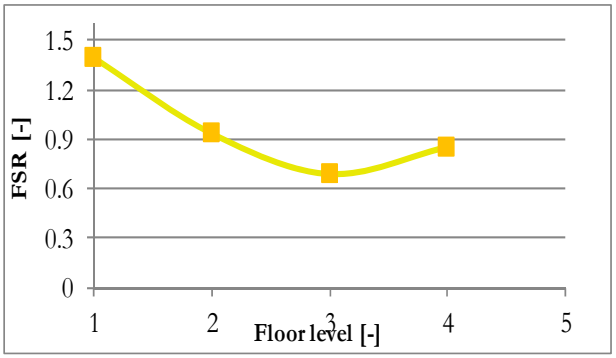

N° floors	Max scaling up to failure	Failure scaling ratio
1	3.71	1.15
2	3.23	1.00
3	3.02	0.93

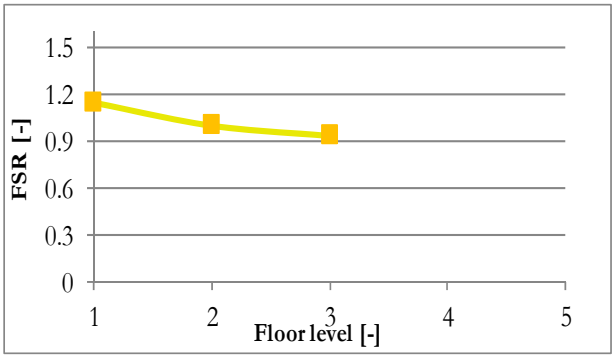

N° floors	Max scaling up to failure	Failure scaling ratio
1	3.50	1.08
2	3.02	0.93

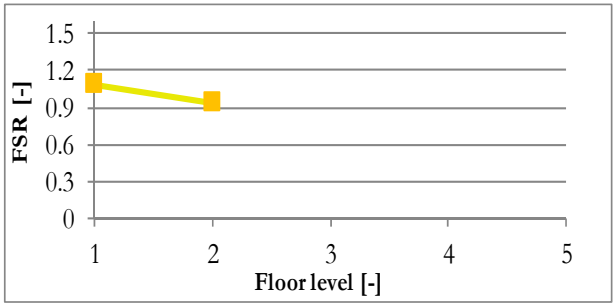

N° floors	Max scaling up to failure	Failure scaling ratio
1	3.23	1.00

Table 34 – Failure scaling ratio for the frame models. Record D. Moment resisting frame stability.

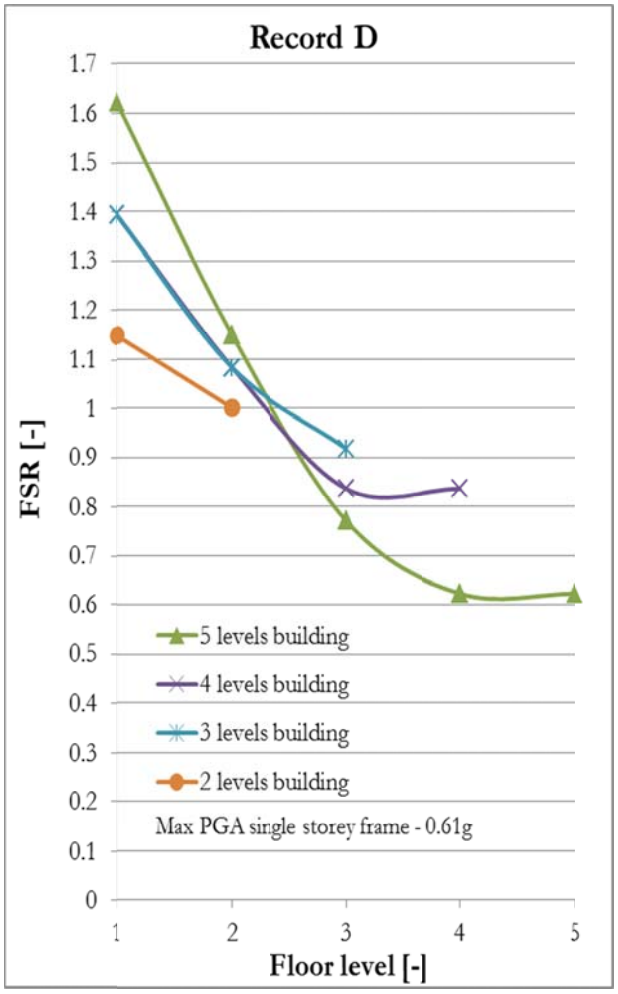

Figure 127 – Signal D. Shear wall stability.

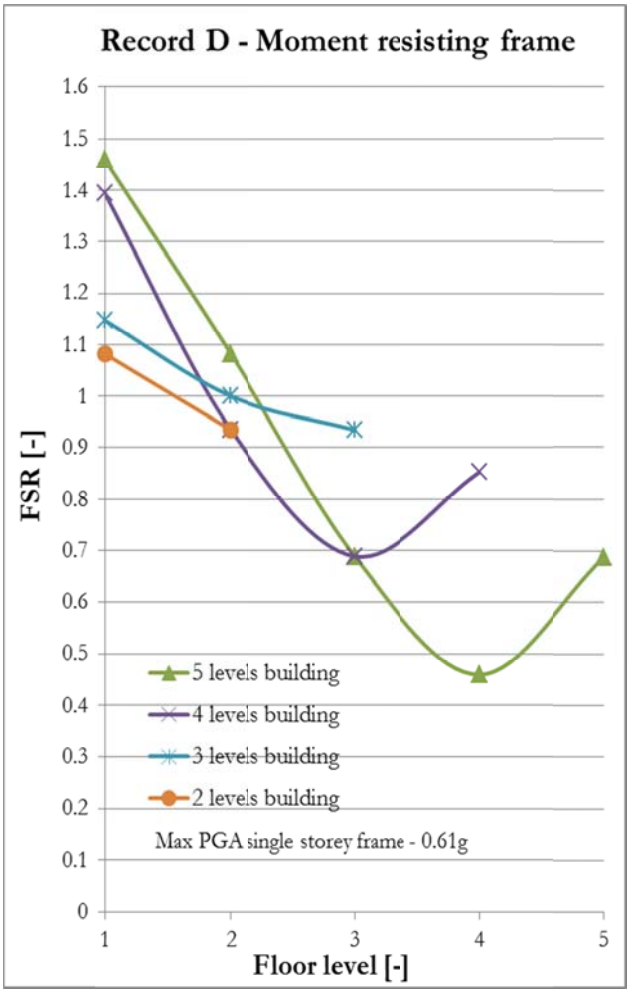

Figure 128 – Signal D. Moment resisting frame stability.

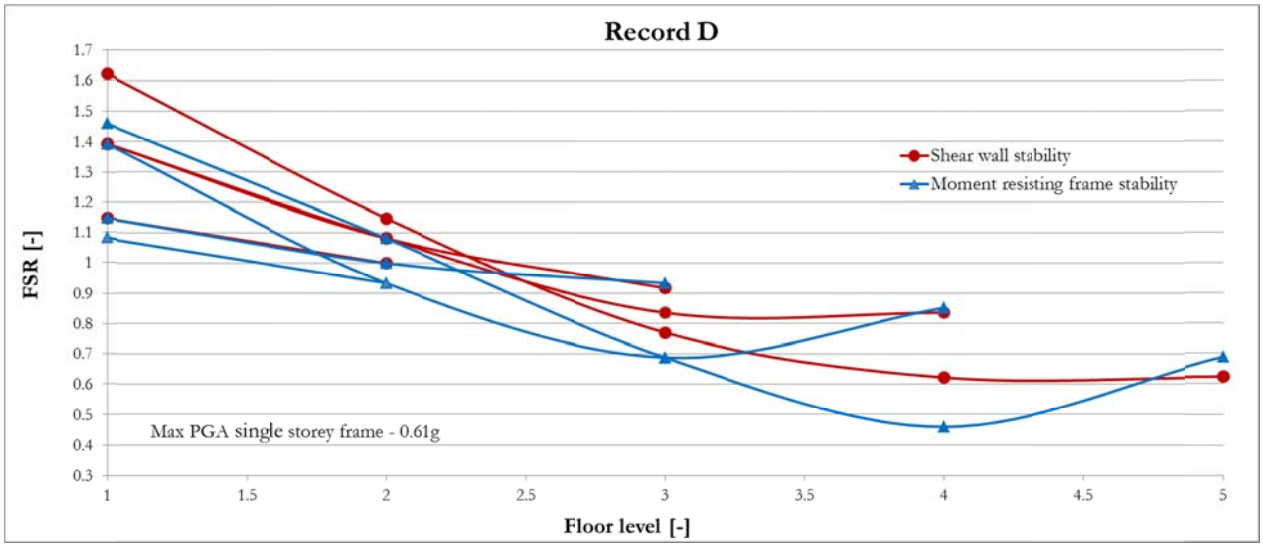

Figure 129 – Signal D. Direct comparison between the two figures above.

5.4.3 Height effects

The observations made on the FSR-graphs suggest that the dynamic response of the walls acting of out-of-plane deserves more investigations, especially when it comes to get a better understanding on the larger PGA that can be resisted by top walls with respect to those beneath them. In general, the main load acting on the wall systems is associated to the inertia forces that originate from the imposed accelerations acting at the ends of the walls in correspondence of their connections with the floor. In order to evaluate the impact of these accelerations on the wall systems acting out-of-plane, it is first necessary to analyze how they develop in the frame models and to assess the maximum values they reach at each of the floor levels under the excitation of a base motion. Therefore the records A, B, C and D are employed to run a set of linear transient analyses on the frame models. The resulting amplification profiles are illustrated in Figure 130 for frames of 1 to 4 storeys. In the y-axis is the amplification of the accelerations as a function of the height, which is represented by the ratio between the maximum accelerations calculated at floor level during the transient analysis and the PGA of the base excitation. That is:

$$Amplification_{(n\_floor)} = \frac{Acc_{n\_floor}}{PGA}$$

Attention is now given to the case of a 5-storey frame model. The maximum absolute values of the accelerations at floors level, for each of the four signals, is illustrated in Figure 130. The response of the frame model to the external excitations shows a tendency of the building to amplify the ground input almost linearly over the height. This might be due to the fact that the response of the 5-storey frame is mainly governed by its first modal shape of vibration.

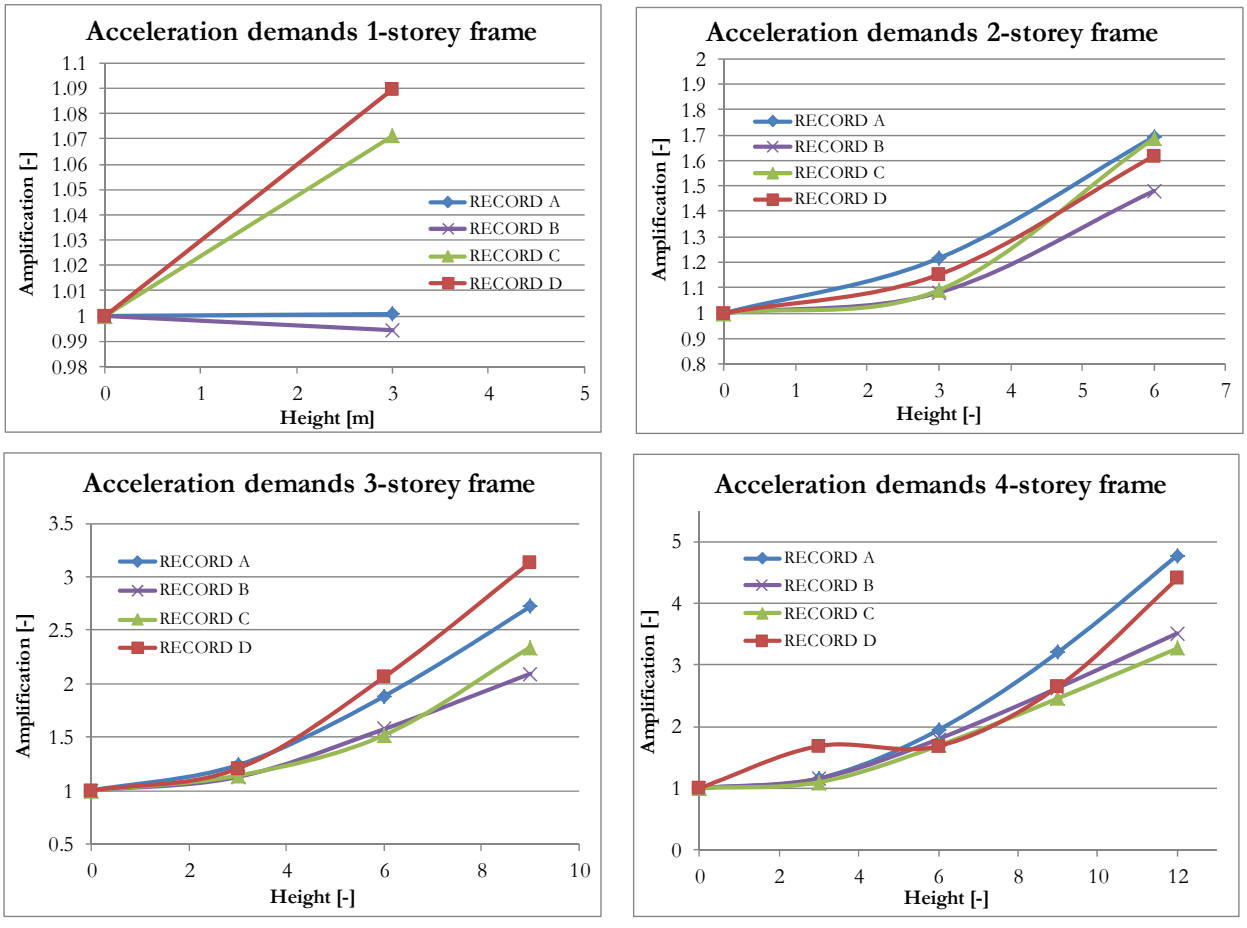

Figure 130 – Amplifications of the acceleration demands at floor level. Frame models, four exciting base signals.

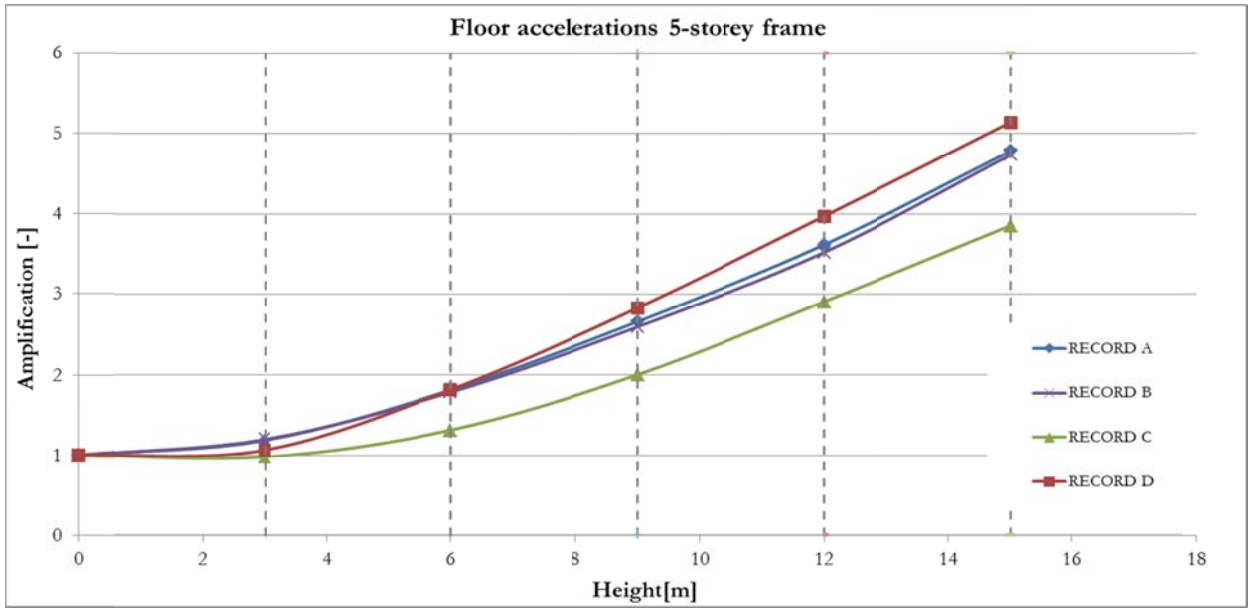

Figure 131 – Amplification profile of acceleration demands for a 5-storey frame subjected to four different base motions.

The amplifications in accelerations demands caused by the response of the primary structure can be classified as height-effects. These are not sufficient for explaining the resistance to the out-of-plane failure demonstrated by the - secondary - wall systems in the NLTHA. In fact, not only there is no evidence of floor accelerations being reduced over the height of the frame, but actually, the curves describe a clear increasing trend up to the top of it. Thus, the performance of the URM walls acting out-of-plane in the frame models needs to be analyzed by taking into account also the extra contribution given by the interaction of the primary and secondary system. Before doing so, the amplification profile of Figure 131 is compared to the curve found in the New Zealand normative (NZS1170.5; Section C8.2).

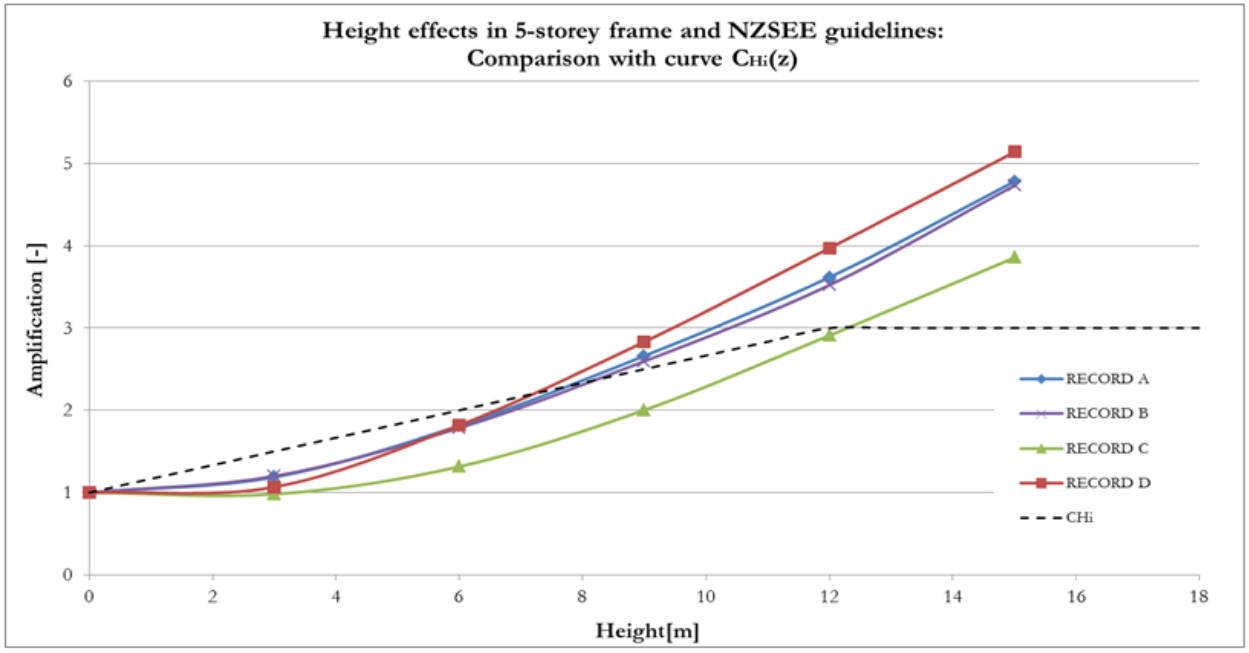

Figure 132 – Amplification profile of acceleration demands for a 5-storey frame: comparison with maximum values found in the New Zealand normative.

Clearly, the acceleration demands found in the numerical representation of the building are larger than those prescribed in the codes. This fact can be explained by the behavior of the primary system which is governed by the first modal shape of vibration. It might be possible that if the frame model was taller, other modes of vibration would have influenced the response of the system on higher floors. This however is not relevant to the 5-storey frame, for which an explanation of such an occurrence may be related to the linear-elastic material properties that were assigned to the frame building model. It is likely that preventing the frame model from yielding results in "un-controlled" amplification in acceleration demands at floor level. Accounting for the ductility of the primary system would have probably activated and delivered more energy to the secondary shapes of vibration resulting in a different response of the model with respect to the acceleration demands at floor levels (see Figure 133). This aspect, however, is not part of this investigation.

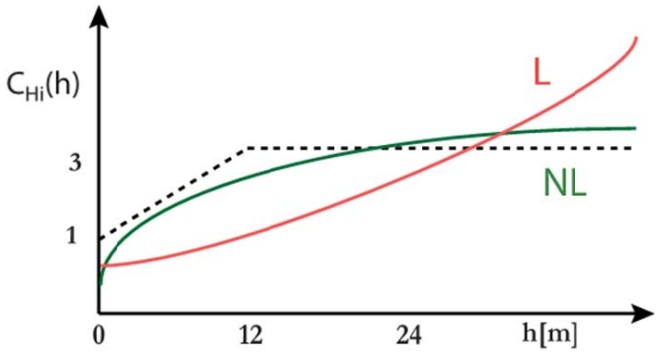

Figure 133 – Supposed trend of amplification in acceleration demands at floor level if nonlinear material properties were used for the primary system of the model.

5.4.4 Part effects

The dynamic response of the primary and secondary systems and the way they interact with each other largely affects the magnitude of the inertia forces that develops on the wall systems on higher floor levels. Aiming to a better understanding of this interaction, elastic floor response spectra for the 5-storey frame model are computed. These are derived through the accelerations output found in the previous linear analyses and an algorithm based on the Fast Fourier Transform. In the elastic response spectra below are also indicated the vibrational period of the frame building, the rocking mechanism calculated in accordance to New Zealand Code and the elastic double-clamped beam (which represents the URM wall in the undamaged condition – linear elastic analysis). The calculations for their derivation are provided in the Appendix F of this report.

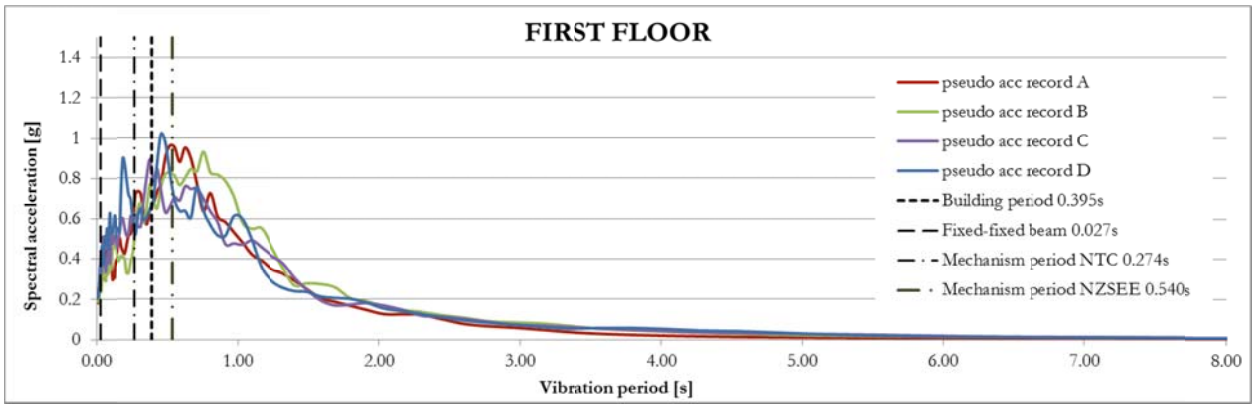

Figure 134 – Elastic floor response spectrum at ground-floor level for the frame building model.

By looking at the Figures 134 it is possible to notice that the elastic spectrum at ground-floor level presents a stocky profile with a peak spectral acceleration of around 1g. That is almost five times the PGA of the four records used to

excite the model. Indeed, when the secondary system has a vibration period smaller than 1,5 seconds, it experiences a larger acceleration than the one acting at the base of the primary system. On the other hand, larger periods of vibration corresponds to a very flexible secondary system for which the acceleration demands drastically reduces down to zero.

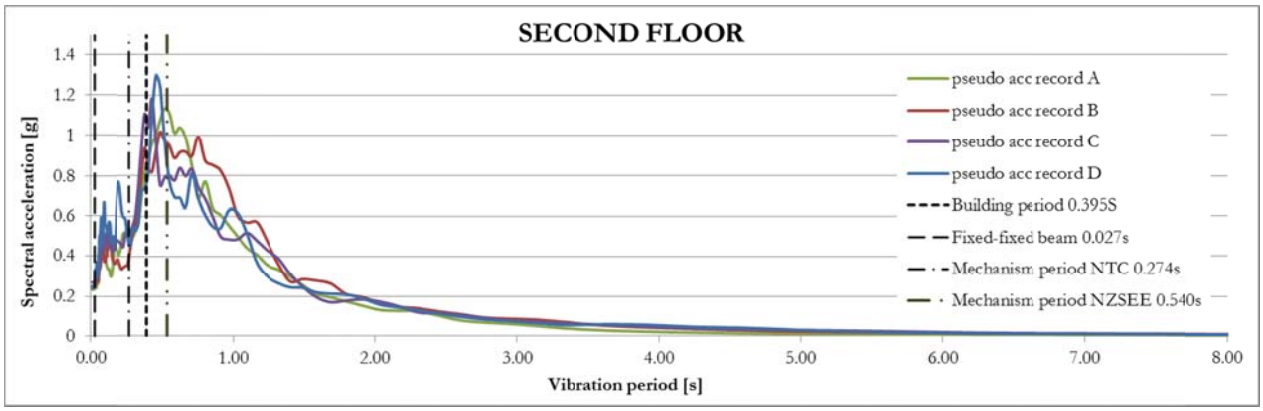

Figure 135 – Elastic floor response spectrum at second-floor level for the frame building model.

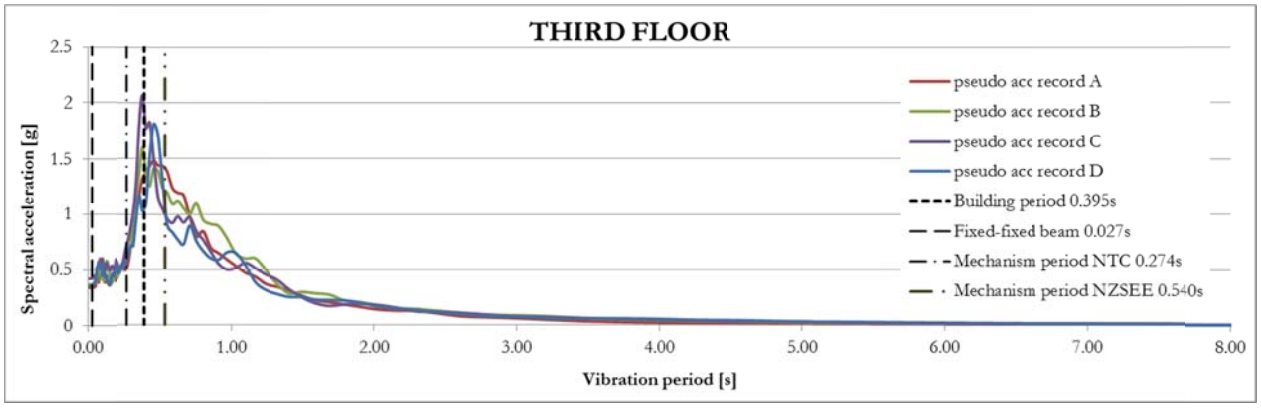

Figure 136 – Elastic floor response spectrum at third-floor level for the frame building model.

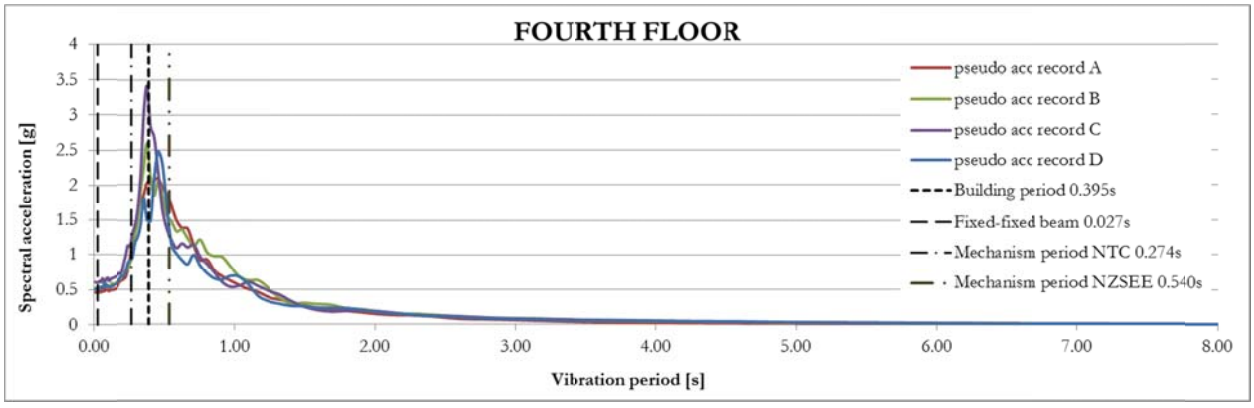

Figure 137 – Elastic floor response spectrum at fourth-floor level for the frame building model.

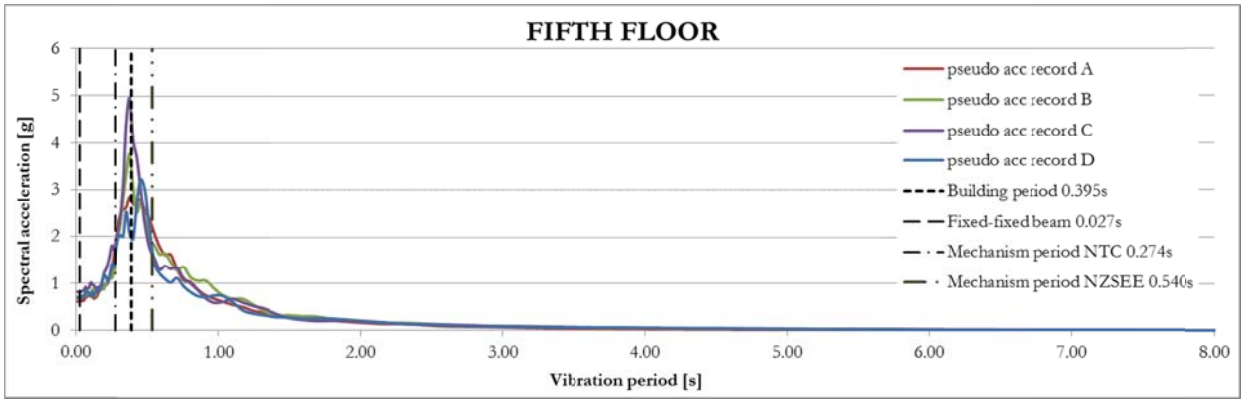

Figure 138 – Elastic floor response spectrum at fifth-floor level for the frame building model.

The amplification in acceleration demands are even more severe for response spectra of top floors. In figures 135-136-137-138 in fact, the bell-shaped curves become progressively more slender and present a tendency to concentrate the larger amplifications around a specific period of vibration: the period of the building. This means that the response of the primary system to the base excitation has an increasing influence on the response of the wall systems the more they are distant from the ground level. In other words, the characteristics of the ground motion are gradually filtered out by the primary system until it eventually governs the behavior of the top floors. At that point, it is no longer possible to discern the input spectrum at ground level. According to Figure 138, the secondary system represented by the rocking wall would be subjected to accelerations of 5g if its period of vibration is close to the one of the frame building. In section 2.8.2 an simplified formula was presented for computing the period of oscillation of a masonry building lower than 40 meters. According to the Italian code, the following formula should be used with the factor C set equal to 0.05 and H being the height of the building:

$$T_1 = C_1 \cdot H^{3/4} = 0.05 \cdot 15^{3/4} = 0.381\ seconds$$

This value is very close to the results obtained through an eigenvalue analysis in Diana, where the period of oscillation of the 5-storey frame was computed as 0.396 seconds (Table 28). Although the effects of resonance phenomena on the response of the walls grow more and more severe with the height, it should be noted that the range of vibrational periods for which the wall is affected becomes smaller. This fact is of great importance on the study of the out-of-plane behavior of rocking walls due to the fact that their period of oscillation is a function of their deformation. A large mid-height displacement in a rocking wall corresponds to a system with a relatively low lateral stiffness and, by consequence of that, with a large vibration period. Therefore the walls located on top levels experience much larger accelerations compared to those present at ground-floor level but only for specific displayed configurations of the walls beyond which the inertial forces acting on them reduce abruptly. As an example, it is possible to derive in an approximated way the values of mid-height displacement of the rocking wall on the fifth floor corresponding to a large magnification of the floor accelerations. Using the Italian approach (see also Appendix F) and assuming that "resonance" of the wall response can be expected between 0.3 and 0.55 seconds (see picture hereunder) it follows that:

$$T_p = 2\pi\sqrt{\frac{d_s^*}{\alpha_s^*}} = 2\pi\sqrt{\frac{\Delta^*_{midheight,secant}}{\alpha_0^*\left(1-\frac{\Delta^*_{midheight,secant}}{\frac{t}{2}}\right)}} \qquad since \qquad \alpha_s^* = \alpha_0^*\left(1-\frac{\Delta^*_{midheight,secant}}{\Delta^*_{midheight,max}}\right)$$

$$\alpha_0^* = \left(1+\frac{P}{W}\right)\frac{4t}{h}g = \left(1+\frac{15000}{5297{,}4}\right)\frac{4\cdot 0{,}2}{3}\cdot 9{,}81 = 10$$

$$T_p = 2\pi\sqrt{\frac{\Delta^*_{midheight,secant}}{10\left(1 - 10\cdot\Delta^*_{midheight,secant}\right)}} \qquad \rightarrow \qquad \Delta^*_{midheight,secant} = \frac{{T_P}^2}{10\cdot T_P^2 + 3{,}94}$$

The spectral displacement $\Delta^*_{midheight,secant}$ should be transformed to its real value which in this case amount to double its value. Hence:

$$T_P = 0.3s \quad \rightarrow \quad \Delta_{midheight} = 0.018\,m$$

$$T_P = 0.55s \quad \rightarrow \quad \Delta_{midheight} = 0.043\,m$$

All the configurations of the wall with a mid-height displacement within the two values above corresponds to cases where the inertia forces acting on the wall are amplified greatly, see picture below.

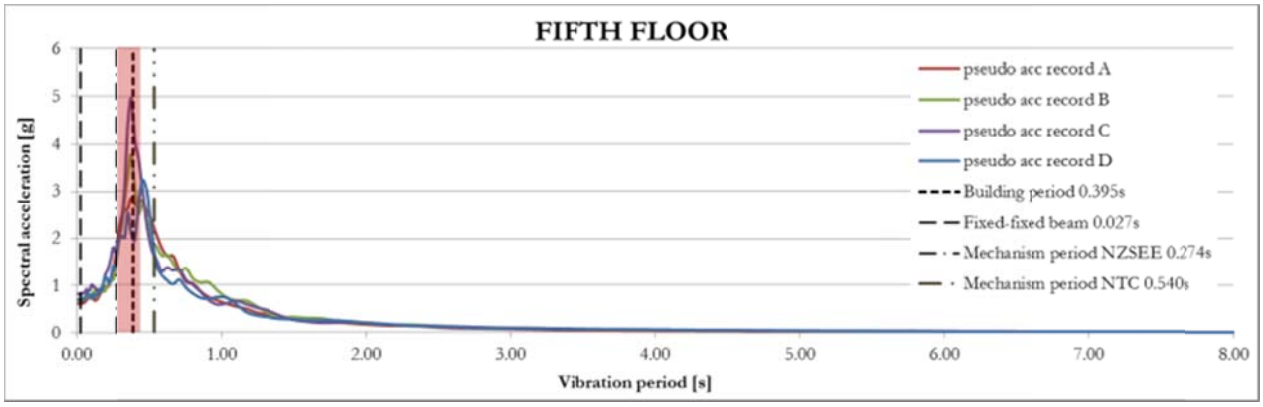

Figure 139 – Range of periods analyzed to estimate the max amplification of inertia forces acting on the wall system during rocking and based on its deformed configurations.

The example above demonstrates that a wall during the rocking motion is subjected to accelerations (and associated inertial forces) that vary as a function of its mid-height displacement. This aspect cannot be studied through a linear elastic transient analysis because the walls do not crack and their period of oscillation would stay equal to that of a clamped-clamped beam, which is close to zero. Thus, no amplification of accelerations (resonance) would occur in linear-elastic circumstances. Nonetheless, the response spectra showed that the role played by the vibration period of the secondary system is of crucial importance for understanding the magnitude of forces acting on walls located on top floors. Although the amplification in acceleration demands may be really large in that situation, the wall systems would experience these accelerations only for a "very short period of time": soon after a wall passes the resonance peak, the imposed accelerations applied to it drastically decrease. On the contrary, for walls located on lower levels, the range of periods for which the secondary system experiences amplifications is larger (the floor response spectrum is wider) and, possibly, leading to more unfavorable effects.

Thus, a correct estimation of the resistance to the out-of-plane failure of a URM wall should not disregard the "period elongation" associated with the deformation of the system. This aspect may explain why the results of the NLTH analyses, plotted in Figures 121-122-123-124, present a FSR curve that is not steadily decreasing as one would expect by only looking at the trend of acceleration amplifications at floor level obtained for the frame model as a function of the height. Also, it should be underlined that the response spectra computed in this Chapter are elastic. Deriving nonlinear response spectra at floor level would probably lead to a more accurate estimation of the inertial forces involved in the problem. In fact, allowing the primary structure to yield would suppress much of the response at first mode period,

accentuating the response at higher modes with proliferation of short-period accelerations spikes of a smaller size than the one found in the case of elastic response spectra on top floors.

Before drawing the final conclusions on the outcome of the previous NLTHA (Section 5.4.1) an additional check is made. The derived elastic response spectra of figures 134-135-136-137-138 can also be employed, theoretically, to derive the amplifications of acceleration demands at floor level, since the spectral values in correspondence of a vibrational period close to zero (secondary system infinitely rigid, i.e. it "follows" the response of the primary structure) should indeed represent the floor accelerations in each of the spectra. To verify this, the accelerations for T=0 are extracted and elaborated:

HAND CHECK HEIGHT AMPLIFICATIONS FROM ELASTIC FLOOR SPECTRA								
	Floor acceleration [g]				Amplification PGA			
Floor level	A	B	C	D	A	B	C	D
5	0.61	0.72	0.82	0.69	3.48	4.00	4.21	3.68
4	0.47	0.53	0.61	0.51	2.66	2.94	3.14	2.71
3	0.33	0.37	0.42	0.35	1.89	2.05	2.16	1.88
2	0.23	0.25	0.27	0.24	1.32	1.40	1.38	1.28
1	0.18	0.19	0.22	0.21	1.05	1.05	1.14	1.10
PGA signals:	A - 0.1759g		B - 0.1798 g		C - 1953g		D - 1886g	

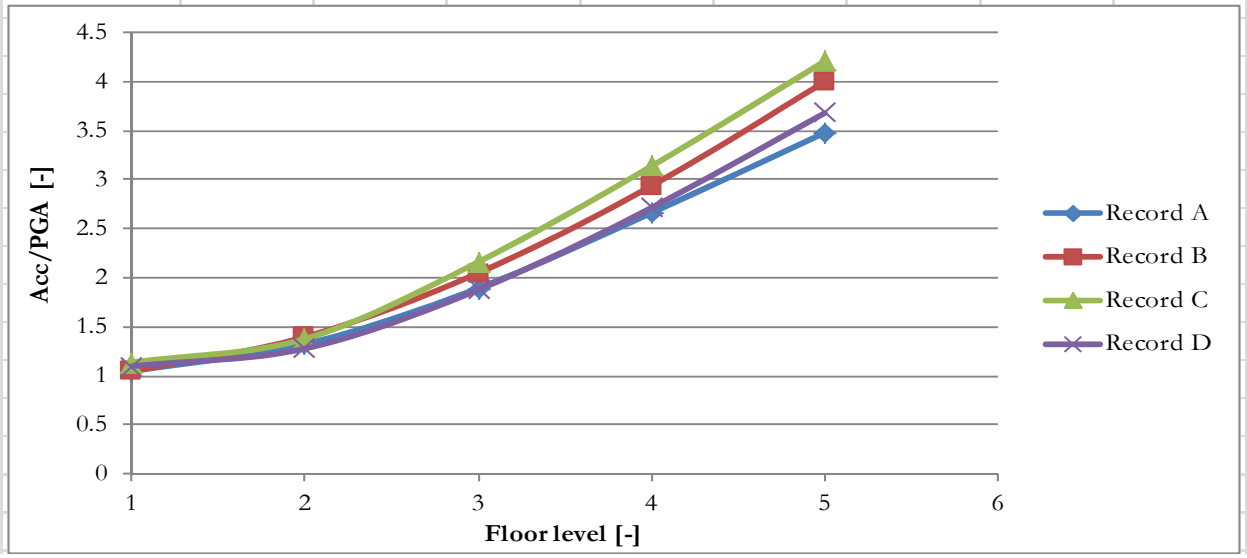

Figure 140 – Amplification of acceleration demands as a function of the height on the frame and obtained through the elastic response spectra at floor level.

The amplification profiles plotted for the 4 signals in Figure 140 show a similar trend to the one depicted in Figure 131. The accelerations increase over the height following the first modal shape of vibration for the frame building as expected. These results are comparable to those presented in the previous section, although not perfectly matching.

5.5 Comparison of numerical results with the foreign normative

The Failure Scaling Ratio presented as an output of the incremental dynamic analysis on the frame models gave an indication of the maximum PGA a unreinforced masonry wall element located on a specific floor of a building is able to withstand before failing out-of-plane with respect to a reference case. The results related to a 5-storey frame and obtained by adopting four signals A, B, C and D as a base excitation can be employed to make a comparison with the maximum PGA a URM wall is able to resist according to the New Zealand and Italian codes. Aiming at this, the curves for a 5-storey frame in Figure 125 should be modified. On the vertical axis, the FSR is converted to the actual value of the max PGA that the wall is able to resist when subjected to one of the signals.

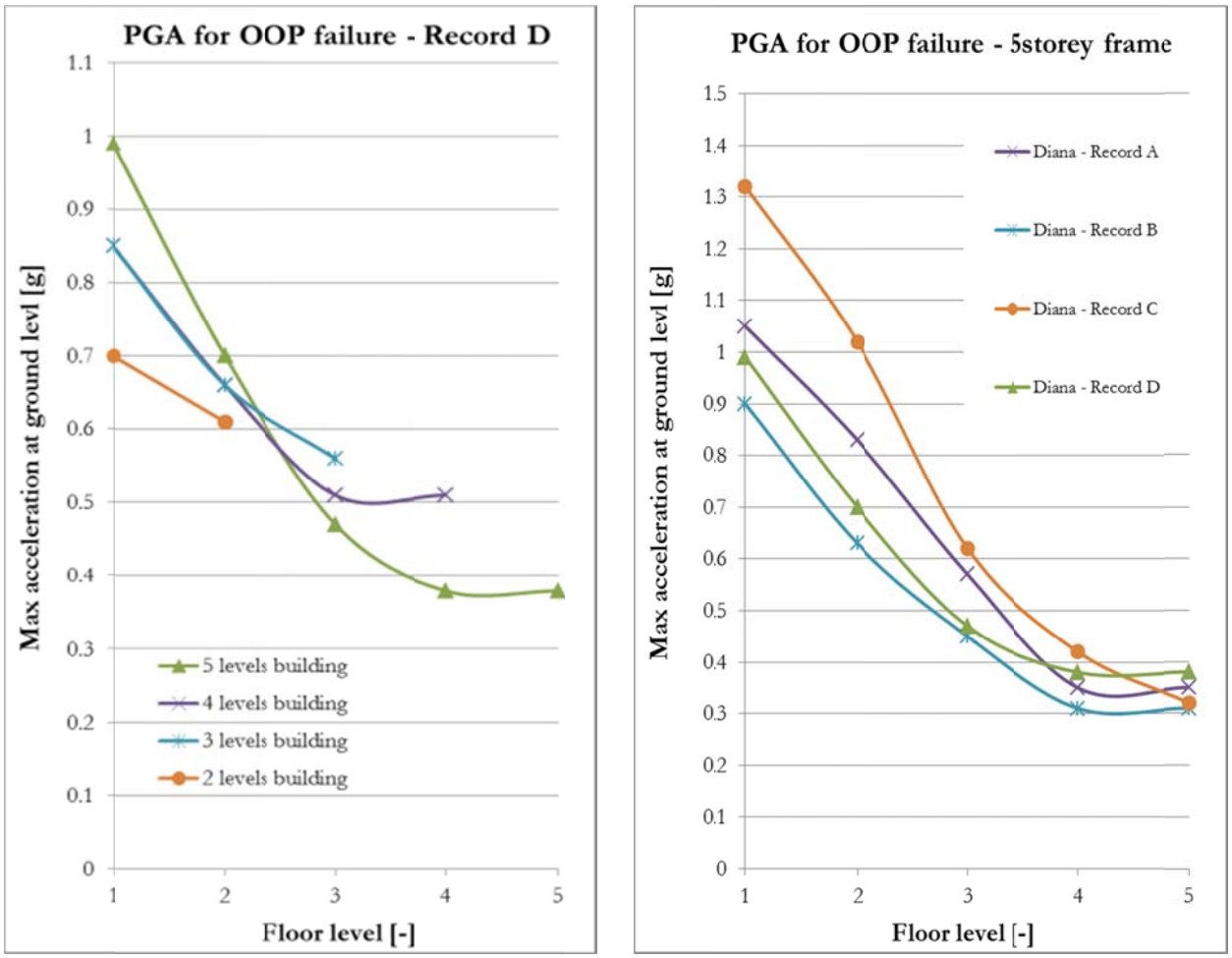

Figure 141 – Max PGA that URM walls are able to resist before failing OOP according to numerical results on DIANA. On the left, the case related to Record D and different frame sizes. On the right, all records on 5-storey frame.

The max peak ground accelerations for the walls according to the foreign normative can be extrapolated from the relevant codes by applying the maximum values to the amplifying coefficients for the calculation of acceleration demands on those walls. This means that height effects, for instance, will always be considered with the maximum amplification possible. For the New Zealand normative the following applies:

$$Max\ PGA \quad \rightarrow \quad 100\%NPR$$

Where the sign %NBS is substituted with %NPR due to the fact that the elastic response spectra used will be the only relevant to the Groningen scenario and, thus, in agreement to the NPR prescriptions. For details on the acronyms used, reference is made to NZSEE 1170.5, section C.

$$100\%NPR \quad \rightarrow \quad D_{ph} = \Delta_m \quad and \quad \Delta_m = \gamma \left(\frac{T_P}{2\pi}\right)^2 \cdot C_P(T_P) R_P \cdot g$$

$$C_P(T_P) = S_e(0) \cdot C_i(T_P) \cdot C_{Hi} \quad \rightarrow \quad C_P(T_P) = \frac{PGA_{Max}}{g} \cdot C_i(T_P) \cdot C_{Hi}$$

The elastic site spectrum employed to do this is derived in accordance to section 3.2.2.2.1 of the NPR9998. The parameters adopted are presented in the table inside the graph of the spectrum.

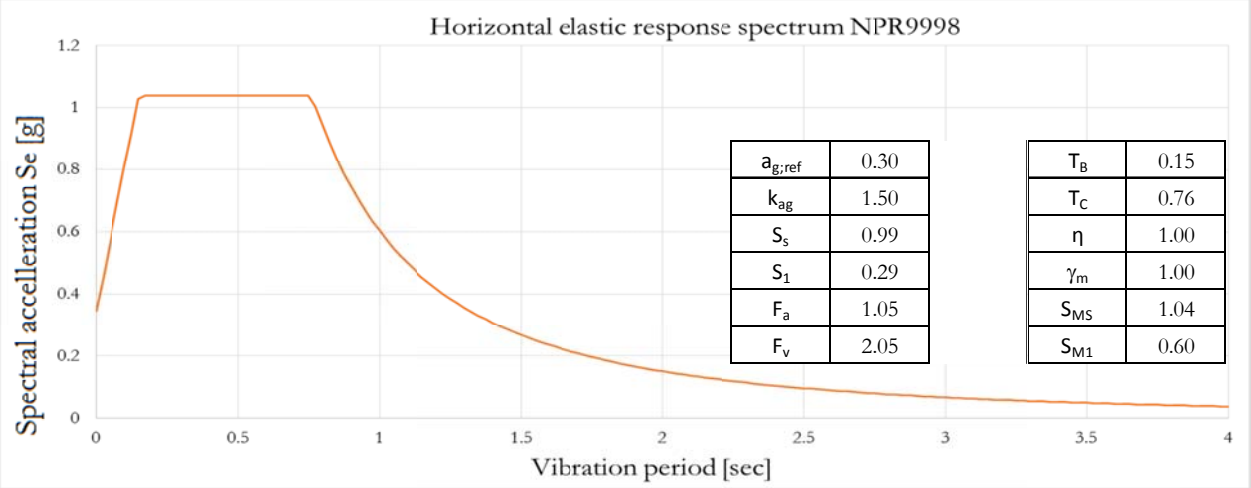

Figure 142 – Elastic response spectrum for horizontal actions derived according to NPR9998 for the area of Groningen.

The C(0) corresponds to the PGA the building is subjected to and it can be substituted with the Se(0) determined by the NPR, shown above. Chi is a factor that magnifies the PGA such that it reflects the acceleration of the main structure at a given height. Finally, the Chc(Tp) is a factor that magnifies the acceleration of the main structure at a given height to reflect also the effect of the period of the part. The curve presenting the values of Chc(Tp) as a function of the period of oscillation can be derived from the NPR9998 spectrum by normalizing it to the PGA and capping it to a maximum of 2 (as it is the case in the NZSEE guidelines, see "BRANZ" report for more details). Therefore:

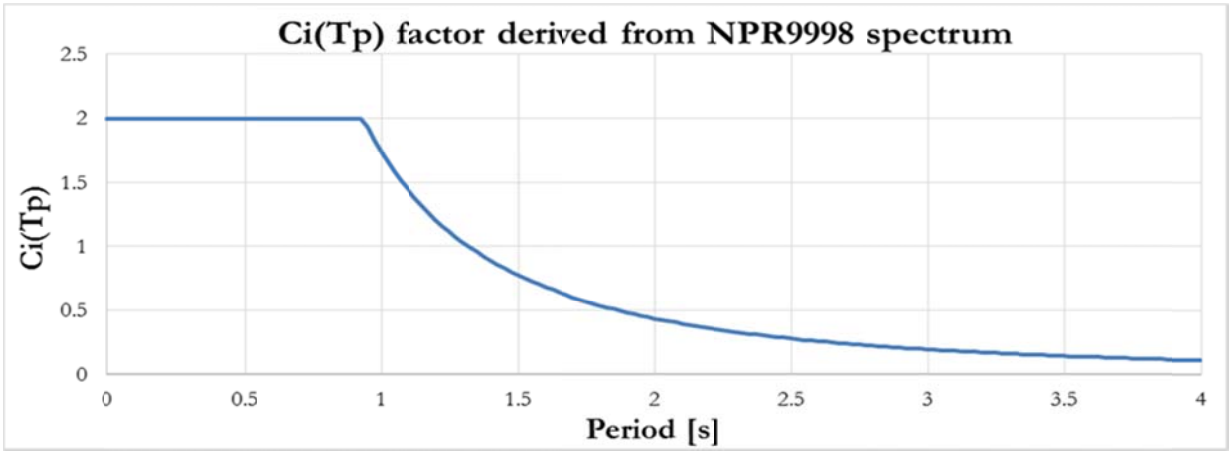

Figure 143 – Adaptation of the spectral shape function to the NPR9998 for the area of Groningen.

It was found before (see Table 29) that the period of the rocking mechanism based on the New Zealand codification is 0.540 seconds. By setting Rp=1 and γ=1.13 (See also Appendix F) one obtains:

$$\Delta_m = \gamma \left(\frac{T_P}{2\pi}\right)^2 \cdot \frac{PGA_{Max}}{g} \cdot C_i(T_P) \cdot C_{Hi}$$

$$PGA_{Max} = \frac{\Delta_m}{\gamma \left(\frac{T_P}{2\pi}\right)^2 \cdot C_i(T_P) \cdot C_{Hi}} = \frac{\Delta_m}{1.13 \left(\frac{0.54}{2\pi}\right)^2 \cdot C_i(0.54) \cdot C_{Hi}}$$

In case of a URM wall located on the 5th floor of a frame building, the value related to height effects is presented hereunder together with the value of the parts coefficient extracted from the Figure 142.

$$C_{Hi} = 3 \qquad since\ h_i = 13.5\ meters$$

$$C_i(0.54)_{NPR} = 2 \qquad since\ h_i = 13.5\ meters$$

Speaking of the maximum mid-height displacement allowed, the NPR specifies that the behavior factor q (generally intended for ULS/LS limit state) can be increased by 1.33 when considering the near-collapse limit state, i.e. to increase the degree of damage allowed. Therefore the 0.6 factor can be increased to 0.8. So:

$$\Delta_m = 0.8 \cdot \Delta_i = 0.150\ meters \qquad (See\ also\ Appendix\ E)$$

$$PGA_{Max} = \frac{0.150}{1.13 \left(\frac{0.54}{2\pi}\right)^2 \cdot 2 \cdot 3} = 2.25 \frac{m}{s^2} = 0.22g$$

Similar calculations are carried out for the walls on lower floors, taking into account that the contribution paid by the height effects is a function of the wall location in the building, as shown in the diagram below.

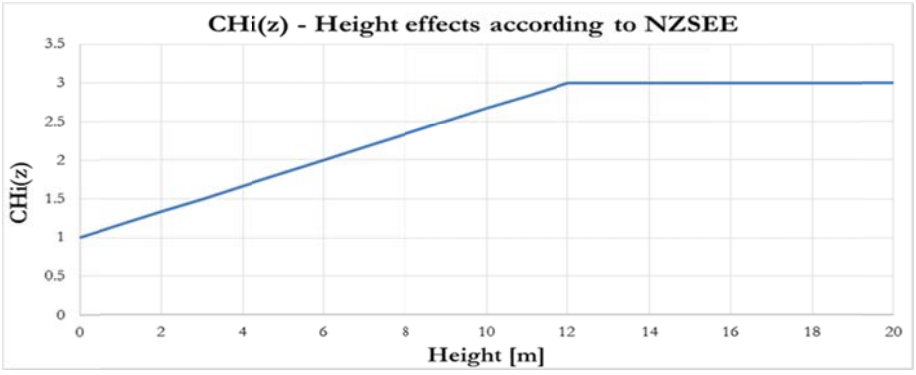

Figure 144 - Height effects coefficient as in the New Zealand guidelines NZS1170.5.

With regards to the Italian normative, the following applies:

$$\alpha_0^* = \frac{S_e(T_1) \cdot \Psi(Z) \cdot \gamma}{q} \qquad with \qquad q = 1 \quad (all\ the\ ductility\ is\ in\ the\ mechanism\ itself)$$

$$\Psi(z) = \frac{Z}{H} = \frac{Z}{15} \qquad where\ H\ is\ the\ total\ height\ of\ the\ building\ and\ Z\ the\ location\ of\ the\ wall$$

$$\alpha_0^* = \alpha_0 \cdot g \quad with \quad \alpha_0 = \frac{4t}{h_w}\left(1 + \frac{P}{W}\right) = 1.04 \qquad (see\ also\ Appendix\ E)$$

$$T_1 = C_1 \cdot H^{3/4} = 0.05 \cdot 15^{3/4} = 0.381\ seconds$$

For such a vibration period of the building the value of elastic response is 3 times larger than the PGA at ground-level (see Figure 141). Then:

$$\gamma = \frac{3N}{2N+1} \quad with\ N\ number\ of\ floors \quad \rightarrow \quad \gamma = 1.36$$

In case of a URM wall located on the 5th floor of a frame building:

$$\Psi(13.5) = 0.9$$

All of this results in the following:

$$PGA_{Max} = \frac{0.104}{0.9 \cdot 1.36 \cdot 3} = 0.28g$$

The results obtained from the two codes and for a 5-storey building are plotted in the graph on the next page together with the curves depicted in Figure 141 (on the right).

PGA(max_normative) NZSEE				
Δm =	0.188	0.6	1.33	0.150024
γ =	1.13		NC factor NPR	
Tp =	0.54			
Ci(0.54) =	2			
floor [-]	Chi(z)		[m/s2]	[g]
5	3		2.9957	0.31
4	2.75		3.2681	0.33
3	2.25		3.9943	0.41
2	1.75		5.1355	0.52
1	1.25		7.1898	0.73

PGA(max_normative) NTC				
Height amplification according to NTC: Ψ(z)				
Z	Ψ	α_0 [g]	floor [-]	[g]
13.5	0.9	1.04	5	0.283224
10.5	0.7		4	0.364146
7.5	0.5	Se(T1)/PGA 3	3	0.509804
4.5	0.3	γ	2	0.849673
1.5	0.1	1.36	1	2.54902

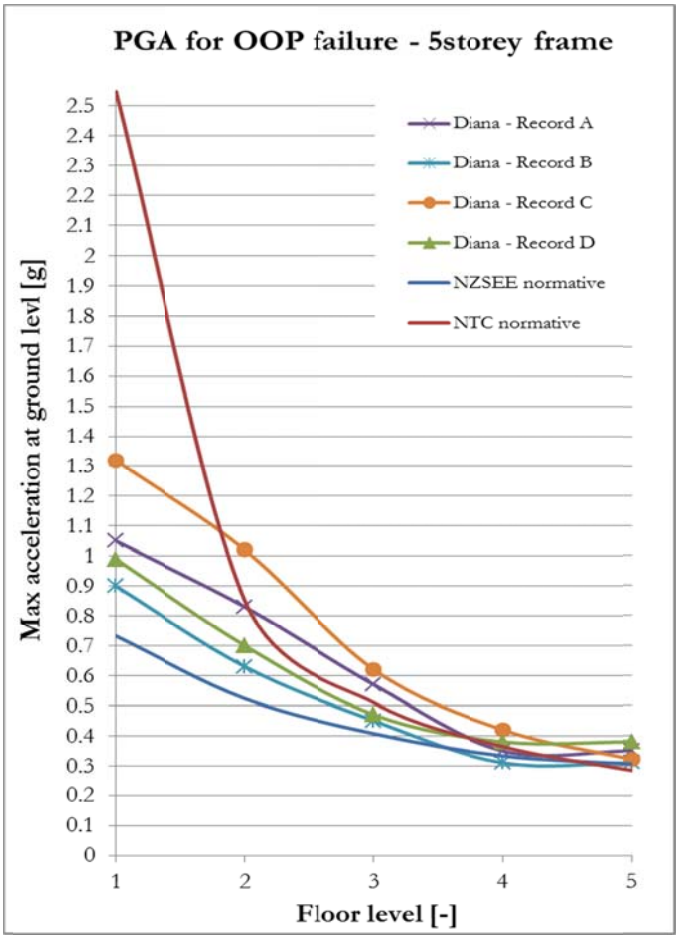

Figure 145 – Max PGA that URM walls are able to resist according to numerical results on four records and foreign codes.

Although it is not possible to accurately estimate the exact contribution of parts effects to the out-of-plane resistance of the walls, the graph evidences that their influence is rather significant on the outcome of the numerical analysis. In the FE models from Diana, the interaction of primary and secondary systems is so big that they seem to greatly counter-act the amplifications in acceleration demands at floor levels caused by height effects. When the walls on higher floors start rocking, the inertia forces act on them for a very short period of time after which, due to the period elongation of the mechanism itself, the detrimental effect of these forces reduce abruptly. Hence, the numerical results show that the unreinforced masonry walls are capable of withstanding much larger PGA than expected on top floors.

With regards to the max PGA's derived from the foreign normative, the graph of Figure 145 can be dived in two parts. For the URM walls on the first level, the numerical model appears to be able to resist larger accelerations than in the case of the New Zealand normative but almost half of the magnitude found in the Italian one, even though the curve for the NTC approach may be considered meaningless at ground-floor level as it is not meant to be used for it. For higher floors, the results obtained though the numerical model are comparable to the prescriptions of both the codes, even though it can be stated that the maximum values of PGA found in the NZSEE seem to be rather conservative for wall located up to the fourth level in the frame building. It can be concluded that there is good agreement between the results of Diana and those of the foreign normative for walls located on higher floor levels.

6 Conclusions and Recommendations

This document starts with a general introduction to the topic of masonry walls acting out-of-plane, the challenges related to the assessment of their stability in the event of an earthquake and a list of associated research questions to guide this investigation. The following chapter now focuses on the results obtained as outcomes of this research. By tracking back the findings of the previous sections, an answer will be given to each of the questions arose after the literature study. Eventually, it will be possible to elaborate on the major research question:

"Is it possible to create an adaptation of foreign methodologies for the out-of-plane assessment of a URM wall to the Groningen scenario, by making use of a simple 2D frame model?"

6.1 Summary of results

The lumped cracking beams model demonstrated that it is possible to construct a discretized representation of the unreinforced masonry wall capable of capturing the geometrical nonlinearity that is specific of the rocking mechanism. The stiffness of the rocking system indeed decreased as the mechanism developed. This behavior was verified for both quasi-static and transient loading as well as for a variety of forcing frequencies and top loads applied on the wall. However, simulating the rigid bodies assumption in a finite elements model produced detrimental effects on the stability of the numerical analyses, particularly when the model was employed in dynamic investigations. For this reason two alternative models were developed.

The smeared cracking plane strain model seemed to be a valid choice for the discretization of the rocking wall. Its resistance to the lateral horizontal loading followed the same trend as in the lumped cracking beams model and it also enabled to implement the physical resisting properties of the masonry material. Nonetheless, in view of the model upgrades it was decided to abandon it due to its complex definition and the associated large computation time required for transient analyses. Still, the plane strain wall model was employed to determine the minimum number of integration points that are necessary over the wall thickness in order to avoid overestimating its displacement capacity at mid-height.

The second research question regarding which structural material aspects should be included in the model for the numerical investigation was better addressed by the other alternative wall discretization, the smeared-cracking beams model. By making use of it, the contribution of the physical nonlinearity of the material to the overall rocking behavior was accounted for. The model proved to be able to respond differently depending on the degree of constraint of its ends and the magnitude of the overburden. This last aspect had a considerable impact in the manifestation of crushing phenomena. Speaking of the ability of the model to give evidence of its material degradation in time, sequential pushover analyses indicated a hysteretic behavior of masonry in the out-of-plane deformation of URM walls which followed a nonlinear elastic law. A sensitivity analysis on the material parameters of the model revealed that it is not recommendable to apply a rotating crack model to the masonry, when in fact a fixed crack orientation seemed to better describe the energy needed to display the wall to its unstable configuration. Also, what came to light in the sensitivity analysis is the central role played by the tensile strength of the masonry, which appeared to be the most influencing property of the model as it determines both the initial lateral resistance of the URM wall as well as its deformation capacity in the estimation of its stability.

Thanks to its ease of operation, the smeared-cracking-beams wall model was chosen for extending the model to include its surrounding structure as well. The frame models were the objects of investigation in the last part of the chapter related to the FE models response. They were developed in a step-by-step procedure, to provide them of sufficient lateral stiffness. Two different stability systems were examined, namely shear walls and moment resisting frames, to evaluate their impact on the dynamic performance of the wall acting out-of-plane inside building. It was noticed that these stabilizing elements could also be interpreting the additional contribution to the lateral stiffness of the frames which is provided by the in-plane action of the return walls and/or perpendicular walls. Since the rocking mechanism of

a wall presents no specific resonant frequencies, its dynamic response needs to be analyzed by means of artificial records so that the system would be excited by a range of frequencies rather than a single one only. Therefore, the set of frame models was subjected to NLTH analyses on four different records selected among those derived from a spectrum in agreement to NPR provisions. The base excitations were used to run several incremental dynamic analyses (IDA) where they were increasingly amplified until the out-of-plane failure of a wall object of investigation would occur. A disadvantage that arose from adopting these frame models in dynamic analyses was that Diana seems not able to warn the user when an element is failing out-of-plane (not always the numerical divergence occurs, the analysis might proceed until its full completion). For this reason it came into view the crucial importance of post-processing the results and defining limit values for the mid-height rocking displacement of walls beyond which the walls were considered as failed. The output of all the IDA provided a means for developing the Failure Scaling Ratio (FSR) curves for the unreinforced masonry walls of the frame structures as they responded to the seismic excitations both within and beyond their elastic range. According to the results obtained, the maximum PGA that the walls were able to resist without failing out-of-their plane decreases the more they are located on higher floors. What is more, it was found that none of the original records employed seemed to be sufficiently strong to cause the direct out-of-plane failure of the walls in the frame models unless scaled appropriately. The main finding of the IDA however was that many of the walls located on top floors of the frame models exhibited the tendency to be less prone to out-of-plane failure than expected. This was reflected by the associated FSR curves which would not be steadily decreasing up to the top levels.

With the aim of achieving a better understanding on the rocking behavior of URM walls, some linear transient analyses were run on the frame models in order to investigate the impact of the height and parts effects in the dynamic response of the wall systems, the so called filtering effects. Since the inertia forces acting on a wall systems during a dynamic analyses are strictly dependent on the accelerations induced on the wall, analyzing how the acceleration demands develops in the frame building, or secondary system, and are subsequently transferred to the wall elements, or secondary systems, is of main importance. The amplification profile of the acceleration at floor level in the frame evidenced a trend resembling its first shape of vibration for all the records used. This would correspond to acceleration demands at floor level that are (almost) linearly increasing with the height. The output of the linear transient analyses was then employed to derive elastic response spectra at floor level through a Fast Fourier Transform procedure. According to the spectral curves, the amplification of accelerations induced on the wall systems increases for higher floors. However, the progressively slenderer shape of the resonance peaks over the height of the frame building results in a smaller range of exciting frequencies for which the secondary system experiences such amplifications. As the rocking mechanism of URM walls on top floors develops due to floor accelerations, the lateral stiffness of the walls decreases and by consequence of that their vibration period may elongate so much that the inertia forces acting on them almost vanish. This strong contribution given by the interaction between the primary and secondary systems explain the trend found in the FSR curves where the walls on higher top floors proved to be able to cope with maximum PGA that are similar in magnitude to those found for lower-level walls.

Finally, the out-of-plane performance of the URM walls resulting from the numerical analyses on the 5-storey buildings is compared to the that resulting from the New Zealand and Italian normative. The comparison showed that for walls on lower floors the maximum PGA tolerable by the numerical model stands in between the values derived from the foreign codes, whereas for wall on higher levels the maximum accelerations at the base of the buildings is similar for the numerical and the analytical models. Also, it was underlined how the values according to the NZS procedure are generally conservative, especially for lower-level walls.

6.2 Conclusions

This conclusive passage addresses the final and major research questions by taking into consideration all the findings brought into the light in the development of this investigation which were briefly reported in the summary at the beginning of this chapter.

At this point in fact, there are sufficient elements to get back to whether it is possible to replicate the results of foreign methodologies by elaborating the results of this research and by deriving demands amplification coefficients to account for the height and the parts effects on walls acting out-of-plane. It appeared that the FE models developed are able to capture the inherent nonlinearity of the unreinforced walls when experiencing the rocking motion. They not only allow

to evaluate the impact of several inelastic material properties (physical nonlinearity) and boundary conditions on the lateral stability of the walls, but are also capable of accounting for the strong geometrical nonlinearities involved in the rocking mechanism. Implementing the wall model, considered as a local or secondary system, into the frame building, representative of the primary system, made it possible to investigate how the two systems interact with each other and the way the primary structure filters out the accelerations from the ground-motion up to the higher floor levels. The derivation of elastic response spectra at floor level clarified the role played by the vibration period of a rocking wall when compared to that of the primary structure. Therefore, the simple 2D-models constructed in this research demonstrated to be effective tools for a numerical investigation on the above topics. In addition to this, the out-of-plane performance of the walls in the 2D models proved to be comparable to that one would obtain by referring to the analytical formulas derived from the foreign normative.

Speaking of the possibility of deriving amplification coefficients for the assessment of the demands on the URM walls in the Groningen scenario, in a similar way to those adopted in the foreign normative to account for height and parts effects, the answer is positive. However, the graphs that one would obtain by making the envelope of the output curves are conservative. This was quite evident in the case of the amplifications due to the height effects: the comparison between the numerical results and the amplifications according to the New Zealand normative clearly showed larger accelerations in the model. With regards to the parts-effects, some remarks should be made. First, the response spectra derived for the FE model are elastic. This means that the bell-shaped curves are likely to have a much higher peak than in the case of an structural element able to take excursions in the inelastic range. Also, the derivation of parts factors in the New Zealand normative was deduced through experimental findings in support of a large-scaled research programme which made it possible to "cap" the maximum amplifications to a certain level. This is not the case for the current research, which is purely numerical. Finally, the response spectra are highly dependent on the level of damping used, and for the presented research the value of damping in both the primary and secondary system was assumed rather than set as a result of a specific investigation. Hence, although it was theoretically possible to draw the parts and height coefficients functions, these would have been much conservative respect to the ones currently used in the codes.

This research demonstrated that the application of procedures based on a combination of spectral and kinematic limit analyses is appropriate for the assessment of the out-of-plane behavior of or URM walls. Overall, the methodology followed generated results which meet the expected behavior of the models, although the accuracy in results for the Groningen scenario did not seem to be increased. In view of a more extensive research on this topic, for instance by making use of detailed fully-nonlinear 3D models and inelastic design spectra from NPR, there is reason to believe that more accurate results can be obtained in order to optimize the assessment of URM walls acting out-of-plane.

6.3 Limitations of this research

The present research showed how complex it is to address the assessment of the stability of rocking walls subjected to seismic motions. Even more so, some of the challenges which result from attempting to describe in a numerical way this deeply nonlinear problem became apparent. Several times it was underlined how limiting and unfavorable it is to underestimate the role of the system surrounding the wall model by making strong simplifying assumptions in the modeling stage. A selection of restrictions associated to this research that is worth mentioning is presented below.

- The out-of-plane failure was addressed as a stability problem of one-way vertically spanning walls. In reality, the failure of walls out-of-plane is a complex 3D phenomenon.
- Assuming the rocking mechanism as a phenomenon that could be analyzed in a 2D environment automatically excludes the possibility of better addressing the filtering effects of the primary structure on the wall. In this way many dissipative mechanisms of the structure under a dynamic load are neglected.
- Target spectra used for the selection of records was the design spectra based on the NPR provisions but only a really small number of signals was employed in the numerical analyses. With regards to this aspect, it is evident that a research aiming to drawing conclusions from processing a large amount of data in a statistical way would have required many more tests. For the same reason, a widened suite of building models to encompass the full

range of structures likely to be encountered in practice should have been used. Hence, it could be said that one of the main limitations of this research is its lack of robustness.

- The energy dissipation in all the NLTH analyses performed was implemented by introducing a fictitious damping through the Rayleigh coefficients. The values used were 2% for the rocking wall system and 4% for the frame structure. The latter was averaged over the sources of the literature study which are based on researches from many different countries. In the same way, when applying the Fourier Transform methodology for the derivation of the floor response spectra a value was set for the damping of the system. It is noted that the models response and the parts effects generated are highly dependent on the assumed value of damping. Therefore, an in-depth investigation on the most appropriate levels of damping to employed should have been first carried out.
- The in-plane action of the wall elements perpendicular to the direction that was investigated for the models of this research was not quantified in detail. Consequently, the outcome of the investigations made should be taken into account this aspect as well.
- The approach used did not permit a "redistribution" of damage in the frame models and did not account for the interaction between simultaneous rocking wall systems. As a matter of fact, the incremental dynamic analysis were performed on models in which only one rocking mechanism was analyzed at each time.
- In the NLTH analyses the wall systems were considered failed either due to numerical divergence, or because the mid-height displacement of the rocking wall reached a limit value equal to its thickness. It should be noted that the latter circumstance is un-conservative, because when the rocking mechanism develops the masonry is subjected to deterioration and the usable thickness for the equilibrium of forces reduces.
- Modeling the primary system with linear elastic properties did not allow it to yield and respond inelastically to the external excitation. As a consequence of that, the acceleration demands at floor level were found to be rather large on top levels of the primary system.

6.4 Recommendations for future studies

This research demonstrated that a complex topic like the out-of-plane action of masonry walls must be addressed by means of a detailed modeling phase in which all the structural aspects pertaining to its nonlinear behavior should be taken into account.

Since this investigation wanted to capture the interactions in behavior occurring between the entire building and parts of it, with special focus to their dynamic response, it could be interesting to embark in a similar study performed on a full 3D model of a masonry structure. Despite the much longer computation times in NLTHA, such discretization would allow a steep decrease in the number of assumptions made, especially with regards to the contribution given by in-plane action of walls and stability system to the lateral stiffness of the model. The out-of-plane deformation is a three dimensional phenomenon which generally occurs in walls spanning in two directions. These walls have a larger lateral degree of constraint which makes them less likely to fail when subjected to inertia loads. A 3D model would be able to better estimate the impact of different boundary conditions such as the flexibility of diaphragms above the walls and the effect of concurring excitations in both the x and y direction.

Creating a model which is able to account for the way the energy is dissipated in the building and how the damage is distributed among the assemblage of structural elements would also make a big difference in the outcome of the analyses, assuring more realistic estimations of filtering effects in the building. For doing so the adoption of a FE software package able to perform sequential analysis in which elements are removed when they fail may be useful.

Finally, it is stressed the added value that cross-validation of numerical results with experimental findings would have brought to the research, in particular for deciding on the appropriate level of damping to use in the model and the degree of ductility of the building to consider.

Appendix A

With reference to the results of section 5.1, experimental results from Doherty used for comparison to the lumped cracking beams model are shown below. Also, more captions showing the results from increasing harmonic transient analyses are presented for the sake of completeness of this report.

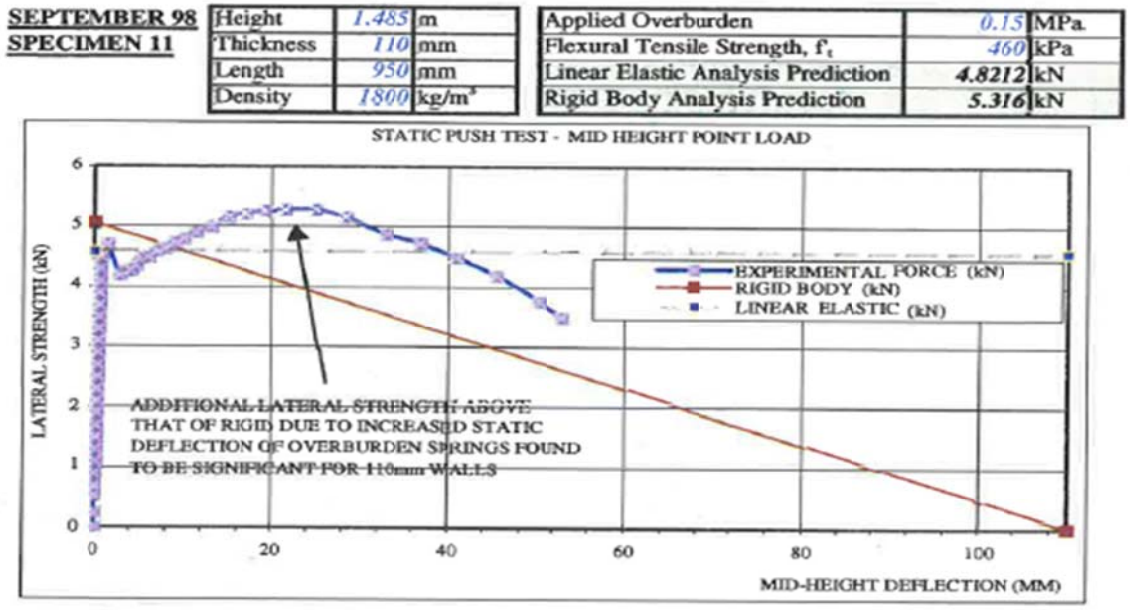

Figure F 8 - Static Push Test – Un-cracked, 110mm, 0.15MPa Overburden

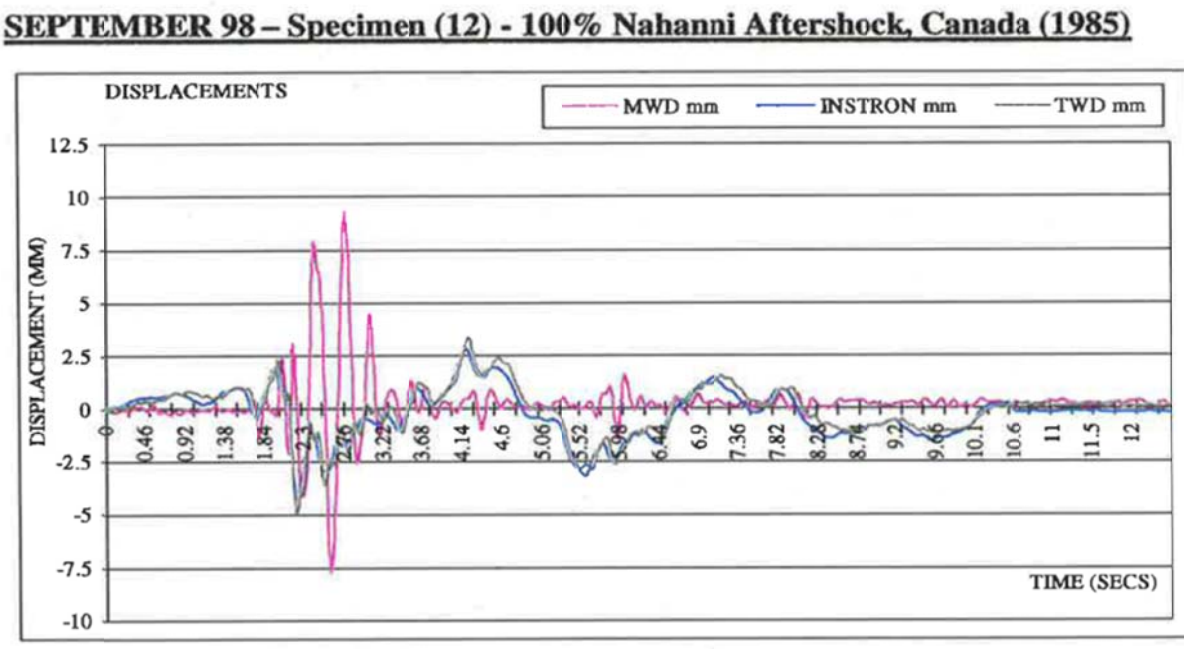

Figure 146 - Experimental results from Doherty (2000): quasi-static and transient analyses on real record (Nahanni).

Appendix B

Hand calculations for the comparison to analytical formulas (Table 2) of numerical results presented in Figure 66 of section 5.1. The graph representing the results found with Diana are reported again after the calculations.

Boundary Condition Number	0	1	2	3
	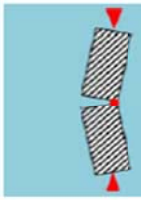	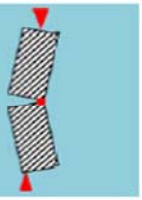	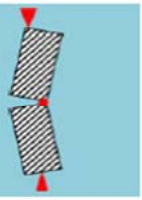	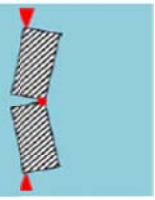
e_p	0	0	$t/2$	$t/2$
e_b	0	$t/2$	0	$t/2$
b	$(W/2+P)t$	$(W+3P/2)t$	$(W/2+3P/2)t$	$(W+2P)t$
a	$(W/2+P)h$	$(W/2+P)h$	$(W/2+P)h$	$(W/2+P)h$
$\Delta = bh/(2a)$	$t/2$	$\frac{(2W+3P)t}{(2W+4P)}$	$\frac{(W+3P)t}{(2W+4P)}$	t
J	$\{(W/12)[h^2+7t^2]+Pt^2\}/g$	$\{(W/12)[h^2+16t^2]+9Pt^2/4\}/g$	$\{(W/12)[h^2+7t^2]+9Pt^2/4\}/g$	$\{(W/12)[h^2+16t^2]+4Pt^2\}/g$
C_m	$(2+4P/W)t/h$	$(4+6P/W)t/h$	$(2+6P/W)t/h$	$4(1+2P/W)t/h$

$$W_{tot} = \rho_w t_w h_w g = 1800\ \frac{Kg}{m^3} \cdot 0.11m \cdot 1.5m \cdot 9.81 \frac{m}{s^2} = 2913.6\ N/m$$

Case 1

$$\Delta_{ins} = \frac{(2W+3P)}{(2W+4P)} t = \frac{(2 \cdot 2913.6\ N + 3 \cdot 17000\ N)}{(2 \cdot 2913.6\ N + 4 \cdot 17000\ N)} 0.11m = 0.084\ m$$

$$C_m = \left(4 + \frac{6P}{W}\right)\frac{t}{h} = \left(4 + \frac{6 \cdot 17000\ N}{2913.6\ N}\right)\frac{0.11}{1.5} = 2.86$$

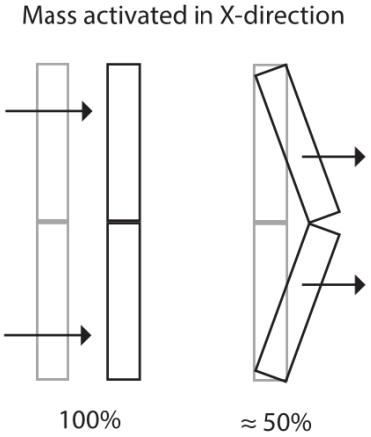

It is now assumed that 50% of the mass of the system is activated along the x-direction during the rocking motion. The product of this mass and the seismic coefficient found gives the maximum horizontal lateral load the wall is able to withstand by making use of rigid bodies theory. The assumption of 50% participating mass is explained by the picture provided on the right.

$$\frac{W_{tot}}{2} \cdot C_m = \frac{2913.6}{2} \cdot 2.86 = 4166\ N$$

$$\textit{This value is} \quad \frac{4166 - 3918.6}{3918.6} \cdot 100 = \mathbf{6.3\%} \quad \textit{larger than in numerical results (graph next pages).}$$

In a similar way, calculations are carried out on the next page for the other three set of boundary conditions on the wall.

Case 2

$$\Delta_{ins}= \frac{(W+3P)}{(2W+4P)}t = \frac{(2913.6\,N + 3\cdot 17000\,N)}{(2\cdot 2913.6\,N + 4\cdot 17000\,N)}0.11m = 0.080\,m$$

$$C_m = \left(2+\frac{6P}{W}\right)\frac{t}{h} = \left(2+\frac{6\cdot 17000\,N}{2913.6\,N}\right)\frac{0.11}{1.5} = 2.71$$

$$\frac{W_{tot}}{2}\cdot C_m = \frac{2913.6}{2}\cdot 2.71 = 3947.9\,N$$

$$\textit{This value is} \quad \frac{3947.9-3716}{3716}\cdot 100 = \mathbf{6.2}\% \quad \textit{larger than in numerical results (graph next page).}$$

Case 3

$$\Delta_{ins}= t = 0.11\,m$$

$$C_m = 4\left(1+\frac{2P}{W}\right)\frac{t}{h} = 4\left(1+\frac{2\cdot 17000\,N}{2913.6\,N}\right)\frac{0.11}{1.5} = 3.71$$

$$\frac{W_{tot}}{2}\cdot C_m = \frac{2913.6}{2}\cdot 3.71 = 5404.7\,N$$

$$\textit{This value is} \quad \frac{5404.7-5092}{5092}\cdot 100 = \mathbf{6.1}\% \quad \textit{larger than in numerical results (graph next page).}$$

Case 0

$$\Delta_{ins}= \frac{t}{2} = \frac{0.11m}{2} = 0.055\,m$$

$$C_m = \left(2+\frac{4P}{W}\right)\frac{t}{h} = \left(2+\frac{4\cdot 17000\,N}{2913.6\,N}\right)\frac{0.11}{1.5} = 1.85$$

$$\frac{W_{tot}}{2}\cdot C_m = \frac{2913.6}{2}\cdot 1.85 = 2695\,N$$

This value is $\frac{2695 - 2541}{2541} \cdot 100 = \mathbf{6.0\%}$ *larger than in numerical results (graph below).*

The results suggest that the correct value of active mass to take into account is a slightly less than half the total: 47%.

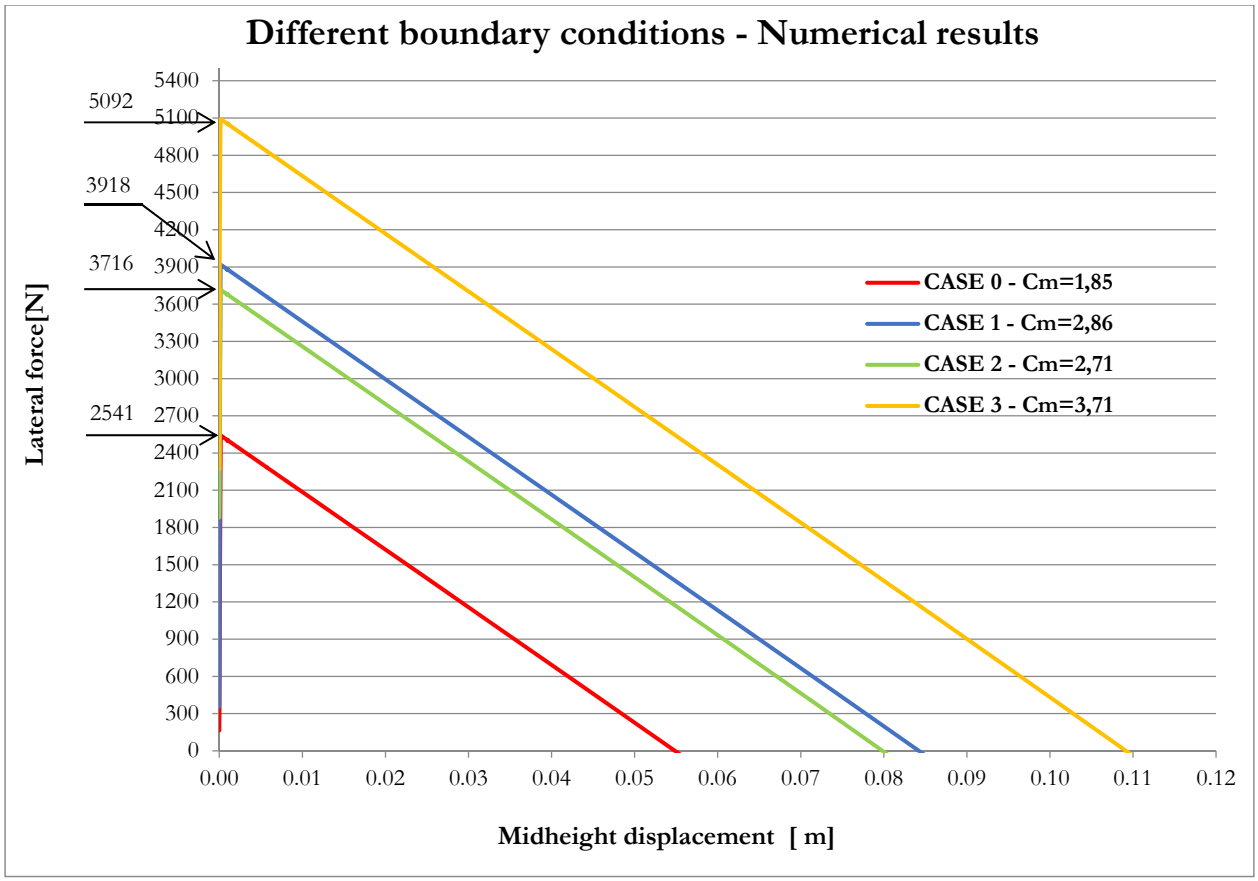

Figures 147 – Numerical results on the lumped cracking beams model subjected to a pushover analysis and with different constraints on the edges of the wall, 17 kN overburden.

Appendix C

More outcomes of the transient analyses carried out on the lumped cracking beams model, increasing harmonic signals.

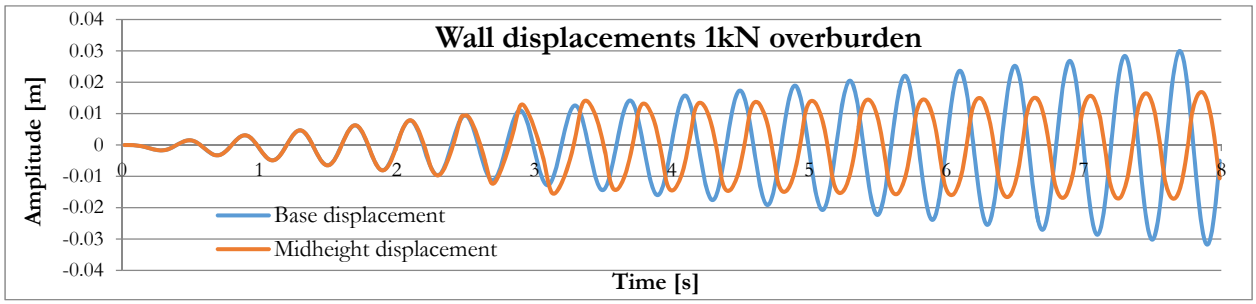

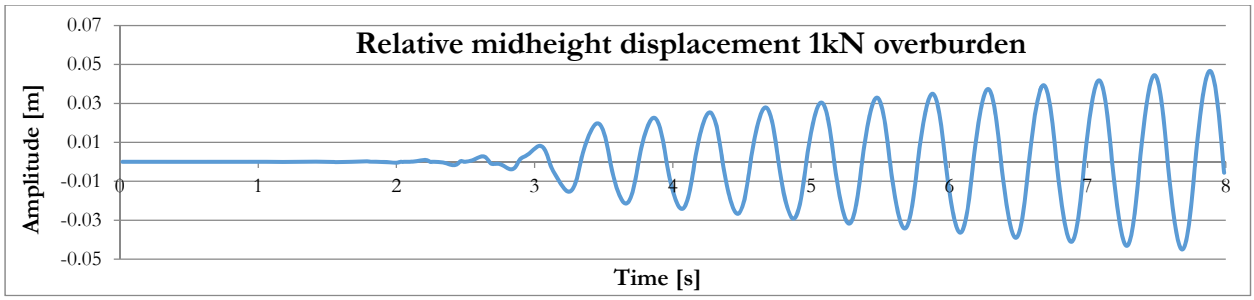

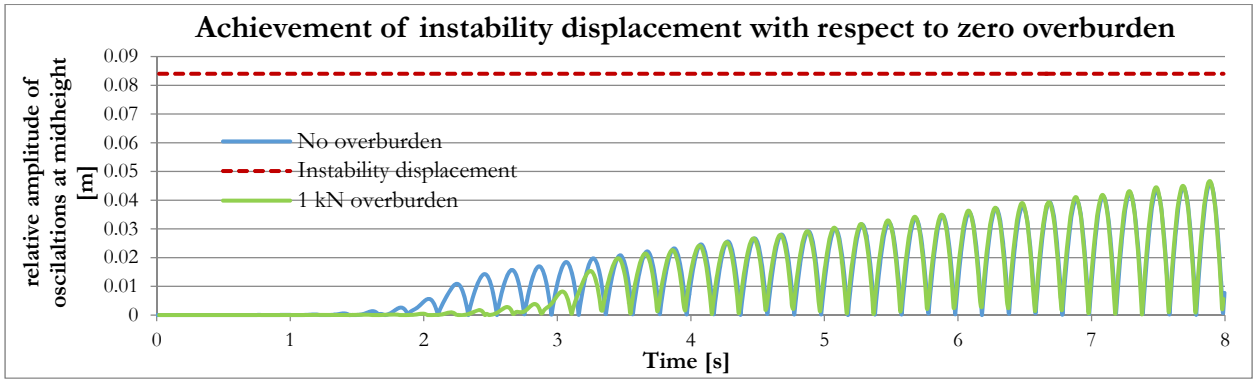

Figures 148 - Increasing harmonic excitation on 1,5 m tall wall. Overburden 1 kN, forcing frequency 2.5 Hertz.

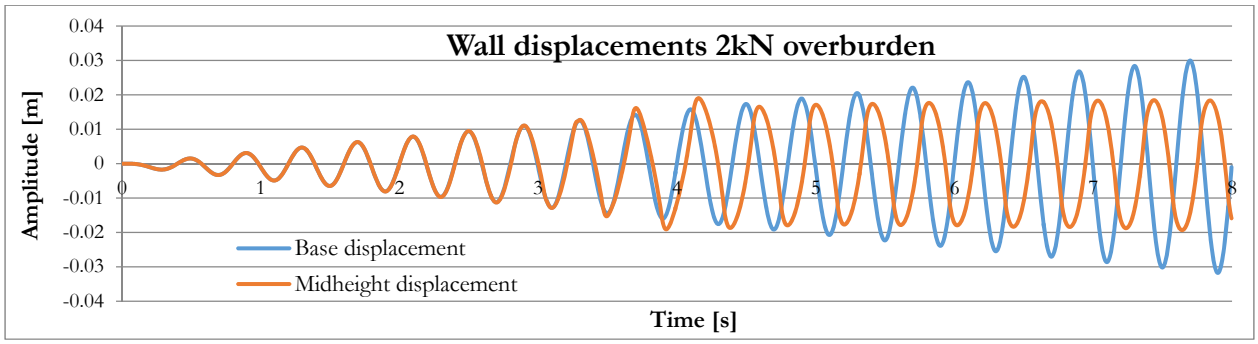

Figure 149 - Increasing harmonic excitation on 1,5 m tall wall. Overburden 2 kN, forcing frequency 2.5 Hertz.

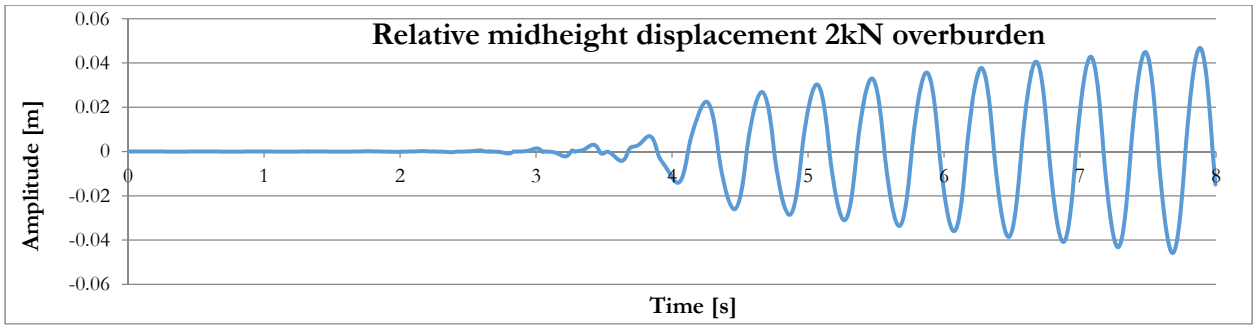

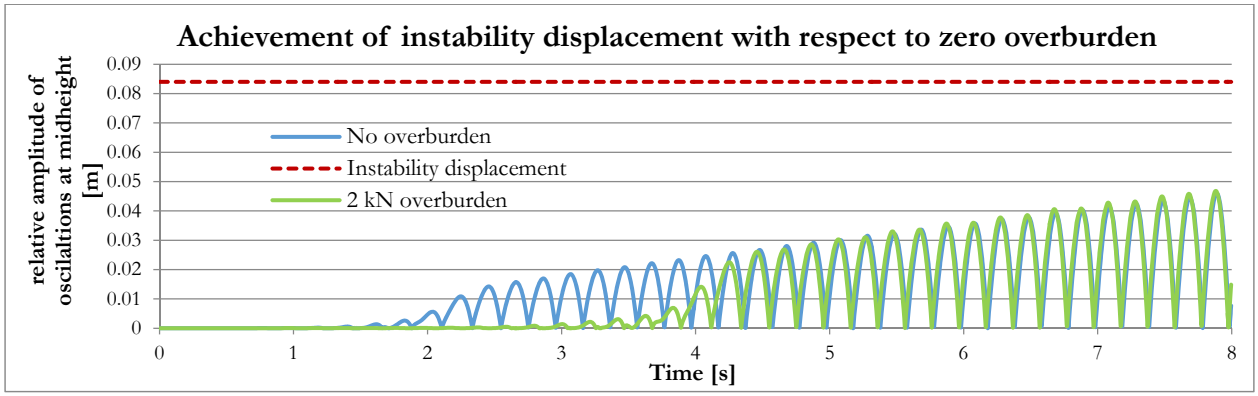

Figures 150 - Increasing harmonic excitation on 1,5 m tall wall. Overburden 2 kN, forcing frequency 2.5 Hertz.

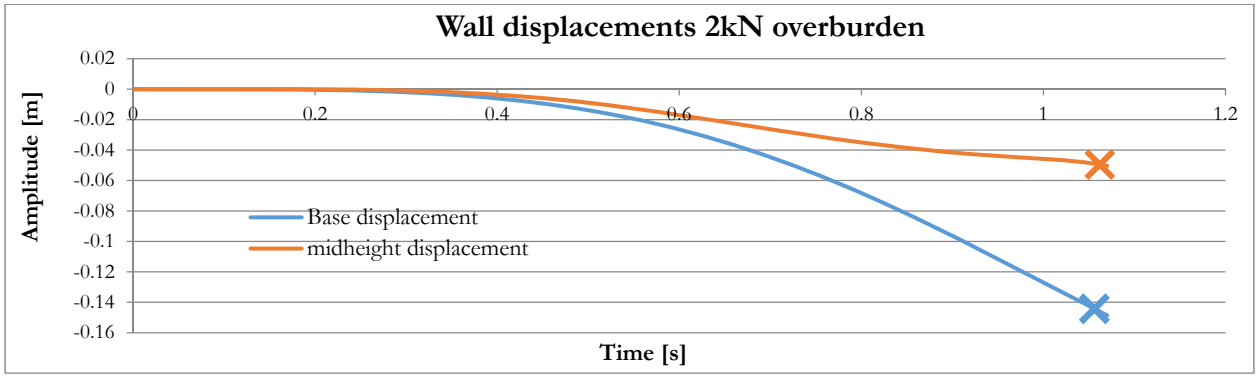

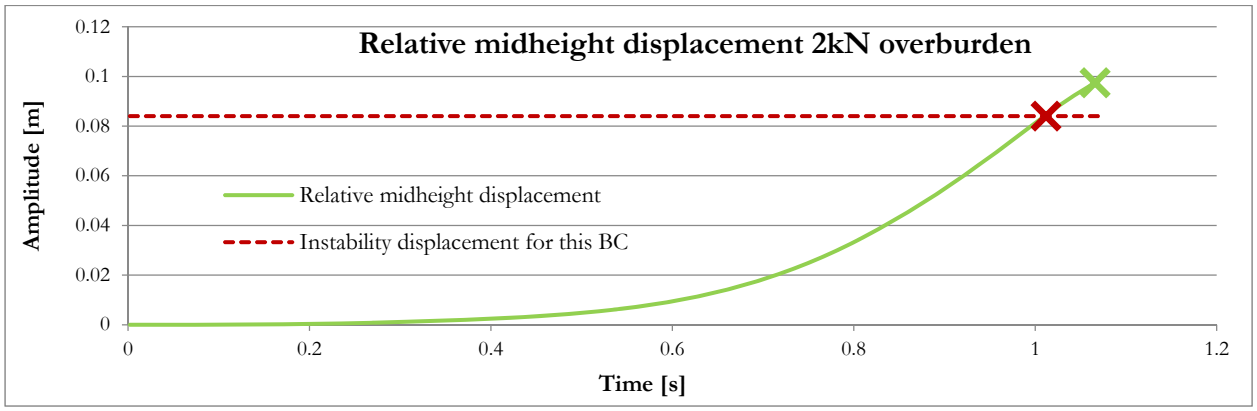

Figure 151 - Increasing harmonic excitation on 1,5 m tall wall. Overburden 2 kN, forcing frequency 0.5 Hertz.

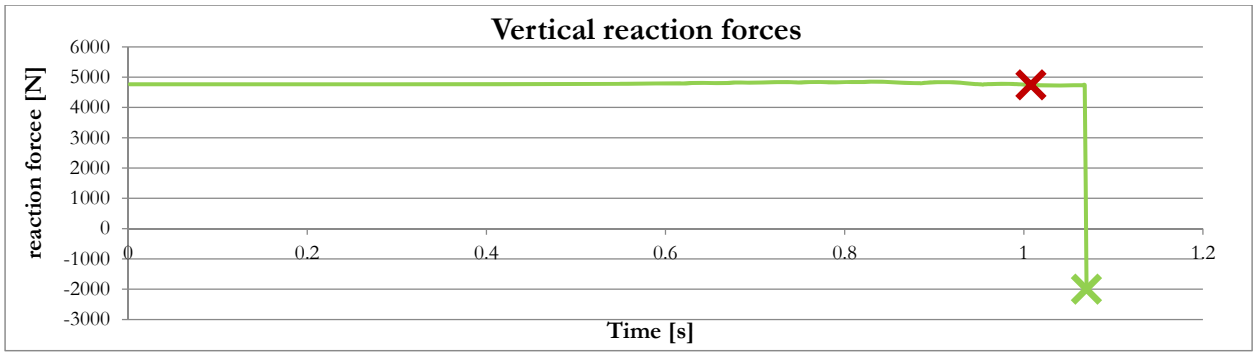

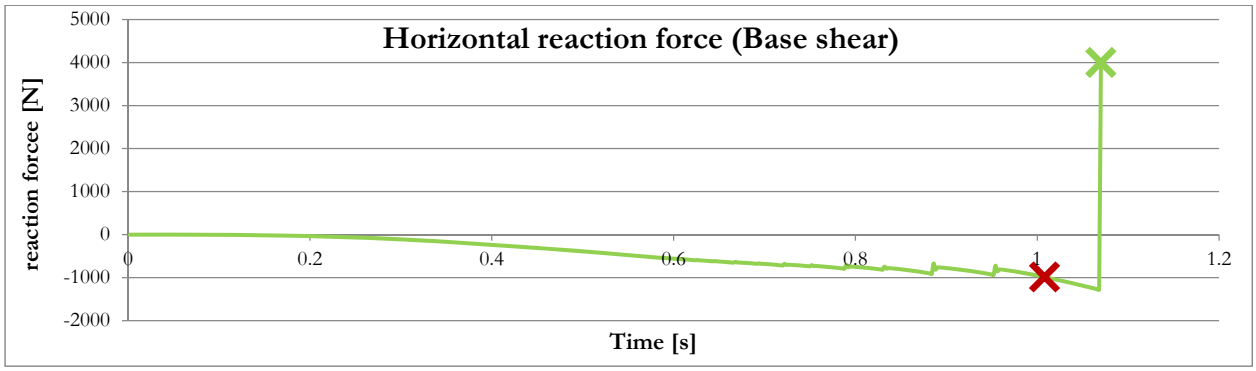

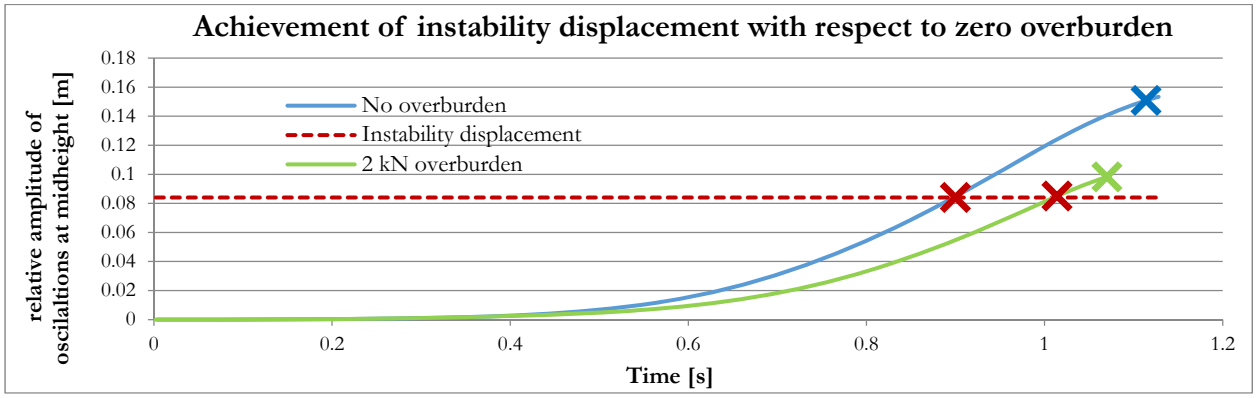

Figure 152 - Increasing harmonic excitation on 1,5 m tall wall. Overburden 2 kN, forcing frequency 0.5 Hertz.

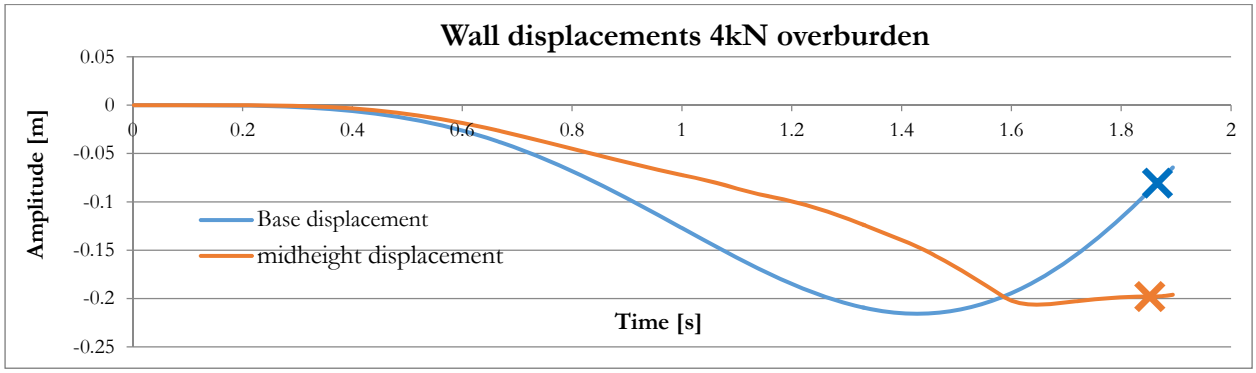

Figures 153 - Increasing harmonic excitation on 1,5 m tall wall. Overburden 4 kN, forcing frequency 0.5 Hertz.

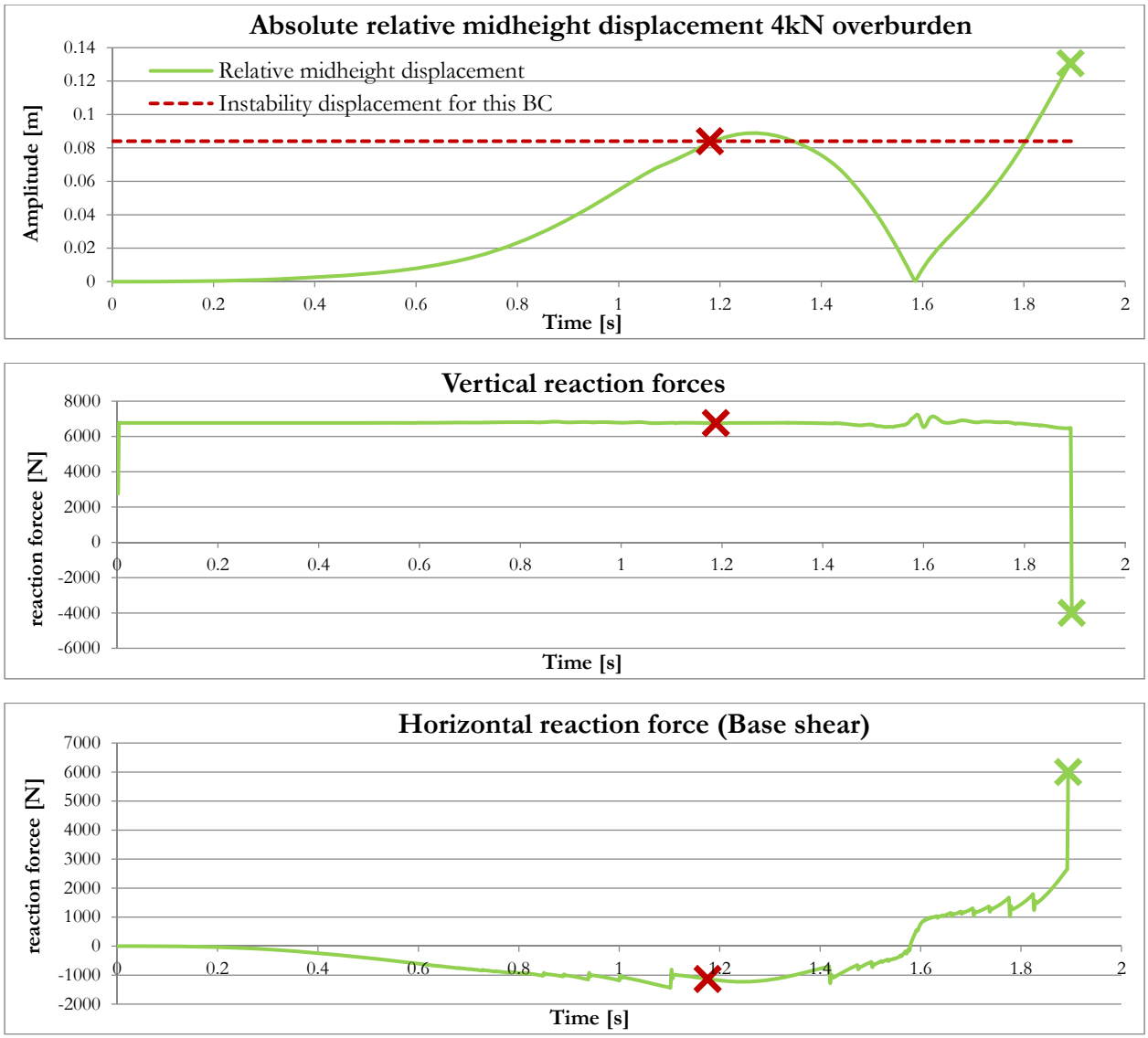

Figures 154 - Increasing harmonic excitation on 1,5 m tall wall. Overburden 4 kN, forcing frequency 0.5 Hertz.

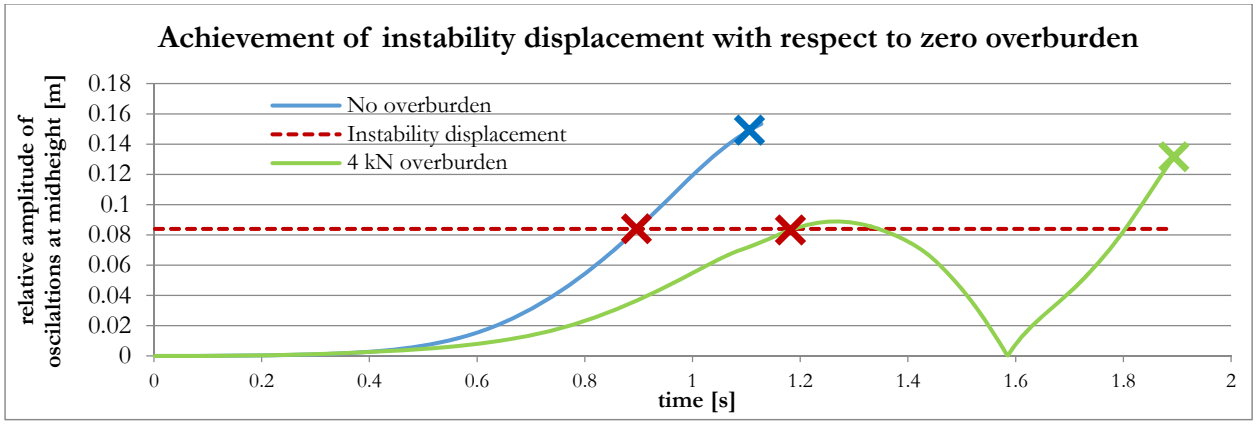

Figures 155 - Increasing harmonic excitation on 1,5 m tall wall. Overburden 4 kN, forcing frequency 0.5 Hertz.

Appendix D

Zoom-in on the first steps of the Figure 79 in section 5.3.1 of this report.

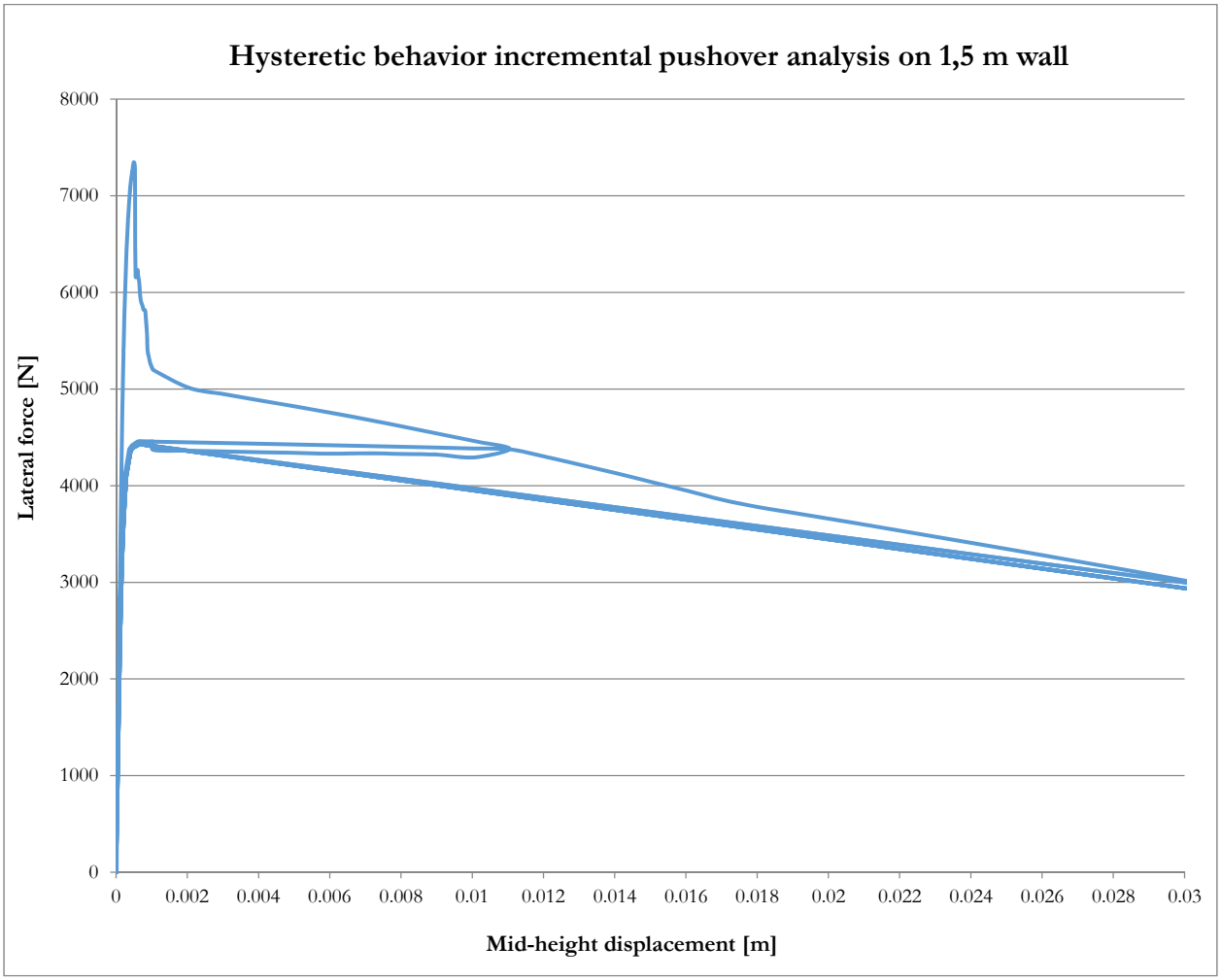

Figure 156 - Hysteretic behavior of the unreinforced masonry material on the wall subjected to the Nahanni excitation. Zoom-in on first steps of Figure 79.

Appendix E

Hand checks to assess the OOP stability of 5th floor URM walls in the frame models.

An hand-check in accordance to the procedure explained in the New Zealand normative may be carried out to confirm the numerical results. The NLTH analyses demonstrated that none of the URM walls of the frame models fails OOP if the primary system is excited at the base with one of the records A, B, C or D. Hence, the NZSEE guidelines for the assessment of the out-of-plane performance of vertically spanning URM walls are now applied to a wall that is located on the last floor of a building which is assumed to be represented by one of the five-storey frame models previously investigated. All the boundary conditions used can be therefore referenced to those of section 5.4.1, and the same accounts for the size of the wall at matter. The elastic site spectrum employed to do this is derived in accordance to section 3.2.2.2.1 of the NPR9998. The latter is presented in Figure 141 of this report and also includes the parameters adopted for its derivation. The following calculations are based on the analytical approach from New Zealand and by adopting the correcting coefficients prescribed in the relevant code for amplifying the demands on the wall.

$$C_P(T_P) = C(0) \cdot C_{Hi} \cdot C_{hc}(T_P)$$

The C(0) corresponds to the PGA the building is subjected to and it can be substituted with the Se(0) determined by the NPR, shown above. C_{hi} is a factor that magnifies the PGA such that it reflects the acceleration of the main structure at a given height. Finally, the $C_{hc}(T_P)$ is a factor that magnifies the acceleration of the main structure at a given height to reflect also the effect of the period of the part. The curve presenting the values of $C_{hc}(T_P)$ as a function of the period of oscillation can be derived from the NPR9998 spectrum by normalizing it to the PGA and capping it to a maximum of 2 (as it is the case in the NZSEE guidelines, see "BRANZ" report for more details). Therefore:

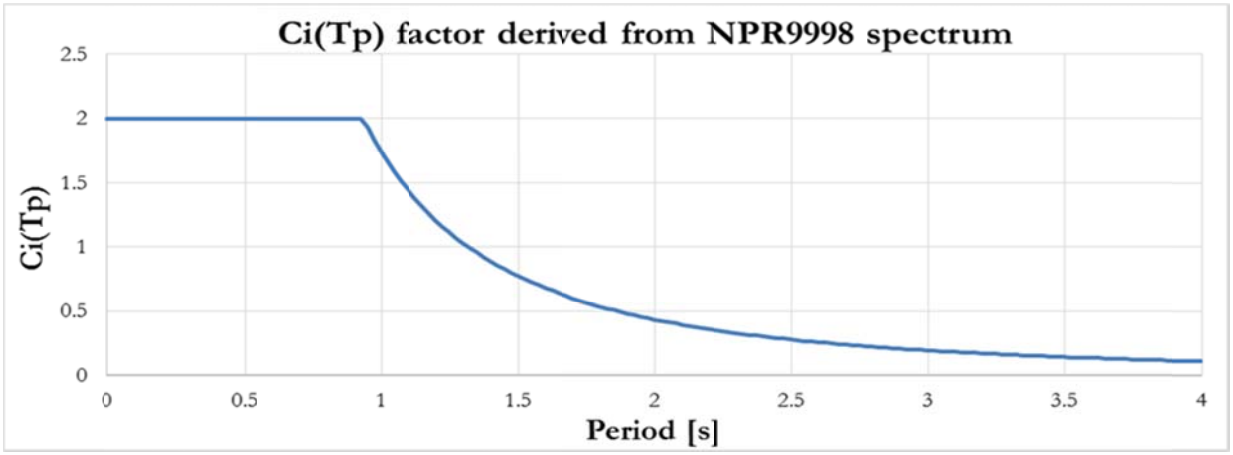

Figure 157 – Adaptation of the spectral shape function to the NPR9998 for the area of Groningen.

It was found before (see Table 29) that the period of the rocking mechanism based on the New Zealand codification is 0.540 seconds. Then one would obtain:

$$C_{Hi} = 3 \quad and \quad C_{hc}(0.54) = 2 \quad then \quad C_P(0.51) = 0.35 \cdot 3 \cdot 2 = 2.07[g]$$

The value obtained for $C_P(T_P)$ is then used to estimate the mid-height displacement demand of the wall following the procedure described in section 10.8.5.2 of the document "Assessment and improvement of the structural performance

of buildings in earthquakes" – Section 10 Revision Seismic Assessment of Unreinforced Masonry Buildings (Included in the bibliography). Thus:

$$D_{ph} = \gamma(T_P/2\pi)^2 C_P(T_P) R_P g \qquad with \qquad \gamma = \frac{(W_b y_b + W_t y_t)h}{2Jg} = 1.13$$

The R_P factor is the part risk coefficients and it tabulated in section 8.1.2 of NZS1170.5-2004. A value of R_P =1 corresponding to parts representing a hazard to life within a structure is chosen. Speaking of the maximum mid-height displacement allowed, the NPR specifies that the behavior factor q (generally intended for ULS/LS limit state) can be increased by 1.33 when considering the near-collapse limit state, i.e. to increase the degree of damage allowed. Therefore the 0.6 factor can be increased to 0.8.

$$\Delta_{max} = 0.8 \times \Delta_{ins} = 0.150\, m \qquad since \qquad \Delta_{ins} = \frac{b \cdot h_{wall}}{2a} \qquad and \qquad a = 60892 \frac{Nm}{m} \qquad and \qquad b = 7692 \frac{Nm}{m}$$

According to the New Zealand code and by making use of the correcting coefficient employed to amplify the rocking demands of walls, the performance of the wall analyzed would be:

$$\%NBS_{(NPR)} = 100 \times \frac{\Delta_{max}}{D_{ph}} = 100 \times \frac{0.150}{0.168} = 89\%$$

The New Zealander normative explains that an element scoring less than 67% should be considered subjected to the seismic risk and that it is earthquake-prone, i.e. it requires strengthening, when scores below 34%. According to the NZSEE regulations the wall analyzed does not need strengthening measures. It is concluded that the NZ guidelines confirm the URM walls in the frame models not to be prone to OOP failure. However, it should be noted that for the Dutch regulations the case of a structural element for which the demands exceed the capacity (ratio shown above < 100%) cannot be considered safe and requires to take action.

Appendix F

Derivation of vibrational periods presented in section 5.4.

1 Period of the rocking mechanism according to the New Zealand Code:

In the following equations, taken from section 10.8.5.2 of *Assessment and Improvement of the Structural Performance of Buildings in Earthquakes", Section 10 Revision (2015)*, the quantity J stands for the rotational inertia of the masses associated with Wb, Wt and P. The factor a derived from virtual work expressions, see Appendix 10B of the over-mentioned document. The calculations refer to a wall with an height of 3 meters, a thickness of 0.2 meters and an applied overburden of 15kN.

$$J = J_{bo} + J_{to} + \frac{1}{g}\left\{W_b[e_b^2 + y_b^2] + W_t[(e_0 + e_b + e_t)^2 + y_t^2] + P\left[\left(e_0 + e_b + e_t + e_p\right)^2\right]\right\}$$

$$W_b = W_t = \frac{\rho_w t_w h_w g}{2} = \frac{1800\ \frac{Kg}{m^3} \cdot 0.2m \cdot 3m \cdot 9.81\frac{m}{s^2}}{2} = 5297.4\ \frac{N}{m}$$

$$y_b = y_t = \frac{h_w}{4} = \frac{3m}{4} = 0.75\ m$$

$$e_0 = e_b = e_t = e_p = \frac{t_p}{2} = \frac{0.188m}{2} = 0.094\ m \qquad where \qquad t_p = \left(0.095 - \left(0.025\frac{P}{W_b + W_t}\right)\right)t_{nom} = 0.188\ m$$

$$J_{bo} = J_{to} = \frac{\frac{W}{2}\left(\left(\frac{h_w}{2}\right)^2 + \left(\frac{t_p}{2}\right)^2\right)}{12g} = \frac{5297.4\ \frac{N}{m}\left(\left(\frac{3m}{2}\right)^2 + \left(\frac{0.188m}{2}\right)^2\right)}{12 \cdot 9.81\frac{m}{s^2}} = 103\ \frac{Kgm^2}{m}$$

$$J = J_{bo} + J_{to} + \frac{1}{g}\left\{W_b[e_b^2 + y_b^2] + W_t[(e_0 + e_b + e_t)^2 + y_t^2] + P\left[\left(e_0 + e_b + e_t + e_p\right)^2\right]\right\}$$

$$W_b[e_b^2 + y_b^2] = 5297.4\ \frac{N}{m}[0.094^2m^2 + 0.75^2m^2] = 3026.6\ Nm$$

$$W_t[(e_0 + e_b + e_t)^2 + y_t^2] = 5297.4\ \frac{N}{m}[(0.094m + 0.094m + 0.094m)^2 + 0.75^2m^2] = 3401\ Nm$$

$$P\left[\left(e_0 + e_b + e_t + e_p\right)^2\right] = 15000\frac{N}{m}[(0.094m + 0.094m + 0.094m + 0.094m)^2] = 2120.6\ Nm$$

$$J = 103\ \frac{Kgm^2}{m} + 103\ \frac{Kgm^2}{m} + \frac{1}{9.81\frac{m}{s^2}}\{3026.6\ Nm + 3401\ Nm + 2120.6\ Nm\} = 1077.4\ \frac{Kgm^2}{m}$$

$$a = W_b y_b + W_t(h - y_t) + Ph = 5297.4\frac{N}{m} \cdot 0.75m + 5297.4\frac{N}{m}(3m - 0.75m) + 15000N \cdot 3m = 60892.2$$

$$T_p = 4.07\sqrt{\frac{J}{a}} = \mathbf{0.54\ seconds}$$

2 Period of oscillation of an elastic fixed-fixed beam:

When the nonlinearities of the wall model are not accounted for, the wall can be seen as an elastic beam clamped on both sides and its vibration period can be derived from the general structural mechanics theory.

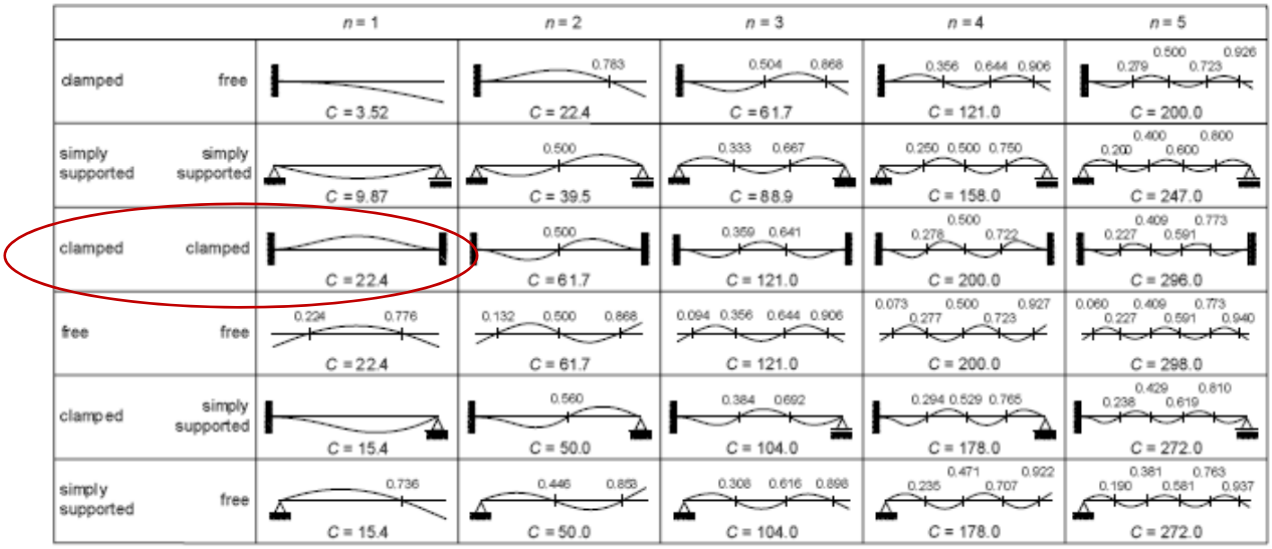

$$\omega_n = \frac{C_n}{L^2}\sqrt{\frac{EI}{\rho A}}$$

Figure 158 - Bending vibrations of a beam: natural frequencies and normal modes.
TU Delft, Structural Dynamics course, CIE4140 (2015).

$$\omega_1 = \frac{22.4}{L^2}\sqrt{\frac{EI}{\rho A}} \qquad where \qquad E = 5 \cdot 10^9\frac{N}{m^2} \qquad and$$

$$I = \frac{1}{12}\ bt^3 = \frac{1}{12}\ 1 \cdot 0.2^3 = 6.67 \cdot 10^{-4}\frac{m^4}{m} \qquad and \qquad A = bt = 1 \cdot 0.2 = 0.2\frac{m^2}{m}$$

$$\omega_1 = \frac{22.4}{{h_w}^2}\sqrt{\frac{EI}{\rho A}} = 237.87\frac{rad}{\sec} \qquad leading\ to \quad T_{beam} = \frac{2\pi}{\omega_1} = \mathbf{0.027\ seconds}$$

3 Period of rocking mechanism according to the Italian normative:

The simply supported wall with applied overburden and no tilt. For the boundary conditions, which reflect the same circumstance as for the calculations according to the New Zealand code above, a picture is also provided. The Italian code requires to solve the nonlinear kinematic problem defined by two rigid bodies rocking around three hinges. The instability of the wall in its OOP deformation is investigated by means of the virtual work theory. The virtual displacement are calculated with respect to the instant centre of rotation of the wall rigid blocks.

$$\mathrm{W_b} = \mathrm{W_t} = \mathrm{W} = \frac{\rho_w t_w h_w g}{2} = 1800\ \frac{\mathrm{Kg}}{\mathrm{m^3}}$$

$$\alpha W\delta_{x,b} + \alpha W\delta_{x,t} + \alpha W\delta_{y,b} + \alpha W\delta_{y,t} - P\delta_{y,p} = 0$$

The factor α is the horizontal multiplication factor which is used to represent the action of the earthquake on the wall. In the New Zealand code this factor is called the seismic coefficient, and it is comparable to an acceleration. The virtual displacement are:

$$\delta_{x,b} = \delta\varphi y_b = \delta\varphi\left(\frac{h}{4} + \frac{t\varphi}{2}\right)$$

$$\delta_{y,b} = \delta\varphi x_b = \delta\varphi\left(\frac{t}{2} - \frac{h\varphi}{4}\right)$$

$$\delta_{x,t} = \delta\varphi y_t = \delta\varphi\left(\frac{h}{4} + \frac{t\varphi}{2}\right)$$

$$\delta_{y,t} = \delta\varphi x_t = \delta\varphi\left(\frac{3t}{2} - \frac{3h\varphi}{4}\right)$$

$$\delta_{y,P} = \delta\varphi x_p = \delta\varphi(2t - \varphi h)$$

By plugging in the virtual displacements in the formula and re-arranging it one would obtain:

$$\alpha(\varphi) = \frac{2t - \varphi h + \frac{P}{W}(2t - \varphi h)}{\frac{h}{2} + \varphi t}$$

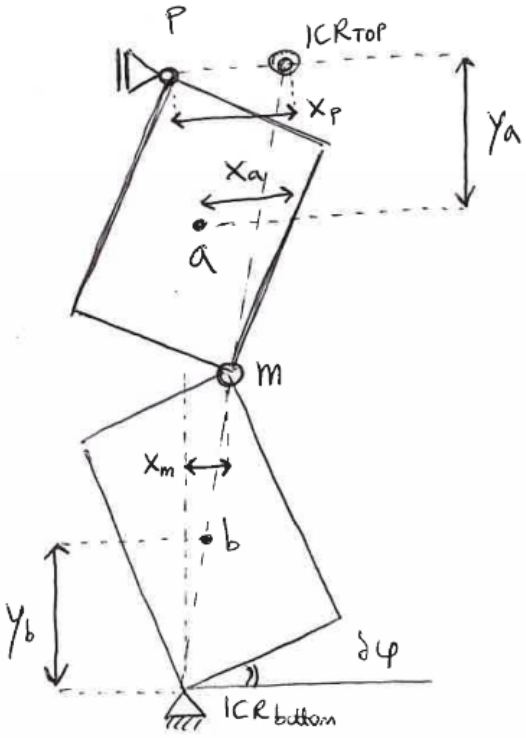

Figure 159 - Sketch used for calculating the virtual displacements of a rocking wall.

The maximum (static) lateral load that the wall is able to withstand in the out-of-plane direction is represented by the multiplier derived for $\varphi = 0$, corresponding to the case of activation of the rocking mechanism. Therefore:

$$\alpha(0) = \alpha_0 = \left(1 + \frac{P}{W}\right)\frac{4t}{h}$$

The ultimate rotation can be obtained, in a similar way, by setting the multiplication factor equal to zero. Once the rotation at incipient instability of the wall is known, the associated mid-height displacement $d_{k,0}$ can be computed:

$$\varphi(\alpha = 0) = \frac{2t}{h} \qquad d_0 = \frac{h}{2} \cdot \varphi_{\alpha=0} = t$$

Since the magnitude of the external forces acting on the wall is assumed to be constant, it is possible to adopt a linear relation between the displacement of the control point (mid-height of the wall) and the multiplier alpha. Then:

$$\alpha = \alpha_0\left(1 - \frac{d}{d_o}\right)$$

This Italian code asks to modify the relation above by referring to an equivalent single-degree-of-freedom system and, thus, to spectral values of accelerations and displacements. The procedure implies calculating the participating mass M^* and the confidence factor FC. The participating mass in this case is assumed to be the total mass of the wall (note: rigid bodies assumption), whereas the confidence factor is set to 1 in line with the clause 4.6.1 of NPR9998. So:

$$\alpha_0^* = \frac{\alpha_0 2W}{M^* FC} = \left(1 + \frac{P}{W}\right)\frac{4t}{h}g \qquad d_0^* = \frac{t}{2}$$

The acceleration-displacement relation is plotted in the caption on the right:

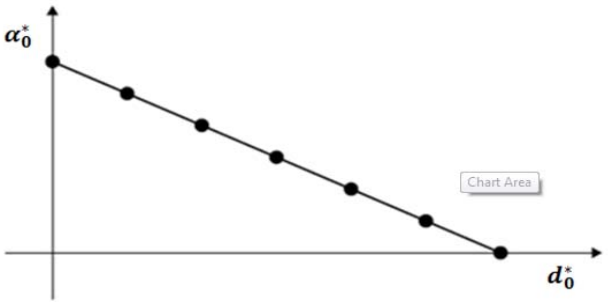

The maximum deformation allowed in the Italian code corresponds to 40% of the ultimate deformation capacity defined by d_0^*. This is explained in more detail in section 2.8.2 of the Literature study in this report. The eigen period of the rocking mechanism according to the NTC2008 is determined by resorting to an average secant stiffness for the lateral capacity of the wall which is taken from the curve above for a spectral displacement of 0.4 times the maximum deformation allowed. Therefore the following applies:

$$T_p = 2\pi\sqrt{\frac{d_s^*}{\alpha_s^*}} = 2\pi\sqrt{\frac{0.16d_0^*}{0.84\alpha_0^*}} = 0.31\sqrt{\frac{h}{\left(1 + \frac{P}{W}\right)}} = 0.31\sqrt{\frac{3m}{\left(1 + \frac{15000N}{5297.4\,N/m}\right)}} = \mathbf{0.274\ seconds}$$

Appendix G

Another example of output from frame models, section 5.4.

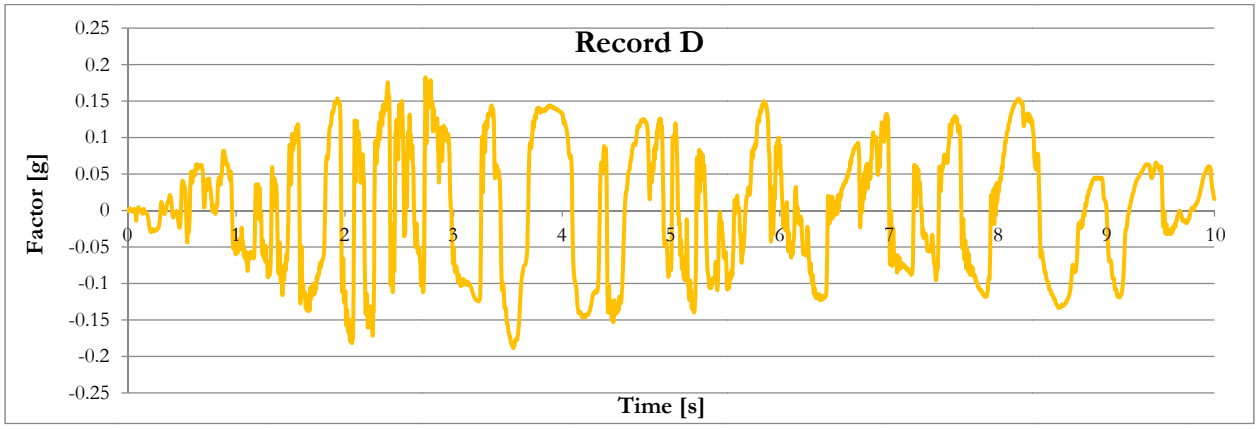

Figure 160 - Representation of the signal D used as an acceleration base motion excitation for the frame models.

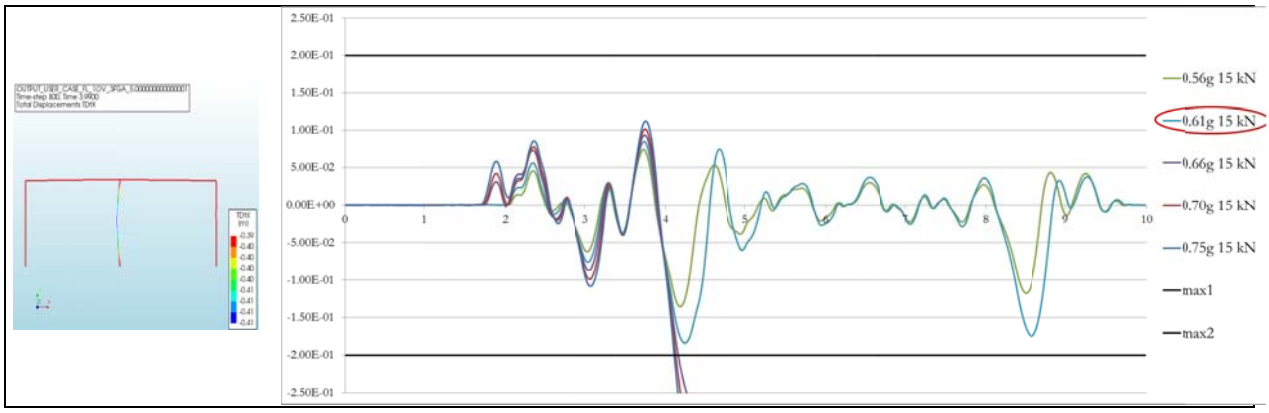

Figure 161 - IDA on frame model with one floor and rocking system at ground floor. Record D.

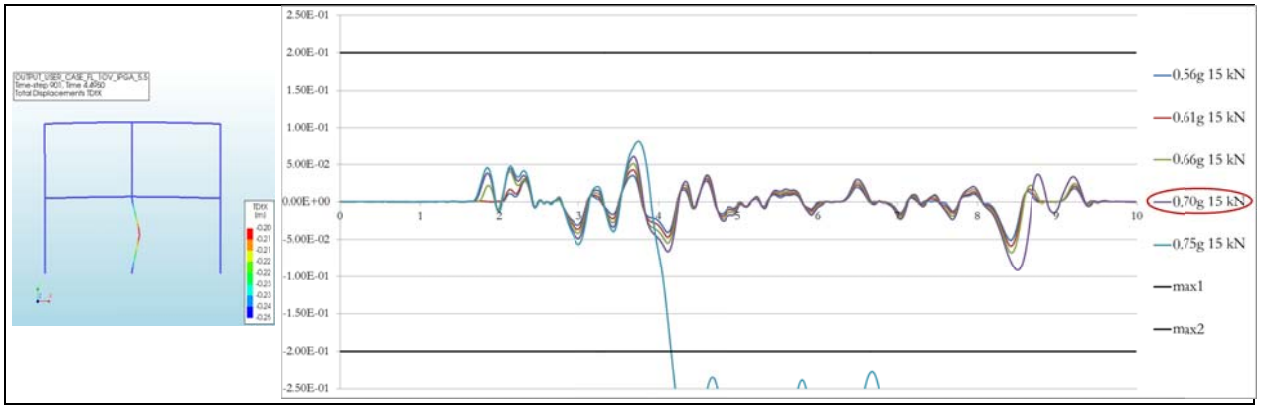

Figure 162 - IDA on frame model with two floors and rocking system at ground floor. Record D.

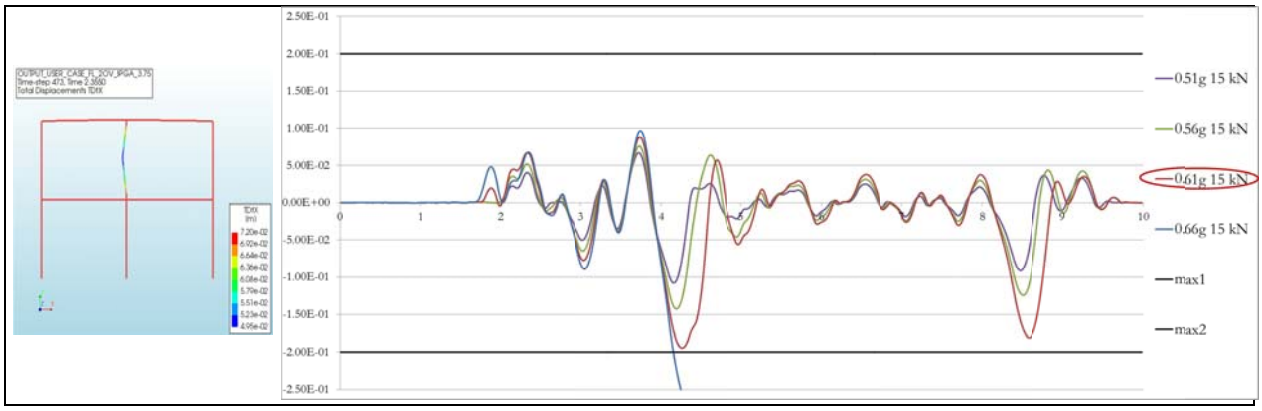

Figure 163 - IDA on frame model with two floors and rocking system at second floor. Record D.

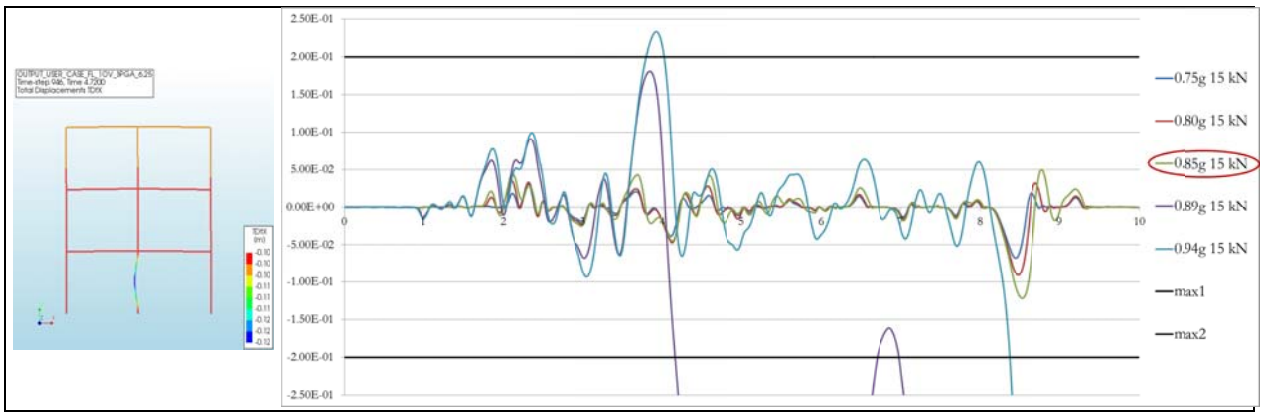

Figure 164 - IDA on frame model with three floors and rocking system at groundfloor floor. Record D.

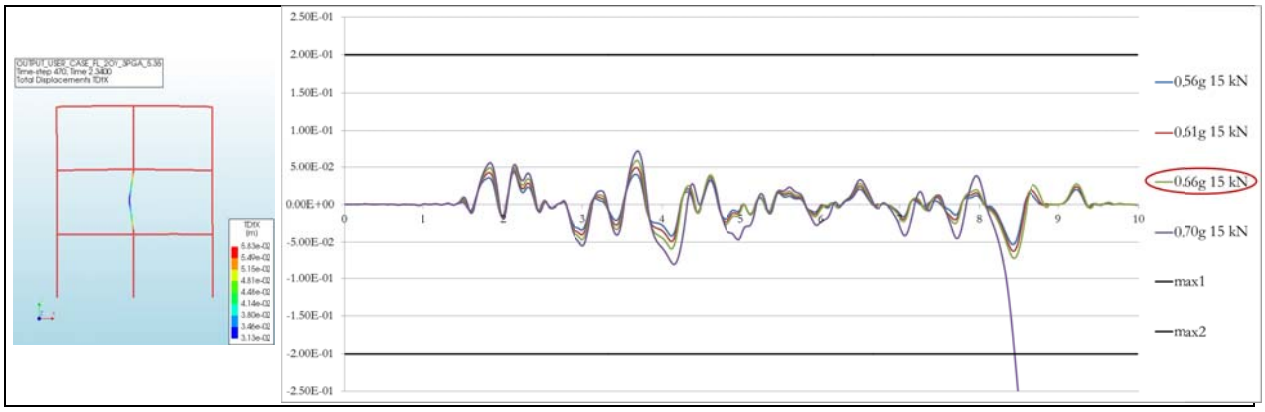

Figure 165 - IDA on frame model with three floors and rocking system at second floor. Record D.

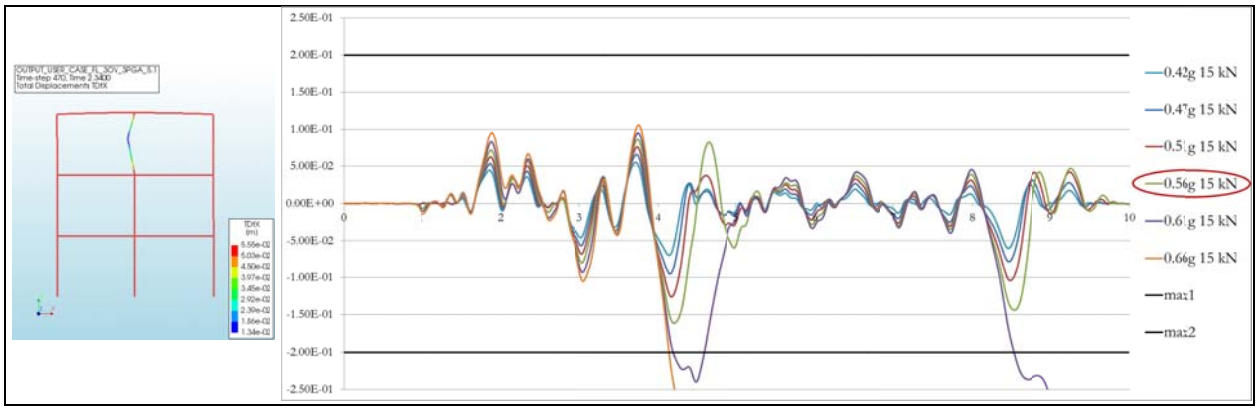

Figure 166 - IDA on frame model with three floors and rocking system at third floor. Record D

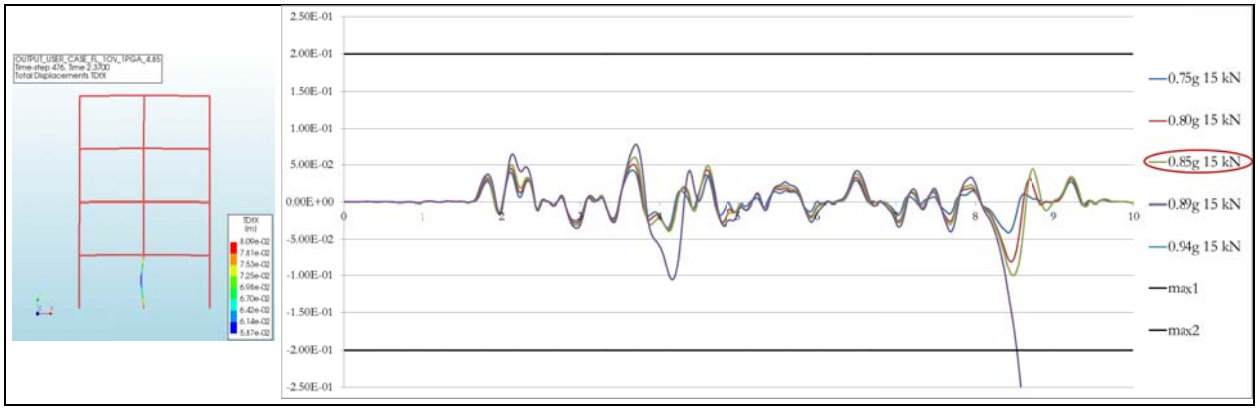

Figure 167 - IDA on frame model with four floors and rocking system at groundfloor floor. Record D.

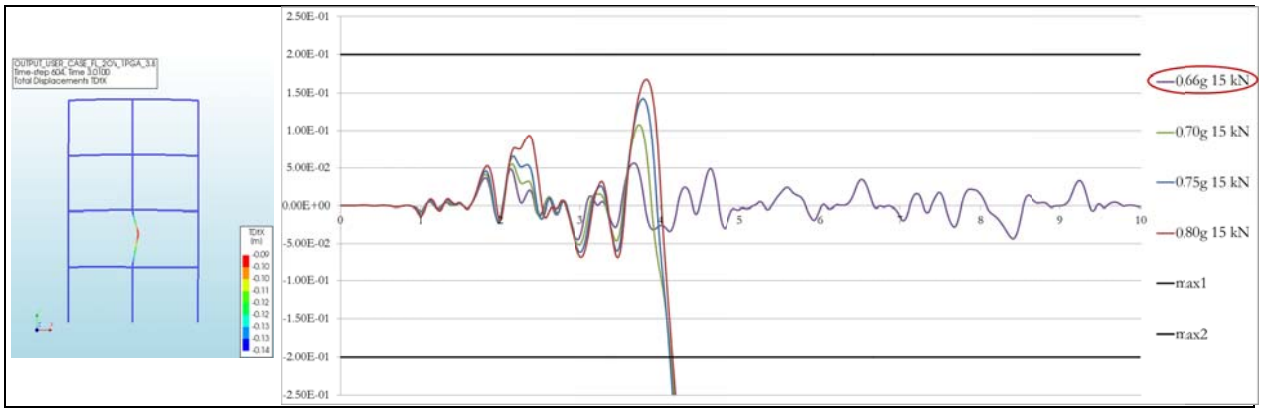

Figure 168 - IDA on frame model with four floors and rocking system at second floor. Record D.

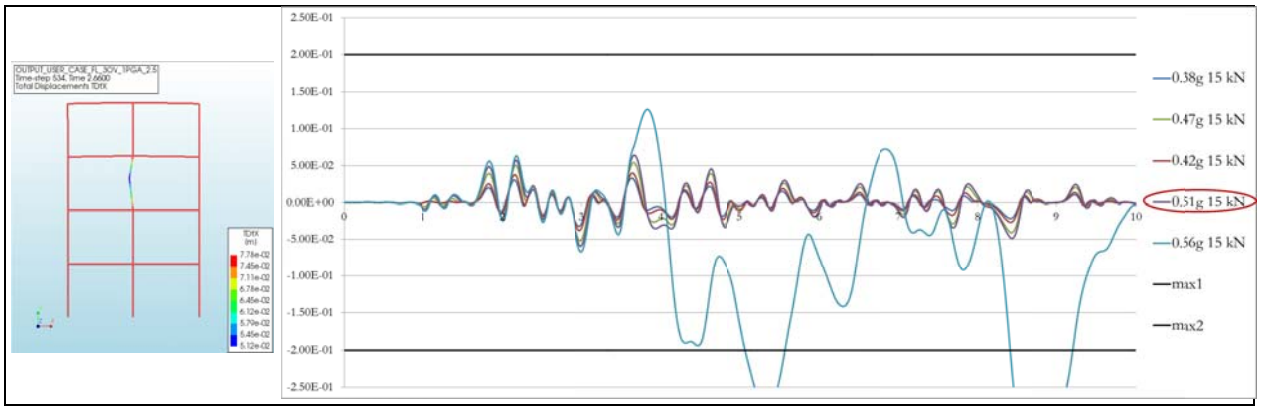

Figure 169 - IDA on frame model with four floors and rocking system at third floor. Record D.

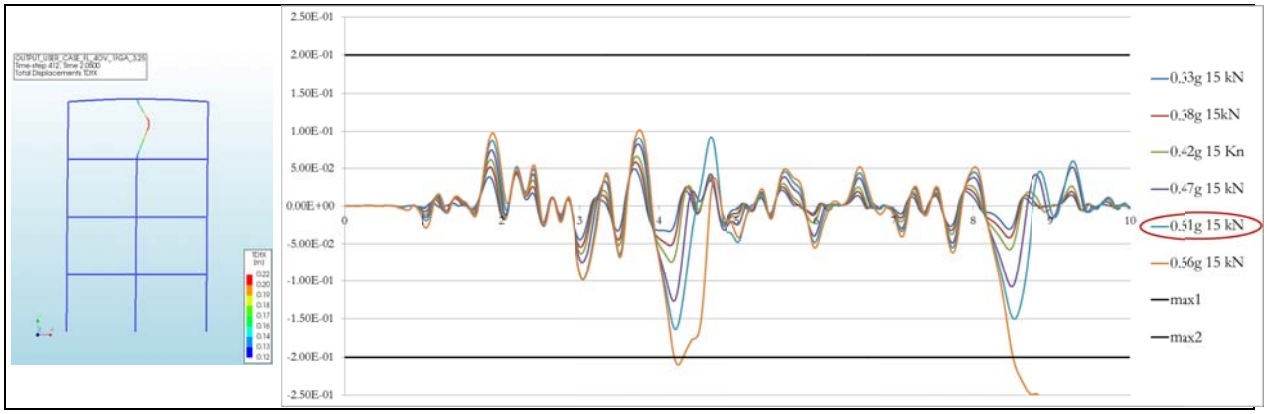

Figure 170 - IDA on frame model with four floors and rocking system at fourth floor. Record D.

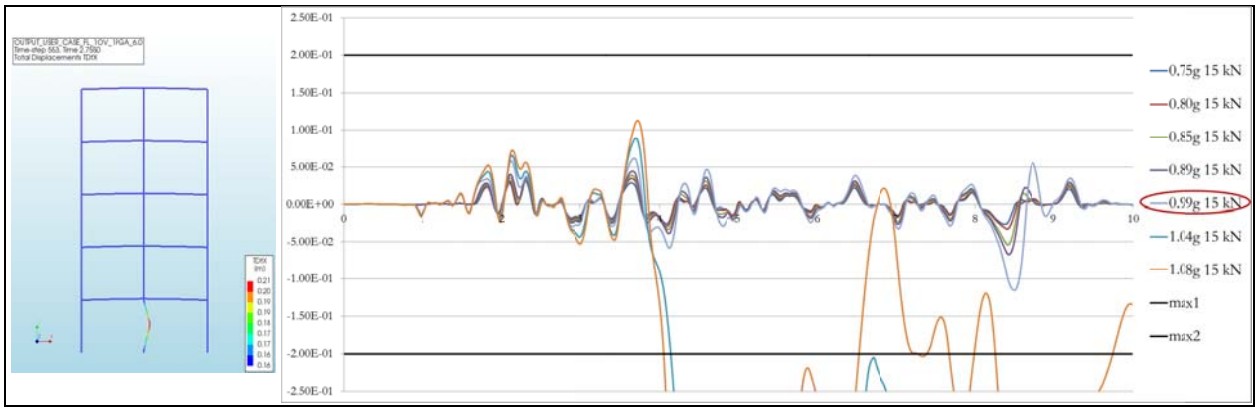

Figure 171 - IDA on frame model with five floors and rocking system at ground floor. Record D.

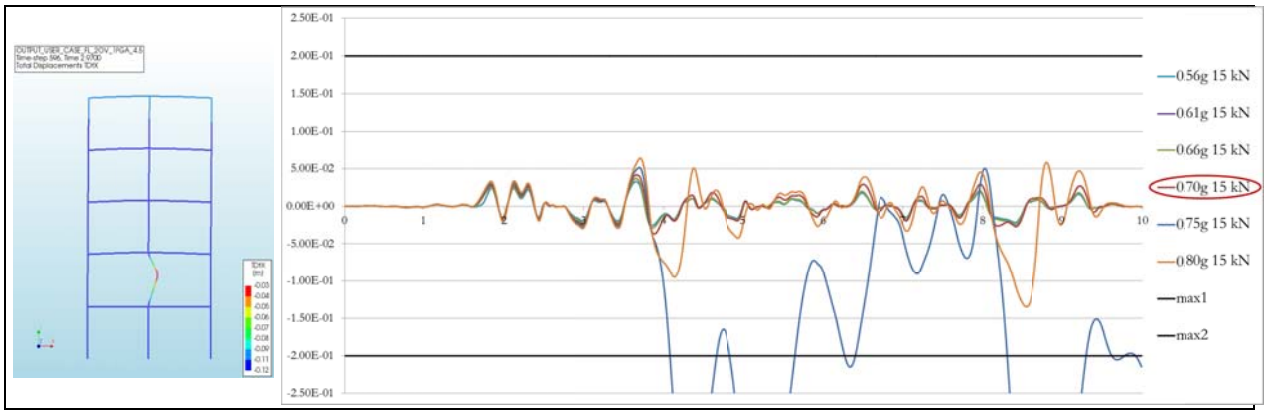

Figure 172 - IDA on frame model with five floors and rocking system at second floor. Record D.

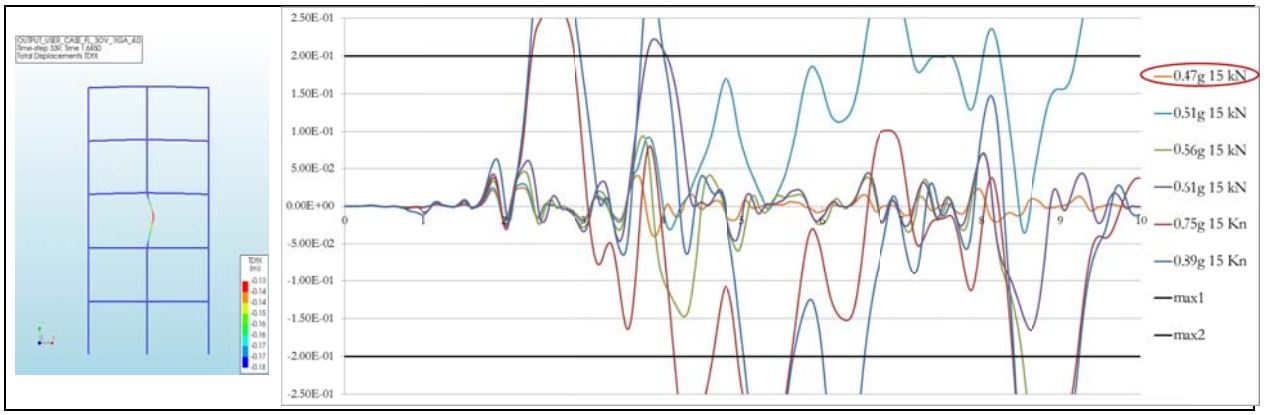

Figure 173 - IDA on frame model with five floors and rocking system at third floor. Record D.

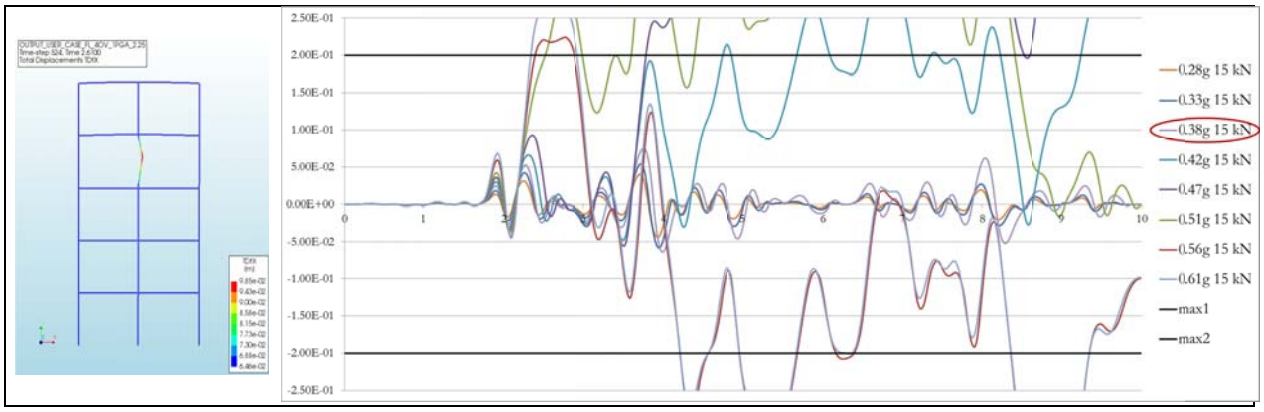

Figure 174 - IDA on frame model with five floors and rocking system at fourth floor. Record D.

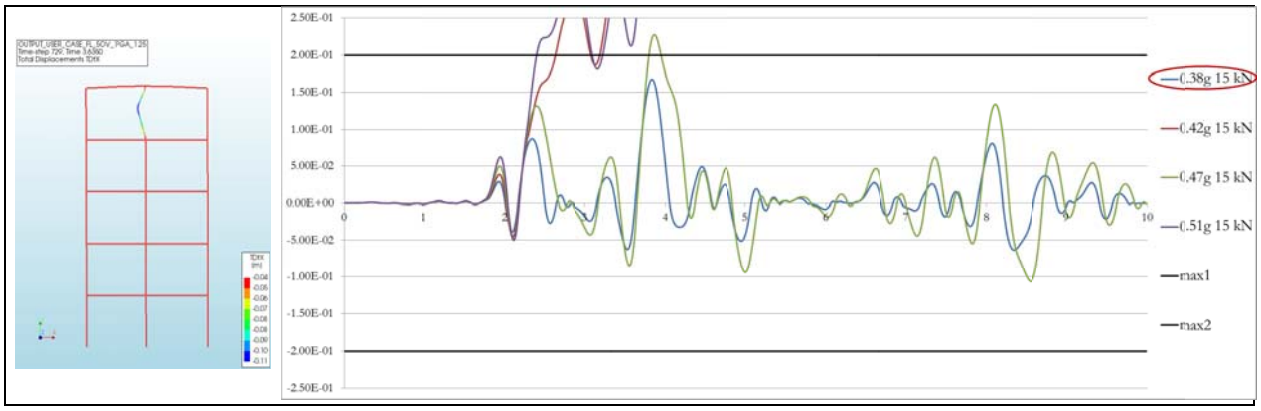

Figure 175 - IDA on frame model with five floors and rocking system at fifth floor. Record D

Bibliography

Allen, C., Masia, M. J. et al, 2013, "What ductility value should be used when assessing unreinforced masonry buildings", NZSEE Conference, Wellington.

Backes, H. P., 1985, "On the Behavior of Masonry Under Tension in the Direction of the Bed Joints", PhD thesis, Aachen University of Technology, Aachen, Germany.

Binda, L., Fontana, A. & Frigerio, G., 1988, "Mechanical Behavior of Brick Masonries derived from Unit and Mortar Characteristics", Proc. 8th Int. Brickand Block Masonry Conf., eds. J.W. de Courcy, Elsevier Applied Science,London, England, pp. 205.

Borri, A., De Maria, A., "Comportamento a taglio delle murature esistenti: esperienze e sperimentazioni anche alla luce del sisma in Emilia", Facoltá di Ingegneria, Univerista' degli studi di Perugia, Italy.

Brebbia, C. A., Maugeri, M., 2011, "Earthquake resistant engineering structures VIII", WITpress.

Casolo, S., 2000, "Modelling the out-of-plane seismic behavior of masonry walls by rigid elements. Earthquake Engineering and Structural Dynamics", Vol. 29, pp 1797-1813.

Chopra, A. K., 2012, "Dynamics of Structures: Theory and Applications to Earthquake Engineering", 4Th edition, Prentice Hall, Englewood Cliffs, New Jersey.

Derakhshan, H. et al, 2014, "Seismic assessment of out-of-plane loaded unreinforced masonry walls in multi storey buildings".

Derakhshan, H., Griffith, M., and Ingham, J., 2013, "Out-of-Plane Behavior of One-Way Spanning Unreinforced Masonry Walls.", J. Eng. Mech., 139(4), 409–417.

Derakhshan, H., 2011, "Seismic Assessment of Out-of-Plane Loaded Unreinforced Masonry Walls", Ph.D. Thesis, Faculty of Engineering, The University of Auckland.

DeJong, M. J., 2009, "Seismic Assessment Strategies for Masonry Structures", PhD thesis, Massachusetts Institute of Technology, Cambridge, United States.

Dhakal, R. P., Sheng, L., Loye, A. K., Evans, S. J., 2013, "Seismic Design Spectra for different soil classes", Bulletin of the New Zealand Society for Earthquake Engineering, Vol. 46, No. 2, pp. 79-87.

Dhanasekar, M., Page, A. W. & Kleeman, P. W., 1985, "The Failure of Brick Masonry Under Biaxial Stresses", Proc. Instn. Civ. Engrs. 2(79), 295-313.

DIANA FEA BV., 2016, "DIANA user's manual", Release 10.0.

Doherty, K. T., 2000, "An investigation of the weak links in the seismic load path of unreinforced masonry buildings", PhD thesis, The University of Adelaide, Adelaide, Australia.

Doherty, K. T., Griffith, M. C., Lam, N. T. K., Wilson, J.L., 2002, "Displacement-based analysis for out-of-plane bending of seismically loaded unreinforced masonry walls", Earthq Eng Struct Dynam, 31(4):833–850.

"Dossier 8550 – Metselwerkwanden belast uit het vlak", 2015, Adviesbureau Ir J.G. Hageman B.V.

Ellsworth, W. L., 2013, "Injection-Induced Earthquakes", Science, 341(6142).

EN 1996-1, 2005, "Eurocode 6 - Design of masonry structures- Part 1-1: General rules for reinforced and unreinforced masonry structures", CEN (European Committee for Standardization), Brussels, Belgium.

EN 1998-1, 2004, "Eurocode 8 - Design of structures for earthquake resistance - Part 1: General rules, seismic actions and rules for buildings", CEN (European Committee for Standardization), Brussels, Belgium.

Gambarotta G., Lagomarsino, S., 1997, "Damage models for the seismic response of brick masonry shear walls.", Earthquake Engineering and Structural Dynamics, Vol. 26, pp 423-439.

Ghali, A., Neville, A. M., Brown, T.G., 2009, "Structural Analysis", Spon Press, 6th edition.

Giuffre' A., Carocci C., 1993, "Statica e dinamica delle costruzioni murarie storiche", Mario Adda Editore, Bari, pp. 539-598.

Griffith, M. C., Vaculik, J., Lam, N. T. K., Wilson, J., and Lumantarna, E., 2007, "Cyclic testing of unreinforced masonry walls in two-way bending", Earthquake Engineering and Structural Dynamics, Vol 36, pp 801–821.

Griffith, M. C., Magenes, G., Melis, G., and Picchi, L., 2003, "Evaluation of out-of-plane stability of unreinforced masonry walls subjected to seismic excitation", Journal of Earthquake Engineering, 7(SPEC. 1):141–169.

"Inspecties en versterkingsadvies aardbevingsbestendiheid QE_R464-N002", Report, Royal Haskoning DHV, 2016.
Lagomarsino, S. (2014) "Seismic assessment of rocking masonry structures", Bull Earthq Eng,, DOI 10.1007/s10518-014-9609-x

KNMI, 2013, "Magnitude beving Huizinge wordt 3.6", Nieuwsbericht 29 January 2013, Koninklijk Nederlands Metereologisch Instituut website.

Lorenco, P. B., Rots, J. G., Blaauwendraad, J., 1995, "Two approaches for the analysis of masonry structures: micro- and macro-modelling", HERON, Vo.40, No.4, pp 313-340.

Lorenco, P. B., Rots, J. G., 1997, "Multi-surface interface model for the analysis of masonry structures", Journal of Engineering Mechanics, ASCE, 127(7), pp 660-668.

Lorenco, P. B., Rots, J. G., Blaauwendraad, J., 1998, "Continuum model for masonry: parameter estimation and validation", Journal of Structural Engineering, 124(6):642-652.

Lourenco, P. B., 2000, "Anisotropic softening model for masonry plates and shells", Journal of Structural Engineering, 126(9):1008–1016.

Lourenco, P. B., 2008, "Structural masonry analysis: recent developments and prospects", Proceedings of the 14th International brick & block masonry conference, Sydney, Australia, pp 1341-1356.

Lorenco, P. B., Mendes, N., Ramos, L., Oliveira, D., 2011, "On the analysis of masonry structures without box behavior".

Lourenco, P. B., 2013, "Types of analysis: linear elastic, linear dynamic and nonlinear static", Presentation, Institute for Sustainability and Innovation in Structural Engineering.

McNary, W. S., & Abrams, D. P., 1985, "Mechanics of masonry in compression", Journal of Structural Engineering, United States, 111(4), 857-870.

Mosalam, K., Glascoe, L., & Bernier, J., 2009, "Mechanical Properties of Unreinforced Brick Masonry".

Naraine, K. and Sinha, S. N., 1989, "Behavior of Brick. Masonry under Cyclic Compressive Loading", Journal of. Struct. Engineering, ASCE.

NEN NPR 9998, 2015, "Nederlandse praktijkrichtlijn: Beoordeling van de constructieve veiligheidvan een gebouw bij nieuwbouw, verbouw enafkeuren - Grondslagen voor aardbevingsbelastingen: Geïnduceerde aardbevingen", Technical report, Nederlands Normalisatie-instituut, Delft, The Netherlands.

NTC – Norme Tecniche per le Costruzioni, 2008, "Circolare Applicazione n.167 ", Ministry of Infrastructures and Transportations, Italy.

NZS 1170.5 , 2004, "Structural Design Actions - Part 5 : Earthquake actions New Zealand", NZS (New Zealand Standards), Wellington, New Zealand.

NZSEE - New Zealand Society for Earthquake Engineering, 2015, "Assessment and Improvement of the Structural Performance of Buildings in Earthquakes", Section 10 Revision, Corrigenda No.4.

Page, A. W., 1981, "The Biaxial Compressive Strength of Brick Masonry", Proc. Intsn. Civ. Engineers 2(71), 893-906.

Pampanin, S., 2002, "Forces or displacements? Alternative seismic design philosophies", ELITE – THe international Journal of Precast Art, Issue n.5 68-75.

Pantazoupoulou, S. J., 2013, "State of the art report for the analysis methods for unreinforced masonry heritage structures and monuments".

Priestley, M. J. N., 1985, "Seismic behavior of unreinforced masonry walls", Bulletin of the New Zealand National Society for Earthquake Engineering, Vol. 18, No. 2, pp 191 – 205.

Priestley, M. J. N, Calvi, G. M, Kowalsky, M. J, 2007, "Displacement based seismic design of structures", IUSS Press, Istituto Universitario Studi Superiori di Pavia.

Shelton, R.H., 2004, "Seismic Response of Building Parts and Non-Structural Components", BRANZ, Study Report, No.124, New Zealand.

Shibata, A., Sozen, M. A., 1976, "Substitute-structure method for seismic design in R/C", Journal of the Structural Division, 102(1):1-18.

Tomazevic, M., 1999, "Earthquake-Resistant Design of Masonry Buildings", Slovenian National Building and Civil Engineering Institute, Imperial College Press.

TU Delft, 2017, "Introduction to Seismic Essentials in Groningen", OpenCourseWare, www.ocw.tudelft.nl.

Van Thienen-Visser, K., Breunese, J.N., 2015, "Induced seismicity of the Groningen gas field: History and recent developments", The leading edge, pag 664-671.

Vinci, M., 2014, "Metodi di calcolo e tecniche di consolidamento per edifice in muratura", Dario Flaccovio Editore, Palermo, Italy.